



**HAL**  
open science

# Synthesis and properties of the Ni-based catalysts for the valorization of ethanol and glycerol via steam reforming reaction for hydrogen production

Marina Arapova

► **To cite this version:**

Marina Arapova. Synthesis and properties of the Ni-based catalysts for the valorization of ethanol and glycerol via steam reforming reaction for hydrogen production. Catalysis. Université de Strasbourg; Boreskov Institute of Catalysis, 2017. English. NNT : 2017STRAF031 . tel-01712030

**HAL Id: tel-01712030**

**<https://theses.hal.science/tel-01712030v1>**

Submitted on 19 Feb 2018

**HAL** is a multi-disciplinary open access archive for the deposit and dissemination of scientific research documents, whether they are published or not. The documents may come from teaching and research institutions in France or abroad, or from public or private research centers.

L'archive ouverte pluridisciplinaire **HAL**, est destinée au dépôt et à la diffusion de documents scientifiques de niveau recherche, publiés ou non, émanant des établissements d'enseignement et de recherche français ou étrangers, des laboratoires publics ou privés.

**ÉCOLE DOCTORALE DES SCIENCES CHIMIQUES**

L'Institut de chimie et procédés pour l'énergie, l'environnement et la santé (ICPEES) UMR 7515 CNRS

**THÈSE** présentée par :

**Marina ARAPOVA**

cotutelle

soutenue le : **01 Novembre 2017**

pour obtenir le grade de : **Docteur de l'université de Strasbourg**

Discipline/ Spécialité : chimie

**Synthèse et propriétés de catalyseurs à base de Ni pour la valorisation d'éthanol et de glycérol par vaporeformage catalytique pour la production d'hydrogène**

**THÈSE dirigée par :**

**Mme Anne-Cécile ROGER** Professeur, université de Strasbourg, France

**M Vladislav SADYKOV** Professeur, université d'Etat de Novossibirsk, Russie

**RAPPORTEURS :**

**Mme Olga VODYANKINA** Professeur, université d'Etat de Tomsk, Russie

**M Mikhail SINEV** Chargé de recherche RAS, Institut de Physique Chimique de Moscou, Russie

---

**AUTRES MEMBRES DU JURY :**

**Mme Ksenia PARKHOMENKO**

Chargé de recherche CNRS, université de Strasbourg, France

## ACKNOWLEDGEMENTS

I would like to express my sincere gratitude to all the people without whom this thesis would have never been possible. First of all, I would like to thank the French Government and French Embassy in Russia, granted me the “Metchnikov” stipend in 2013, for the priceless opportunity to work with the great scientists in a modern laboratories between two leading scientific countries.

I am especially grateful to my French supervisor, Anne-Cécile Roger for her hospitality, for all the valuable advices she gave me and for sharing her highly effective experience how to set scientific tasks, conduct and analyze experiments and achieve the goals desired. As well, I am gratefully acknowledged for my Russian scientific supervisor Vladislav Sadykov, who inspired me with real interest in catalysis science and showed great confidence, allowing me to become a part of this international cooperation.

I owe a great deal of gratitude to Svetlana Pavlova for her immense role and continuous support of my study, encouraging my research and for allowing me to grow as a research scientist.

Special words of thanks to Ksenia Parkhomenko, who have always been a major source of support for me in a moments of difficulties, helped me on every academician, bureaucratic and personal questions, showed me the wonderful world of French cuisine and culture and always was there for me as the best example of optimistic and confident person.

I would also like to thank my jury members, Dr. Olga Vodyankina and Dr. Mikhail Sinev for investing time and providing interesting and valuable feedback that helped to make this work better, I feel proud and honored that you have accepted to be in my committee. Thanks are also in order for a number of the colleagues and friends at ICPEES – both past and present: Laetitia, Miriam, Charlotte, Killian, Dmitry, Qian, QinQin, Sebastian, Audrey, Pauline, Valentin, Rogeria and Geraldine who made me feel so welcome during my French staying periods of research.

A special thanks to Yvan Zimmermann for his tremendous patience to my French language and technical skills and his ongoing help with the practical aspects essential to my work.

I am also very grateful to all the teaching and research staff in both Boreskov Institute of Catalysis and ICPEES, which have taken some time to discuss and enrich my work.

My deepest appreciation belongs to my parents for their patience, support and understanding. A very special word of thanks goes for my husband Pavel, who always supports, encourages and motivates me and never let me give up in the way I go.

# RESUME en Français

## Introduction

Parmi les défis actuels auxquels l'humanité a fait face au XXI<sup>e</sup> siècle, la question des ressources et des technologies d'énergie verte renouvelable est l'une des plus urgentes, essentielles et vitales. De nos jours, la biomasse est l'une des matières premières alternatives les plus prometteuses qui pourraient être transformées en l'énergie utile. Aujourd'hui, il existe des dizaines de méthodes de la transformation de la biomasse, qui permettent d'obtenir trois principales matières premières: les combustibles solides, gazeux et liquides, dont la composition peut varier selon les conditions de traitement. Les produits d'intérêt élevé sont issus de la biomasse par la pyrolyse rapide des composants oxygénés légers de la bio-huile. Cette fraction, comme l'éthanol, le glycérol etc, semble extrêmement prometteuse en raison de la possibilité d'être utilisée directement comme combustible dans des *piles à combustible à oxyde solide à température intermédiaire*. Le principal problème de ce procédé à haute efficacité énergétique est la cokéfaction et le frittage lourds lors de la réaction des catalyseurs les plus appropriés contenant du Ni. L'une des approches les plus approfondies pour augmenter la stabilité des catalyseurs consiste à utiliser des pérovskites contenant du Ni comme précurseur du catalyseur, qui forment des nanoparticules Ni-Fe métalliques résistants au frittage, qui interagissent fortement avec la pérovskite restante lors du prétraitement réducteur. Ces catalyseurs sont actifs et stables, mais en raison d'une surface spécifique pas très élevée - environ 10 m<sup>2</sup>/g - ils ne peuvent pas fournir des performances requises étant supportés sur des supports structurés. Ce problème pourrait être résolu en chargeant des pérovskites sur les supports avec surface spécifique plus élevée tel que  $\gamma$ -Al<sub>2</sub>O<sub>3</sub> avec l'incorporation d'éléments alcalins, ce qui contribuera à créer des systèmes catalytiques structurés de haute efficacité pour la réaction de vaporeformage d'éthanol et de glycérol.

## ***L'objectif du travail:***

Développement de catalyseurs efficaces à base de pérovskite pour la transformation des bio-huiles en le gaz de synthèse et l'hydrogène (réactions modèles - vaporeformage d'éthanol et de glycérol). Conformément à l'objectif, les tâches suivantes ont été formulées:

1. Synthèse de trois familles de catalyseurs:

- a. Les pérovskites massives  $\text{LnFe}_{1-x-y}\text{M}_x\text{Ru}_y\text{O}_3$  (Ln = La, Pr, M = Ni, Co)
- b. Les pérovskites supportées  $m\text{LnNi}_{0,9-x}\text{Fe}_x\text{Ru}_{0,1}\text{O}_3/n\text{Mg-}\gamma\text{-Al}_2\text{O}_3$  (Ln = La, Pr, x = 0 - 0.6, m = 10-20%mass, n = 6-15% mass.



- c. Les pérovskites structurées  $[\text{LnNi}_{0.9}\text{Ru}_{0.1}\text{O}_3/\text{nMg-}\gamma\text{-Al}_2\text{O}_3]/\text{mousses structurées}$
2. La caractérisation physique et chimique détaillée pour toutes les familles à l'aide des méthodes BET, DRX, MET avec EDX, TPR- $\text{H}_2$ , XPS, IR de CO adsorbées et UV-Vis
  3. L'étude d'activité catalytique et de la stabilité des matériaux préparés dans les réactions modèles - vaporéformage d'éthanol et vaporéformage de glycérol.

### **Résultats et discussions.**

Les résultats expérimentaux et la discussion des résultats ont été divisés en trois chapitres: chapitre III, IV et V.

Le **chapitre III** est consacré à la synthèse, à la caractérisation et à l'étude de l'activité catalytique dans les réactions de vaporeformage d'éthanol et de glycérol de la famille de pérovskites massives  $\text{LnFe}_{1-x-y}\text{M}_x\text{Ru}_y\text{O}_3$  ( $\text{Ln} = \text{La}, \text{Pr}, \text{M} = \text{Ni}, \text{Co}$ ), ainsi que des échantillons de comparaison de 5%  $\text{Ni}(\text{Co})/\text{PrFeO}_3$ . En utilisant les méthodes DRX et MET, il a été montré que les échantillons initiaux  $\text{PrFeO}_3$  et  $\text{LnFe}_{1-x-y}\text{M}_x\text{Ru}_y\text{O}_3$  contiennent principalement la phase de pérovskite avec la structure orthorhombique. La surface spécifique moyenne des pérovskites initiales est de 4-10  $\text{m}^2/\text{g}$ . Les diffractogrammes DRX des échantillons 5% $\text{Ni}(\text{Co})/\text{PrFeO}_3$  montrent qu'ils sont constitués d'oxydes orthorhombiques  $\text{PrFeO}_3$  et  $\text{NiO}$  ( $\text{Co}_3\text{O}_4$ ) avec une taille de cristallites de  $\sim 35$  nm et  $\geq 100$  nm dans les cas de supports calcinés à 700 et 900  $^\circ\text{C}$ , respectivement. La capacité de réduction des pérovskites a été étudiée par la méthode TPR- $\text{H}_2$  avec une étude ultérieure par DRX et MET (Fig.1). Pour les échantillons monophasés  $\text{LnFe}_{1-x-y}\text{M}_x\text{O}_3$  qui ne contiennent pas de ruthénium, le traitement dans l'hydrogène à 500  $^\circ\text{C}$  n'affecte pas leur structure; pour les échantillons contenant du Ru à des températures  $\sim 300\text{-}320$   $^\circ\text{C}$ , la réduction de Ru est observée. Une augmentation de la température de réduction à 800  $^\circ\text{C}$  entraîne une décomposition partielle de la pérovskite avec la formation d'oxydes de La, Pr et de Ni-Fe (Ru), des particules d'alliage de Co-Fe avec une taille moyenne de 10 nm stabilisée sur la phase de la pérovskite restante (Fig. 1).

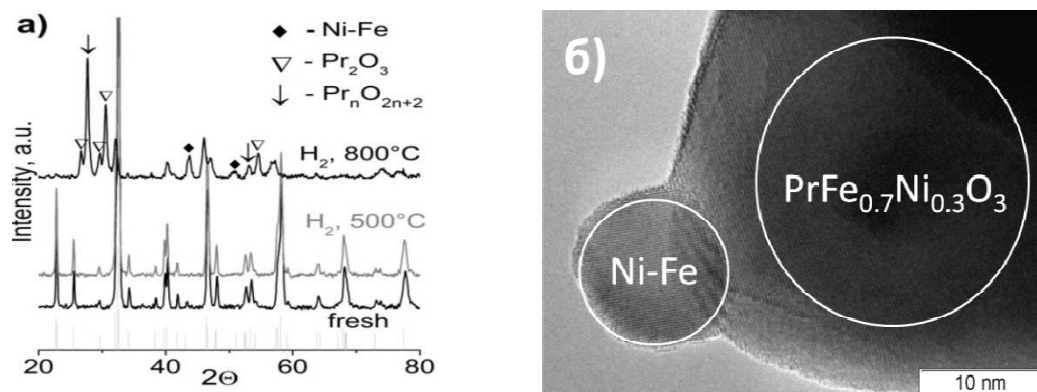


**Fig. 1.** a – Résultats DRX d'échantillons  $\text{PrFe}_{0.7}\text{Ni}_{0.3}\text{O}_3$ : frais et réduit à 500 et 800  $^\circ\text{C}$ ,  
 b – Image MET d'échantillon  $\text{PrFe}_{0.7}\text{Ni}_{0.3}\text{O}_3$  après la réduction à 800  $^\circ\text{C}$ .

La formation de particules bimétalliques nanométriques de Ni-Fe liées avec la pérovskite a été confirmée par MET (Fig. 1b). Selon les données du TPR-H<sub>2</sub>, la réduction du cobalt de la pérovskite se produit à des températures plus élevées que celles des nickels. Dans les échantillons à 5% de Ni(Co)/PrFeO<sub>3</sub>, la réduction de NiO et de Co<sub>3</sub>O<sub>4</sub> se produit à T ~ 450-500 °C, et la taille des particules métalliques formées est dépendante de la température de calcination du support: pour PrFeO<sub>3</sub> avec T<sub>calc</sub> = 700 °C est de l'ordre de 10 à 20 nm ; dans le cas de PrFeO avec T<sub>calc</sub> = 900 °C, des particules sont beaucoup plus grandes.

Les catalyseurs de cette famille ont été préalablement réduits dans un flux d'hydrogène à 800 °C avant les essais catalytiques dans la réaction de *vaporeformage de l'éthanol* à des températures de 600 à 850 °C (certaines données sont présentées dans le Tableau 1). Les tests catalytiques montrent que pour tous les échantillons de composition LnFe<sub>1-x-y</sub>M<sub>x</sub>Ru<sub>y</sub>O<sub>3</sub>, des taux élevés de conversion de l'éthanol sont déjà observés à une température de 700 °C. Les principaux produits de la réaction sont H<sub>2</sub>, CO et CO<sub>2</sub>.

**Tableau 1.** Conversion d'éthanol, rendement en hydrogène et sélectivité de CO et C<sub>2</sub>H<sub>4</sub> (%)

T, °C	X <sub>C<sub>2</sub>H<sub>5</sub>OH</sub>		Y <sub>H<sub>2</sub></sub>		S <sub>CO</sub>		S <sub>C<sub>2</sub>H<sub>4</sub></sub>	
	650	700	650	700	650	700	650	700
Catalyst:								
PrFe <sub>0.7</sub> Ni <sub>0.3</sub> O <sub>3</sub>	64	98	68	89	57	73	1	0
LaFe <sub>0.7</sub> Ni <sub>0.3</sub> O <sub>3</sub>	49	75	44	67	53	60	3	3
PrFe <sub>0.7</sub> Co <sub>0.3</sub> O <sub>3</sub>	29	60	12	29	20	38	9	10
PrFe <sub>0.6</sub> Ni <sub>0.3</sub> Ru <sub>0.1</sub> O <sub>3</sub>	80	100	76	90	57	75	0	0
5% Ni/ PrFeO <sub>3</sub> <sup>700</sup>	96	100	82	85	57	63	1	0
5% Ni/ PrFeO <sub>3</sub> <sup>900</sup>	100	100	93	97	63	78	0	0
10PrNi <sub>0.9</sub> Ru <sub>0.1</sub> /6Mg-Al <sub>2</sub> O <sub>3</sub>	98	98	57	76	37	60	31	11
10PrNi <sub>0.9</sub> Ru <sub>0.1</sub> /10Mg-Al <sub>2</sub> O <sub>3</sub>	100	100	86	90	62	71	0	0
10PrNi <sub>0.9</sub> Ru <sub>0.1</sub> /15Mg-Al <sub>2</sub> O <sub>3</sub>	100	100	78	85	53	72	8	0
10LaNi <sub>0.9</sub> Ru <sub>0.1</sub> /10Mg-Al <sub>2</sub> O <sub>3</sub>	100	100	85	91	57	75	5	0
20PrNi <sub>0.9</sub> Ru <sub>0.1</sub> /10Mg-Al <sub>2</sub> O <sub>3</sub>	100	100	96	97	59	70	0	0

Les échantillons contenant Pr présentent une activité et une stabilité supérieures à celles contenant La, ce qui peut être expliqué par la forte réactivité de l'oxygène dans l'oxyde de praséodyme formé pendant la réduction, ce qui contribue à l'oxydation des précurseurs de coke. L'activité des échantillons à base de Co est beaucoup plus faible que pour les analogues contenant du Ni sur toute la gamme de température. En même temps, un rendement élevé en l'acétaldéhyde (non donné pour la brièveté) et l'éthylène indique un faible taux de conversion de ces intermédiaires en les produits cibles. Les résultats obtenus sont compatibles avec la difficulté de la réduction de Co à partir de la structure de la pérovskite montrée par la méthode TPR-H<sub>2</sub>. La comparaison de l'activité des

catalyseurs  $\text{LnFe}_{1-x-y}\text{M}_x\text{Ru}_y\text{O}_3$  et  $5\% \text{Ni}/\text{PrFeO}_3$  (Tableau 1) montre que les échantillons imprégnés de  $5\% \text{Ni}/\text{PrFeO}_3$  sont plus actifs à  $T \leq 700^\circ\text{C}$ , ce qui est dû à une réduction plus facile de nickel, selon les données TPR- $\text{H}_2$ . Cependant, les essais de la stabilité de ces échantillons à une température constante de  $650^\circ\text{C}$  pendant 7 heures (Fig. 2) ont montré une désactivation rapide et les images MET (Fig. 3) des catalyseurs après tests indiquent un frittage important des particules métalliques pour les échantillons imprégnés. Ainsi, les catalyseurs à base de ferrites substituées  $\text{LnFe}_{1-x-y}\text{M}_x\text{Ru}_y\text{O}_3$  démontrent une résistance accrue au frittage de particules métalliques et dépôt de carbone grâce à une forte interaction des particules métalliques avec le support et une dilution des ensembles de nickel en raison de la formation d'un alliage Ni-Fe.

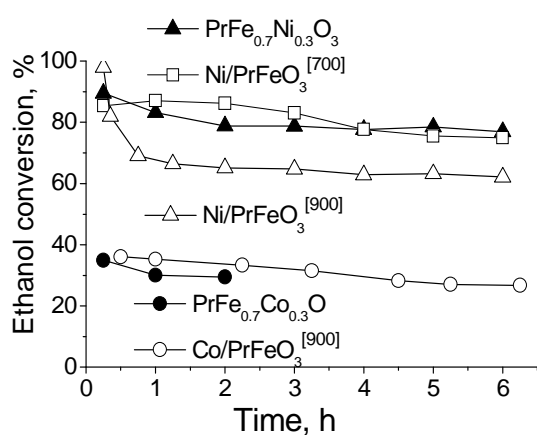


**Fig. 2.** La conversion d'éthanol pendant le vaporeformage d'éthanol à  $650^\circ\text{C}$  pour les catalyseurs à base de  $5\% \text{Co}(\text{Ni})/\text{PrFeO}_3$  et  $\text{PrFe}_{0.7}\text{Co}(\text{Ni})_{0.3}\text{O}_3$ .

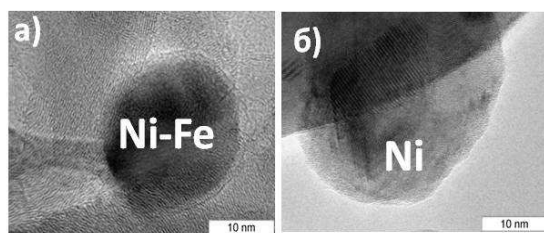


**Fig. 3.** Images MET de a)  $\text{PrFe}_{0.7}\text{Ni}_{0.3}\text{O}_3$  et b)  $5\% \text{Ni}/\text{PrFeO}_3^{[900]}$  après le vaporeformage d'éthanol à  $650^\circ\text{C}$  pendant 7 h.

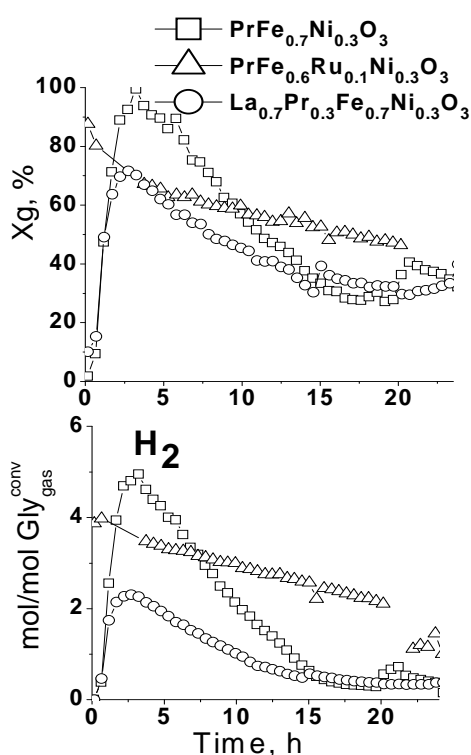


**Fig. 4.** La conversion du glycérol en phase gazeuse  $X_g$  (%) et la productivité en hydrogène ( $\text{mol}/\text{mol Gly}_{\text{gas}}^{\text{conv}}$ ) pendant le vaporeformage du glycérol à  $650^\circ\text{C}$  en présence de  $\text{LnFe}_{1-x-y}\text{Ni}_x\text{Ru}_y\text{O}_3$

Les catalyseurs  $\text{LnFe}_{1-x-y}\text{M}_x\text{Ru}_y\text{O}_3$  ont été préalablement réduits dans de l'hydrogène à  $500^\circ\text{C}$  et testés dans une réaction de *vaporeformage de glycérol* à  $650^\circ\text{C}$ . Pour les échantillons à base de nickel  $\text{PrFe}_{0.7}\text{Ni}_{0.3}\text{O}_3$ ,  $\text{La}_{0.7}\text{Pr}_{0.3}\text{Fe}_{0.7}\text{Ni}_{0.3}\text{O}_3$ ,  $\text{PrFe}_{0.6}\text{Ni}_{0.3}\text{Ru}_{0.1}\text{O}_3$ , il a été montré (Fig. 4) que la conversion du glycérol et le rendement en hydrogène dépendent fortement de la composition de la pérovskite. Pour  $\text{PrFe}_{0.7}\text{Ni}_{0.3}\text{O}_3$  et  $\text{La}_{0.7}\text{Pr}_{0.3}\text{Fe}_{0.7}\text{Ni}_{0.3}\text{O}_3$ , un maximum sur les courbes de la conversion est observé en raison de la réduction supplémentaire de la pérovskite dans le mélange

réactionnel et, par la suite, une diminution rapide de l'activité due à la formation de carbone. L'activité initiale élevée du catalyseur  $\text{PrFe}_{0.6}\text{Ni}_{0.3}\text{Ru}_{0.1}\text{O}_3$  s'explique par la présence de Ru, qui est réduite à  $T \leq 300$  °C. La diminution lente de l'activité pour cet échantillon indique sa plus grande stabilité. Les essais de catalyseurs à base de cobalt ont montré qu'ils présentent une faible activité dans les réactions: malgré la conversion du glycérol en phase gazeuse  $X_g$  de 70%, le rendement en hydrogène pour les systèmes contenant du cobalt, même avec l'addition de l'oxygène (oxy-vaporeformage) reste faible ( $0,8 \text{ mol H}_2/\text{mol}_{\text{Gly}}$ ), ce qui correspond à la valeur de l'échantillon sans composant actif  $\text{PrFeO}_3$ . La sélectivité élevée en l'éthylène pour ces échantillons indique également la faible sélectivité du groupe de catalyseurs à base de Co. L'ajout d'oxygène au mélange réactionnel peut améliorer considérablement la stabilité du catalyseur tout en maintenant un haut rendement en hydrogène réduisant la formation de dépôts carbonés.

Le **chapitre IV** est consacré à la synthèse, à la caractérisation et à l'étude de l'activité catalytique dans les réactions de vaporeformage d'éthanol et de glycérol de la famille sur support  $m\text{LnNi}_{0.9-x}\text{Fe}_x\text{Ru}_{0.1}\text{O}_3/n\text{Mg-}\gamma\text{-Al}_2\text{O}_3$  ( $\text{Ln} = \text{La}, \text{Pr}, x = 0 - 0.6, m = 10\text{-}20\% \text{mass}, n = 6\text{-}15\% \text{mass}$ ). Pour cette famille, on a constaté que l'état de l'agent actif et les propriétés acides de la surface de support, déterminant l'activité catalytique des échantillons, dépendaient de la quantité et du procédé d'introduction du magnésium, le procédé de la synthèse, la quantité et la composition chimique de la pérovskite déposée. La surface spécifique du  $\gamma\text{-Al}_2\text{O}_3$  initial est de  $177 \text{ m}^2/\text{g}$  et elle diminue avec la charge de Mg et pérovskite jusqu'à  $100\text{-}160 \text{ m}^2/\text{g}$  selon la méthode d'incorporation de Mg et de sa concentration.

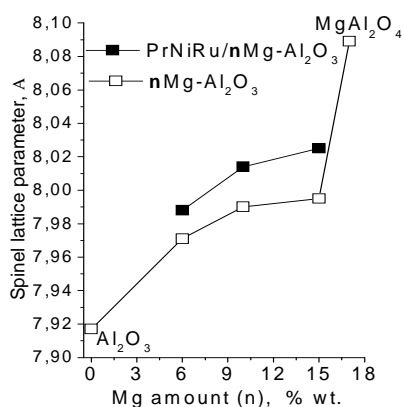


**Fig. 5.** Paramètre de maille de spinelle en fonction de taux de Mg en n% Mg- $\gamma\text{Al}_2\text{O}_3$  et en catalyseur supporté sur n% Mg- $\gamma\text{Al}_2\text{O}_3$

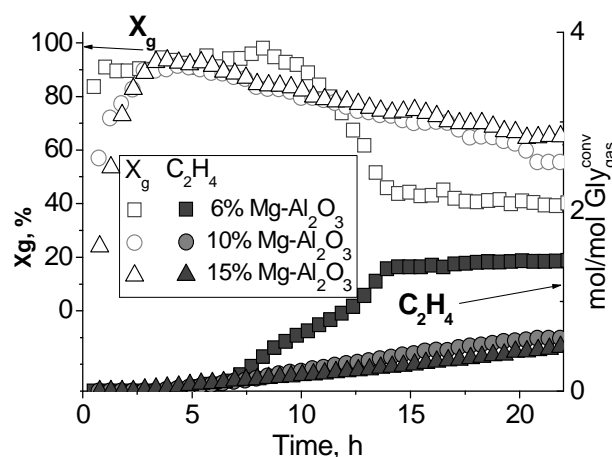


**Fig. 6.** La conversion du glycérol en phase gazeuse  $X_g$  (%) et la productivité en hydrogène ( $\text{mol}/\text{molGly}_{\text{gas}}^{\text{conv}}$ ) pendant le vaporeformage du glycérol à  $650$  °C en présence de  $10\% \text{PrNi}_{0.9}\text{Ru}_{0.1}\text{O}_3/[n\% \text{Mg-}\gamma\text{Al}_2\text{O}_3]$

L'étude des catalyseurs supportés par DRX, la spectroscopie UV-Vis-NIR et MET a montré que le Ni avec Mg sont incorporés dans la structure spinelle (Fig. 5) pour former une phase mixte de  $\text{Ni}_x\text{Mg}_{1-x}\text{Al}_2\text{O}_4$ , alors qu'à  $\text{Mg} \geq 10$  % la solution solide MgO-NiO est également formée. La

formation de structures de surface de type pérovskite  $\text{PrNi}_x\text{Ru}_{1-x}\text{O}_3$  and  $\text{Pr}_2\text{Ni}_x\text{Ru}_{1-x}\text{O}_4$  est montrée par MET pour des échantillons avec une teneur en pérovskite de 20%. L'étude des supports modifiés par Mg par la spectroscopie infrarouge avec du CO adsorbé montre une diminution de l'acidité de surface avec une augmentation de la concentration superficielle du Mg. La réduction des échantillons avec la formation de particules métalliques de Ni et de Ni-Ru a lieu dans la gamme de températures de 600 à 900 °C. Dans ce cas, en raison de la forte interaction métal-support, la taille des particules métalliques formées est assez petite ~ 6-15 nm.

L'étude de la performance des catalyseurs dans la réaction de *vaporeformage d'éthanol* montre que tous les catalyseurs fournissent des valeurs élevées de la conversion de l'éthanol, tandis que la sélectivité et la stabilité des catalyseurs dépendent principalement de la teneur en magnésium. La diminution de la force des sites acides de l'oxyde d'aluminium, montrée par la spectroscopie IR, entraîne une diminution de la sélectivité de l'éthylène en supprimant la voie de déshydratation, ce qui donne une forte résistance au dépôt de carbone à ces échantillons. Lorsque la teneur en magnésium dans le catalyseur est  $\geq 10\%$ , les catalyseurs à base de La et Pr présentent une activité similaire (Tableau 1). La conversion élevée d'éthanol est déjà atteinte à 600 °C tout en conservant des rendements élevés en  $\text{H}_2$  et en CO, ainsi qu'une faible sélectivité pour les sous-produits.

Dans le cas de la réaction de *vaporeformage de glycérol*, une tendance à la désactivation dans les tests de longue durée a été révélée. La conversion du glycérol et le rendement en hydrogène, comme cela a été démontré dans le cas d'échantillons massifs du chapitre III, sont plus élevés pour les catalyseurs contenant le Pr. On a montré une corrélation entre la teneur en Mg et l'état Ni et la performance catalytique de ces catalyseurs. La conversion de glycérol et la productivité de l'éthylène (précurseur de coke le plus important) (Fig. 6) démontrent une augmentation de la stabilité de l'échantillon avec une augmentation de la teneur en Mg dans l'échantillon à 15%. Pour toutes les familles de catalyseurs, la stabilisation de la performance catalytique a été observée lorsque l'oxygène était ajouté au mélange réactionnel.

Le **chapitre V** est consacré aux résultats des tests des catalyseurs  $10\%\text{LnNi}_{0,9}\text{Ru}_{0,1}\text{O}_3/\text{Mg-}\gamma\text{-Al}_2\text{O}_3$  supporté sur des plaquettes de mousse structurée. Il a été montré que, à des températures inférieures à 750 °C, la conversion d'éthanol et le rendement en hydrogène sont plus élevés pour le composant actif optimisé chargé sur la mousse Ni-Al métallique par rapport à la mousse céramique. Évidemment, la performance du catalyseur supporté en mousse de Ni-Al est meilleure grâce à sa haute conductivité thermique qui fournit un transfert de chaleur efficace le long du lit catalytique. Un essai à long terme de ce catalyseur dans vaporeformage d'éthanol et oxy-vaporeformage d'éthanol utilisant un mélange de gaz réaliste (30% d'éthanol) montre sa grande activité et sa stabilité dans les deux réactions pendant 40 heures.

## Conclusion générale

1. Il a été démontré que, la synthèse de précurseurs d'oxyde mixtes utilisant la méthode Pechini modifiée suivie d'une calcination à  $700 \pm 900$  °C, permet d'obtenir la pérovskite monophasée  $\text{LnFe}_{1-x-y}\text{M}_x\text{Ru}_y\text{O}_3$  (Ln = La, Pr, M = Ni, Co) de la structure orthorhombique à  $x \leq 0,3$  pour Ni et  $x \leq 0,4$  pour Co;  $y = 0-0.1$ . Dans le cas d'échantillons de 5% M/PrFeO<sub>3</sub> obtenus par imprégnation, Ni (Co) ne sont pas inclus dans la structure de la pérovskite et sont présents sous forme d'oxydes individuels de NiO ou Co<sub>3</sub>O<sub>4</sub>.
2. Il a été établi que, lors de la réduction à 800 °C les pérovskites  $\text{LnFe}_{1-x-y}\text{M}_x\text{Ru}_y\text{O}_3$  se transforment en les catalyseurs actifs comprenant des nanoparticules d'oxyde de LnO<sub>x</sub> et un alliage métallique (Ni-Fe, Co-Fe ou Ni-Fe-Ru) avec une taille de ~ 10 nm fortement lié à la surface de la pérovskite restante. Il est démontré que ces matériaux activés ont une plus grande stabilité dans les réactions du vaporeformage d'éthanol et de glycérol par rapport aux catalyseurs 5%M/PrFeO<sub>3</sub> obtenus par imprégnation. Les catalyseurs les plus actifs et les plus stables sont les échantillons à base des pérovskites  $\text{PrFe}_{0.7}\text{Ni}_{0.3}\text{Ru}_y\text{O}_3$  ( $y = 0-0.1$ ), ce qui est dû à la facilité de leur réduction et aux propriétés red-ox de l'oxyde de praséodyme formé.
3. Il a été montré que, pour la famille supportée  $\text{Ln}(\text{Fe})_x\text{Ni}_{0.9-x}\text{Ru}_{0.1}\text{O}_3$  / n% Mg- $\gamma$ -Al<sub>2</sub>O<sub>3</sub> ( $m = 10-20\%$  mass,  $n = 6-10\%$  mass), le magnésium et le nickel sont introduit dans  $\gamma$ -Al<sub>2</sub>O<sub>3</sub>, ce qui réduit l'acidité de  $\gamma$ -Al<sub>2</sub>O<sub>3</sub> et la concentration de Mg affecte l'interaction du nickel avec le support: à  $n = 6\%$ , le nickel est principalement incorporé dans  $\gamma$ -Al<sub>2</sub>O<sub>3</sub> pour former le spinelle  $\text{Ni}_x(\text{Mg}_{1-x})\text{Al}_2\text{O}_4$ , à  $n \geq 10\%$  NiO-MgO. Avec un contenu de 20% de pérovskite, une partie du nickel peut également faire partie des structures superficielles de  $\text{PrNi}_x\text{Ru}_{1-x}\text{O}_3$  and  $\text{Pr}_2\text{Ni}_x\text{Ru}_{1-x}\text{O}_4$ .
4. Il a été montré que la réduction de  $m\text{Ln}(\text{Fe})_x\text{Ni}_{0.9-x}\text{Ru}_{0.1}\text{O}_3$  / n% Mg- $\gamma$ -Al<sub>2</sub>O<sub>3</sub> avec la formation de particules de Ni métalliques fortement dispersées et l'alliage Ni-Ru est déterminée par la forte interaction de nickel avec le support, qui dépend de la concentration de Mg et de pérovskite.
5. Il a été établi que l'activité et la stabilité des catalyseurs supportés à base de  $m\text{Ln}(\text{Fe})_x\text{Ni}_{0.9-x}\text{Ru}_{0.1}\text{O}_3$  / n% Mg- $\gamma$ -Al<sub>2</sub>O<sub>3</sub> dans toutes les réactions étudiées augmentent avec l'augmentation de la concentration de magnésium, en raison d'une diminution de la concentration des sites acides sur la surface de support. Il a été démontré que les catalyseurs de la composition optimale de 10 à 20% de  $\text{PrNi}_{0.9}\text{Ru}_{0.1}\text{O}_3$ /10% Mg- $\gamma$ -Al<sub>2</sub>O<sub>3</sub> fournissent le meilleur rendement en hydrogène (~ 90%) et la stabilité pour ~ 20 heures dans le vaporeformage d'éthanol.
6. Une activité élevée de catalyseurs structurés à base de supports macroporeux Ni-Al, SiC/Al-Si-O et Ni-Al-SiC/ $\alpha$ -Al<sub>2</sub>O<sub>3</sub> dans le vaporeformage d'éthanol dans un réacteur pilote a été montré. Un catalyseur structuré optimisé à base de support Ni-Al métallique fournit un rendement d'hydrogène de 80 à 87% dans les réactions de oxy-vaporeformage d'éthanol avec l'alimentation réaliste de gaz

(concentration d'éthanol 30%) dans le réacteur pilote pendant 40 heures ( $T = 850\text{ }^{\circ}\text{C}$ , temps de contact 1 s).

---

## LISTE DES PRESENTATIONS

1. Pavlova S., Arapova M., Alikina G., Rogov V., Krieger T., Sadykov V., Roger A.-C., Chan –Thaw C. E., «Hydrogen and syngas production by steam reforming of ethanol using  $\text{LnFeNiMO}_3$  ( $M=\text{Co, Mn, Ru}$ ) perovskites as catalyst precursors», 11th European Congress on Catalysis–EuropaCat-XI, Lyon, France, 2013, P.585.
2. Pavlova S., Arapova M., Alikina G., Rogov V., Krieger T., Sadykov V., Roger A.-C. «Steam reforming of ethanol for hydrogen and syngas production over perovskite-type  $\text{Ni}(\text{Co, Ru})$  ferrites as catalyst precursors», The Seventh Tokyo Conference on Advanced Catalytic Science and Technology - TOCAT7, Kyoto, Japan, 2014, Poster O-A22 (19).
3. Arapova M. V., Pavlova S. N., Larina T. V., Rogov V. A., Krieger T. A., Sadykov V. A., Smorygo O., Parkhomenko K., Roger A.-C., «Hydrogen and syngas production via ethanol steam reforming over supported ferrites-nikelates», Energy&Materials, Research Conference - EMR2015 Madrid, Spain, 2015, P.138.
4. Sadykov V., Arapova M., Smal E., Pavlova S., Roger A.-C., van Veen A., «Nanocomposite catalysts of biofuels transformation into syngas: design and performance», 6<sup>th</sup> Annual Global Congress of Catalysis, Xian, China, 2015, P.45.
5. M. Arapova, S. Pavlova, V. Sadykov, K. Parkhomenko, A.-C.Roger., «Perovskite-based catalysts for steam/autothermal reforming of bioethanol», GDRI French – Russian Meeting, «Catalytic transformation of biomass into valuable products», Strasbourg, France, 15-17.07.2015, oral presentation
6. M. Arapova, S. Pavlova, T. Larina, V. Rogov, T. Krieger, V. Sadykov, T. Glazneva, O. Smorygo, K. Parkhomenko, A.-C. Roger., «Hydrogen production via ethanol steam reforming over supported nikelates: from powders to structured catalysts», 12th European Congress on Catalysis – EuropaCat-XI, Kazan, Russia, 30 August – 4 September, 2015, poster
7. Arapova M.V., Pavlova S.N., Parkhomenko K.V., Glasneva T.S., Larina T.V., Rogov V.A., Krieger T.A., Sadykov V.A., Roger A.-C., «Hydrogen production via steam reforming of bio-oil's light components – ethanol and glycerol – over supported nickelates», 4th International School-Conference on Catalysis for Young Scientists "CATALYST DESIGN. From Molecular to Industrial level", 5-6 September, Kazan, Russia, oral presentation

8. Arapova M., Pavlova S., Parkhomenko K., Glasneva T., Larina T., Sadykov V., Roger A.-C., Smorygo O., “Steam reforming of ethanol and glycerol over functionally graded nickelate-based catalysts: from grain to structured catalysts”, FCCat, the 1st French Conference on Catalysis, 23-27 May, Frejus, France, poster
  9. M. Arapova, K. Parkhomenko, A.-C. Roger, S. Pavlova and V. Sadykov, “Perovskite-like nicketales for hydrogen production via sream reforming of oxygenates”, 2nd EFCATS-CNRS European Summer School on Catalyst Preparation: Fundamental Concepts and Industrial Requirements”, 12-17 June, Ardeche, France, poster
  10. Pavlova S., Arapova M., Alikina G., Rogov V., Krieger T., Sadykov V., Roger A.-C. Steam reforming of ethanol for hydrogen and syngas production over perovskite-type Ni(Co, Ru) ferrites as catalyst precursors // The Seventh Tokyo Conference on Advanced Catalytic Science and Technology (TOCAT7). – 2014. - Kyoto, Japan. – P. O-A22 (19).
- 

## **LISTE DES PUBLICATIONS**

1. Ni(Co)-Containing Catalysts Based on Perovskite-Like Ferrites for Steam Reforming of Ethanol, Arapova M. V., Pavlova S. N., Rogov V. A., Krieger T. A., Ishchenko A.V., Roger A.-C. // *Catalysis for Sustainable Energy*.-V.1.-2014.-P. 10-20. DOI: 10.2478/cse-2014-0002
2. Hydrogen and syngas production via ethanol steam reforming over supported nickelates, Arapova M. V., Pavlova S. N., Larina T. V., Glazneva T.S., Rogov V. A., Krieger T. A., Sadykov V. A., Smorygo O., Parkhomenko K., Roger A.-C. // *Materials and Technologies for Energy Efficiency* / Ed. A. Mendes-Vilas. - Boca Raton, USA: Brown Walker Press, 2015. - P. 131-135. ISBN 1627345590.
3. Perovskite-based Catalysts for Transformation of Natural Gas and Oxygenates into Syngas, Sadykov V. A., Pavlova S. N., Alikina G. M., Sazonova N. N., Mezentseva N. V., Arapova M. V., Rogov V. A., Krieger T. A., Ishchenko A. V., Gulyaev R. V., Zadesenets A. V., Roger A. C., Chan-Thaw C. E., Smorygo O. L. // *Perovskite: Crystallography, Chemistry and Catalytic Performance* / Eds.: J. Zhang, H. Li. – InTech.Nova Science publishers – 2013. – P. 1-58. ISBN 978-1-62417-800-9.
4. Mechanism of ethanol steam reforming over Pt/(Ni+Ru)-promoted oxides by FTIRS in situ, Sadykov V. A., Chub O., Chesalov Yu., Mezentseva N., Pavlova S. N., Arapova M. V., Rogov V.A., Simonov M.N., Roger A.-C., Parkhomenko K., Van Veen A. C. // *Topics in Catalysis*. V. – 59. 2016. – P. - 1332–1342. DOI: 10.1007/s11244-016-0659-y
5. Structured nanocomposite catalysts of biofuels transformation into syngas and hydrogen: Design and performance, Sadykov V., Mezentseva N., Simonov M., Smal E., Arapova M., Pavlova S., Fedorova Y., Chub O., Bobrova L., Kuzmin V., Ishchenko A., Krieger T., Roger A.-C., Parkhomenko K., Mirodatos C.,



Smorygo O., Ross J. // International Journal of Hydrogen Energy.– V. 40. – I. 24. -2015. – P. 7511-7522.  
DOI: 10.1016/j.ijhydene.2014.11.151

6. Structured Catalysts for Biofuels Transformation into Syngas with Active Components Based on Perovskite and Spinel Oxides Supported on Mg-Doped Alumina, Sadykov V., Pavlova S., Smal E., Arapova M., Simonov M., Mezentseva N., Rogov V., Glazneva T., Lukashevich A., Roger A-C., Parkhomenko K., van Veen A., Smorygo O // Catalysis Today. - V. 293-294. - 2017. - P. 176-185. DOI: 10.1016/j.cattod.2017.05.055

## ANNOTATION

This cotutelle PhD thesis investigation was carried out in the frames of the joint French-Russian PhD funding by French Embassy in Russia, the financial support was guaranteed by the “Metchnikov” stipend obtained in 2013. The research work was distributed between two scientific establishments: Boreskov Institute of Catalysis (BIC), Novosibirsk, Russia and ICPEES, UMR7515, University of Strasbourg, France. The work was divided between two institutions as follows: the catalysts’ synthesis, as well as catalytic tests in the steam reforming of ethanol reaction were carried out at the BIC, the characterization of the samples before and after tests was carried out in both institutes, and catalytic tests in the steam reforming of glycerol reaction were performed at the University of Strasbourg. The author directly participated in formulating of goals and tasks to be solved within the presented work, synthesized all the catalysts and performed catalytic experiments on steam and oxy-steam reforming of glycerol, processed and analyzed results of the experiments on steam reforming of ethanol; took part in processing and discussion of the data obtained by physical-chemical methods and performed necessary preparative and auxiliary operations; contributed to the preparation of papers, presented the obtained data at conferences, collected and analyzed literature data related to the subject of the study.

The thesis consists of an introduction, five chapters, conclusions and references. The work is set out on 144 pages, contains 9 tables, 59 figures and a list of literature used mentioning 273 items.

The *introduction* provides the justification of the relevance of the topic chosen; the goal, the tasks and the main steps of the work are also formulated.

The *first chapter*, which is a literature review, proves the prospects of the developments in the field of hydrogen and synthesis gas production from bio-renewable sources in accordance with the main problems of modern hydrogen energy. The processes of hydrogen and synthesis gas production from oxygenates, including steam reforming of ethanol and glycerol, are considered. The analysis of the existing data on the steam reforming reactions catalysts is carried out; oxides with the perovskites structure as precursor of stable processes’ catalysts are considered in details. Literature data on the development of structured catalysts, their application to bio-oils conversion reactions are analyzed.

The *second chapter* describes materials and synthesis methods used for the preparation of all catalysts’ families, as well as specification of the physicochemical methods used in the study, such as BET, XRD, TPR-H<sub>2</sub>, IRS ads. CO, UV-Vis, XPS, HR TEM, TPR-C<sub>2</sub>H<sub>5</sub>OH. Also, the chapter describes the conditions of catalytic tests in reactions of steam and oxy-steam reforming of ethanol and glycerol.

The *third chapter* is devoted to the study of catalysts based on substituted ferrites of rare-earth elements with a perovskite structure  $\text{LnFe}_{1-x-y}\text{M}_x\text{Ru}_y\text{O}_3$ , as well as comparison samples of

5% Ni(Co)/PrFeO<sub>3</sub>. The effects of the chemical composition and synthesis method on the structural and textural properties, as well as reducibility of initial samples are studied. Further, the chapter presents the results of catalytic tests in the reactions of ethanol and glycerol stream reforming using preliminarily activated perovskites. The activity, stability and dependence of these parameters on the composition and properties of precursors are analyzed; conclusions on the most suitable samples are drawn.

The *fourth chapter* is devoted to the investigation of the supported on magnesium-modified alumina catalysts  $m\text{LnNi}_{0.9}\text{Ru}_{0.1}\text{O}_3/n\text{Mg-}\gamma\text{-Al}_2\text{O}_3$ . Data on the study of the structural properties of supports and catalysts, aimed at revealing the influence of the magnesium introduction method, its content and the perovskite composition on the surface acidity, Ni state and the formation of the active phase of metallic nickel in the process of reduction treatment are established. The second section of the chapter contains the results of catalytic tests in the reactions of ethanol and glycerol stream reforming. The effect of the physical-chemical properties of the supported precursors on the stability and selectivity is investigated and discussed. Conclusions on the most suitable samples are made.

In the *fifth chapter* the results obtained for the structured catalytic systems [10%LaNi<sub>0.9</sub>Ru<sub>0.1</sub>O<sub>3</sub>/6%Mg- $\gamma$ -Al<sub>2</sub>O<sub>3</sub>/metal-ceramic foams] tested in a pilot reactor are shown. The activity and stability of the catalysts in conditions close to real industrial ones is demonstrated.

The *sixth chapter* concludes the overall results obtained. Based on this, the main fundamental regularities in the formation of active and stable to carbonization catalysts were proposed, depending on the parameters as composition, synthesis method that can be regulated during the design of the precursors.

The lists of figures, tables and contents, as well as abbreviations are given at the beginning of the manuscript. The literature used is listed in the end of the thesis.

## FIGURES LIST

Figure 1-1 World consumption and distribution of primary sources of energy (MTOE) in the period from 1971 to 2014 .....	5
Figure 1-2 The world distribution of hydrogen production processes in 2007.....	7
Figure 1-3 A solid oxide fuel cell system with external or internal reforming of biofuels.....	7
Figure 1-4 The temperature dependence of products concentration in ethanol steam reforming in thermodynamic equilibrium at a water/ethanol ratio (S/E) = 3 and 6 .....	14
Figure 1-5 Distribution of ethanol steam reforming products (a) and selectivity for hydrogen and carbon deposits (b) in thermodynamic equilibrium versus temperature and water/ethanol (S/E) ratio.....	15
Figure 1-6 A scheme of main transformations in steam reforming of glycerol.....	17
Figure 1-7 The distribution of selectivities for the reaction products of glycerol steam reforming in thermodynamic equilibrium versus temperature at the water to ethanol ratio of 3: $\diamond$ – H <sub>2</sub> , $\square$ – CO <sub>2</sub> , $\Delta$ – CO, $\times$ – CH <sub>4</sub> , $\circ$ – H <sub>2</sub> O.....	17
Figure 1-8 Distribution of the main reaction products H <sub>2</sub> , CO, CO <sub>2</sub> , CH <sub>4</sub> in steam reforming of glycerol in thermodynamic equilibrium: dependence on temperature and water/glycerol ratio.....	17
Figure 1-9 The polyhedral structure of the ideal perovskite ABO <sub>3</sub> . Red spheres correspond to oxygen atoms, yellow – to cations of sublattice A, and gray – to cations of sublattice B .....	25
Figure 1-10 The formation of the polymeric matrix including metal cation, citric acid and ethylene glycol during Pechini synthesis .....	28
Figure 2-1 A photo of the foam supports used for preparation of structured catalytic systems .....	33
Figure 2-2 A scheme of the setup for glycerol steam reforming .....	38
Figure 2-3 A scheme of the pilot unit reactor for reforming of oxygenates in concentrated mixtures...39	
Figure 3-1-1 X-ray diffraction patterns obtained for initial sample PrFeO <sub>3</sub> , calcined at 700 and 900 °C for 2θ a) 20-80° и б) 31-34°. The histogram corresponds to the phase PrFeO <sub>3</sub> [JCPDF 47-0065] .....	42
Figure 3-1-2 X-ray diffraction patterns obtained for LaFe <sub>0.7</sub> Ni <sub>0.3</sub> O <sub>3</sub> и PrFe <sub>0.7</sub> Ni <sub>0.3</sub> O <sub>3</sub> for 2θ a) 20-80° and b) 31-34° .....	43
Figure 3-1-3 X-ray diffraction patterns obtained for LnFe <sub>0.7</sub> Ni <sub>0.3</sub> (Ru <sub>0.1</sub> )O <sub>3</sub> : influence of the composition and doping metal amount (Ni, Co, Ru) for 2θ a) 20-80° and b) 31-34° .....	43
Figure 3-1-4 TEM micrographs and calculated from EDX microanalysis element's molar fractions (%) of PrFe <sub>0.7</sub> Ni <sub>0.3</sub> O <sub>3</sub> .....	44
Figure 3-1-5 X-ray diffraction patterns obtained for supported 5%Ni(Co)/PrFeO <sub>3</sub> <sup>[700]</sup> for 2θ a) 20-80° and b) 35-39°.....	45
Figure 3-1-6 TEM micrographs of 5%Ni/PrFeO <sub>3</sub> <sup>[700]</sup> (above) и 5%Ni/PrFeO <sub>3</sub> <sup>[900]</sup> (bottom) .....	46
Figure 3-1-7 TPR-H <sub>2</sub> spectra of LnFe <sub>1-x-y</sub> Ni <sub>x</sub> M <sub>y</sub> O <sub>3</sub> , calcined at 900 °C .....	47
Figure 3-1-8 X-ray diffraction patterns obtained for PrFe <sub>0.6</sub> Co <sub>0.4</sub> O <sub>3</sub> : (1) initial, reduced at (2) 600 and (3) 800 °C .....	48
Figure 3-1-9 a – X-ray diffraction patterns obtained for PrFe <sub>0.7</sub> Ni <sub>0.3</sub> O <sub>3</sub> : initial (1) and reduced at (2) 600 and (3) 800 °C. The histogram corresponds to the phase PrFeO <sub>3</sub> [JCPDF 47-0065], b – TEM micrograph of PrFe <sub>0.7</sub> Ni <sub>0.3</sub> O <sub>3</sub> after reduction at 800 °C .....	49
Figure 3-1-10 TPR-H <sub>2</sub> spectra of PrFeO <sub>3</sub> <sup>[700]</sup> and supported 5%Ni(Co)/PrFeO <sub>3</sub> .....	50
Figure 3-2-1 TPR-C <sub>2</sub> H <sub>5</sub> OH patterns of Ni-based perovskites: dependency of the H <sub>2</sub> , CO и CO <sub>2</sub> concentrations on temperature.....	52

Figure 3-2-2 TPO-H <sub>2</sub> O patterns of LaFe <sub>0.7</sub> Ni <sub>0.3</sub> O <sub>3</sub> after TPR-C <sub>2</sub> H <sub>5</sub> OH: dependency of the H <sub>2</sub> , CO и CO <sub>2</sub> concentrations on temperature .....	53
Figure 3-2-3 Ethanol conversion, hydrogen yield and products selectivity obtained for the blank experiment in the temperature range 650-825 °C.....	54
Figure 3-2-4 Temperature dependences of ethanol conversion, hydrogen yield, and selectivities for main products for Ni-containing catalysts in steam reforming of ethanol. Catalyst grain size 0.25-0.5 mm, contact time 0.07 s, H <sub>2</sub> O:EtOH = 4.....	55
Figure 3-2-5 Temperature dependences of ethanol conversion, hydrogen yield, and selectivities for main products for the catalysts with different active metal (Ni/Co) and synthesis method (massive/supported) in steam reforming of ethanol .....	57
Figure 3-2-6 Results of the long-term steam reforming of ethanol tests at 650 °C: a) ethanol conversion for the catalysts with different active metal (Ni/Co) and synthesis method (massive/supported); b) hydrogen yield and products selectivities for the PrFe <sub>0.6</sub> Ni <sub>0.3</sub> O <sub>3</sub> catalyst.....	58
Figure 3-2-7 TEM images with EDX data for PrFe <sub>0.7</sub> Ni <sub>0.3</sub> O <sub>3</sub> (top) and 5% Ni/PrFeO <sub>3</sub> <sup>[900]</sup> (bottom) samples after tests in ethanol steam reforming at 650 °C .....	59
Figure 3-2-8 TEM images with EDX data for a) PrFe <sub>0.6</sub> Ni <sub>0.3</sub> Ru <sub>0.1</sub> O <sub>3</sub> и б) 5% Ni/PrFeO <sub>3</sub> <sup>[700]</sup> after tests in ethanol steam reforming at 650 °C.....	59
Figure 3-2-9 Glycerol conversion to gas X <sub>g</sub> and productivities to the gaseous products P <sub>i</sub> in the blank experiment with the reactor filled with SiC (C <sub>3</sub> H <sub>8</sub> O <sub>3</sub> : H <sub>2</sub> O=1:9, GHSV=28000 h <sup>-1</sup> , T=650 °C) .....	60
Figure 3-2-10 a) Hydrogen productivity and glycerol conversion to gas products X <sub>g</sub> obtained for PrFe <sub>0.6</sub> Ni <sub>0.3</sub> Ru <sub>0.1</sub> O <sub>3</sub> reduced at 500 and 800 °C in GSR (C <sub>3</sub> H <sub>8</sub> O <sub>3</sub> : H <sub>2</sub> O = 1:9, GHSV = 28000 h <sup>-1</sup> , T=650 °C); б) XRD patterns of PrFe <sub>0.6</sub> Ni <sub>0.3</sub> Ru <sub>0.1</sub> O <sub>3</sub> : initial and after GSR reaction with different pretreatment.....	61
Figure 3-2-11 Glycerol conversion to gas X <sub>g</sub> and productivities to the gaseous products P <sub>i</sub> in the glycerol steam reforming reaction (C <sub>3</sub> H <sub>8</sub> O <sub>3</sub> : H <sub>2</sub> O=1:9, GHSV=28000 h <sup>-1</sup> , T=650 °C) obtained for PrFe <sub>0.7</sub> Ni <sub>0.3</sub> O <sub>3</sub> , PrFe <sub>0.6</sub> Ni <sub>0.3</sub> Ru <sub>0.1</sub> O <sub>3</sub> and La <sub>0.7</sub> Pr <sub>0.3</sub> Fe <sub>0.7</sub> Ni <sub>0.3</sub> O <sub>3</sub> samples .....	62
Figure 3-2-12 Glycerol conversion to gas X <sub>g</sub> and productivities to the gaseous products P <sub>i</sub> in the glycerol steam reforming reaction (C <sub>3</sub> H <sub>8</sub> O <sub>3</sub> : H <sub>2</sub> O=1:9, GHSV=28000 h <sup>-1</sup> , T=650 °C) obtained for PrFeO <sub>3</sub> , PrFe <sub>0.7</sub> Co <sub>0.3</sub> O <sub>3</sub> и PrFe <sub>0.7</sub> Ni <sub>0.3</sub> O <sub>3</sub> samples .....	63
Figure 3-2-13 Glycerol conversion to gas X <sub>g</sub> and productivities to the gaseous products P <sub>i</sub> obtained for PrFe <sub>0.7</sub> Ni <sub>0.3</sub> O <sub>3</sub> sample in glycerol steam reforming reaction (C <sub>3</sub> H <sub>8</sub> O <sub>3</sub> : H <sub>2</sub> O=1:9, GHSV=28000 h <sup>-1</sup> , T=650 °C) and glycerol oxy-steam reforming reaction (C <sub>3</sub> H <sub>8</sub> O <sub>3</sub> :H <sub>2</sub> O:O <sub>2</sub> = 1:9:0.25, GHSV=28000 h <sup>-1</sup> , T=650 °C) .....	64
Figure 3-2-14 TPO-O <sub>2</sub> data after reaction of GSR and GOSR for PrFe <sub>0.7</sub> Ni <sub>0.3</sub> O <sub>3</sub> and PrFe <sub>0.6</sub> Ni <sub>0.3</sub> Ru <sub>0.1</sub> O <sub>3</sub> catalysts .....	65
Figure 4-1-1 A scheme of the methods used to modify the support .....	69
Figure 4-1-2 a) X-ray diffraction patterns of nMg-γ-Al <sub>2</sub> O <sub>3</sub> supports synthesized by different methods; b) The dependence of the spinel lattice parameter on magnesium content and introduction method for n%Mg-γAl <sub>2</sub> O <sub>3</sub> supports .....	70
Figure 4-1-3 X-ray diffraction patterns of nMg-γ-Al <sub>2</sub> O <sub>3</sub> supports for 2θ a) 25-80° and b) 60-70° .....	72
Figure 4-1-4 X-ray diffraction patterns of 10% PrNi <sub>0.9</sub> Ru <sub>0.1</sub> O <sub>3</sub> / n% Mg-γ-Al <sub>2</sub> O <sub>3</sub> samples: 1) n = 6%, 2) n = 10% , and 3) n = 15% .....	73
Figure 4-1-5 TEM images and EDX spectra for the 20%PrNi <sub>0.9</sub> Ru <sub>0.1</sub> O <sub>3</sub> /[10%Mg-γ-Al <sub>2</sub> O <sub>3</sub> ] sample. Left – MgAl <sub>2</sub> O <sub>4</sub> spinel, right – Pr <sub>2</sub> Ni <sub>1-x</sub> Ru <sub>x</sub> O <sub>4</sub> perovskite .....	74

Figure 4-1-6 UV-Vis spectra for 10%PrNi <sub>0.9</sub> Ru <sub>0.1</sub> O <sub>3</sub> /n%Mg-γ-Al <sub>2</sub> O <sub>3</sub> catalysts: 1) 6% Mg, 2) 10% Mg, and 3) 15% Mg.....	75
Figure 4-1-7 Ni <sup>2p</sup> XPS spectra of 10%PrRuNi/6%Mg-γAl <sub>2</sub> O <sub>3</sub> (bottom) and 10%PrRuNi/10%Mg-γAl <sub>2</sub> O <sub>3</sub> .....	76
Figure 4-1-8 Data on IR spectroscopy of CO adsorbed for 6%Mg-γ-Al <sub>2</sub> O <sub>3</sub> and 10%Mg-γ- Al <sub>2</sub> O <sub>3</sub> supports after pretreatment in hydrogen: a)IR spectra of CO adsorbed at 77 K and CO pressure of 0.1 – 10 Torr; b) The difference IR spectrum of CO adsorbed at 77 K and CO pressure of 10 Torr .	77
Figure 4-1-9 Data on IR adsorption of CO for 10%PrNi <sub>0.9</sub> Ru <sub>0.1</sub> O <sub>3</sub> /[6%Mg-γ-Al <sub>2</sub> O <sub>3</sub> ] and 10%PrNi <sub>0.9</sub> Ru <sub>0.1</sub> O <sub>3</sub> /[10%Mg-γ-Al <sub>2</sub> O <sub>3</sub> ] catalysts after pretreatment in hydrogen: a) IR spectra of CO adsorbed at 77 K and CO pressure of 0.1 – 10 Torr; b) The difference IR spectrum of CO adsorbed at 77 K and CO pressure of 10 Torr.....	78
Figure 4-1-10 TPR-H <sub>2</sub> spectra for LnNi <sub>0.9</sub> Ru <sub>0.1</sub> O <sub>3</sub> /0-15%Mg-γAl <sub>2</sub> O <sub>3</sub> samples.....	80
Figure 4-1-11 TPR-H <sub>2</sub> spectra for mPrNi <sub>0.9</sub> Ru <sub>0.1</sub> O <sub>3</sub> /n%Mg-γ-Al <sub>2</sub> O <sub>3</sub> samples: the effect of m - percentage of the perovskite supported samples .....	81
Figure 4-2-1 The effect of Mg concentration and its introduction method on the activity and selectivity of LaNi <sub>0.9</sub> Ru <sub>0.1</sub> O <sub>3</sub> /6-10%Mg-γAl <sub>2</sub> O <sub>3</sub> catalysts in steam reforming of ethanol. Catalyst grain size 0.25-0.5 mm, contact time 0.07 s, H <sub>2</sub> O:EtOH = 4 .....	83
Figure 4-2-2 Temperature dependences of ethanol conversion, hydrogen yield, and selectivities for CO and C <sub>2</sub> H <sub>4</sub> for praseodymium-containing catalysts with different magnesium content. Catalyst grain size 0.25-0.5 mm, contact time 0.07 s, H <sub>2</sub> O:EtOH = 4 .....	84
Figure 4-3-1 Glycerol conversion to gas X <sub>g</sub> and productivities to the gaseous products P <sub>i</sub> for the 10%LaNi <sub>0.9</sub> Ru <sub>0.1</sub> O <sub>3</sub> /[6%Mg-γ-Al <sub>2</sub> O <sub>3</sub> <sup>D</sup> ] sample in a) GSR (C <sub>3</sub> H <sub>8</sub> O <sub>3</sub> : H <sub>2</sub> O=1:9, GHSV=28000 h <sup>-1</sup> , T=650 °C) and b) GOSR (C <sub>3</sub> H <sub>8</sub> O <sub>3</sub> :H <sub>2</sub> O:O <sub>2</sub> = 1:9:0.25, GHSV=28000 h <sup>-1</sup> , T=650 °C) reactions .....	87
Figure 4-3-2 Glycerol conversion to gas X <sub>g</sub> and productivities to the gaseous products P <sub>i</sub> in the glycerol steam reforming reaction (C <sub>3</sub> H <sub>8</sub> O <sub>3</sub> : H <sub>2</sub> O=1:9, GHSV=28000 h <sup>-1</sup> , T=650 °C) obtained for 10%PrNi <sub>0.9</sub> Ru <sub>0.1</sub> O <sub>3</sub> /[n%Mg-γ-Al <sub>2</sub> O <sub>3</sub> ] samples with different magnesium content in the support .....	88
Figure 4-3-3 Glycerol conversion to gas X <sub>g</sub> and H <sub>2</sub> productivity in the glycerol steam reforming reaction (C <sub>3</sub> H <sub>8</sub> O <sub>3</sub> : H <sub>2</sub> O=1:9, GHSV=28000 h <sup>-1</sup> , T=650 °C) obtained for 10%LnNi <sub>0.9</sub> Ru <sub>0.1</sub> O <sub>3</sub> /[n%Mg-γ-Al <sub>2</sub> O <sub>3</sub> ] (Ln = La, Pr) samples with different Ln cation .....	89
Figure 4-3-4 Glycerol conversion to gas X <sub>g</sub> and H <sub>2</sub> productivity in the glycerol steam reforming reaction (C <sub>3</sub> H <sub>8</sub> O <sub>3</sub> : H <sub>2</sub> O=1:9, GHSV=28000 h <sup>-1</sup> , T=650 °C) obtained for samples with different perovskites amount .....	90
Figure 4-3-5 Glycerol conversion to gas X <sub>g</sub> and productivities to the gaseous products P <sub>i</sub> for the 10%PrNi <sub>0.9</sub> Ru <sub>0.1</sub> O <sub>3</sub> /[15%Mg-γ-Al <sub>2</sub> O <sub>3</sub> ] sample in a) GSR (C <sub>3</sub> H <sub>8</sub> O <sub>3</sub> : H <sub>2</sub> O=1:9, GHSV=28000 h <sup>-1</sup> , T=650 °C) and b) GOSR (C <sub>3</sub> H <sub>8</sub> O <sub>3</sub> :H <sub>2</sub> O:O <sub>2</sub> = 1:9:0.25, GHSV=28000 h <sup>-1</sup> , T=650 °C) reactions .....	90
Figure 5-1 a - The photography of Ni-Al foam, b - SEM pictures with EDX analysis of the wall section: as prepared (top) and calcined at 900°C (bottom)	
Figure 5-2 a – H <sub>2</sub> and CO concentrations in the EOSR products for the 10%LaNi <sub>0.9</sub> Ru <sub>0.1</sub> O <sub>3</sub> /6%Mg-γ-Al <sub>2</sub> O <sub>3</sub> catalyst supported on (I) Ni-Al, (II) SiC/Al-Si-O and (III) corundum/Al-Si-O foam supports. b – H <sub>2</sub> and CO concentrations in the reaction products during stability testing performed consecutively for EOSR and ESR reactions using the 10%LaNi <sub>0.9</sub> Ru <sub>0.1</sub> O <sub>3</sub> /6%Mg-γ-Al <sub>2</sub> O <sub>3</sub> catalyst with the Ni-Al foam support.....	93
Figure 5-3 SEM pictures of the structured catalysts based on 10%LaNi <sub>0.9</sub> Ru <sub>0.1</sub> O <sub>3</sub> /6%Mg-γ-Al <sub>2</sub> O <sub>3</sub> supported on (I) Ni-Al, (II) SiC/Al-Si-O and (III) α-Al <sub>2</sub> O <sub>3</sub> /Al-Si-O foam supports after EOSR reaction	

## TABLES LIST

Table 1-1 Reactions accompanying steam reforming of ethanol.....	13
Table 2-1 Reagents used to synthesize catalysts for the study.....	31
Table 3-1 Synthesized compositions, their some physical and chemical properties and values of the tolerance factor t.....	41
Table 4-1-1 Synthesis method, specific surface area and spinel lattice parameter of supports n%Mg- $\gamma$ -Al <sub>2</sub> O <sub>3</sub> and catalysts based on it.....	68
Table 4-1-2 Surface composition of 6%Mg- $\gamma$ -Al <sub>2</sub> O <sub>3</sub> and 6%Mg- $\gamma$ -Al <sub>2</sub> O <sub>3</sub> <sup>D</sup> supports revealed by XPS.....	70
Table 4-1-3 Surface composition of some supports and 10%LnNi <sub>0.9</sub> Ru <sub>0.1</sub> O <sub>3</sub> /6-10%Mg- $\gamma$ -Al <sub>2</sub> O <sub>3</sub> catalysts.....	76
Table 4-1-4 Position, shift and proton affinity (PA) of a.b. for CO complexes adsorbed on OH groups.....	79
Table 4-2 Selectivity for C <sub>2</sub> H <sub>4</sub> and proton affinity (PA) (from IR data about CO adsorption* on hydroxyl groups – a.b. 3730 cm <sup>-1</sup> ) versus magnesium content for catalysts 10%PrNi <sub>0.9</sub> Ru <sub>0.1</sub> O <sub>3</sub> /n%Mg- $\gamma$ -Al <sub>2</sub> O <sub>3</sub> , n = 6, 10.....	85
Table 5-1 Main characteristics of structured substrates.....	92

## LIST OF CONTENTS

Abbreviations .....	1
Introduction .....	2
<b>CHAPTER 1. LITERATURE REVIEW .....</b>	<b>5</b>
1.1. Hydrogen energy and fuel cells.....	6
1.2. Liquid products from biomass processing: bio-oil, ethanol and glycerol.....	8
1.3. Hydrogen production from oxygenates.....	9
1.3.1. Steam reforming of oxygenates.....	11
1.3.1.1. Steam reforming of ethanol.....	13
1.3.1.2. Steam reforming of glycerol .....	16
1.3.2. Coke formation in steam reforming as the main route of catalyst's deactivation .....	19
1.4. Catalysts for steam reforming of oxygenates.....	20
1.4.1. Activity of metals of different nature in catalysts for steam reforming .....	20
1.4.2. The size effect and approaches to enhancing the stability of nickel-containing catalysts .....	21
1.4.3. The effect of support properties on activity and selectivity of nickel-containing catalysts .....	23
1.5. Mixed oxides with the perovskite structure .....	25
1.5.1. Structural features.....	25
1.5.2. Perovskites as the precursors of catalysts for fuel reforming .....	26
1.5.3. Methods for the perovskites synthesis .....	28
1.6. Structured catalysts: supports and additional requirements .....	29
1.7. Conclusion to the literature review, the goals of the thesis .....	30
<b>CHAPTER 2. EXPERIMENTAL TECHNIQUES.....</b>	<b>31</b>
2.1. Materials preparation.....	31
2.1.1. Reagents and materials .....	31
2.1.2. Synthesis of lanthanide ferrites $\text{LnFe}_{1-x-y}\text{M}_x\text{Ru}_y\text{O}_3$ and 5% M/PrFeO <sub>3</sub> .....	31
2.1.3. Synthesis of supported $\text{mLnNi}_{0.9}\text{Ru}_{0.1}\text{O}_3/\text{n}\% \text{Mg-}\gamma\text{-Al}_2\text{O}_3$ samples .....	32
2.1.4. Synthesis of structured catalysts.....	33
2.2. Materials characterization .....	34
2.2.1. Specific surface area measurements .....	34
2.2.2. X-ray diffraction analysis (XRD).....	34
2.2.3. Temperature-programmed reduction with hydrogen (TPR-H <sub>2</sub> ) .....	34
2.2.4. Infrared spectroscopy of adsorbed CO (IRS ads. CO) .....	34
2.2.5. Diffuse reflectance electron spectroscopy (UV-Vis).....	35
2.2.6. X-ray photoelectron spectroscopy (XPS).....	35
2.2.7. High resolution transmission electron microscopy (HRTEM).....	36
2.2.8. Temperature-programmed reduction with ethanol (TPR-C <sub>2</sub> H <sub>5</sub> OH).....	36
2.3. Catalytic tests .....	37
2.3.1. Catalytic tests in steam reforming of ethanol .....	37
2.3.2. Catalytic tests in steam/steam-oxygen reforming of glycerol .....	37
2.3.3. Catalytic tests in ethanol steam reforming on the structured support in a pilot reactor .....	38



<b>CHAPTER 3. MASSIVE CATALYSTS' FAMILY <math>\text{LnFe}_{1-x-y}\text{M}_x\text{Ru}_y\text{O}_3</math> (Ln = Pr, La, M= Ni, Co, x = 0.3; 0.4 y = 0; 0.1): PHYSICOCHEMICAL PROPERTIES AND CATALYTIC ACTIVITY IN STEAM REFORMING OF ETHANOL AND STEAM/OXY-STEAM REFORMING OF GLYCEROL</b> .....	40
3.1. Structural and textural properties of initial perovskites .....	40
3.1.1. Effect of the chemical composition and synthesis method on the structural and textural properties of initial samples.....	41
3.1.2. Effect of the chemical composition and synthesis method on the formation of the catalyst active phase upon reduction of perovskite precursors.....	46
3.1.3. Conclusion to Section 3.1 .....	51
3.2. Study of the catalytic activity in steam reforming of oxygenates .....	52
3.2.1. Temperature-programmed reduction with ethanol (TPR- $\text{C}_2\text{H}_5\text{OH}$ ).....	52
3.2.2. Catalytic activity in steam reforming of ethanol .....	54
3.2.3. Effect of the perovskite composition and method of the active phase formation on catalyst stability in steam reforming of ethanol.....	58
3.2.4. Catalytic activity in steam/oxy-steam reforming of glycerol .....	60
3.2.5 Conclusion to Section 3.2 .....	66
<b>CHAPTER 4. SUPPORTED CATALYSTS' FAMILY <math>m\text{Ln}(\text{Fe})_x\text{Ni}_{0.9-x}\text{Ru}_{0.1}\text{O}_3/n\%\text{Mg-}\gamma\text{-Al}_2\text{O}_3</math>: PHYSICOCHEMICAL PROPERTIES AND CATALYTIC ACTIVITY IN STEAM REFORMING OF ETHANOL AND STEAM/OXY-STEAM REFORMING OF GLYCEROL</b> .....	67
4.1. Structural and textural properties of initial oxides .....	68
4.1.1. Effect of magnesium content and its introduction method on the support properties.....	69
4.1.2. Effect of magnesium content on the state of nickel in precursors and activated catalysts.....	72
4.1.3. Effect of magnesium content on the surface composition of initial catalysts. ....	75
4.1.4. Effect of magnesium content on the surface acidity of the support and catalysts.....	77
4.1.5. Effect of magnesium content and its introduction method on the ability to reduce nickel from catalyst precursors.....	79
4.1.6. Conclusion to Section 4.1 .....	82
4.2. Catalytic activity in steam reforming of ethanol.....	83
4.3. Catalytic activity in steam/oxy-steam reforming of glycerol.....	87
4.4. Conclusion to Chapter 4 .....	91
<b>CHAPTER 5. STRUCTURED CATALYTIC <math>\text{LnNi}_{0.9}\text{Ru}_{0.1}\text{O}_3/n\text{Mg-}\gamma\text{-Al}_2\text{O}_3</math> SYSTEMS DEPOSITED ON DIFFERENT FOAM SUPPORTS: ASSESSMENT OF CATALYTIC PROPERTIES AND STABILITY IN STEAM AND OXY-STEAM REFORMING OF ETHANOL IN CONCENTRATED MIXTURES</b> .....	92
5.1. Structural and textural properties of initial supports and catalysts .....	92
5.2. Catalytic activity in steam/oxy-steam reforming of ethanol .....	92
<b>CHAPTER 6. MAIN CONCLUSIONS</b> .....	94
List of publications on the subject of the dissertation.....	98
References .....	99

## Abbreviations

BET method – the Brunauer-Emmett-Teller method for estimating specific surface area

Bio-oil or pyrolysis oil – liquid products from fast pyrolysis of biomass

ESR – ethanol steam reforming

GSR – glycerol steam reforming

GOSR – glycerol oxy-steam reforming

HR TEM – high resolution transmission electron microscopy

IRS ads. CO – infrared spectroscopy of adsorbed CO

MT-SOFC – medium-temperature solid oxide fuel cells

PA – proton affinity

RSE – renewable sources of energy

SEM - scanning electron microscope

SR – steam reforming

TPR – temperature-programmed reduction

UV-Vis – diffuse reflectance electron spectroscopy

XPS – X-ray photoelectron spectroscopy

XRD – X-ray diffraction analysis

## Introduction

**Relevance.** The growing demand for energy along with global warming, climate change, and the need for harmonious exploitation of natural resources determine the world's interest in renewable sources of energy. To ease the dependence on mineral resources, such as coal, oil and gas, and to improve the environmental situation in the world, it is necessary to search for new highly efficient processes based on alternative sources of energy. Biomass, being a renewable and CO<sub>2</sub>-neutral feedstock, is not only the object of many research works but in some countries replaces, to a large extent, the conventional fossil sources of energy. One of the most promising methods for transformation of biomass to fuel and energy is now the catalytic steam reforming of liquid products from processing of biomass, the so-called bio-oil, to hydrogen and syngas. Hydrogen is known to be the most environmentally friendly fuel for various energy and heat generators (fuel cells, internal combustion engines, mobile power plants), whereas bio-syngas can serve as a feedstock for the synthesis of various chemical products and liquid fuel in the Fischer–Tropsch process. However, the wide application of this technology is hindered by the drawbacks of available catalysts: despite the intensive studies, the main problem related to low stability of the known catalysts due to coking remains unresolved.

It is known that the most active and inexpensive nickel-containing catalysts with conventional supports having a high surface area (alumina, aluminosilicates, etc.) rapidly deactivate due to sintering of nickel and coking, which is promoted by acid sites on the support surface. The application of basic oxides (MgO, La<sub>2</sub>O<sub>3</sub>) as the supports enhances stability of the catalysts; however, they possess a relatively low activity due to small surface area. The use of nickel-doped mixed oxides of rare-earth elements with the perovskite structure as the catalyst precursors makes it possible to obtain highly active coke-resistant catalysts. This occurs because a highly disperse metallic nickel strongly bound to the oxide matrix is formed in the reducing reaction medium, and coke precursors are oxidized by oxygen of the highly mobile oxide. Perovskites as the catalyst precursors were studied mostly in numerous works devoted to methane reforming but were not well studied in steam reforming of oxygen-containing hydrocarbons. In spite of high activity and stability, the low specific surface area of perovskites and the high cost of rare-earth elements limit their practical application. Thus, stable inexpensive catalysts for transformation of biofuels to syngas and hydrogen have not been devised as yet.

A promising approach to enhancing the activity and stability of steam reforming catalysts consists in depositing the layers of nickel-containing mixed oxides with the perovskite structure onto supports possessing high specific surface area and basic properties. Such catalysts are highly active and resistant to coking due to high surface area and thermal stability of disperse nickel

particles and owing to a decreased acidity of the support and high mobility and reactivity of oxygen from the mixed oxide. It is known also that nickel alloys with cobalt, ruthenium or iron are more resistant to coking due to dilution of nickel ensembles.

Bio-oil is a mixture of oxygen-containing hydrocarbons, such as alcohols, acids, aldehydes, ketones, etc. Fundamental studies aimed to reveal a relationship between catalyst properties and its activity and stability in steam reforming of bio-oil are commonly performed using model compounds of bio-oil, for example, ethanol and glycerol. Also, reforming of bio-oil is carried out at short contact times in the presence of structured catalysts deposited on heat-conducting supports provides a high yield of hydrogen and syngas, which is very important for practical applications.

**The goal of this work** was the development of active and coke-resistant catalysts with nickel-containing mixed oxides as the precursors for steam and steam-oxygen reforming of ethanol and glycerol, which are the model components of bio-oils.

Within the goal, the following **tasks** were formulated:

1. Synthesis of *bulk* and *supported* on magnesium-doped alumina *Ni-, Co-, and Ru-containing catalysts* based on mixed oxides of rare-earth metals with the perovskite structure using various methods.

2. Investigation of the chemical composition effect and the synthesis method on the structural, textural and redox properties of the oxide precursors and their relations with the activity and the stability of the corresponding catalysts in steam reforming of ethanol (ESR) as well as in steam (GSR) and oxy-steam (GOSR) reforming of glycerol.

3. Synthesis and study of structured catalysts based on  $\text{LnNi}_{0.9}\text{Ru}_{0.1}\text{O}_3/n\text{Mg-}\gamma\text{-Al}_2\text{O}_3$  deposited on different porous foam supports, estimation of their activity and stability in steam and steam-oxygen reforming of ethanol in concentrated mixtures.

Thereby, three catalysts family were chosen:

1. Massive perovskite-like  $\text{LnFe}_{1-x-y}\text{Ni}_y\text{M}_x\text{O}_{3-\delta}$  (Ln=La, Pr; B=Co, Mn, Ru;  $x=0\div 0.4$ ,  $y=0\div 0.4$ )
2. Supported perovskite-like  $m\text{LnNi}_{0.9}\text{Ru}_{0.1}\text{O}_3/n\text{Mg-}\gamma\text{-Al}_2\text{O}_3$  (Ln = La, Pr,  $m=10\text{-}20\%$  wt,  $n=6\text{-}15\%$  wt)
3. Structured catalyst based on  $m\text{LnNi}_{0.9}\text{Ru}_{0.1}\text{O}_3/n\text{Mg-}\gamma\text{-Al}_2\text{O}_3$  supported on metallic and ceramic foams specialized for SOFC conditions

Thus, the global scheme of the work can be represented as follows:

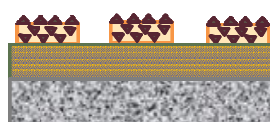
**1. Ni, Fe-containing perovskites**



**2. Ni-containing perovskites/high SSA basic oxides**



**3. Structured Ni-containing perovskites/high SSA supports**



- ✓ High active
- ✗ Low SSA
- ✓ Strong Me-S interaction

- ✓ High active
- ✓ High SSA
- ✓ Strong Me-S interaction
- ✓ Stable

- ✓ High active
- ✓ High SSA
- ✓ Stable
- ✓ Scalable

## CHAPTER 1. LITERATURE REVIEW

The 21<sup>st</sup> century is characterized by high rates of industrial intensification, growth of population and the living standards. The dynamic development of civilization increases demand for energy in all spheres of industry, transport and dwelling complexes. According to data provided by the International Energy Agency, the world consumption of energy resources increased by a factor of 1.5 from 1970 to 2008, and in 2030 the expected world demand for energy resources will increase by 65-70% as compared to the level reached in 2007 (Figure 1.1) [1, 2].

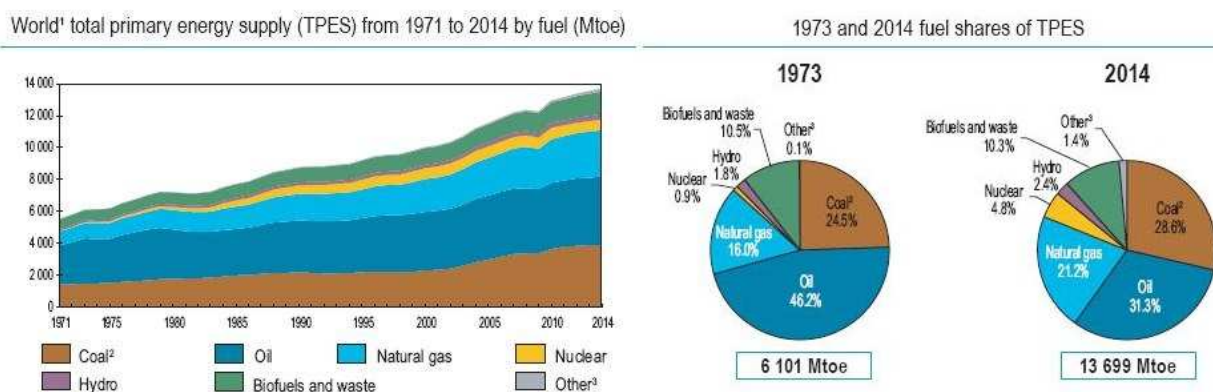


**Figure 1.1.** World consumption and distribution of primary sources of energy (MTOE) in the period from 1971 to 2014

As it shown on the diagram (Figure 1.1), 85% of the world energy demands in 2014 were satisfied by fossil feedstocks (oil, gas and coal) [3]. The depletion of fossil resources is a matter of great concern nowadays. Moreover, as the most accessible deposits are being developed, handling of less energy density and more hard-to-get types of feedstock will increase the cost of production and processing of such energy carriers. Therewith, a great problem is the detrimental effect from processing of fossil sources, which are the main cause of environmental contamination and a growing concentration of greenhouse gases in the atmosphere. In this situation, the only way for **sustainable development of the world power industry** is a transformation of existing technologies the way the production and consumption of energy will not be accompanied by a growing deficit of non-renewable natural resources and will not lead to destructive environmental processes. This includes the development of advanced efficient technologies for the production of electric and thermal energy and a gradual transition from conventional fuel to alternative renewable sources of energy (ARSE), which is being implemented now. In 2008, renewable sources of energy constituted ca. 19% of the world consumption of primary sources of energy, with biofuels produced from biomass, solar and wind energies being its main segments [2, 4].

**Biomass**, as a renewable CO<sub>2</sub>-neutral resource, is not only the subject of comprehensive research but is already used in some countries to replace a considerable fraction of conventional fossil feedstock [5, 6]. The use of biomass preserves natural resources, radically solves the problem of CO<sub>2</sub> greenhouse gas emission, decreases contamination of the atmosphere with waste SO<sub>2</sub>, NO<sub>x</sub> and ash, and reduces the cost of the produced energy [7, 8]. In 2014, first and second generation fuels obtained from biomass satisfied 14% of the world demand for energy [9]. Russia, taking a leading place in the world with respect to renewable energy resources, both vegetable and other types, only starts to develop its biofuel industry [10, 34]. The main cause is a relatively low cost of conventional energy resources and large oil and gas supplies. According to the RF President Decree No. 889 of June 4, 2008 “Some measures for enhancing energy and environmental efficiency of the RF economics”, the increase in power efficiency and the development of renewable sources of energy (RSE) for reducing energy intensity of the RF gross national product by at least 40% in comparison with the level of year 2007 are the strategic priorities of the Russian Federation [11].

In recent years, **hydrogen energy** was considered as a promising approach to solving the environmental problems of energy production. A particular interest in hydrogen as a fuel is caused by a rapid progress in the development of fuel cell technology [12]. At present, hydrogen energy is at the implementation step of development and its future directly depends on the efficiency of solving the problems of hydrogen production and application; so, studies in this field are carried out in all the developed countries of the world [13, 14].

### **1.1. Hydrogen energy and fuel cells**

Hydrogen energy complies with all the requirements of “Green energy of the future”. Hydrogen as a fuel stands out among conventional energy carriers due to its high energy capacity and absolutely environmental combustion [15, 16]. In addition, advanced technologies of its conversion to energy (like fuel cells) increase an energy efficiency of the process in comparison with the existing outdated combustion engine technologies [17]. It should be noted that the pure form of hydrogen does not occur in the nature in sufficient amounts, so hydrogen is not a resource but rather a secondary fuel, which should be produced.

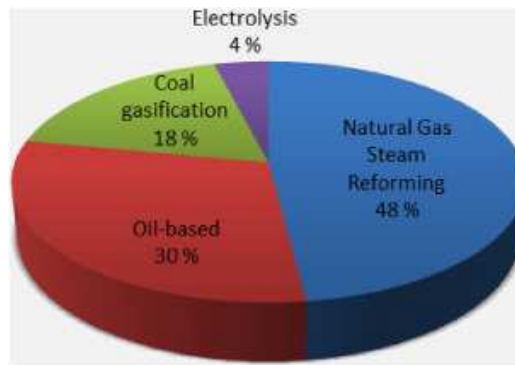


**Figure 1.2.** The world distribution of hydrogen production processes in 2007

A rapid development of hydrogen energy engineering is hindered by the absence of a developed infrastructure as well as by the high cost and environmental unfriendliness of the implemented methods of hydrogen production. Nowadays, 96 % of all hydrogen is produced industrially from fossil sources (Figure 1.2) [18].

Thus, the hydrogen produced is employed now only in the industries that cannot operate without it – the production of ammonia as well as oil and food industries. The development of methods for hydrogen production from eco-friendly and inexpensive sources will radically change the situation in this field and is the key strategic vector of studies in the world [13].

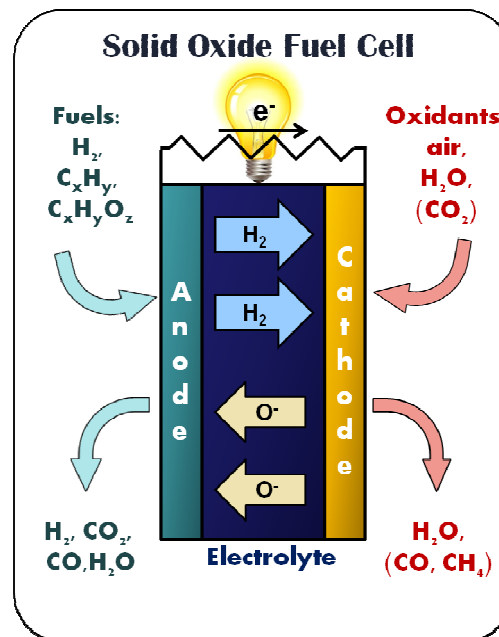


**Figure 1.3.** A solid oxide fuel cell system with external or internal reforming of biofuels

A promising direction of research and development is the creation of power plants – electrochemical generators – based on fuel cells with the use of inexpensive renewable resource –



bio-oil [19]. The technology is based on fuel to syngas conversion, which occurs in the external fuel processor over structured monolithic catalysts [20, 21], or in the case of solid oxide fuel cell with the internal reformer, directly at the fuel cell anode with simultaneous generation of electricity [22, 23, 24] (Figure 1.3).

Fuel cell power plants become very promising due to their compactness, high efficiency, the absence of moving and rubbing parts, silent operation, and absence of harmful wastes [25]. Along with the production of electric energy by stationary plants, such devices can form a basis for a new generation of vehicle engines [26, 27]. Thus, the application of renewable biofeedstocks for hydrogen production, especially using a highly efficient fuel cell technology with internal or external reformer of fuels, is the most important and promising field of green energy engineering combining high eco-friendliness and energy efficiency [28, 29].

## **1.2. Liquid products from biomass processing: bio-oil, ethanol and glycerol**

For today, there are a dozens of biomass processing methods, which allows one to obtain three main types of raw materials: solid, gaseous and liquid fuels, which composition could be varying by the treatment conditions depends on the requirements. The production of hydrogen and syngas from biomass can be performed both directly via gasification processes [30, 31] and consecutively via the “biomass → liquid biofuel → hydrogen/syngas” transformation. The second route is more energy advantageous and reduces the cost of the initial feedstock storage and transportation [32]. The composition and properties of liquid products from biomass processing depend on the valorization methods and conditions. One of the most promising biofuel is bio-oil obtained by fast pyrolysis of biomass. Main parameters of the fast pyrolysis include a moderate temperature (450-650°C), high heating rate (103-105 °C/s), short contact time (< 2 s), and sharp cooling of pyrolytic vapor to suppress secondary reactions [33]. In such a process, the yield of liquid products attains 75%, and composition of the resulting bio-oil varies in dependence on the feedstock and process conditions. A typical bio-oil is a dark-brown liquid comprising a substantial amount of water (from 15% to 35%) and a wide set of organic compounds: acids, alcohols, ketones, aldehydes, phenols, esters, sugars, and aromatic hydrocarbons [34]. However, the direct use of bio-oil is hindered primarily by its instability in storage and high corrosive ability [35].

Ethanol and glycerol are oxygenates often considered as the model components of bio-oil; moreover, both compounds are the most abundant biofuels that are annually produced on industrial scale. In 2014, bio-ethanol and bio-diesel constituted about 90% of the world consumption of biofuel [36, 37].

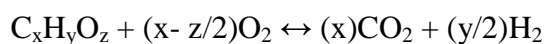
Ethanol is produced mostly by fermentation of sugar cane, corn and other vegetable cultures with a high starch content, which are successfully cultivated for this purpose in Brazil, Africa, and southern regions of Russia [38]. Recent studies were aimed to produce bio-ethanol from lignocellulosic biomass (the so-called second generation bio-ethanol). This technology will make it possible to use various low-cost types of biomass as a feedstock, for example, agricultural and woodworking wastes; as a result, the production of ethanol as a fuel will not compete for resources with food industry [39]. Ethanol has some essential advantages: due to low toxicity and volatility, it is convenient for storage, transportation and use. In 2008, the ethanol output from edible raw materials in Russia was ca. 1.5 billion liters, and its annual consumption was 0.7-0.8 billion liters, 80% of which was used for the production of alcoholic beverages [10].

Glycerol is the main by-product of transesterification reaction in the production of bio-diesel and constitutes 10 wt% of the resulting target fuel [40, 41]. In 2009, the world output of bio-diesel reached 16.6 billion liters. The use of glycerol for hydrogen production is attractive not only in terms of renewability but also because this will substantially reduce the cost of bio-diesel and make it competitive at the market of modern fuels [42].

### 1.3. Hydrogen production from oxygenates

Various technologies are employed to produce hydrogen from liquid biofuels [43, 44, 45]; of special interest are partial oxidation, steam and autothermal reforming [46, 47, 48, 49].

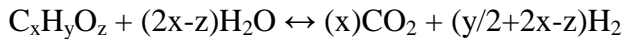
Partial oxidation of oxygenates is an exothermic process with general equation is written as



The reaction is initiated by oxygenate combustion at relatively low temperatures and does not require an additional heat supply until a steady state is established [50]. Cost-effectiveness of the process is provided also by the use of air oxygen as the oxidant. The process is characterized by low yields of by-products, including methane and carbon monoxide, which is very important for the units that feed fuel cells, because carbon monoxide is a poison for them. Partial oxidation units are relatively compact, mobile and have a fast start, so they are convenient for use, for example, in hybrid engines [26]. The main drawback of partial oxidation in comparison with all existing methods is the lowest yield of hydrogen even at the optimal C/O ratio and temperature [47]. In addition, the formation of hot spots in the catalyst is reported often as a cause of its sintering and deactivation [51].

A high yield of hydrogen is a typical characteristic of the **steam reforming reaction**. Thus, over 90% of industrial hydrogen is produced by steam reforming of hydrocarbons, mostly natural gas [14].

Steam reforming of oxygenates [52] is described by the equation:



In this reaction water serves as an oxidant. It is a huge advantage in case of reforming of oxygenates derived from biomass: expensive preliminary separation of the aqueous fraction whose content in biofuel can reach 35% limiting its application, for example, in internal combustion engines [52].

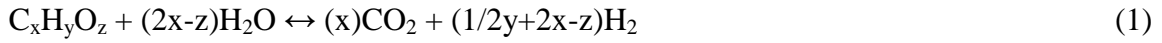
However, the process has some essential drawbacks. First of all, high endothermicity consumes much energy for maintaining a high (600-800°C) temperature. Another problem is the complexity of the process itself, which can be accompanied, depending on the process conditions and catalyst, by parallel or consecutive side reactions that decrease the yield of hydrogen and syngas and contaminate them with by-products [45]. In addition, the reaction is thermodynamically limited, so in practice the real yield of products is always lower than the theoretical value [49]. And finally, the existing steam reforming catalysts demonstrate insufficient stability due to their strong coking, and attempts to improve their stability lead to a decrease in selectivity or an increase in their cost [53].

To diminish carbon deposits, oxygen is introduced in the reaction mixture used for steam reforming and this process is known as oxy-steam reforming. For each individual oxygenate it could be calculated the O<sub>2</sub>/H<sub>2</sub>O ratio when the sum of all thermal effects of exo- and endothermic reactions is close to zero [54, 46]. Such a process is called autothermal [55, 56], and its main advantage is a substantial decrease in the coke amount and energy consumption in comparison with the steam reforming process [57]. Selectivity for hydrogen depends on the oxygen concentration in the mixture.

Some technologies allow enhancing the efficiency of the above listed processes, for example, the recovery of CO<sub>2</sub> or hydrogen directly from the reaction mixture or at the reactor outlet. In such cases, the yield of hydrogen can be as high as 99% [58, 59]. However, this step will be reasonable only after optimization of the catalyst's activity and stability those are the key parameters of efficient implementation of the process.

### 1.3.1. Steam reforming of oxygenates

Steam reforming of oxygenates is described by the overall equation:



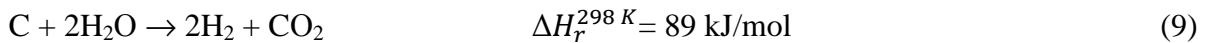
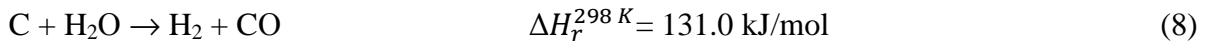
This is an endothermic process that runs at high ( $\geq 500^\circ\text{C}$ ) temperatures and atmospheric pressure, and is irreversible for the majority of reagents and catalysts under the indicated conditions. The steam reforming process is complicated by the presence of competing reactions in the system. A number of side reactions as thermal decomposition, WGS, methanation and others, depending on thermodynamical conditions and substrate nature used, could take place in the system:



The formation of carbon proceeds by the following general reactions:



Steam gasification of coke may occur under a high partial pressure of water in the reaction:



The main factors determining the composition of products and the conversion depth of reagents are the catalyst nature and the reaction conditions: temperature, pressure,  $H_2O/C$  ratio, contact time, and the presence of oxygen. Overall, similar trends are observed for steam reforming of all oxygen-containing hydrocarbons. According to thermodynamic calculations, a rise in temperature increases the  $CO/H_2$  ratio, shifting the equilibrium to the formation of  $CO$  and  $H_2O$  and thus decreasing the concentration of hydrogen, and facilitates steam reforming of the produced methane. High temperature is required also for a complete conversion of oxygenate [49]. According to theoretical calculations and experimental data, the lower is the pressure, the higher is the yield of gaseous products and conversion of oxygenate [85]. The formation of carbon deposits also decreases due to weakening the bonds between the adsorbed coke precursors and the catalyst surface [69]. A

pressure of 1-2 atm is accepted as optimal for steam reforming because it is economically unreasonable to create a decreased ( $<1$  atm) pressure in the reaction system. The partial pressure of reagents can be decreased by diluting the reaction mixture with an inert [85]. The  $H_2O/C$  ratio is also the key parameter: at a fixed temperature, an increase in the  $H_2O/C$  ratio above the stoichiometric value increases the conversion of oxygenate and decreases the  $CO/H_2$  ratio and the amount of carbon deposits. A reason is that a high partial pressure of water vapor increases the contribution of steam reforming of the oxygenate and steam reforming of CO (water gas shift reaction, WGS); in addition, steam gasification of carbon may occur [60]. However, the amount of overstoichiometric water is strongly limited by technological expenditures: the cost of the diluted mixture evaporation sharply increases as compared to undiluted one. The choice of the optimal contact time is important for efficient catalyst operation. Overall, for all oxygenates, short contact times not only decrease the substrate conversion and the yields of  $H_2$  and CO but also increase the selectivity for by-products, including coke [69].

The introduction of oxygen in the reaction medium is widely applied for reducing the amount of carbon deposits. In the case of transition metal catalysts, the optimal O/C ratio prevents the formation of filamentous carbon. As was shown in the studies, the amount of amorphous carbon also decreases. Depending on the O/C ratio, partial or complete oxidation of both the oxygenate and all intermediate and final compounds, including hydrogen, can occur. The addition of oxygen increases the initial conversion of the oxygenate, decreases the yield of hydrogen, and increases the yield of  $CO_2$  for all the catalysts [46].

In the next two sections, the latest advances in the steam reforming of ethanol and glycerol reactions investigation will be considered in more detail.

### 1.3.1.1. Steam reforming of ethanol

The total equation of ethanol steam reforming can be written as



Hydrogen production by steam reforming of ethanol is being intensively studied now. Recent advances in this field are summarized in reviews [61, 62, 14, 63], particularly those devoted to the reaction mechanism [64, 65, 66]. The main reactions accompanying steam reforming of ethanol are listed in Table 1.1.

**Table 2.1.** Reactions accompanying steam reforming of ethanol

Reaction	General equation
SRE in sufficient amount of water	$\text{C}_2\text{H}_5\text{OH} + 3\text{H}_2\text{O} \rightarrow 2\text{CO}_2 + 6\text{H}_2$
SRE at a water deficit	$\text{C}_2\text{H}_5\text{OH} + \text{H}_2\text{O} \rightarrow 2\text{CO} + 4\text{H}_2$
Dehydrogenation	$\text{C}_2\text{H}_5\text{OH} \rightarrow \text{C}_2\text{H}_4\text{O} + \text{H}_2$
Decomposition of acetaldehyde	$\text{C}_2\text{H}_4\text{O} \rightarrow \text{CH}_4 + \text{CO}$
Steam reforming of acetaldehyde	$\text{C}_2\text{H}_4\text{O} + \text{H}_2\text{O} \rightarrow 3\text{H}_2 + 2\text{CO}$
Dehydration	$\text{C}_2\text{H}_5\text{OH} \rightarrow \text{C}_2\text{H}_4 + \text{H}_2\text{O}$
Water-gas shift reaction	$\text{CO} + \text{H}_2\text{O} \rightarrow \text{CO}_2 + \text{H}_2$
Steam reforming of methane	$\text{CH}_4 + \text{H}_2\text{O} \rightarrow \text{CO} + 3\text{H}_2$
Dry reforming of methane	$\text{CH}_4 + \text{CO}_2 \rightarrow 2\text{CO} + 2\text{H}_2$
Thermal decomposition	$\text{C}_2\text{H}_5\text{OH} \rightarrow \text{CO} + \text{CH}_4 + \text{H}_2$ $2\text{C}_2\text{H}_5\text{OH} \rightarrow \text{C}_3\text{H}_6\text{O} + \text{CO} + 3\text{H}_2$ $2\text{C}_2\text{H}_5\text{OH} \rightarrow \text{CO}_2 + 3\text{CH}_4$
Acetone formation	$2\text{C}_2\text{H}_5\text{OH} + \text{H}_2\text{O} \rightarrow \text{CH}_3\text{COCH}_3 + \text{CO}_2 + 4\text{H}_2$
Methanation	$\text{CO} + 3\text{H}_2 \rightarrow \text{CH}_4 + \text{H}_2\text{O}$ $\text{CO}_2 + 4\text{H}_2 \rightarrow \text{CH}_4 + 2\text{H}_2\text{O}$ $\text{C}_2\text{H}_5\text{OH} + 2\text{H}_2 \rightarrow 2\text{CH}_4 + \text{H}_2\text{O}$
Polymerization of ethylene	$\text{C}_2\text{H}_4 \rightarrow \text{polymerized deposits}$
Decomposition of methane	$\text{CH}_4 \rightarrow 2\text{H}_2 + \text{C}$
The Boudouard reaction	$2\text{CO} \rightarrow \text{CO}_2 + \text{C}$

Lots of studies are devoted to thermodynamic analysis of ethanol steam reforming [67, 68, 69]. Figure 1.4 shows the distribution of ethanol steam reforming products at a fixed stoichiometric water/ethanol ratio equal to 3 and 6, and a pressure of 1 atm versus the process temperature. Ethanol conversion over the entire temperature range is 100%, while hydrogen, CO, CO<sub>2</sub> and CH<sub>4</sub> are sole products of the reaction at 200-1000 °C. As the temperature is raised, concentrations of methane and CO<sub>2</sub> decrease, whereas those of H<sub>2</sub> and CO increase, and at a temperature above 700 °C hydrogen, CO and CO<sub>2</sub> become the sole products of the reaction. This is related to an increased

contribution from steam reforming of CO and methane. The hydrogen concentration has a maximum in the region of 650-700 °C.

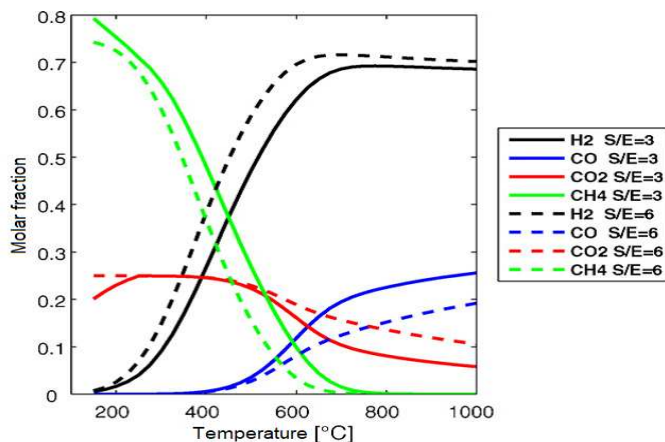


**Figure 1.4.** The temperature dependence of products concentration in ethanol steam reforming in thermodynamic equilibrium at a water/ethanol ratio (S/E) = 3 and 6.

The dependence of reaction products distribution on the water content is displayed on Figure 1.5. Overall, the addition of overstoichiometric water increases the selectivity for hydrogen, and when the water/ethanol ratio exceeds 4, carbon disappears from the reaction products. Thus, in terms of thermodynamics, the optimal conditions for ethanol steam reforming are the temperature range of 550-650 °C and the water/ethanol ratio  $\geq 4$ . Under the indicated conditions, a theoretical yield of hydrogen exceeds 4 mol H<sub>2</sub>/mol EtOH, and coke formation becomes thermodynamically disadvantageous [67]. Numerous experimental data for these conditions demonstrate that ethanol conversion and selectivity for reaction products strongly depend on the chosen catalyst (see Section “Catalysts for steam reforming”).

The reaction mechanism of ethanol steam reforming is not clear as yet. As for the majority of heterogeneous catalytic reactions, the key to understanding the mechanism is related to identification of the intermediates formed at the catalyst active sites. However, the spectroscopic methods studying the intermediates formed on the catalyst surface, are difficult to use under real reaction conditions at high temperatures. The analysis of kinetic data on the distribution of products at the reactor outlet gives possible transformation routes of ethanol and its derivatives [70, 71, 72, 73, 74]. A combination of such studies, theoretical calculations and spectroscopy studies under conditions differ from the reaction conditions made it possible to suggest different reaction mechanisms [64, 65, 66].

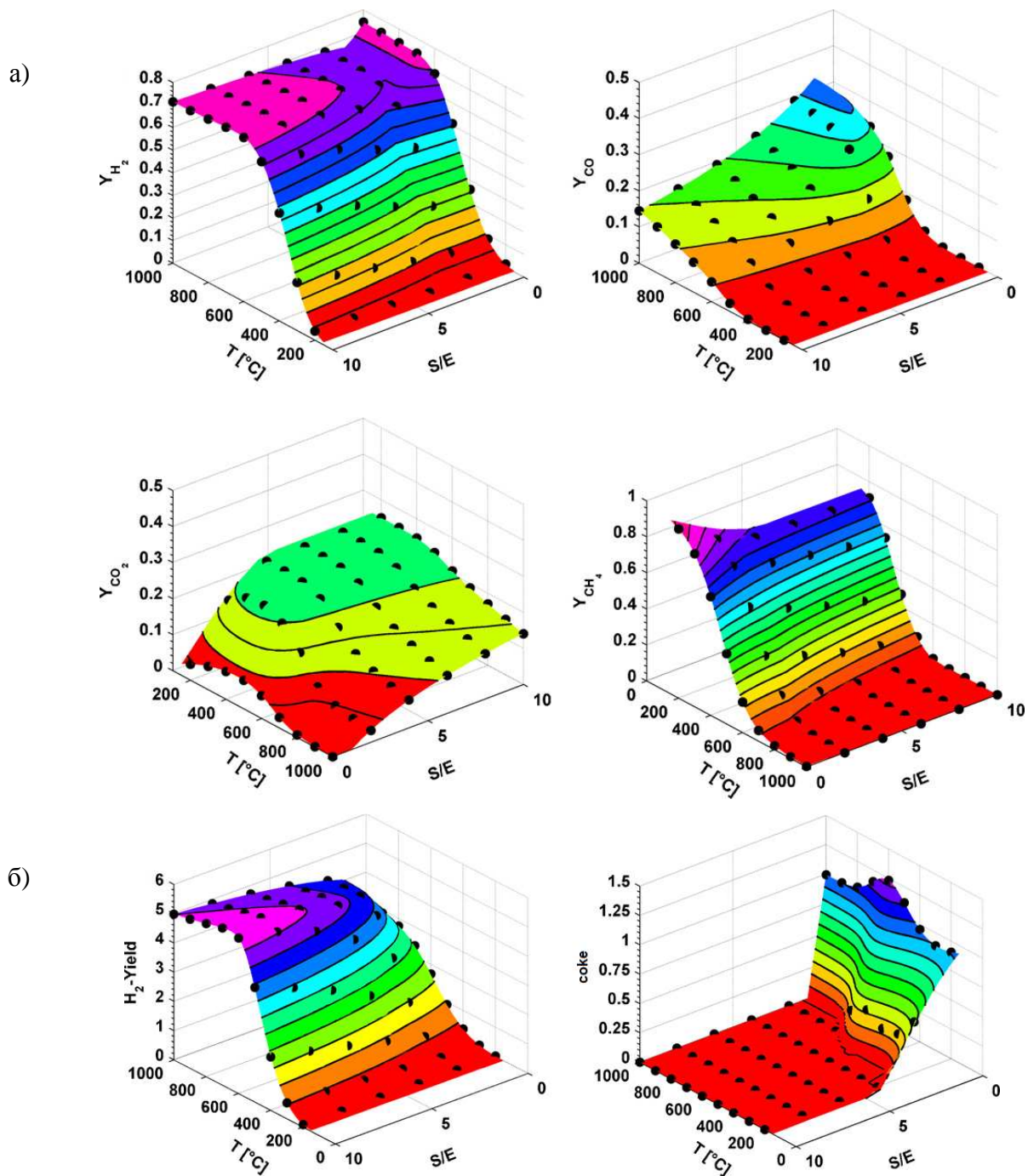


**Figure 1.5.** Distribution of ethanol steam reforming products (a) and selectivity for hydrogen and carbon deposits (b) in thermodynamic equilibrium versus temperature and water/ethanol (S/E) ratio.

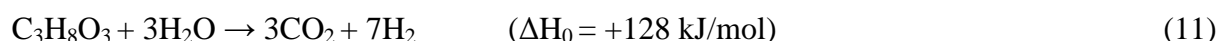
Overall, the researchers have agreed on the main regularities of ethanol steam reforming. Thus, in the first step, ethanol is dissociatively adsorbed on the catalyst surface; depending on the nature of the active metal, cleavage of either the O-H (transition and noble metals) or C-H (noble metals) bond occurs. Although in the gas phase the binding energy of C-O is lower as compared to that of O-H, the transfer of an electron pair from oxygen to the catalyst surface results in the formation of an energetically advantageous ethoxy species with the retention of the C-O bond [64].



The transformation of this ethoxy intermediate can proceed by two competitive routes – dehydrogenation and dehydration. In the first case, acetaldehyde is formed, and its further transformations lead to consecutive hydrogen abstraction and formation of surface  $C_xH_yO_z$  species. The cleavage of the C-C bond becomes energetically advantageous in the last steps of the process and results in the formation of  $*CH_x$  species, which can be hydrated to form methane or dehydrated with subsequent oxidation of  $*C$  species to CO and  $CO_2$ . Dehydration of ethanol takes place when the catalyst contains acid Lewis sites decreasing the activation barrier for C-O bond cleavage, which leads to the formation of the C=C double bond, i.e. ethylene. Ethylene is the main precursor of carbon deposits and polymerizes on metallic sites of the catalyst [75].

### *1.3.1.2 Steam reforming of glycerol*

The total equation of glycerol steam reforming can be written as



A considerable progress in the study of glycerol steam reforming over recent years was summed up in reviews [76, 77, 78, 79]. Along with thermal decomposition and, in the case of oxygen introduction, partial oxidation of glycerol,



a large number of parallel reactions proceed in the system, the main displayed on Figure 1.6 [80]. As can be seen on the scheme, the process can include the formation of liquid by-products, such as acetaldehyde, methane, acrolein [81, 82], acetone, hydroxyacetone, acetic acid, allyl alcohol, and others [83]. Further transformations of these compounds depend on the catalyst properties and process conditions.

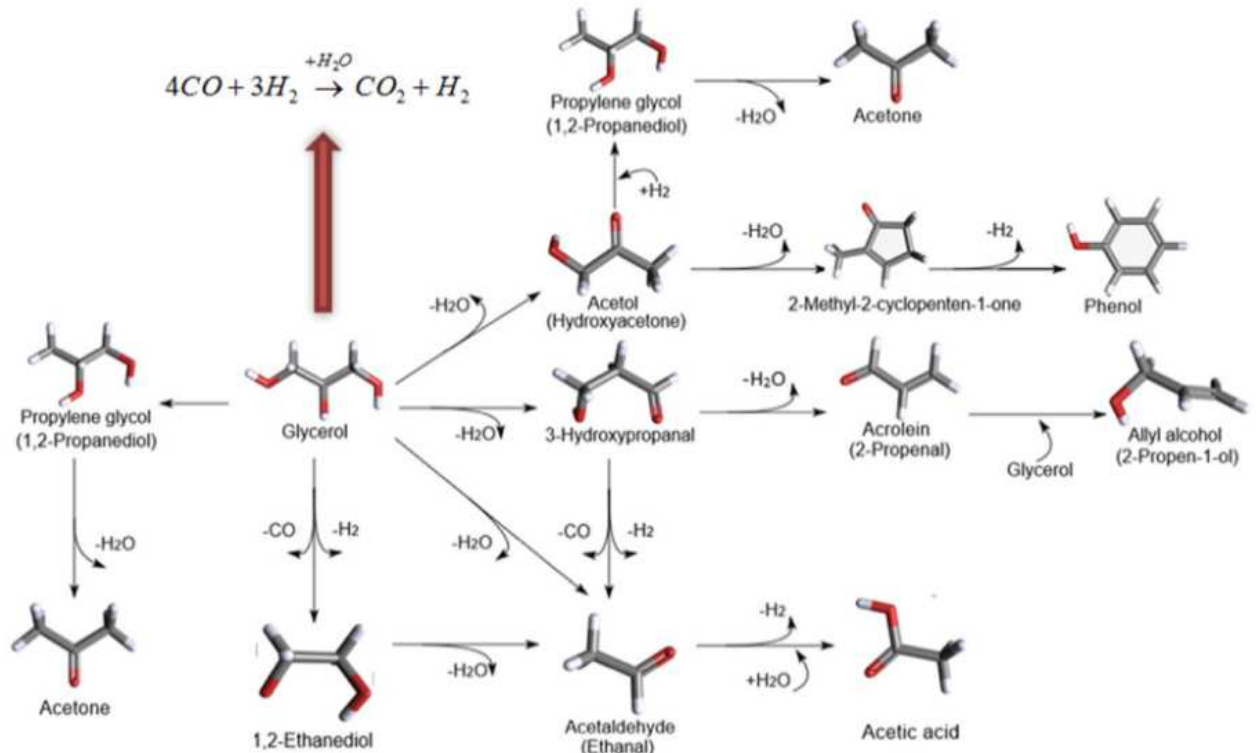


**Figure 1.6.** A scheme of main transformations in steam reforming of glycerol.

The reaction is thermodynamically limited [84, 85 ,86]. Detailed calculations were earlier made also at ICPEES, University of Strasbourg, and presented in the PhD Thesis by M. Arago [87].

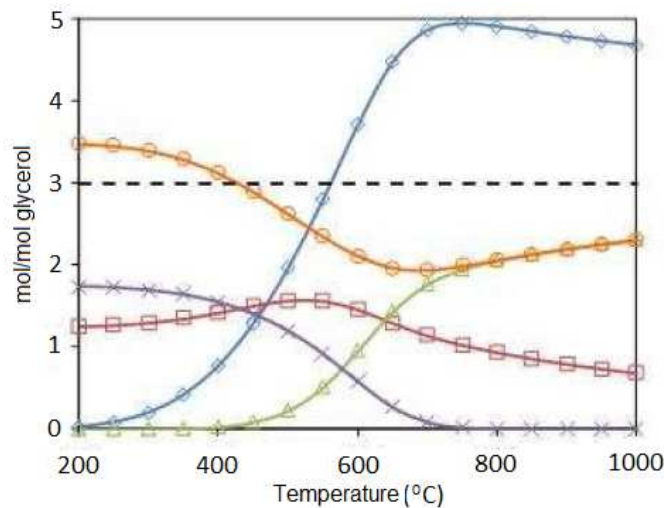


**Figure 1.7.** The distribution of selectivities for the reaction products of glycerol steam reforming in thermodynamic equilibrium versus temperature at the water to ethanol ratio of 3:  $\diamond$  –  $H_2$ ,  $\square$  –  $CO_2$ ,  $\Delta$  –  $CO$ ,  $\times$  –  $CH_4$ ,  $\circ$  –  $H_2O$  [87]

Figure 1.7 displays the temperature dependence of selectivity for glycerol steam reforming products at a fixed stoichiometric ratio water/glycerol = 3 and a pressure of 1 atm. [87]. Three main temperature ranges can be distinguished: below 400 °C water is not a reagent, and its role is reduced to shifting the equilibrium of methane and carbon monoxide steam reforming. In a temperature range of 300-800 °C, the formation of hydrogen and carbon dioxide increases with a maximum in the region of 700 °C; and at temperatures above 800 °C, H<sub>2</sub>, CO and CO<sub>2</sub> are the main products of the reaction.

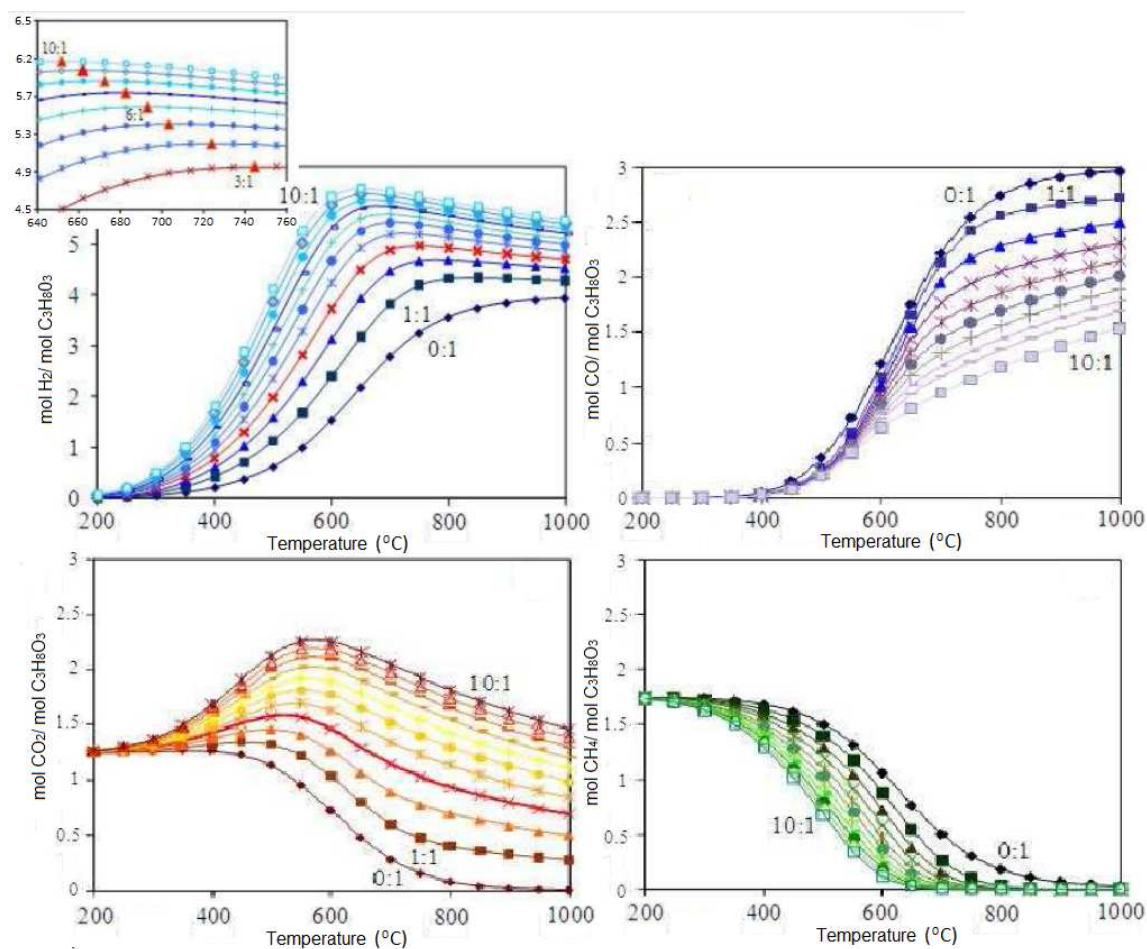


**Figure 1.8.** Distribution of the main reaction products H<sub>2</sub>, CO, CO<sub>2</sub>, CH<sub>4</sub> in steam reforming of glycerol in thermodynamic equilibrium: dependence on temperature and water/glycerol ratio [87]

Investigation of the effect produced by water content in the reaction mixture on the products distribution (Figure 1.8) revealed that the maximum hydrogen yield is observed at 600-700 °C and increases with the water/glycerol ratio [87]. Wang and co-authors examined also the effect of oxygen introduction in the reaction medium and concluded that an increase in the oxygen content above O/glycerol = 0.4 decreases the hydrogen yield [88]. Summarizing all the listed data, one can

obtain the optimal conditions of the process: a temperature of 580-700 °C, a water/glycerol ratio of 9-12, and atmospheric pressure [88, 84, 85, 87, 89].

In the case of glycerol steam reforming, elucidation of a detailed reaction mechanism is complicated by a large amount of intermediates and strongly depends on the process conditions and catalyst [90, 91, 92]. By now, the overall effect exerted by the nature of adsorption sites on the main steps of glycerol transformation has been revealed [93] and possible reaction mechanism for platinum-containing catalysts have been proposed [94].

### ***1.3.2. Coke formation in steam reforming as the main route of catalysts' deactivation***

Carbon formed in steam reforming is usually divided into two main types – amorphous and filamentous. Amorphous carbon is attributed to stable forms of deposits which could be oxidized at temperatures above 800 °C. Amorphous carbon is formed by two different routes: via dehydration and cyclization of alkenes on acid sites of the oxide support [94, 126] and via decomposition of adsorbed  $\text{CH}_x$  species formed at metal sites [128]. Such a carbon covers both the metallic particles and the support surface, thus blocking active sites, which leads to deactivation of steam reforming catalysts. In the case of transition metals, the produced carbon can dissolve in a metal with subsequent growth of carbon fibers. The formed filamentous carbon is less stable and can be oxidized already at the reaction temperatures ( $<700$  °C) [120, 121]. Catalyst's deactivation in this case takes place due to detachment of a metal particle from the support surface during the growth of fibers (the “intrusion” mechanism) [95]. The isolated metal particle is still active in steam reforming reactions; however, after regeneration the catalyst activity is not restored and the number of its working cycles sharply decreases.

## 1.4. Catalysts for steam reforming of oxygenates

In recent 15 years, many studies were devoted to investigation of ethanol and glycerol steam reforming. Studies on the activity and stability of catalysts of different chemical composition as well as methods of their synthesis, which demonstrate some progress in the field, are reported in reviews [61, 62, 96, 97]. However, the problem of deactivation of the highly active catalysts for steam reforming of oxygen-containing hydrocarbons due to their coking in the long-term testing remains unsolved, and the design of inexpensive active and stable catalysts is still a topical task.

A typical catalyst for steam reforming is an active metal deposited on the oxide support, most often with different modifying additives. The key factors determining activity and stability of such catalysts in steam reforming reactions are the nature and dispersion of a metal, its interaction with the support and promoters, as well as the specific surface area and acidity of the support.

### *1.4.1. Activity of metals of different nature in catalysts for steam reforming*

Noble and transition metals are highly active in steam reforming reactions. Among noble metals, most active in steam reforming are Rh [98, 99, 100, 101], Pt [94, 102, 103, 104], Pd [72, 105, 106, 107, 108] and Ru [109, 110, 111] in the temperature range of 300-750 °C at a metal content in the catalyst of 0.5-5 wt.%. These metals show high activity in the cleavage of C-C bond due to their electronic structure [112, 113, 114]. As a result, a complete conversion of ethanol is reached already at 400 °C irrespective of the support. Such catalysts ensure the high yields of hydrogen and syngas as well as the low formation rates of carbon deposits [115]. In spite of their efficiency, the high cost of noble metals hinders their industrial application. Among all noble metals active in steam reforming of oxygen-containing hydrocarbons, ruthenium is the most accessible one; however, in steam reforming catalysts it is employed more often as a promoter but not as the main active phase. In some studies it was noted that in the synthesis under similar conditions, the dispersion of supported ruthenium can be much lower as compared to other noble metals. This substantially decreases the activity due to fast deactivation caused by both the coking and the further coarsening of the particles as a result of sintering in the reaction [116, 117]. Nevertheless, when highly disperse ruthenium particles are stabilized on the surface, such an additive, for example, to transition metals essentially enhances the catalytic activity [118].

Among transition elements, most used are Ni and Co as well as Fe and Cu. The content of these metals in the catalysts ranges from 1 to 25 wt.%, the working temperature in steam reforming is 500-800 °C, and the catalytic activity decreases in the sequence: Ni → Co → Fe → Cu [80]. Such a dependence is related to the fact that nickel and cobalt are able to cleave both the C-C and C-H bond, whereas iron is active mostly toward the cleavage of only the C-C bond, and copper – only

for the C-H bond [80, 119]. The activity of nickel and cobalt compares well with that of noble metals; however, their main drawback is fast coking [120]. It is well known that only amorphous coke is formed over noble metals, while transition metal catalysts are characterized by the formation of both the amorphous and filamentous carbon, which substantially deteriorates their stability in the long-term testing [95, 121]. However, the low cost of transition metals attracts considerable interest in such catalysts and inspires researchers to search for solutions of the problem.

Catalysts based on cobalt show high activity in diluted mixtures in steam reforming of both ethanol [122] and glycerol [123] along with fast deactivation due to strong coking. In addition to coke formation, an essential drawback of cobalt-containing catalysts is their deactivation under the reaction conditions due to the oxidation of active metal particles [124]. At present, nickel is the most studied, inexpensive and promising component of steam reforming catalysts. High activity of nickel catalysts along with their strong coking were demonstrated in many studies [125, 126, 127, 128].

#### ***1.4.2. The size effect and approaches to enhancing the stability of nickel-containing catalysts***

The effect of metal particle size on resistance to coking was first revealed for nickel-containing catalysts in methane reforming reactions [129]. It was shown that dissociation of methane with the formation of carbon takes place on the ensembles consisting of seven and more nickel atoms. If the size of ensembles is smaller than the critical value, the dissociation does not occur and coking is not observed [130]. Filamentous carbon is formed on the particles with the diameter greater than 6 nm [131]. The larger the metal particles are, the higher the reaction intensity is [132, 128]. The decrease or inhibition of coking at an increased dispersion of nickel was revealed in many studies, particularly for ethanol [133] and glycerol [134] steam reforming catalysts.

The size of metal particles and the strength of their interaction with the support are determined by the state of nickel in the oxidized catalyst precursor. The interaction strength can be estimated from the position and intensity of hydrogen absorption peaks when studying the reduction of nickel-containing precursors using temperature-programmed reduction of hydrogen (TPR-H<sub>2</sub>). Thus, the reduction of nickel from bulk NiO oxide occurs at a temperature of 300-400 °C [153]. Supported catalysts (NiO/TiO<sub>2</sub>, NiO/ZnO, NiO/CeO<sub>2</sub>, NiO/SiO<sub>2</sub>, NiO/Al<sub>2</sub>O<sub>3</sub>) prepared by impregnation are characterized by a weak interaction with the support. Nickel particles, which are formed at 300-600 °C in this case, commonly have a size above 100 nm and show a tendency to further sintering in the reaction [80, 134, 135, 140, 142, 136]. Nickel can be incorporated in the support structure with the formation of solid solutions (for example, NiO-MgO) and mixed oxides,

which results in the appearance of highly disperse nickel metal particles due to strong interaction with the support [137]. The formation of  $\text{NiAl}_2\text{O}_4$  spinel is well known for the most popular  $\gamma$ - $\text{Al}_2\text{O}_3$  support. In this case, to obtain active metal particles, the reduction should be performed at high temperatures (about 900 °C). Surface modification of alumina with alkali-earth or rare-earth elements decreases the interaction strength and increases the dispersion of the produced particles [138]. A substantial decrease in the nickel reduction temperature at a strong interaction is observed for mesoporous structures, and the size of the formed particles commonly does not exceed 6 nm [139]. It was shown [157] that in mesoporous  $\text{Ca}(\text{Mg})\text{Al}_2\text{O}_4$  spinels nickel resides in non-stoichiometric highly disperse oxides that are reduced at 600-650°C. Thus obtained nickel particles have the mean size of 3-5 nm after the reduction at 800°C and do not sinter (6-8 nm) after 40 hours of operation in combined steam and dry reforming of methane at 800°C.

The size of metal particles can be decreased substantially also by the synthesis of catalysts from perovskite precursors [140, 141]. It was shown [193, 195] that after the reduction at temperatures above 400 °C, the catalysts obtained from the  $\text{LaNiO}_3$  perovskite precursor consist of 15-20 nm nickel metal particles anchored on the surface of lanthanum oxide  $\text{La}_2\text{O}_3$ . The resistance to sintering of such systems is determined by the chemical composition of the initial perovskite. For example, a comparison of nickel particle sizes in the  $\text{CeNiO}_3$  catalyst before and after the reaction revealed a pronounced sintering (30 → 109 nm), whereas for the  $\text{LaNiO}_3$  sample virtually no coarsening of the particles (20 → 21 nm) occurred [198]. In [196], a similar resistance to sintering observed for  $\text{LaNiO}_3$  in autothermal ethanol reforming was attributed to a strong interaction of nickel with the  $\text{La}_2\text{O}_2\text{CO}_3$  phase formed in the reaction. Iron-containing perovskites of the  $\text{AFe}_x\text{Ni}_{1-x}\text{O}_3$  type are able to retain their structure after the reduction up to 900 °C. Nevertheless, under reduction conditions at temperatures close to 650 °C, nickel and iron cations partially segregate to produce a highly disperse (6-30 nm) Ni-Fe alloy. In some cases, the process is reversible and such perovskites can restore their structure after reoxidation [199].

A highly efficient way enhancing the stability of nickel-containing catalysts is the dilution of the active component ensembles using bimetallic systems where the formation of an alloy may occur: Ni-Co [142, 143], Ni-Cu [26], Ni-Fe [144] or Co-Fe [145]. The addition of iron is accompanied by a synergetic effect, owing to which iron facilitates steam reforming of carbon monoxide and increases the selectivity for hydrogen.

The promotion with noble metals, for example ruthenium, diminishes the formation of filamentous carbon due to dilution of nickel atoms and stabilization of highly disperse particles in the long-term testing [146, 147], as well as lowering the reduction temperature of nickel via hydrogen spillover [118]. Some researchers noted a significant decrease in the amount of carbon

deposits in the case of nickel-containing catalysts promoted with molybdenum [148, 149, 150]. In [151], an essential decrease in the carbon formation rate was attributed to the ability of molybdenum to activate water with subsequent oxidation of Ni-C and Ni-CH<sub>x</sub> particles adsorbed on the surface of metallic nickel.

#### ***1.4.3. The effect of support properties on activity and selectivity of nickel-containing catalysts***

To ensure efficient distribution and anchoring of the active metal on the surface, it is necessary, first of all, to use those supports with a high specific surface area, which are able to provide a strong metal-support interaction in order to prevent sintering and coking of metal particles in the reaction. The “high” specific surface area is commonly above 100 m<sup>2</sup>/g; it facilitates high dispersion of the active component and diminishes sintering of the particles. Various supports are reported in the literature:  $\gamma$ -Al<sub>2</sub>O<sub>3</sub> [119], SiO<sub>2</sub> [152], CeO<sub>2</sub> [172, 181, 182], ZrO<sub>2</sub> [136], TiO<sub>2</sub> [153], more rarely carbon [154], and mesoporous oxides [155, 156, 157].

Alumina is chosen most often as a support owing to its low cost, high specific surface area and high thermal stability. However, its application in unmodified form is unacceptable because the surface concentration of acid sites is too high. The coordination of aluminum with respect to oxygen atom corresponds to the Lewis acid-base interactions; the stronger is the interaction, the higher is the proton acidity. Such sites were found to catalyze the dehydration of an oxygen-containing hydrocarbon resulting in the formation of C<sub>2+</sub> compounds with the double C=C bond, which are further polymerized on metal sites to form stable carbon deposits leading to catalyst deactivation [94, 126]. The relationship between surface acidity and catalytic activity in coke-formation reactions is well studied in the literature. Surface acidity is analyzed using temperature-programmed adsorption/desorption of ammonia, pyridine and formic acid, as well as IR spectroscopy [158, 159, 160, 161, 162, 163]. The studies revealed that a decrease in the strength and concentration of Lewis acid sites makes it possible to avoid undesirable route of the reaction and significantly decrease the amount of carbon deposits formed in the reaction. In this connection, widely accepted is the approach based on promoting a support with the elements whose oxides possess basic properties. Surface modification with alkali-earth elements, primarily magnesium and calcium, not only decreases the surface acidity [164, 165, 166, 167] but also stabilizes nickel on the surface [168, 169, 170]. The enhancement of stability and selectivity for hydrogen after the addition of alkali metals was also noted in the literature. In particular, it was shown that potassium [171, 172] and sodium [173] can inhibit the methanation reaction, thus sharply decreasing the amount of coke and increasing the selectivity for hydrogen. The promotion of the support surface by rare-earth elements suppresses the growth of nickel crystallites, thus preventing the formation of large



particles that are necessary for coke formation, and hinders the reoxidation of metallic nickel in the reaction [174, 175, 176, 177, 128].

Resistance to coking can be improved significantly by using oxides with high oxygen mobility as the supports. These are the mixed oxides having the spinel, fluorite or perovskite structure, and some oxides of rare-earth elements, the most popular of which is  $\text{CeO}_2$ . Ceria is employed as both the support and the promoter of more inexpensive supports [178].  $\text{CeO}_2$  minimizes coke deposits due to active oxygen [179], facilitates high dispersion of nickel, and increases selectivity for hydrogen by promoting steam reforming of methane and carbon monoxide, which are the main intermediates that are formed in steam reforming of oxygen-containing hydrocarbons [46, 180, 181, 182].

Mixed oxides with the perovskite structure possess not only high oxygen mobility but also some additional unique properties due to which they are sometimes considered as «the substitutes of noble metals for catalysis» [183].

## 1.5. Mixed oxides with the perovskite structure

### 1.5.1. Structural features

Oxides with the perovskite structure have long been known and widely applied in catalysis due to a unique set of physicochemical properties [183].

Perovskite-like oxides include a wide range of mixed oxides with the general formula  $ABO_3$ , where A and B cations can be represented by metal cations satisfying the condition of electroneutrality (the total charge +6) and the specified steric relationships. Cations A commonly have the ionic radii close to that of oxygen and can be represented by rare-earth (La, Pr, Sm, Ce), alkali-earth (Ca, Mg, Ba, Sr) or alkali (Na, K) metals. Cations in position B should have a much smaller ionic radius and can be represented by the majority of transition metals (Fe, Ni, Co, Cu, Ti, Cr, Ru, Mn and others).

The perovskite structure is the framework consisting of  $BO_6$  octahedra jointed at all their vertices – oxygen atoms, and  $AO_{12}$  cuboctahedra formed between them (where A and B atoms reside at the centers of polyhedra, respectively) (Figure 1.9).

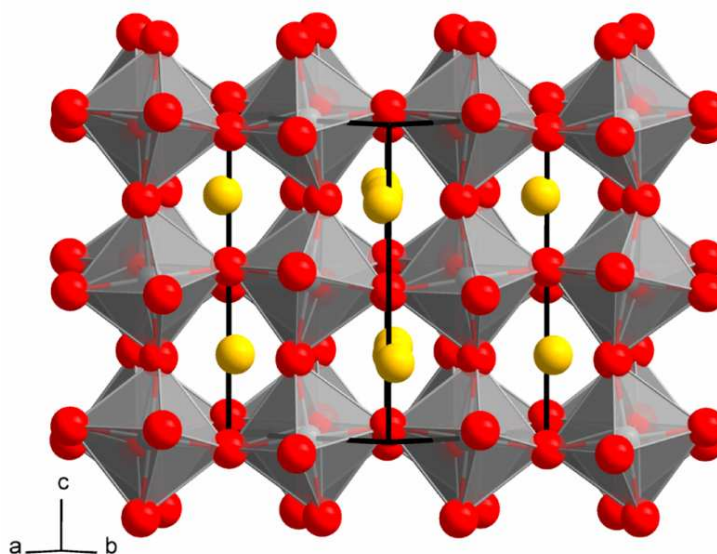


**Figure 1.9.** The polyhedral structure of the ideal perovskite  $ABO_3$ . Red spheres correspond to oxygen atoms, yellow – to cations of sublattice A, and gray – to cations of sublattice B.

Perovskite's structure is to a large extent flexible and can undergo substantial changes with a possible lowering of symmetry or formation of defects, remaining within the perovskite structural type. Distortions can be caused by polyvalence of both the rare-earth and transition metals as well as by the substitution of atoms in positions A and/or B, which are compensated by changes in the

bond length, mutual shift of octahedra, and formation of oxygen and cation vacancies. Such flexibility ensures the following nontrivial properties of perovskites:

1. Depending on external conditions, perovskites can accumulate non-stoichiometry oxygen due to the ability of a transition metal to have several oxidation states. Strictly speaking, it is more correct to write the perovskite formula as  $ABO_{3-\delta}$ , where  $\delta$  indicates a deviation from the ideal composition in real samples and theoretically can vary in a range of  $0 \leq \delta \leq 1$  [184]. As a result, such defect structures have oxygen mobility and are able to generate active oxygen on the surface. Being applied to the reforming of biofuels, this helps to burn the coke precursors, which are formed during the reaction at the metal-oxide interface, and this way strongly increases stability of the catalysts [185].

2. Under reduction atmosphere a partial segregation of cations occurs with the formation of a defect perovskite structure and highly dispersed metal particles strongly bound to its surface [188].

3. The perovskite composition can be modified by a partial substitution of cations in both the A and B positions. In this case, the perovskite formula is written as  $A_xA'_{1-x}B_yB'_{1-y}O_{3-\delta}$ ; stability of the resulting structure and its substitution limits are theoretically estimated using the Goldschmidt tolerance factor  $t = \frac{r_A+r_o}{\sqrt{2}(r_B+r_o)}$ , where  $r_i$  denotes the ionic radii of A and B cations and oxygen ion, respectively. The lattice geometry determines a tolerable distortion within the tolerance factor variation from 0.8 to 1 [186]. Due to the difference in the properties of cations B and B'/A and A', the number of oxygen vacancies in the substituted perovskite can increase several-fold. As a result, such systems possess much higher oxygen mobility as compared to unsubstituted perovskites [187].

### ***1.5.2. Perovskites as the precursors of fuel reforming catalysts***

The above listed properties make perovskites very promising for application in catalysis [188]. The efficiency of perovskite catalysts in oxidation reactions was first demonstrated for the partial oxidation and dry reforming of methane, where coking is the main cause of deactivation [189]. As was shown earlier, perovskites-based catalysts require a preliminary activation, and the metal-oxide active phase is formed in a reducing medium with a partial or complete removal of cations from the lattice. For the catalysts synthesized from perovskite precursors, resistance to coking is caused by a high dispersion of metal particles, which decreases or inhibits coke formation according to the theory of ensembles, and by oxygen mobility facilitating the reoxidation of coke precursors [190, 191].

Many works deal with investigation of the  $LaNiO_3$  oxide as a perovskite precursor of catalysts for steam and steam-oxygen reforming of ethanol [192, 193, 194, 195, 196, 197, 198]. In work [193], stability of two catalysts was compared. The first catalyst was obtained by the reduction of

LaNiO<sub>3</sub> perovskite, while the second one was synthesized by impregnation of lanthanum oxide with a nickel nitrate solution followed by calcination of Ni/La<sub>2</sub>O<sub>3</sub>. In the case of supported sample, the amount of carbon deposits after ethanol steam reforming was found to be 6-fold greater. A considerable decrease in the coke amount on LaNiO<sub>3</sub> samples as compared to Ni/La<sub>2</sub>O<sub>3</sub> was demonstrated also in [196]. For a series of La<sub>x</sub>Ce<sub>1-x</sub>NiO<sub>3</sub> catalysts, a direct dependence of carbon deposits on the size of nickel particles was revealed [198].

High activity of the catalysts with substituted precursors in ethanol steam reforming was shown for various perovskites: LaFeNiO<sub>3</sub> [199], La<sub>1-x</sub>A<sub>x</sub>Fe<sub>1-y</sub>Ni<sub>y</sub>O<sub>3</sub> (A = Ca, Sr) [200, 201], La<sub>1-x</sub>Sr<sub>x</sub>Fe<sub>1-y</sub>Co<sub>y</sub>O<sub>3</sub> [202], La<sub>1-x</sub>Ca<sub>x</sub>Fe<sub>1-x</sub>Co<sub>x</sub>O<sub>3</sub> [203], and LaXCoO<sub>3</sub> (X = Mg, Ca, Sr, Ce) [204]. The formation of the Ni-Fe alloy essentially enhances the catalyst stability in the long-term testing and provides high yields of hydrogen due to acceleration of CO steam reforming [205]. The incorporation of noble metals in the perovskite structure facilitates a further increase in its stability. An earlier study performed in our laboratory demonstrated a high stability of the catalysts based on LnFe<sub>1-y</sub>Ni(M)<sub>y</sub>O<sub>3</sub> (Ln = La, Pr, Ce, Sm; M = Mn, Ru) in dry reforming of methane. Stability was most pronounced in the ruthenium-doped catalysts due to formation of intermetallide nanoparticles strongly anchored on the oxide support surface [206, 207, 208, 209, 210, 211, 212].

Perovskites can be used also as the supports with high oxygen mobility; in this case, the active metal (Ni/Co or Pt) is deposited on the oxide formed (LaAlO<sub>3</sub>, SrTiO<sub>3</sub>, BaTiO<sub>3</sub> [213], CaTiO<sub>3</sub> [214], LaFeO<sub>3</sub> [215]) by classical methods. Overall, such catalysts have larger metal particles that tend to sintering under the reaction conditions.

Perovskites as the catalyst precursors were studied in steam and autothermal reforming of glycerol [216, 217], bio-oil (La<sub>1-x</sub>K<sub>x</sub>MnO<sub>3</sub>) [218] and heavier oxygen-containing hydrocarbons [219], which revealed their high activity.

In spite of the listed advantages, perovskites have an essential drawback (in addition to a high cost of their components): standard values of specific surface area for such systems are usually not higher than 10-20 m<sup>2</sup>/g [220]. Recently, a promising approach was reported in the literature: it allows not only decreasing the percentage of a perovskite in the catalyst, which significantly reduces its cost, but also increasing the specific surface area of the synthesized catalyst. The proposed method consists in the deposition of a perovskite on the oxides having high specific surface areas. The supports can be represented by Al<sub>2</sub>O<sub>3</sub> [221, 222, 223], SiO<sub>2</sub> [196], ZrO<sub>2</sub> [224, 225, 226], cordierite [227], etc. There are only a few studies in the literature where supported perovskites are used in the reforming of oxygen-containing hydrocarbons; therewith, optimal results were obtained when the surface was preliminarily modified to decrease its acidity [197, 228].

### 1.5.3. Methods for the perovskites synthesis

The first perovskites for catalytic applications were obtained by the solid-phase sintering or the ceramic method requiring high temperatures and a long-term synthesis. Thus obtained perovskites had a poorly developed specific surface area ( $\sim 0.5 \text{ m}^2/\text{g}$ ), as in the case of multicomponent systems – a non-uniform distribution of cations over the oxide volume [229]. At present, there are many methods that allow optimizing both the structural and textural characteristics of the produced perovskites. The literature provides various techniques based on coprecipitation [193], complexation [192, 199, 200, 201, 230], mechanical activation [231] and freeze drying [232], as well as sol-gel methods in inorganic [233] and organic [185, 198, 216, 234] media. To obtain the maximum specific surface areas, these methods can be combined with the use of solid mesoporous templates [235, 236, 237, 238].

An efficient approach to the synthesis of complex multication perovskites has been proposed by an American chemist M. P. Pechini [239].

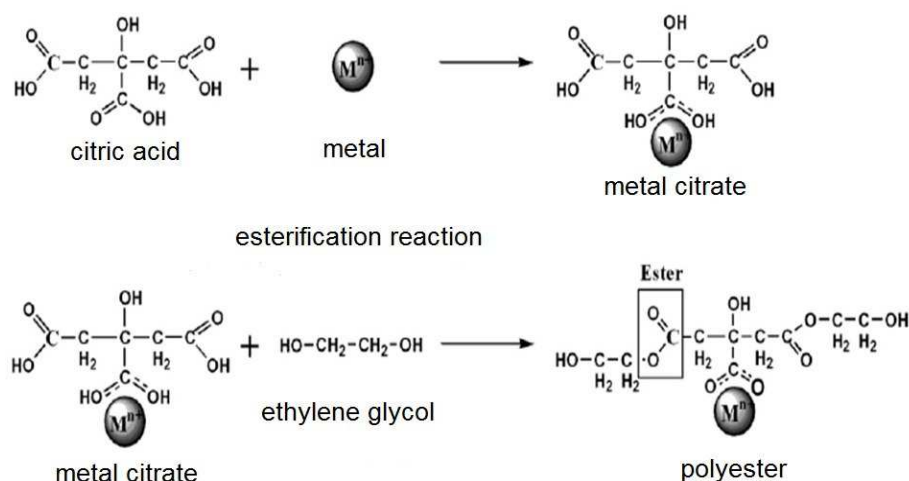


**Figure 1.10.** The formation of the polymeric matrix including metal cation, citric acid and ethylene glycol during Pechini synthesis.

The Pechini method, or the method of the polymerized precursors, is a particular case of the sol-gel method and consists in a gradual formation of the organic polymer matrix with metal atoms that can reside in its nodes (Figure 1.10). In the process, organic precursors are represented by citric acid (CA) and ethylene glycol (EG), and a source of metals – by nitrates, which are readily removed by annealing. The process occurs under vigorous stirring performed for a long time to ensure the most uniform distribution of cations in the reaction mixture. The synthesis does not require many laboratory facilities, complicated setups or expensive reagents.

The synthesis methods for supported perovskites described in the literature include depositing active metal precursors from aqueous or organic solutions on the preliminarily prepared oxide supports [197, 240].

### **1.6. Structured catalysts: supports and additional requirements**

It was shown recently that the maximum efficiency of various industrial catalytic processes is reached with the use of structured catalytic systems [241, 242, 243]. The main advantage of structured catalysts in comparison with granulated ones is the high efficiency of mass transfer at a low hydraulic resistance, which makes it possible to perform the process at short contact times. In this connection, it is possible to decrease dimensions of the reactor and a necessary amount of the catalyst without a loss in productivity.

Such technologies are being developed intensively also for the transformation of biofuels to syngas and hydrogen [20, 21, 244, 245, 246, 247]. Catalysts for such processes should be highly active in the target reaction, compatible with materials of the structured support (or anode of the fuel cell), and strongly anchored on their surface. Various structured supports can be used to obtain monolithic catalysts for transformation of biofuels: ceramic [20, 21, 244-247], metallic [248, 249], and cerametallic [250]. In recent years, technologies appeared for the production of structured foam carbon-containing supports with the surface protected by a layer of metal and/or oxide stable under the working conditions. Such supports possess high thermal and electric conductivity, unique strength, low specific weight and compatibility with different types of materials (metals, oxides, etc.). Nickel is most promising for use as a metal compatible with carbon, and corundum – as a protecting oxide [251].

The structured platelets containing catalysts which demonstrated high performance in diluted mixtures as fractions should be produced and tested in pilot reactors. This will be the next step toward industrial implementation of the technology that will help to estimate compatibility, efficiency and stability of the catalytic system in operation under real conditions.

## 1.7. Conclusion to the literature review

The analysis of the literature data revealed a high interest of researchers in studying the transformations of liquid products from biomass processing to hydrogen and syngas, in particular, steam reforming of oxygen-containing hydrocarbons. A typical steam reforming catalyst is the active metal deposited on the oxide support, commonly with different modifying additives. Activity in the reaction can be provided by noble (Pt, Pd, Rh, Ru, etc.) and transition (Ni, Co, Fe, Cu) metals. It is well known that on noble metals only amorphous coke is formed, whereas transition metal catalysts are characterized by the formation of both the amorphous and filamentous carbon, which substantially decreases their stability in the long-term testing. Nevertheless, the use of noble metal catalysts is economically disadvantageous. In this connection, the best studied, inexpensive and promising component of steam reforming catalysts is nickel. High activity of nickel catalysts was demonstrated in many studies, along with their strong coking.

As follows from the analysis of the literature, the formation of a stable and selective nickel-containing catalyst for steam reforming of oxygen-containing hydrocarbons should start from optimization of a set of parameters determining the catalyst behavior in carbon formation processes. In steam reforming, carbon is produced by the two different routes: via decomposition of the adsorbed  $\text{CH}_x$  particles that are formed on metal sites, and via dehydration and cyclization of alkenes on acid sites of the oxide support. The carbon produced can be dissolved in the metal with subsequent growth of carbon filaments.

In the first case, nickel particles should be stabilized in a highly disperse state to suppress coking. Highly efficient approaches to the synthesis of such systems include the use of mixed oxides, for example perovskites or spinels as the catalyst precursors, as well as the dilution of nickel atoms and stabilization of highly disperse particles of the active component in bimetallic systems (Ni-Fe, Ni-Co, Ni-Ru) where an alloy can form [252, 253]. In addition, to provide efficient distribution and anchoring of the active metal on the surface, it is necessary to use supports with a high specific surface area, which can ensure a strong metal-support interaction to prevent both coking and sintering of metal particles in the reaction.

A decrease in the strength and concentration of Lewis acid sites of the support makes it possible to avoid the undesirable dehydration route and essentially decrease the amount of carbon formed in the reaction. In this connection, the obligatory step of catalyst optimization is its modification providing basic properties of the support surface. Alumina is the most often selected support due to its low cost, high specific surface area and thermal stability. Modification of alumina is performed by depositing basic oxides of alkali and alkali-earth elements, the most commonly used is magnesium.

## CHAPTER 2. EXPERIMENTAL TECHNIQUES

### 2.1. Materials preparation

#### 2.1.1. Reagents and materials

The reagents listed in Table 2.1 were used for preparation of solutions and served as the precursors.

**Table 2.1.** Reagents used to synthesize catalysts for the study

Reagent	Chemical purity	Manufacturer
Ni(NO <sub>3</sub> ) <sub>2</sub> *6H <sub>2</sub> O	pure for analysis	Reakhim
Co(NO <sub>3</sub> ) <sub>2</sub> *6H <sub>2</sub> O	pure for analysis	Reakhim
Fe(NO <sub>3</sub> ) <sub>2</sub> *9H <sub>2</sub> O	pure for analysis	Reakhim
La(NO <sub>3</sub> ) <sub>2</sub> *6H <sub>2</sub> O	chemically pure	Vekton
Pr(NO <sub>3</sub> ) <sub>2</sub> *6H <sub>2</sub> O	chemically pure	Vekton
RuOCl <sub>3</sub>	chemically pure	Reakhim
Mg(NO <sub>3</sub> ) <sub>2</sub> *6H <sub>2</sub> O	chemically pure	Reakhim
AlOOH Disperal	highly pure	Sasol
Citric acid (CA)	chemically pure	Reakhim
Ethylene glycol (EG)	pure for analysis	Laverna

#### 2.1.2. Synthesis of lanthanide ferrites $LnFe_{1-x-y}M_xRu_yO_3$ and 5%M/PrFeO<sub>3</sub>

The catalyst precursors – substituted ferrites of rare-earth elements with the general formula  $LnFe_{1-x-y}M_xRu_yO_3$  (Ln = Pr, La, M= Ni, Co, x = 0.3; 0.4 y = 0; 0.1) – were synthesized by the organic polymeric precursor method, which is the modified Pechini method [239]. The synthesis was performed using crystalline hydrates of nitrates of the corresponding cations, citric acid (CA, chemically pure), and ethylene glycol (EG, pure). Exact molar masses of the nitrates were found by thermal analysis. Ethylene glycol and citric acid were used as complex formers. The reagents were taken at a molar ratio CA : EG :  $\Sigma v$  (metals) = 3.75:11.25:1. Citric acid was dissolved in ethylene glycol under vigorous stirring and weak heating (60-80 °C). The solution cooled to room temperature was supplemented with a necessary amount of crystalline hydrates of metal nitrates under vigorous stirring. A complete homogenization took ca. 2 hours. The resulting mixture was evaporated under stirring to obtain a thick polymer, and calcined in a muffle furnace to 700 or 900 °C for 5 hours.



Supported reference catalysts 5%Ni(Co)/PrFeO<sub>3</sub> were prepared by impregnation of the PrFeO<sub>3</sub> perovskite, which was synthesized by the modified Pechini method and calcined at 700 or 900 °C, with aqueous solutions of cobalt or nickel nitrate followed by drying under an IR lamp and calcination at 500 °C.

### ***2.1.3. Synthesis of supported $m\text{LnNi}_{0.9}\text{Ru}_{0.1}\text{O}_3/n\%\text{Mg-}\gamma\text{-Al}_2\text{O}_3$ samples***

Catalysts  $m\text{LnNi}_{0.9}\text{Ru}_{0.1}\text{O}_3/n\%\text{Mg-}\gamma\text{-Al}_2\text{O}_3$  (Ln = La, Pr, x= 0; 0.6, m=10; 20, n = 6; 10; 15) were obtained by impregnation of magnesia-doped alumina with a joint aqueous solution of La, Ni and Ru salts taken in a specified ratio with subsequent calcination at 700 °C for 2 hours.

Modification of the support with magnesium was conducted by different procedures:

1. Impregnation of the formed gamma-alumina with an aqueous solution of magnesium nitrate (denoted in the text as  $[\text{Mg-}\gamma\text{-Al}_2\text{O}_3]$ ). Aluminum hydroxide Disperal was calcined in a muffle furnace at 500 °C for 4 hours. The obtained  $\gamma\text{-Al}_2\text{O}_3$  was impregnated with an aqueous solution of magnesium nitrate taken in a specified amount; this was followed by drying under an IR lamp and calcination in a muffle furnace at 700 °C for 1 hour.

2. Impregnation of the formed gamma-alumina with an organic solution of magnesium nitrate (denoted as  $[\text{Mg-}\gamma\text{-Al}_2\text{O}_3^{\text{P}}]$ ). Aluminum hydroxide Disperal was calcined in a muffle furnace at 500 °C for 4 hours. A citric acid solution in ethylene glycol was prepared separately and supplemented with magnesium nitrate at a ratio of CA : EG : v(Mg) = 3.75:11.25:1; the resulting solution was homogenized at room temperature for 2 hours.  $\gamma\text{-Al}_2\text{O}_3$  was introduced into the gel, vigorously stirred for another 2 hours, and then heated under stirring on a sand bath to obtain a solid polymer precursor. This was followed by calcination in a muffle furnace up to 500 °C for 2 hours.

3. Magnesium introduction by impregnation from an aqueous solution at the aluminum hydroxide step (denoted as  $[\text{Mg-}\gamma\text{-Al}_2\text{O}_3^{\text{D}}]$ ). Aluminum hydroxide Disperal was impregnated with an aqueous solution of magnesium nitrate taken in a stoichiometric amount; this was followed by drying under an IR lamp and calcination in a muffle furnace at 700 °C for 4 hours.

MgAl<sub>2</sub>O<sub>4</sub> spinel was synthesized by the modified Pechini method from Mg and Al nitrates (denoted as MgAl<sub>2</sub>O<sub>4</sub>). The reagents were taken in the molar ratio CA : EG :  $\Sigma\text{V}(\text{metals}) = 3.75:11.25:1$ . Citric acid was dissolved in ethylene glycol under vigorous stirring and weak heating (60-80 °C). Necessary amounts of crystalline hydrates of metal nitrates were introduced under vigorous stirring in the obtained solution that was cooled to room temperature. A complete homogenization took ca. 2 hours. The resulting mixture was evaporated under stirring to obtain a thick polymer, which was then calcined in a muffle furnace up to 700 °C for 4 hours.

#### 2.1.4. Synthesis of structured catalysts

Porous platelets displayed on Figure 2.1 were afforded by our colleagues from the Institute of Powder Metallurgy NAS Belarus within the joint project and had the following characteristics:

1. Nickel-aluminum alloy foam platelets with a low density ( $0.5 \text{ g/cm}^3$ );
2. SiC/Al-Si-O foam composite (density  $0.5 \text{ g/cm}^3$ );
3. Corundum/Al-Si-O ceramic composite platelets (density  $0.5 \text{ g/cm}^3$ ).



**Figure 2.1.** A photo of the foam supports used for preparation of structured catalytic systems.

The platelets were manufactured by duplication of the polyurethane foam samples by suspension of SiC or  $\alpha\text{-Al}_2\text{O}_3$  powders with an aluminosilicate binder containing low-temperature fluxes (feldspar) followed by sintering under air at  $1200 \text{ C}$  [254]. Nanocomposite active components (loading up to 10 wt.%) were supported on structured substrates by slip casting slurries in isopropanol with addition of polyvinyl butyral followed by drying and calcination under air at  $700 \text{ }^\circ\text{C}$  for 2 hours. To prepare the structured catalysts for testing in the pilot-scale reactor in real feeds, substrates with typical sizes  $38 \times 38 \times 5$  or  $35 \times 35 \times 1 \text{ mm}$  were used.

The active component  $m\text{LnNi}_{0.9}\text{Ru}_{0.1}\text{O}_3/n\%\text{Mg-}\gamma\text{-Al}_2\text{O}_3$  was deposited from a suspension of the powdered catalyst in polyvinyl butyral and isopropyl alcohol. The suspension was obtained by ultrasonic dispersion of 7.5 wt.% powdered oxide in 70 ml isopropanol with the addition of 1.5 ml polyvinyl butyral. The foam support was immersed in the suspension, purged with air, dried under an IR lamp, and calcined in a furnace at  $800 \text{ }^\circ\text{C}$  for 2 hours. The procedure was repeated until 10 %wt. of the active component was deposited.

## **2.2. Materials characterization**

### ***2.2.1. Specific surface area measurements***

Textural characteristics of the reduced catalysts were measured from N<sub>2</sub> physical adsorption at the liquid nitrogen temperature using an ASAP-2400 (Micromeritics Instrument. Corp., Norcross, GA, USA) automated volumetric adsorption unit. Before the analysis, samples were outgased at 150 °C for 4 h at a pressure of  $1 \cdot 10^{-3}$  mm Hg. The analysis time was chosen for each sample. The obtained adsorption isotherms were used to calculate the specific surface area  $S_{sp}$ .

Specific surface areas were measured by T.Ya. Efimenko at the Laboratory of catalyst texture, BIC.

### ***2.2.2. X-ray diffraction analysis (XRD)***

Diffraction patterns were taken on a Bruker Advance D8 diffractometer with a CuK<sub>α</sub> source. Scanning was performed in a  $2\Theta$  angular range of 15 – 90° at a 0.05° step. Identification of the obtained phases and quantitative calculations were made using the ICDD database.

XRD data were acquired by T.A. Krieger at the Laboratory of structural methods, BIC.

### ***2.2.3. Temperature-programmed reduction with hydrogen (TPR-H<sub>2</sub>)***

Properties of the materials under reducing conditions were studied on a flow kinetic setup with a quartz U-shaped reactor equipped with a Tsvet-500 chromatograph and a thermal conductivity detector. All the measurements were performed using the catalyst grain size of 0.25-0.5. Before the reduction, the samples were treated in flowing oxygen at 500 °C for 30 minutes and then cooled to room temperature. The reduction was carried out at 900 °C with a heating rate of 10 °C/min in a flow of 10 % hydrogen in argon at a flow rate of 2.5 L/h.

The TPR-H<sub>2</sub> data were obtained by G.V. Bondarenko and V.A. Rogov at the Laboratory of catalytic reaction mechanisms, BIC.

### ***2.2.4. Infrared spectroscopy of adsorbed CO (IRS ads. CO)***

Surface properties of the samples were examined by low-temperature IR Fourier spectroscopy of adsorbed carbon monoxide. Before recording the IR spectra, a sample was pressed in a pellet with an area of 2 cm and total weight of 30-35 mg. The pellet was placed in an IR cell and pretreated in a vacuum, in an oxygen or hydrogen medium. Studies with different pretreatments were performed consecutively using the same pellet. The vacuum pretreatment included calcination

of a sample in a vacuum at 500 °C. During the pretreatment in a hydrogen medium, 100 Torr H<sub>2</sub> was admitted in a cell, and the sample was calcined in a hydrogen medium for 1 h at 500 °C; after that, the sample was evacuated to a residual gas pressure not lower than 10<sup>-3</sup> Torr and cooled to room temperature. For pretreatment in an oxygen medium, 100 Torr O<sub>2</sub> was admitted in a cell, and the sample was calcined in an oxygen medium for 1 h at 500 °C; after that, the sample was cooled in an oxygen medium to room temperature and evacuated to a residual gas pressure not lower than 10<sup>-3</sup> Torr. After the pretreatment, 60 Torr CO was admitted in a sampler using a gas admission unit. IR spectra of the initial sample and the sample after CO admission were recorded at the liquid nitrogen temperature on a Shimadzu FTIR-8300 spectrometer in the region of 400-6000 cm<sup>-1</sup> with a resolution 4 cm<sup>-1</sup> and accumulation of 100 scans. After recording the spectra at the liquid nitrogen temperature, the sample was heated to room temperature, and the spectrum was recorded. The obtained absorption spectra were normalized to the optical thickness of the pellets. All the reported IR spectra are the difference spectra.

Data on IR spectroscopy of adsorbed CO were obtained by T.S. Glazneva at the Laboratory of spectral methods, BIC.

#### ***2.2.5. Diffuse reflectance electron spectroscopy (UV-Vis)***

The electronic states of the support and all supported samples were investigated using diffuse reflectance electron spectroscopy (UV-Vis) on a UV-2501 PC (Shimadzu) spectrophotometer with an ISR-240 A diffuse reflectance attachment. Powdered samples were placed in a quartz cuvette with the optical path length of 2 mm, and diffuse reflectance spectra of the samples were recorded against BaSO<sub>4</sub> as the reflection standard in a wavelength range of 190-900 nm (11 000–53 000 cm<sup>-1</sup>). The obtained diffuse reflectance factors were converted into absorption factors using the Kubelka-Munk function  $F(R) = (1 - R)^2/2R$ , and wavelengths were transformed into wave numbers. All UV-Vis data were presented in the ‘Kubelka-Munk function F(R) – wave number’ coordinates.

UV-Vis data were obtained by T.V. Larina at the Laboratory of spectral methods, BIC.

#### ***2.2.6. X-ray photoelectron spectroscopy (XPS)***

The study was carried out on a KRATOS ES 300 photoelectron spectrometer. Before loading in the spectrometer, samples were ground in an agate mortar and deposited on a conducting carbon scotch. Photoelectron spectra were recorded after reaching a 1\*10<sup>-8</sup> Torr vacuum. To estimate the qualitative surface composition and detect the presence of impurities, the survey

spectra were obtained in a range of 0 – 1100 eV with an energy step 1 eV and the analyzer pass energy HV = 50 eV (Fig. 1). The quantitative composition of the surface and the charge states of elements were determined from precision spectra of individual photoelectron lines with a 0.1 eV step at the analyzer pass energy HV = 25 eV. The spectrometer analyzer was calibrated against the Au<sup>4f</sup> and Cu<sup>2p</sup> lines of metallic gold and copper with the corresponding positions of 84.0 and 932.7 eV. The obtained spectra were calibrated against the Al2p line, the binding energy of which was taken equal to 74.5 eV. The K<sub>α</sub> line of magnesium (hv = 1253.6 eV) served as the primary radiation. The depth of XRD analysis was ca. 30 – 40 Å.

XPS data were acquired by R.V. Gulyaev at the Group of supported metal-oxide catalysts, BIC.

### ***2.2.7. High resolution transmission electron microscopy (HRTEM)***

Electron microscopy images were obtained on a JEM-2010 (Jeol, Japan) transmission electron microscope. Local analysis of the elemental composition of samples was performed using a Phoenix energy dispersive EDX spectrometer with a Si(Li) detector and energy resolution not higher than 130 eV.

HRTEM data were obtained by A.V. Ischenko at the Laboratory of structural methods, BIC.

### ***2.2.8. Temperature-programmed reduction with ethanol (TPR-C<sub>2</sub>H<sub>5</sub>OH)***

The temperature dependence of the interaction of materials with ethanol was studied using a flow kinetic unit with a quartz reactor equipped with a Tsvet-500 chromatograph and a thermal conductivity detector.

All the measurements were made with the catalyst grain size of 0.25-0.5 mm. Prior to the reduction, the samples were treated in flowing oxygen.

TPR-C<sub>2</sub>H<sub>5</sub>OH with pretreatment in oxygen at 500 °C and fast cooling upon termination of the experiment was followed by TP-reoxidation with water vapor and steam reforming of ethanol (SR-ethanol). In the experiments on ethanol steam reforming, first the stationary activity in the reaction mixture was obtained at 800 °C, and then a steady state of the sample was reached at each chosen temperature upon cooling with a step of ~ 50-100 °C.

Data of TPR-C<sub>2</sub>H<sub>5</sub>OH followed by TPO-H<sub>2</sub>O were acquired by G.M. Alikina at the Laboratory of deep oxidation catalysts, BIC.

## 2.3. Catalytic tests

### 2.3.1. Catalytic testing in steam reforming of ethanol

Catalytic testing in steam reforming of ethanol (SRE) was conducted in a flow U-shaped reactor at atmospheric pressure, ethanol to water ratio of 1:4, contact time 0.07 s, and temperature 500-800 °C. A 0.18 g sample of the catalyst with the grain size 0.25-0.5 mm was diluted with quartz in a weight ratio of 1:10. The reductive pretreatment of catalysts was carried out in flowing hydrogen 10% $H_2$ /Ar at 800 or 500 °C for 1 h. Gaseous products were analyzed on an LHM-8 gas chromatograph equipped with thermal conductivity and flame-ionization detectors.

The catalytic data were obtained by N.F. Saputina at the Group of catalyst testing, BIC.

The conversion of ethanol, selectivity for carbon-containing products, and hydrogen yield were calculated using the following formulas:

$$x_{EtOH} = \frac{mol_{EtOH}^{inlet} - mol_{EtOH}^{outlet}}{mol_{EtOH}^{inlet}} \times 100\% \quad S_i = \frac{v_i \cdot mol_i}{\sum_i^n v_i \cdot mol_i} \times 100\% \quad Y_{H_2} = \frac{mol_{H_2}}{6 \cdot mol_{EtOH}^{inlet}} \times 100\%$$

where  $mol_{EtOH}^{inlet}$  and  $mol_{EtOH}^{outlet}$  are moles of ethanol at the reactor inlet and outlet, respectively;  $mol_i$  is the number of moles of i-th product; and  $n_i$  is the number of carbon atoms in i-th product.

### 2.3.2. Catalytic testing in steam/steam-oxygen reforming of glycerol

Steam and oxy-steam reforming of glycerol was carried out for 24 hours in a flow reactor at the inlet concentration of glycerol 3.8%, ratio of glycerol : water = 1 : 9, weight hourly space velocity  $28000 \text{ h}^{-1}$ ,  $T = 650 \text{ °C}$ , and catalyst grain size 0.25-0.5 mm. In the case of oxy-steam reforming of glycerol, the  $O_2$  concentration was 3%, other parameters remaining unchanged. The reductive pretreatment of the catalysts was performed in a 10% $H_2$ /Ar at a flow rate 40 ml/min, heating rate  $2^\circ\text{C}/\text{min}$ ,  $T = 500 \text{ °C}$ , and retention time 1.5 h.

The catalyst was mixed with SiC in a 1:1 weight ratio [ $m(\text{cat}) = m(\text{SiC}) = 0.055 \text{ g}$ ]. Quartz grains were placed in a tubular reactor with a 0.5 cm diameter at 1/3 of the furnace height and fixed with quartz wool from two sides. The diluted catalyst fixed with quartz wool was placed at the center of the reactor. Quartz wool with a height of ca. 2 cm was mounted at the reactor inlet to provide a better dispersion of the reaction mixture in the flow. Gaseous products ( $H_2$ , CO,  $CO_2$ ,  $CH_4$ ,  $C_2H_4$ ) were analyzed on-line each 30 minutes of the reaction using a gas chromatograph

Network GC system Agilent Technologies 6890N with a TCD detector. Liquid products (methanol, acetic acid, ethylene glycol, acetone, acrolein, hydroxyacetone, propanediols, propionic acid) were collected by two traps at  $T_1 = T_{\text{room}}$  and  $T_2 = 0\text{ }^{\circ}\text{C}$  and analyzed after 8 and 24 hours using a gas chromatograph Network GC system Agilent Technologies 6890N with a flame-ionization detector.

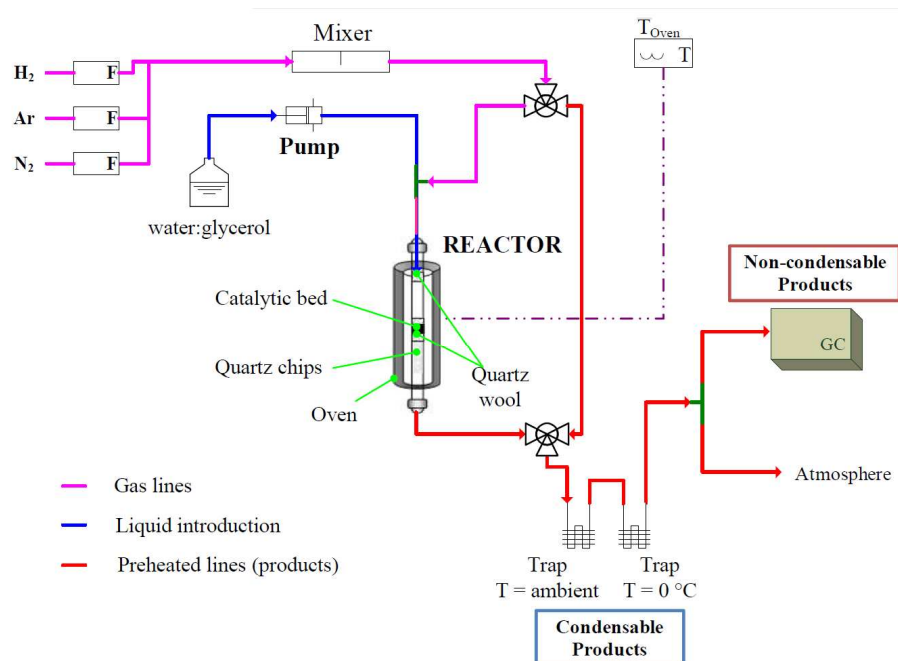


**Figure 2.2.** A scheme of the setup for glycerol steam reforming

The catalytic data were obtained by the author in collaboration with her French colleagues at the Institute of Chemistry and Processes for Energy, Environment and Health (ICPEES), Strasbourg.

Steam reforming of glycerol can be accompanied by the formation of a wide range of liquid by-products, which quantitative identification is difficult. In this connection, glycerol conversion to the gas phase and productivity for gaseous products were introduced to compare the catalytic activity of different samples. Glycerol conversion to the gas phase was calculated as a ratio of the sum of gaseous products multiplied by the number of carbon atoms in a molecule to the glycerol fed to the reactor. Productivity was calculated in the (mol/mol) units, where (mol) denotes the moles of glycerol converted to gaseous products.

$$x_g = \frac{\sum_i^n v_i \cdot \text{mol}_i^{\text{gas}}}{\text{mol}_G^{\text{in}}} \times 100\%$$

$$P_i = \frac{v_i \cdot \text{mol}_i^{\text{gas}}}{\sum_i^n v_i \cdot \text{mol}_i^{\text{gas}}} \times 100\%$$

### 2.3.3. Catalytic testing in ethanol steam reforming on the structured support in a pilot reactor

To test the structured catalysts in steam and oxy-steam reforming of ethanol in concentrated mixtures, a special plane reactor was used. A scheme of the reactor is displayed on Figure 2.3. Platelets with the size of  $1*0.5*0.2$  cm were employed in the study. A seal was placed between the reactor walls and the catalyst. The temperature was measured in several points at the reactor inlet and outlet. The catalytic activity of different foam supports was compared in a flow reactor at a contact time  $150 \mu\text{s}$ , temperature  $800 \text{ }^\circ\text{C}$ , and reaction mixture composition 10%  $\text{C}_2\text{H}_5\text{OH}$  + 40%  $\text{H}_2\text{O}$  + 50%  $\text{N}_2$ .

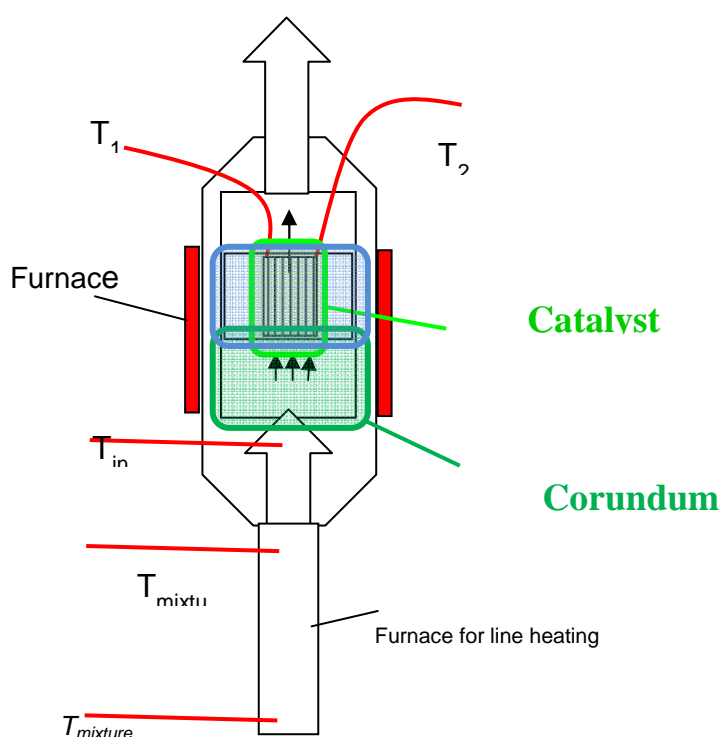


**Figure 2.3.** A scheme of the pilot unit reactor for reforming of oxygenates in concentrated mixtures.

Catalytic studies on stability in steam and oxy-steam reforming of ethanol were carried out at a contact time of 150 ms ( $\text{GHSV} = 3600 \text{ h}^{-1}$ ) and a constant temperature of  $850 \text{ }^\circ\text{C}$  using the reaction mixture 3%  $\text{O}_2$  + 57%  $\text{H}_2\text{O}$  + 29%  $\text{C}_2\text{H}_5\text{OH}$  + 10%  $\text{N}_2$  for 20 hours, which was then replaced by the 10%  $\text{C}_2\text{H}_5\text{OH}$  + 40%  $\text{H}_2\text{O}$  + 50%  $\text{N}_2$  mixture.

The catalytic data were obtained by Z.Yu. Vostrikov at the Laboratory of deep oxidation catalysts, BIC.



## CHAPTER 3. MASSIVE CATALYST'S FAMILY $\text{LnFe}_{1-x-y}\text{M}_x\text{Ru}_y\text{O}_3$ (Ln = Pr, La, M= Ni, Co, x = 0.3; 0.4 y = 0; 0.1): PHYSICOCHEMICAL PROPERTIES AND CATALYTIC ACTIVITY IN STEAM REFORMING OF ETHANOL AND STEAM/OXY-STEAM REFORMING OF GLYCEROL

This chapter is devoted to the investigation of the  $\text{LnFe}_{1-x-y}\text{M}_x\text{Ru}_y\text{O}_3$  and 5%M/PrFeO<sub>3</sub> mixed oxide precursors synthesized and catalysts obtained upon their reduction. The  $\text{LnFe}_{1-x-y}\text{M}_x\text{Ru}_y\text{O}_3$  precursors were synthesized by the modified Pechini method, a family of 5% Co(Ni)/PrFeO<sub>3</sub> comparison samples was prepared by impregnating the perovskite PrFeO<sub>3</sub> with the Ni(Co) nitrates solution. Physical-chemical properties and its relationship with the activity and stability in steam reforming of ethanol (ESR) as well as steam (GSR) and oxy-steam (GOSR) reforming of glycerol are considered in a three main sections.

In the first section, the effect of the chemical composition and synthesis method on structural and textural properties of the oxides synthesized was studied using BET, XRD and TEM methods. Reducibility of the precursors was explored by the TPR-H<sub>2</sub> method. The second section describes the catalytic activity of preliminary reduced  $\text{LnFe}_{1-x-y}\text{M}_x\text{Ru}_y\text{O}_3$  and 5%M/PrFeO<sub>3</sub> samples in the steam reforming of ethanol reaction in the temperature range of 650-800 °C and at the constant T = 650 °C. The third section contains results of the catalytic tests of preliminary reduced  $\text{LnFe}_{1-x-y}\text{M}_x\text{Ru}_y\text{O}_3$  samples in the steam and oxy-steam reforming of glycerol reactions at the constant T = 650 °C during 24 hours. The main conclusions about the effect of the composition and the method of precursor's synthesis on the activity and stability in the reactions studied were postulated.

### *3.1. Structural and textural properties of initial perovskites*

Catalysts with the general formula  $\text{LnFe}_{1-x-y}\text{M}_x\text{Ru}_y\text{O}_3$  (Ln = Pr, La, M= Ni, Co, x = 0.3; 0.4 y = 0; 0.1) were synthesized by the modified Pechini route described in the Chapter 2. To study the effect of the synthesis method, a series of impregnation catalysts 5 % M/PrFeO<sub>3</sub> (M = Ni, Co) was prepared. In Table 3.1. some data on the composition, method and conditions of synthesis, as well as the properties of synthesized perovskites are given. As can be seen from the table, the specific surface area of the samples is in the range of 3-10 m<sup>2</sup>/g, which are typical values for perovskites of this composition [183, 190, 255].

**Table 3.1.** Synthesized compositions, their some physical and chemical properties and values of the tolerance factor t

Composition	Method of synthesis	T <sub>calc</sub> , °C	S <sub>BET</sub> , m <sup>2</sup> /g	a*, Å	b, Å	c, Å	V, Å <sup>3</sup>	t
LaFe <sub>0.7</sub> Ni <sub>0.3</sub> O <sub>3</sub>	Pechini	900	7	5,511	7.808	5,537	238.25	0,97
LaFe <sub>0.6</sub> Ni <sub>0.4</sub> O <sub>3</sub>	Pechini	900	9	5,529	7,787	5,495	236.58	0,97
PrFe <sub>0.7</sub> Ni <sub>0.3</sub> O <sub>3</sub>	Pechini	900	7	5,522	7,742	5,462	233.5	0,84
PrFe <sub>0.6</sub> Ni <sub>0.4</sub> O <sub>3</sub>	Pechini	900	10	5,534	7,750	5,470	234.60	0,84
LaFe <sub>0.6</sub> Co <sub>0.4</sub> O <sub>3</sub>	Pechini	900	4	5,509	7,746	5,465	233.24	0,97
PrFe <sub>0.7</sub> Co <sub>0.3</sub> O <sub>3</sub>	Pechini	900	3	5.494	7.730	5.454	231.6	0,84
PrFe <sub>0.6</sub> Co <sub>0.4</sub> O <sub>3</sub>	Pechini	900	3	5.474	7.694	5.438	229.0	0,84
La <sub>0.7</sub> Pr <sub>0.3</sub> Fe <sub>0.7</sub> Ni <sub>0.3</sub> O <sub>3</sub>	Pechini	900	4	5,53	7,74	5,46	237.4	0,93
PrFe <sub>0.6</sub> Ni <sub>0.3</sub> Ru <sub>0.1</sub> O <sub>3</sub>	Pechini	900	4	5.584	7.777	5.478	237.6	0,97
PrFeO <sub>3</sub> <sup>[700]</sup>	Pechini	700	7	5.567	7.790	5.491	237.9	0,82
PrFeO <sub>3</sub> <sup>[900]</sup>	Pechini	900	4	5,575	7,787	5,483	237.2	0,82
5 % Ni/PrFeO <sub>3</sub> <sup>[700]</sup>	impregnation	500**	7	5.566	7.788	5.488	237.9	—
5 % Ni/PrFeO <sub>3</sub> <sup>[900]</sup>	impregnation	500**	4	5.572	7.784	5.482	237.9	—
5 % Co/PrFeO <sub>3</sub> <sup>[700]</sup>	impregnation	500**	7	5.571	7.791	5.489	238.2	—

\* reference data for PrFeO<sub>3</sub> [JCPDF 47-0065]: a = 5.48 Å, b = 5.59 Å, c = 7.78 Å, V = 238.72

\*\* T<sub>calc</sub> after impregnation

### 3.1.1. Effect of the chemical composition and synthesis method on the structural and textural properties of initial samples

#### Substituted LnFe<sub>1-x-y</sub>M<sub>x</sub>Ru<sub>y</sub>O<sub>3</sub>

The XRD patterns of the initial perovskites are given in Fig. 3.1.1. For the non-substituted PrFeO<sub>3</sub> both calcined at 700 and 900 °C all peaks refer to the orthorhombic perovskite phase [JCPDF 47-0065]. The literature data confirm that the formation of an iron-containing AFe<sub>x</sub>B<sub>1-x</sub>O<sub>3</sub> perovskite structure is possible at temperatures above 650 °C [205]. For the sample calcined at 700 °C, the broadened peaks on the X-ray diffraction pattern (Fig. 3.1.1, b) correlate with the larger specific surface area (Table 3.1) as compared with PrFeO<sub>3</sub><sup>[900]</sup>, indicating greater dispersion in the PrFeO<sub>3</sub><sup>[700]</sup> sample. (The size of the perovskite phase crystallites calculated from XRD data for these samples are 35-40 and > 100 nm, respectively).

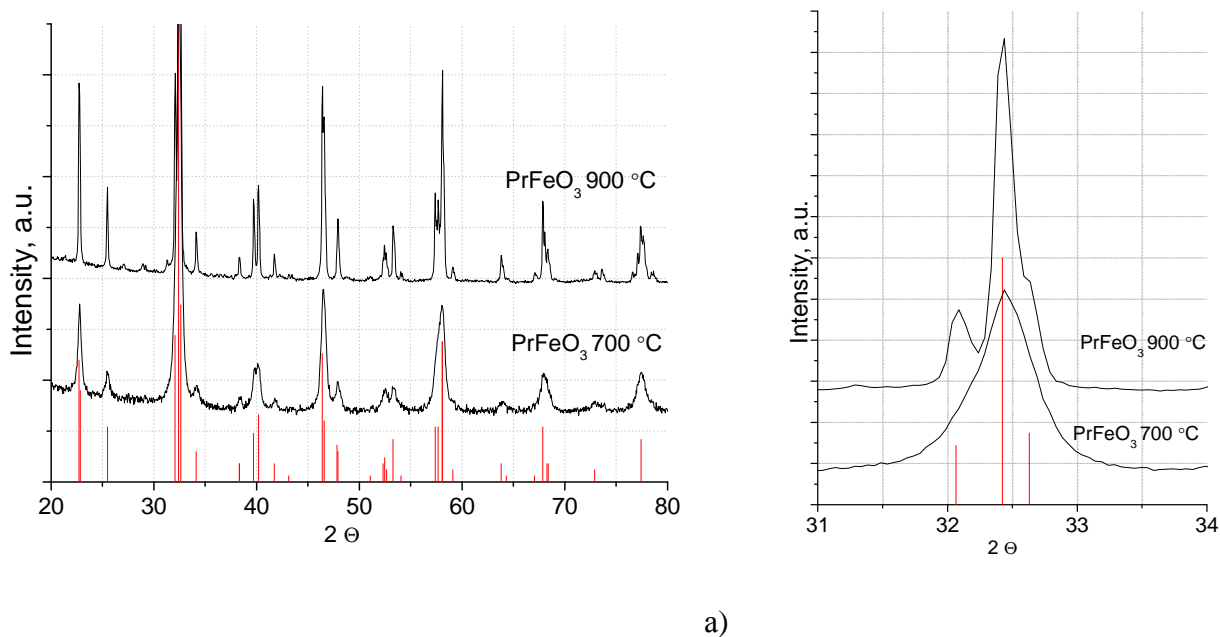


**Figure 3.1.1.** X-ray diffraction patterns obtained for initial sample  $\text{PrFeO}_3$ , calcined at 700 and 900 °C for  $2\theta$  a) 20-80° and b) 31-34°. The histogram corresponds to the phase  $\text{PrFeO}_3$  [JCPDF47-0065]

The main phase of all initial substituted samples  $\text{LnFe}_{1-x-y}\text{Ni}_x\text{M}_y\text{O}_3$  is orthorhombic perovskite (Figures 3.1.1-3.1.3) with intensity approximately equal to theoretical. Peak shifts depending on cation's nature are close to those described in the literature [256]. The theoretical possibility of the existence of perovskites with compositions used was confirmed by the tolerance factor calculating for all samples (Table 3.1).

For the lanthanum-containing perovskites, whose cation radius is greater than the radius of the praseodymium cation ( $r(\text{La}^{3+}) = 1.36 \text{ \AA}$ ,  $r(\text{Pr}^{3+}) = 1.179 \text{ \AA}$ ), all peaks are shifted to a region of smaller angles, which indicates an increase in the lattice parameter comparing with praseodymium-containing ones (Figure 3.1.2, Table 3.1).

Similar regularities were shown in the works [190, 257, 258], as well as in earlier works of our laboratory [206, 209].

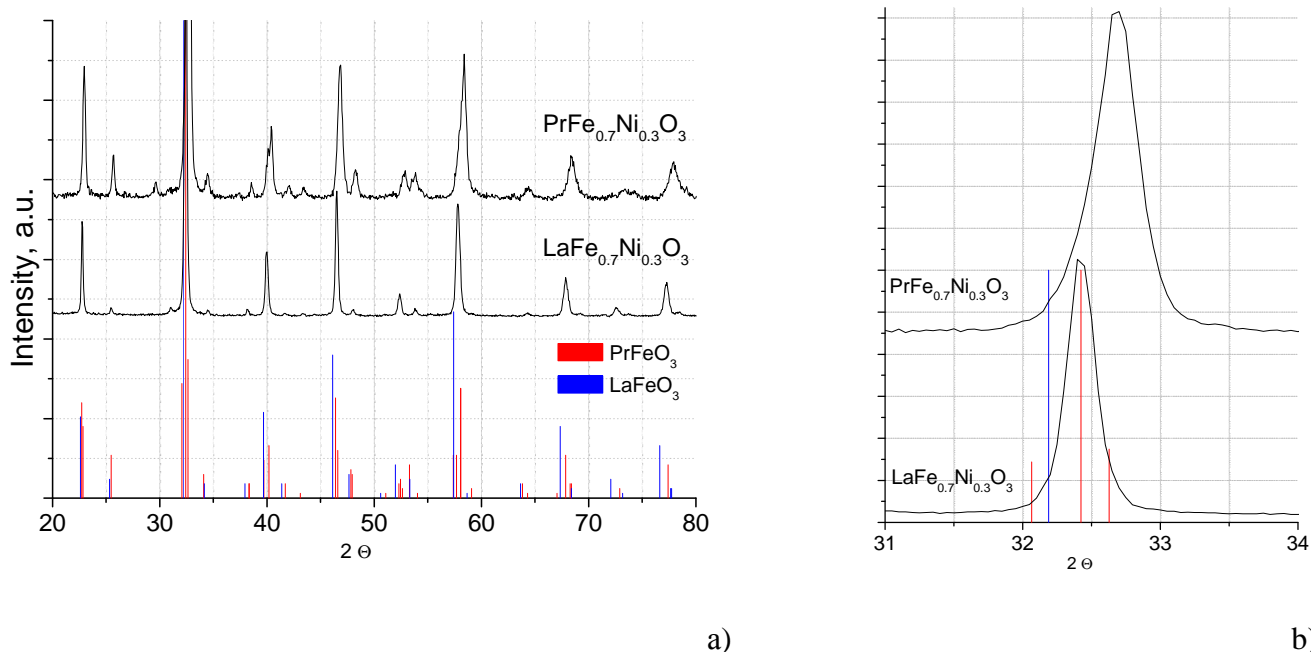


**Figure 3.1.2.** X-ray diffraction patterns obtained for  $\text{LaFe}_{0.7}\text{Ni}_{0.3}\text{O}_3$  и  $\text{PrFe}_{0.7}\text{Ni}_{0.3}\text{O}_3$  for  $2\theta$  **a)**  $20\text{-}80^\circ$  and **b)**  $31\text{-}34^\circ$

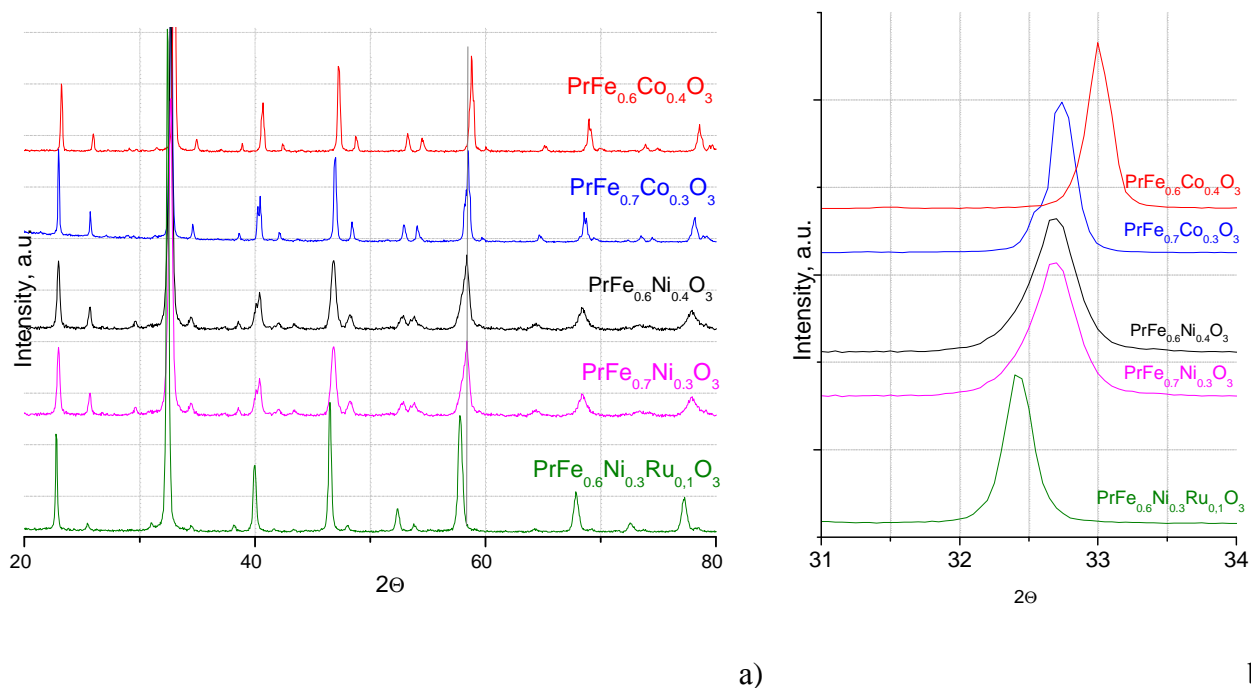
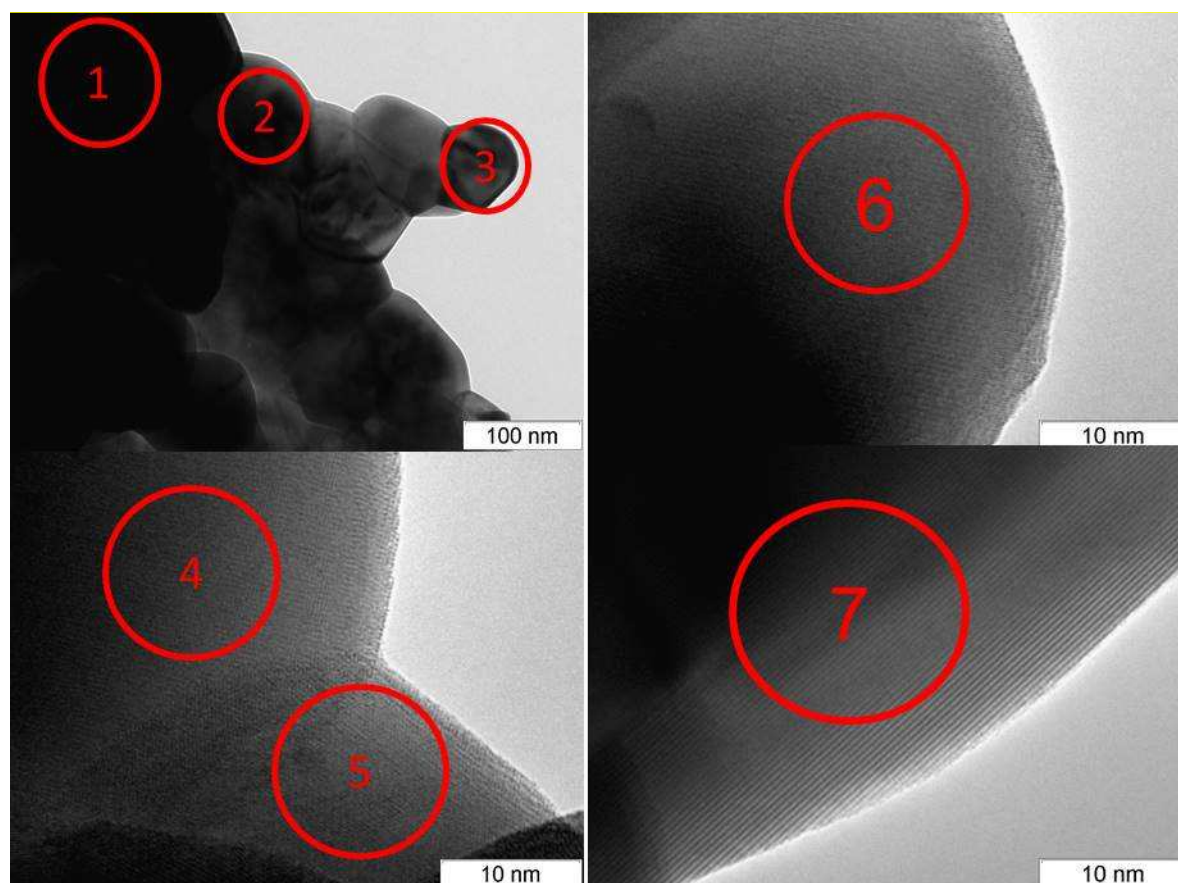


**Figure 3.1.3.** X-ray diffraction patterns obtained for  $\text{LnFe}_{0.7}\text{Ni}_{0.3}(\text{Ru}_{0.1})\text{O}_3$ : influence of the composition and doping metal amount (Ni, Co, Ru) for  $2\theta$  **a)**  $20\text{-}80^\circ$  and **b)**  $31\text{-}34^\circ$

Figure 3.1.3 shows the X-ray diffraction patterns of perovskites  $\text{PrFe}_{1-x-y}\text{Ni}_x\text{M}_y\text{O}_3$  with different cations in the iron position. When iron is replaced by nickel and cobalt with the smaller cations radius ( $r(\text{Fe}^{3+}) = 0.645 \text{ \AA}$ ,  $r(\text{Ni}^{3+}) = 0.60 \text{ \AA}$ ,  $r(\text{Co}^{3+}) = 0.61 \text{ \AA}$ ), the lattice parameters decrease (Table 3.1), as evidenced by the perovskite phase peaks shift to the region of larger angles. The

regularities obtained agree with the data described in the literature for similar systems. [259]. Ruthenium introduction into perovskite composition, whose cation size  $r(\text{Ru}^{3+}) = 0.68 \text{ \AA}$ , leads to an increase in lattice parameters (Table 3.1), and also to the appearance of weak reflections of the nickel oxide phase and praseodymium oxychloride on the XRD patterns. The appearance of the peaks corresponding to trace amounts of praseodymium  $\text{PrOCl}$  oxychloride is due to the use as a ruthenium precursor of the chlorinated  $\text{RuOCl}_3$  [211].



	1	2	3	4	5	6	7
Pr	64,6	66,6	62,9	63,5	67,0	66,1	64,8
Fe	24,1	24,5	29,6	26,8	24,4	23,1	26,5
Ni	11,3	8,9	7,5	9,8	8,6	10,8	8,7

**Figure 3.1.4.** TEM micrographs and calculated from EDX microanalysis element's molar fractions (%) of  $\text{PrFe}_{0.7}\text{Ni}_{0.3}\text{O}_3$

The presence of impurity phases for the initial perovskites  $\text{LnFe}_{1-x-y}\text{Ni}_x\text{M}_y\text{O}_3$  is determined by the nature and content of the cation replacing Fe. The XRF data for some compositions are presented in Figure 3.1.3. Samples with a nickel and cobalt content of 0.3 do not contain impurity phases. With an increase in the nickel content to  $x = 0.4$ , an NiO impurity [JCPDF 47-1049]

appears, whereas all samples containing Co are single-phase. The homogeneous distribution of the elements in single-phase samples was confirmed by electron microscopy with EDX analysis (Figure 3.1.4).

### Supported 5%Ni(Co)/PrFeO<sub>3</sub>

The XRD patterns of the Ni and Co supported on PrFeO<sub>3</sub><sup>[700]</sup> are given in Fig. 3.1.5. For the sample 5%Co/PrFeO<sub>3</sub><sup>[700]</sup>, apart from the peaks of orthorhombic perovskite, the peaks corresponding to Co<sub>3</sub>O<sub>4</sub> oxide [JCPDF 80-1541] were observed. For the 5% Ni/PrFeO<sub>3</sub><sup>[700]</sup>, an absence of nickel oxide peaks can be explain by the high dispersy of the phase.

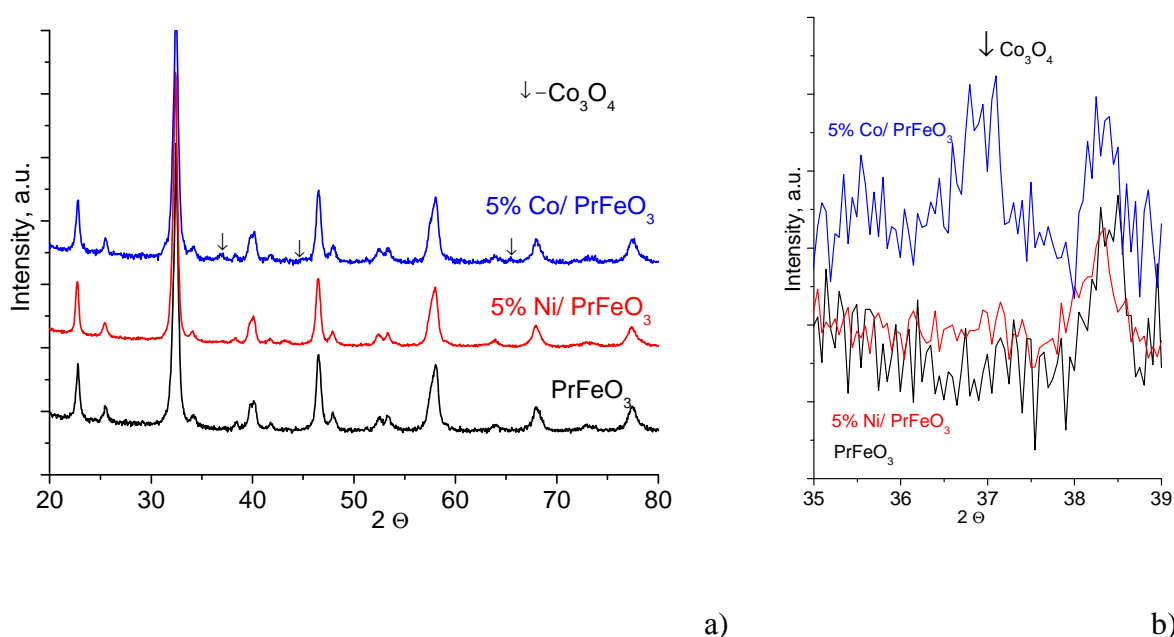


**Figure 3.1.5.** X-ray diffraction patterns obtained for supported 5%Ni(Co)/PrFeO<sub>3</sub><sup>[700]</sup> for 2 $\theta$  **a)** 20-80° and **b)** 35-39°

To understand the state of Ni in the samples 5%Ni/PrFeO<sub>3</sub><sup>[700]</sup> and 5%Ni/PrFeO<sub>3</sub><sup>[900]</sup>, the TEM microscopy was used. The images of 5% Ni/PrFeO<sub>3</sub><sup>[700]</sup> and 5% Ni/PrFeO<sub>3</sub><sup>[900]</sup> samples (Fig. 3.1.6) indicate nickel oxide formation of on the surface with the considerable difference in the particle size depending on the support's calcinations temperature. In the case of 5% Ni/PrFeO<sub>3</sub><sup>[900]</sup>, large particles of nickel oxide forming agglomerates on the surface are observed, while for the 5% Ni/PrFeO<sub>3</sub><sup>[700]</sup> NiO particles are well dispersed and have an average size of 5-30 nm. The data obtained are consistent with the support's textural properties revealed: because of the higher specific surface area of PrFeO<sub>3</sub> calcined at 700 °C (Table 3.1.1) compared with the PrFeO<sub>3</sub><sup>[900]</sup> one, the dispersion of the NiO phase formed after deposition in this case is much higher and the particles are more evenly distributed over the surface.



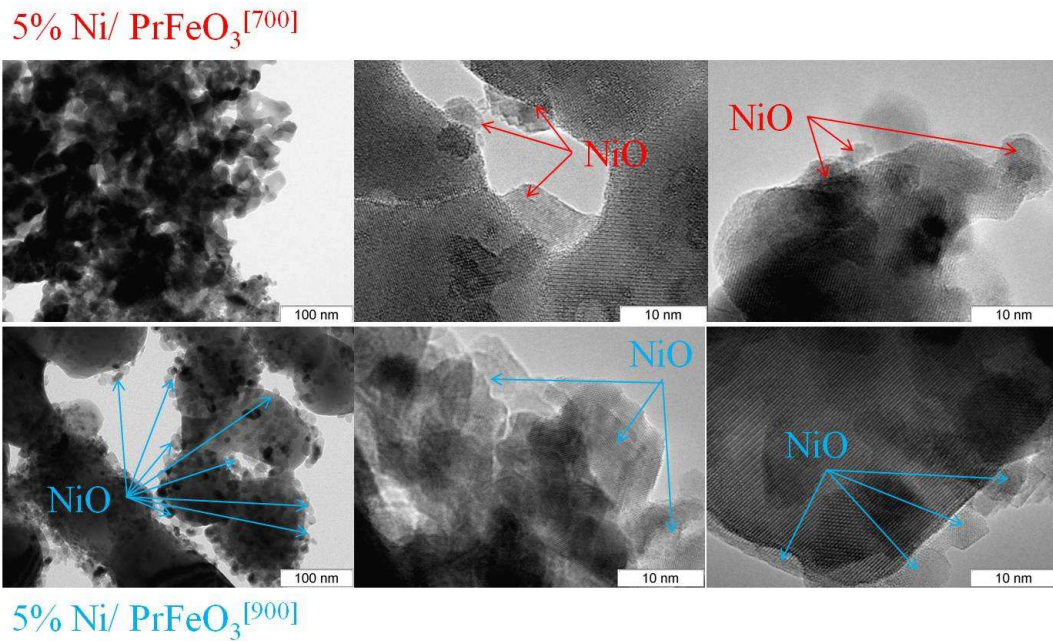


**Figure 3.1.6.** TEM micrographs of 5%Ni/PrFeO<sub>3</sub><sup>[700]</sup> (above) и 5%Ni/PrFeO<sub>3</sub><sup>[900]</sup> (bottom)

### 3.1.2. Effect of the chemical composition and synthesis method on the perovskite reducibility

Reducibility of the perovskites was studied using temperature-programmed reduction with hydrogen (TPR-H<sub>2</sub>). The results obtained are shown in Figures 3.1.7, a-d.

#### *Massive LnFe<sub>1-x-y</sub>M<sub>x</sub>Ru<sub>y</sub>O<sub>3</sub>*

The reduction patterns of the unsubstituted sample PrFeO<sub>3</sub><sup>[900]</sup> (Fig. 3.1.7, a) show two weakly intense broad peaks with maxima at 412 and 480 °C, corresponding to the reduction of Fe<sup>4+</sup> to Fe<sup>3+</sup> and Fe<sup>3+</sup> to Fe<sup>2+</sup> within the perovskite structure without changing the phase composition [220, **Erreur ! Signet non défini.**]. The absorption of hydrogen at temperatures above 600 °C corresponds to a further partial reduction of the iron cations to the Fe<sup>0</sup> state [260]. For the substituted perovskites LnFe<sub>1-x-y</sub>Ni<sub>x</sub>M<sub>y</sub>O<sub>3</sub>, the active metal's (Ni or Co) reduction temperature depends on the perovskite chemical composition (Figures 3.1.7 b-d).

For the perovskites LnFe<sub>0.7</sub>Ni<sub>0.3</sub>O<sub>3</sub> and LnFe<sub>0.7</sub>Co<sub>0.3</sub>O<sub>3</sub>, (Ln = La, Pr), which do not contain ruthenium, there are two peaks of hydrogen absorption on the TPR-H<sub>2</sub> patterns (Fig. 3.1.7, b). A weak-intensive peak in the temperature range below 500 °C corresponds to the reduction of cations Ni<sup>3+</sup> → Ni<sup>2+</sup> (Co<sup>3+</sup> → Co<sup>2+</sup>) and Fe<sup>4+</sup> → Fe<sup>3+</sup> in the perovskite structure, with cobalt reduction occurring at higher temperatures (380-390 °C) compared to nickel one (350- 360 °C) [255, 256].

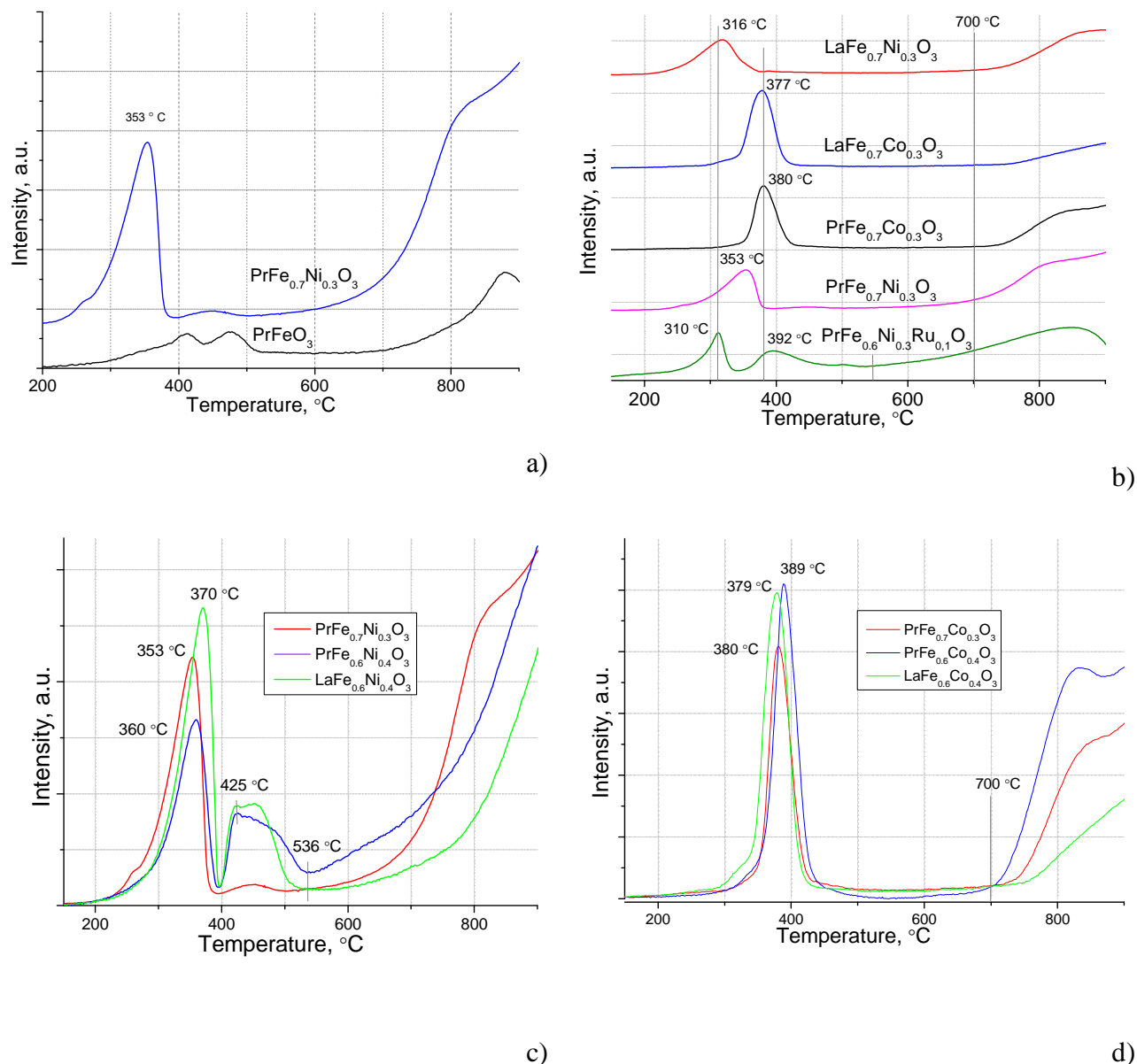


**Figure 3.1.7.** TPR-H<sub>2</sub> spectra of LnFe<sub>1-x-y</sub>Ni<sub>x</sub>M<sub>y</sub>O<sub>3</sub>, calcined at 900 °C

The unresolved intense peak above 600 °C refers to the further reduction of nickel/cobalt cations to the metal state  $\text{Ni}^{2+} \rightarrow \text{Ni}^0$  ( $\text{Co}^{2+} \rightarrow \text{Co}^0$ ), as well as partial reduction of iron  $\text{Fe}^{2+} \rightarrow \text{Fe}^0$  [205]. Furthermore, for Pr-containing samples the high-temperature reduction peak is shifted to low temperatures with respect to La-containing one (Fig. 3.1.7, b). It can be explained by the less stable praseodymium-based perovskite structure due to the contraction of the perovskite lattice shown by XRD and confirmed also by the tolerance factor values for these compositions [Table 3.1].

The Ru introduction in the perovskite composition  $\text{PrFe}_{0.6}\text{Ni}_{0.3}\text{Ru}_{0.1}\text{O}_3$  (Figure 3.1.7, b) leads to the appearance of two medium-intensity hydrogen absorption peaks in the low-temperature region (310 and 392 °C), corresponding to the reduction of cations  $\text{Ru}^{3+} \rightarrow \text{Ru}^0$  and/or  $\text{Ni}^{3+} \rightarrow \text{Ni}^{2+}$



<sup>+</sup> in the perovskite structure [206, 261, 262]. The high-temperature peak becomes much wider, appears already at 550 °C and has a maximum at 850 °C, which indicates an easier reduction of nickel from the structure.

The TPR-H<sub>2</sub> data for samples with different nickel and cobalt contents are presented in Figures 3.1.7, c), d). With the nickel content increase to  $x = 0.4$  both in the La- and Pr-containing perovskites, a peak at the 420-500 °C region appears corresponding to the reduction of the individual NiO oxide whose presence is shown by the XRD method (Figure 3.1.3).

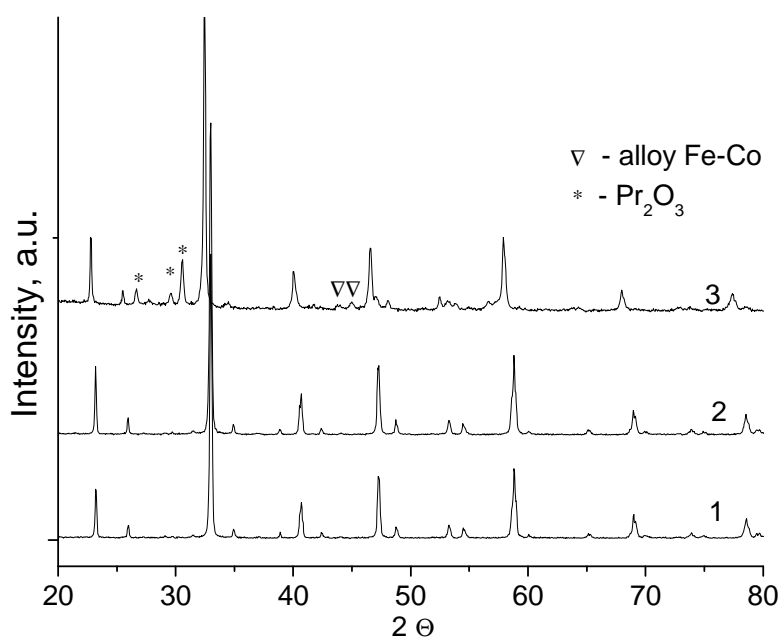
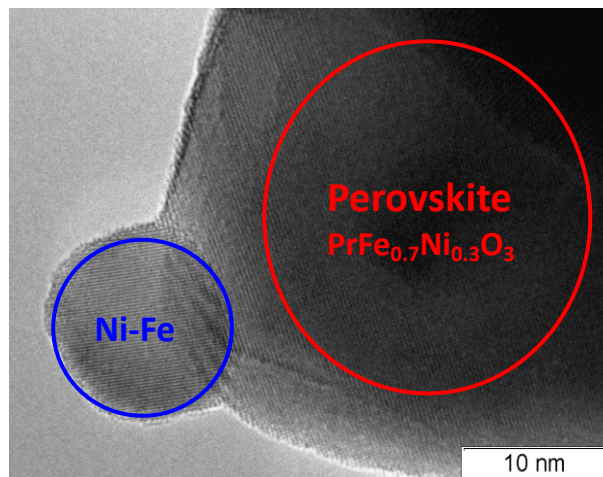
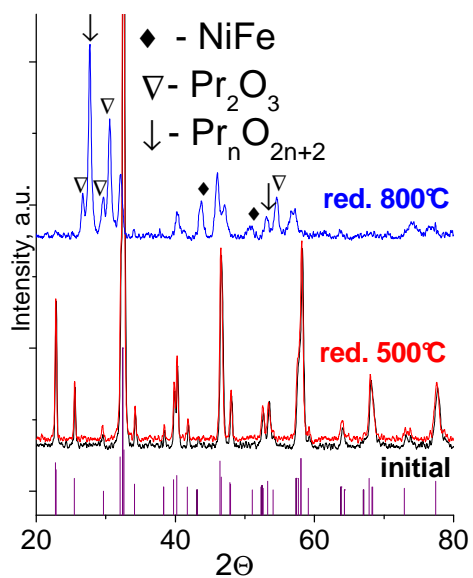


**Figure 3.1.8.** X-ray diffraction patterns obtained for PrFe<sub>0.6</sub>Co<sub>0.4</sub>O<sub>3</sub>: (1) initial, reduced at (2) 600 and (3) 800 °C

In the case of cobalt-containing perovskites, the cobalt content increase to  $x = 0.4$  does not lead to changes in the reducibility (Figure 3.1.7, d). For all compositions of cobalt-containing perovskites, stability under reducing conditions is observed at temperatures below 600 °C. The formation of the Co-Fe alloy for these systems was demonstrated by the XRD method (Figure 3.1.8) after reduction at 700 °C.



a)

b)

**Figure 3.1.9, a)** – X-ray diffraction patterns obtained for  $\text{PrFe}_{0.7}\text{Ni}_{0.3}\text{O}_3$ : initial (1) and reduced at (2) 600 and (3) 800 °C. The histogram corresponds to the phase  $\text{PrFeO}_3$  [JCPDF 47-0065].

**b)** – TEM micrograph of  $\text{PrFe}_{0.7}\text{Ni}_{0.3}\text{O}_3$  after reduction at 800 °C.

### Supported 5%Ni(Co)/PrFeO<sub>3</sub>

Figure 3.1.10 shows the spectra of TPR-H<sub>2</sub> for PrFeO<sub>3</sub><sup>[700]</sup> and 5% Ni (Co)/PrFeO<sub>3</sub> samples with the supports PrFeO<sub>3</sub> calcined at 700 and 900 °C.

The spectra profiles for the samples 5% Ni/PrFeO<sub>3</sub><sup>[700]</sup> and 5% Ni/PrFeO<sub>3</sub><sup>[900]</sup> show significant differences in the peak position corresponding to the nickel reduction to metallic state.

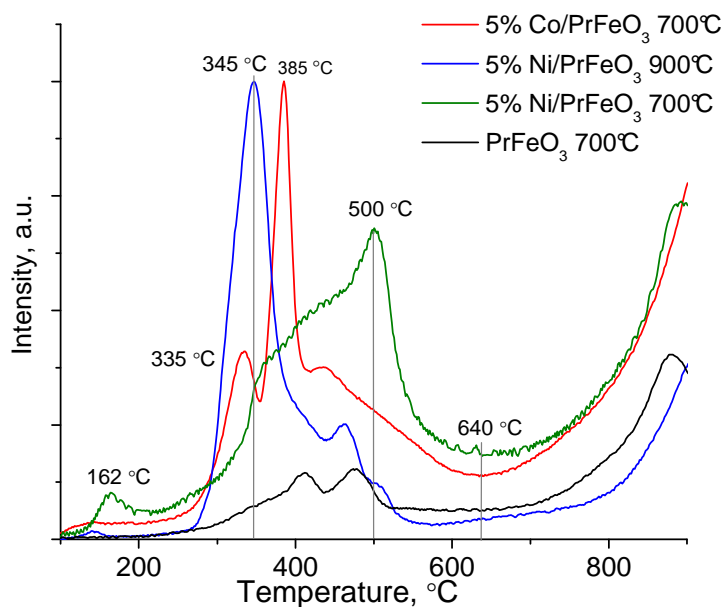


**Figure 3.1.10.** TPR-H<sub>2</sub> spectra of PrFeO<sub>3</sub><sup>[700]</sup> and supported 5%Ni(Co)/PrFeO<sub>3</sub>.

The results obtained are in good agreement with the XRD and TEM data on the size of the nickel oxide phase particles for these samples (Figure 3.1.4). Thus, in the 5% Ni/PrFeO<sub>3</sub><sup>[900]</sup> spectrum with a low SSA, a rather narrow peak at 345 °C with a shoulder at 463 °C is observed, which is related to the reduction of large NiO oxide particles [263], while the pattern for the 5% Ni/PrFeO<sub>3</sub><sup>[700]</sup> is characterized by a broad peak of hydrogen absorption with a maximum at 500 °C, corresponding to the reduction of the oxidized nickel forms firmly bound to the perovskite surface. Peaks with a maximum above 650 °C refer to the reduction of iron in perovskite.

On the TPR pattern of 5% Co/PrFeO<sub>3</sub><sup>[700]</sup>, two peaks with maxima at 335 and 385 °C correspond to the reduction of cobalt from the mixed oxide Co<sub>3</sub>O<sub>4</sub>, the shoulder at 345 °C refers to the reduction of Fe<sup>3+</sup> to Fe<sup>2+</sup> in the support structure [264].

### 3.1.3. Conclusion to Section 3.1

The properties of the mixed ferrites with the general formula  $\text{LnFe}_{1-x-y}\text{Ni}_x\text{M}_y\text{O}_3$  ( $\text{M} = \text{Co}, \text{Ru}, \text{Ln} = \text{Pr}, \text{La}$ ) synthesized by the modified Pechini method, as well as the reference impregnated samples 5%Co(Ni)/PrFeO<sub>3</sub> were studied using a physicochemical method's complex (BET, XRD, TEM with EDX analysis and TPR-H<sub>2</sub>). The shortcut of the results obtained is as follows:

- For all compositions proposed  $\text{LnFe}_{1-x-y}\text{M}_x\text{Ru}_y\text{O}_3$  (including PrFeO<sub>3</sub>) in this work using the modified Pechini synthesis method followed by the calcinations at 900 °C the formation of orthorhombic perovskites was shown with the structural features depending on the nature and/or amount of the cation. In the case of reference impregnated samples 5%Co(Ni)/PrFeO<sub>3</sub>, the embedding of the Ni(Co) cations into the structure does not occur. The samples consist of NiO(Co<sub>3</sub>O<sub>4</sub>) oxides supported on the PrFeO<sub>3</sub> with the particles size depending on a  $T_{\text{calc}}$  of the support: small well-dispersed particles can be obtained only in case of PrFeO<sub>3</sub>, calcined at 700 °C.
- The average SSA of all samples obtained is about 4-10 m<sup>2</sup>/g.
- The presence of impurity phases for the initial perovskites  $\text{LnFe}_{1-x-y}\text{Ni}_x\text{M}_y\text{O}_3$  is determined by the nature and content of the cation replacing Fe. All samples are single-phased except the ones with the nickel content of  $x = 0.4$  - NiO impurity appears in this case.
- Reducibility of individual perovskite depends on its composition and doping cations, but in general for all perovskites the same reduction tendency is observed: up to 500°C in hydrogen flow the structure remains stable (according to TPR-H<sub>2</sub> data up to 100% of Ni<sup>3+</sup>(Co<sup>3+</sup>) reduced to Ni<sup>2+</sup>(Co<sup>2+</sup>) within the perovskite structure). Further increasing of temperature up to 800°C leads to a Ni(Co) and Fe metallic particles partially emerge from the perovskite and stabilized on the surface of oxide with simultaneous formation of Pr oxides phases. Perovskite reducibility depends both on the nature of the lanthanide and transition metal: Pr-containing samples are reduced more easily than La-containing, and Ni-containing are reduced more easily than Co-containing.

### 3.2. Catalytic activity of the $\text{LnFe}_{1-x-y}\text{M}_x\text{Ru}_y\text{O}_3$ in steam reforming of oxygenates.

#### 3.2.1. TPR- $\text{C}_2\text{H}_5\text{OH}$

The TPR- $\text{C}_2\text{H}_5\text{OH}$  method used for the study of the most promising nickel containing samples provides important information on the ethanol conversion route, depending on the catalyst composition. The results obtained are presented in Figure 3.2.1.

In general, for the samples studied, the ethanol interaction with initial oxidized perovskites occurs by the similar regularities. The main products ( $\text{H}_2$ ,  $\text{CO}$  and  $\text{CO}_2$ ) formation begins at 350-400 °C, the concentrations increase with the temperature increasing.

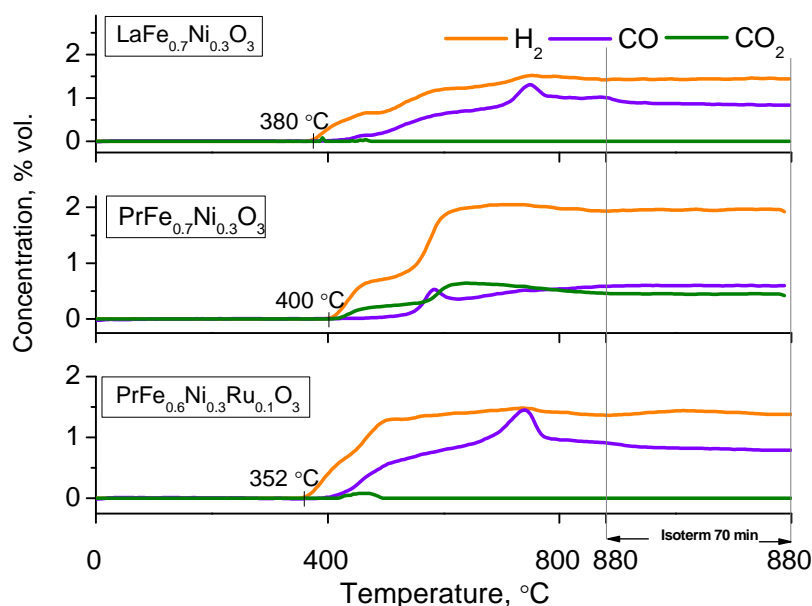


**Figure 3.2.1.** TPR- $\text{C}_2\text{H}_5\text{OH}$  patterns of Ni-based perovskites: dependency of the  $\text{H}_2$ ,  $\text{CO}$  и  $\text{CO}_2$  concentrations on temperature

Onset temperature of the products appearance grows for the catalysts in a row  $\text{PrFe}_{0.6}\text{Ni}_{0.3}\text{Ru}_{0.1}\text{O}_3 < \text{LaFe}_{0.7}\text{Ni}_{0.3}\text{O}_3 < \text{PrFe}_{0.7}\text{Ni}_{0.3}\text{O}_3$ , which is in a good agreement with the TPR- $\text{H}_2$  data (Figure 3.1.7, b). It should be noted that in the case of  $\text{PrFe}_{0.7}\text{Ni}_{0.3}\text{O}_3$  sample, unlike  $\text{LaFe}_{0.7}\text{Ni}_{0.3}\text{O}_3$ , a large amount of carbon dioxide is formed throughout the temperature range, which is due to the high oxidizing power of  $\text{Pr}^{4+}$ - $\text{Pr}^{3+}$  in praseodymium oxide [265, 266]. The ruthenium introduction not only leads to a decrease in the temperature of the interaction initiation, but also to a

simultaneous decrease in the concentrations of hydrogen and CO<sub>2</sub> and an increase in the concentration of CO, indicating a reverse water-gas shift reaction takes place.

For all catalysts, formation of the H<sub>2</sub>, CO, and CO<sub>2</sub> continues in the isothermal regime at 880 °C, after the formation of the active metal phase Ni-Fe (Ru) (according to the data of TPR-H<sub>2</sub> and TEM that was described in detail in the previous section). Decomposition of ethanol and stable operation of catalysts in the isothermal regime despite the fact that, undoubtedly, the formation of surface carbonaceous deposits occur indicates its weak connection with the surface [267, 268]. This is confirmed by the data of temperature-programmed oxidation by water (TPO-H<sub>2</sub>O) on the samples after reduction by ethanol. A typical distribution of products during TPO-H<sub>2</sub>O is shown in Figure 3.2.2 for the sample LaFe<sub>0.7</sub>Ni<sub>0.3</sub>O<sub>3</sub>. The simultaneous absorption of water and the formation of hydrogen at 400 °C indicate the oxidation of the perovskite reduced. When a certain surface concentration is reached, the reactive oxygen formed begins to interact with the carbonaceous sediments, releasing CO and CO<sub>2</sub>. For all catalysts, the carbon oxidation process is generally complete at a temperature below 800 °C, which indicates the high reactivity of loosely bound carbonaceous deposits.

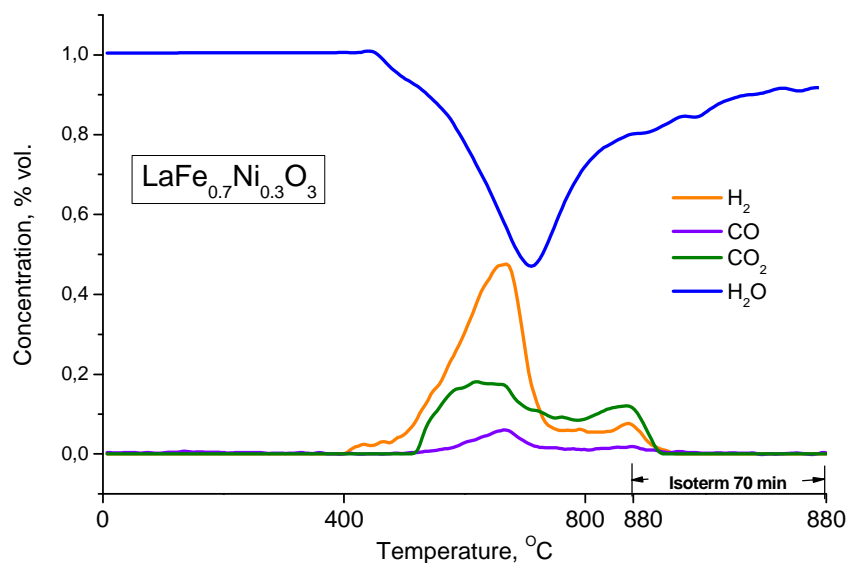


**Figure 3.2.2.** TPO-H<sub>2</sub>O patterns of LaFe<sub>0.7</sub>Ni<sub>0.3</sub>O<sub>3</sub> after TPR-C<sub>2</sub>H<sub>5</sub>OH: dependency of the H<sub>2</sub>, CO и CO<sub>2</sub> concentrations on temperature

### 3.2.2. Catalytic activity in ethanol steam reforming

Figure 3.2.3 shows the ethanol conversion, hydrogen yield and product distribution obtained in a blank experiment (quartz-filled reactor, the contact time of 70 ms, the composition of the reaction mixture  $C_2H_5OH:H_2O:N_2 = 1:4:5$ , the temperature range 650- 825 °C). As can be seen from the graphs, the ethanol conversion at temperatures below 700 °C does not exceed 20% and increases with temperature, reaching a maximum value of 94% at 825 °C. The hydrogen yield remains low and does not exceed 20% over the entire temperature range. The main reaction products are carbon monoxide, methane and ethylene; selectivity for  $CO_2$  is zero throughout the temperature range.

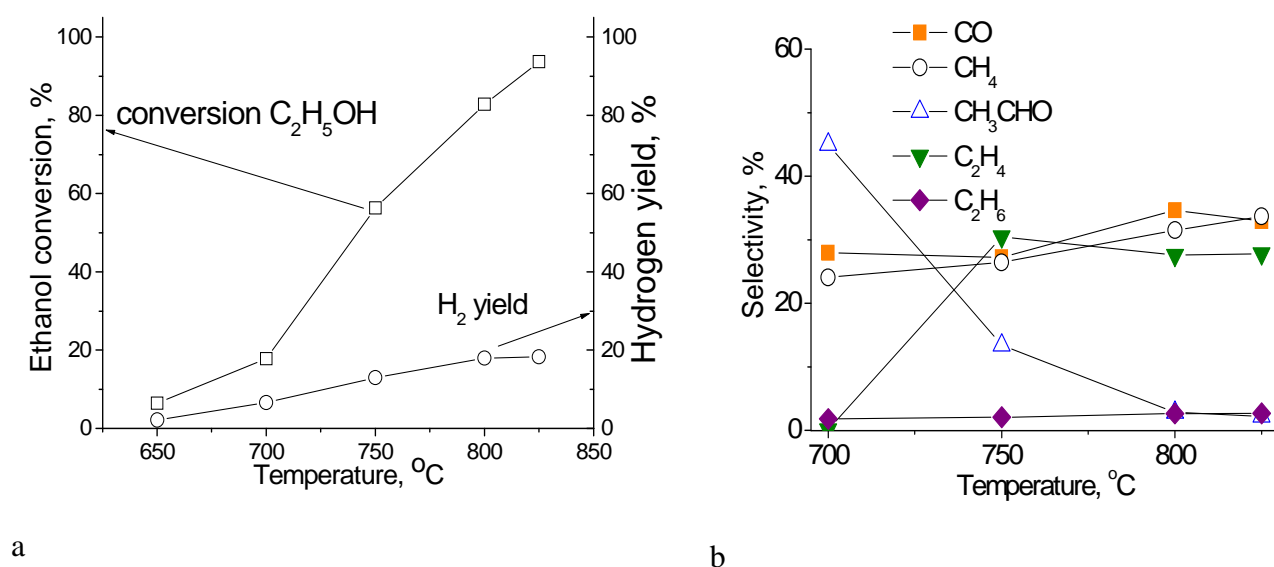
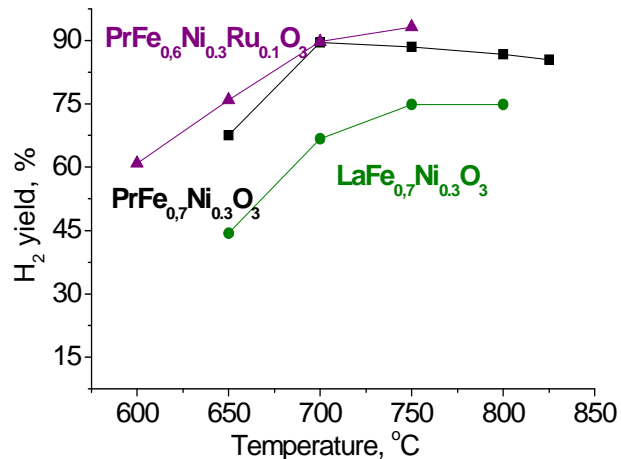
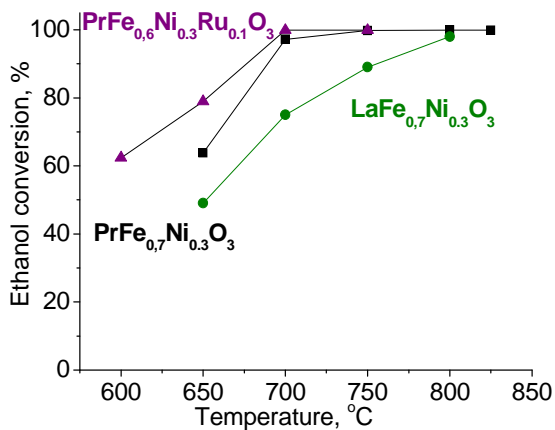


**Figure 3.2.3.** Ethanol conversion, hydrogen yield and products selectivity obtained for the blank experiment in the temperature range 650-825 °C.

All catalysts based on  $LnFe_{1-x-y}Ni_xM_yO_3$  perovskites were tested in a steam reforming reaction of ethanol under conditions used in the blank experiment. Taking into account the TPR- $H_2$  data, the initial perovskites were preliminarily reduced in hydrogen at 800 °C to form the active phase.

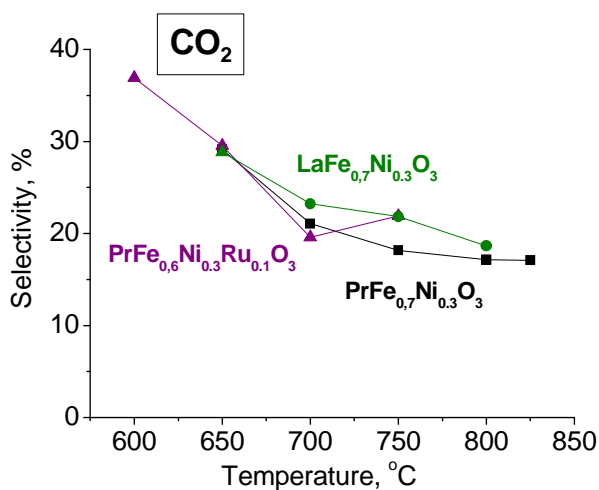
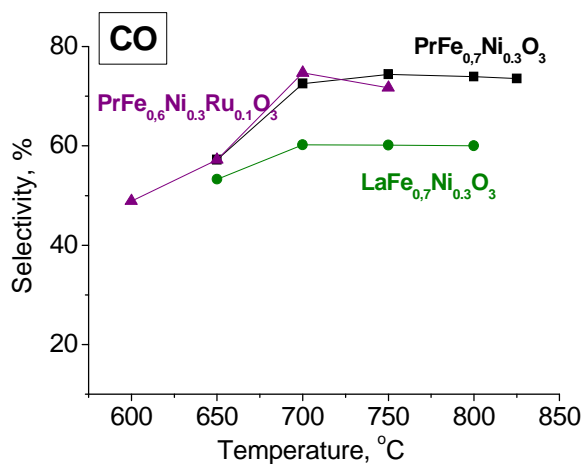
The temperature dependences of the ethanol conversion, hydrogen yield and selectivities for the main and by-products are shown in Figures 3.2.4 to 3.2.6.

Figure 3.2.4 shows the results of tests of nickel-containing samples. In general, similar dependences are observed for all samples of  $LnFe_{1-x-y}Ni_xRu_yO_3$  – high values of ethanol conversion are achieved already at a temperature of 700 °C, and the main products of the reaction are hydrogen, CO and  $CO_2$ .



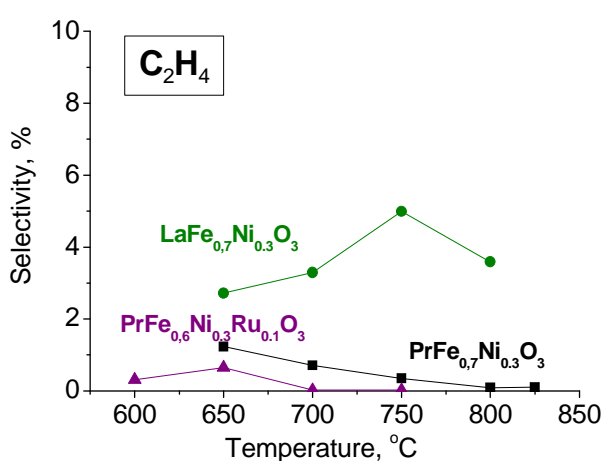
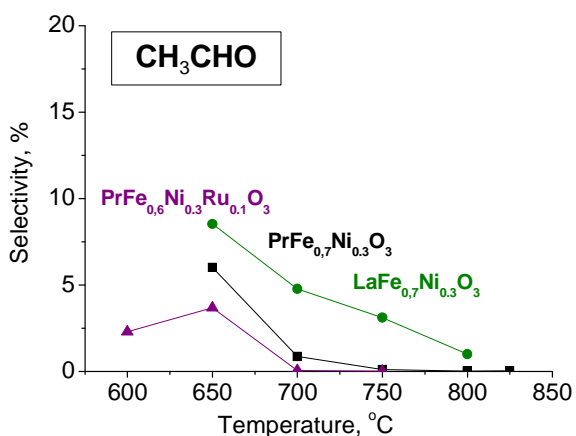
a)

b)



c)

d)



e)

f)

**Figure 3.2.4.** Temperature dependences of ethanol conversion, hydrogen yield, and selectivities for main products for Ni-containing catalysts in steam reforming of ethanol. Catalyst grain size 0.25-0.5 mm, contact time 0.07 s, H<sub>2</sub>O:EtOH = 4



Wherein, samples containing praseodymium show higher activity. As can be seen from Figures 3.2.4a), b), for the  $\text{PrFe}_{0.7}\text{Ni}_{0.3}\text{O}_3$  sample at 700 °C, the ethanol conversion reaches 100% and the hydrogen yield is 90%, whereas for the  $\text{LaFe}_{0.7}\text{Ni}_{0.3}\text{O}_3$  sample under these conditions these values are 75% and 60%, respectively. The presence of ruthenium in the catalyst helps to lower the temperature of the reaction start, which is consistent with the data of TPR- $\text{H}_2$  and TPR- $\text{C}_2\text{H}_5\text{OH}$  for the sample  $\text{PrFe}_{0.6}\text{Ni}_{0.3}\text{Ru}_{0.1}\text{O}_3$ . Low selectivity for ethylene (<10%) and the presence of acetaldehyde (selectivity 15-60%) is observed for all massive perovskite catalysts, which indicates the dehydrogenation reaction of ethanol as the main route for its steam reforming.

The activity of cobalt-based catalysts is significantly lower than nickel-containing ones. The data on ethanol conversion and hydrogen yield for  $\text{PrFe}_{0.7}\text{Ni}_{0.3}\text{O}_3$  and  $\text{PrFe}_{0.7}\text{Co}_{0.3}\text{O}_3$  presented in Fig. 3.2.5 indicate low activity of cobalt-containing samples even at high temperature. High selectivities for acetaldehyde and ethylene confirm low rate of the further transformation of these intermediates to  $\text{C}_1$  products and  $\text{H}_2$ . An increase in the cobalt content to  $x = 0.4$  does not lead to significant improvements in catalytic activity, most likely due to the difficulty of cobalt reduction from the perovskite structure shown by the TPR- $\text{H}_2$  method.

Comparison of the catalytic activity of massive and supported catalysts is also shown in Figure 3.2.5. In general, the supported catalysts are more active at low temperatures. Among the catalysts deposited on  $\text{PrFeO}_3$ , the conversion of ethanol increases in the series of 5% Ni /  $\text{PrFeO}_3$  <sup>[700]</sup> < 5% Co /  $\text{PrFeO}_3$  <sup>[700]</sup> < 5% Ni /  $\text{PrFeO}_3$  <sup>[900]</sup>. The high conversion of ethanol 5% Ni /  $\text{PrFeO}_3$  <sup>[900]</sup> below 600 ° C is explained by easier reduction of nickel, shown by the TPR- $\text{H}_2$  method.

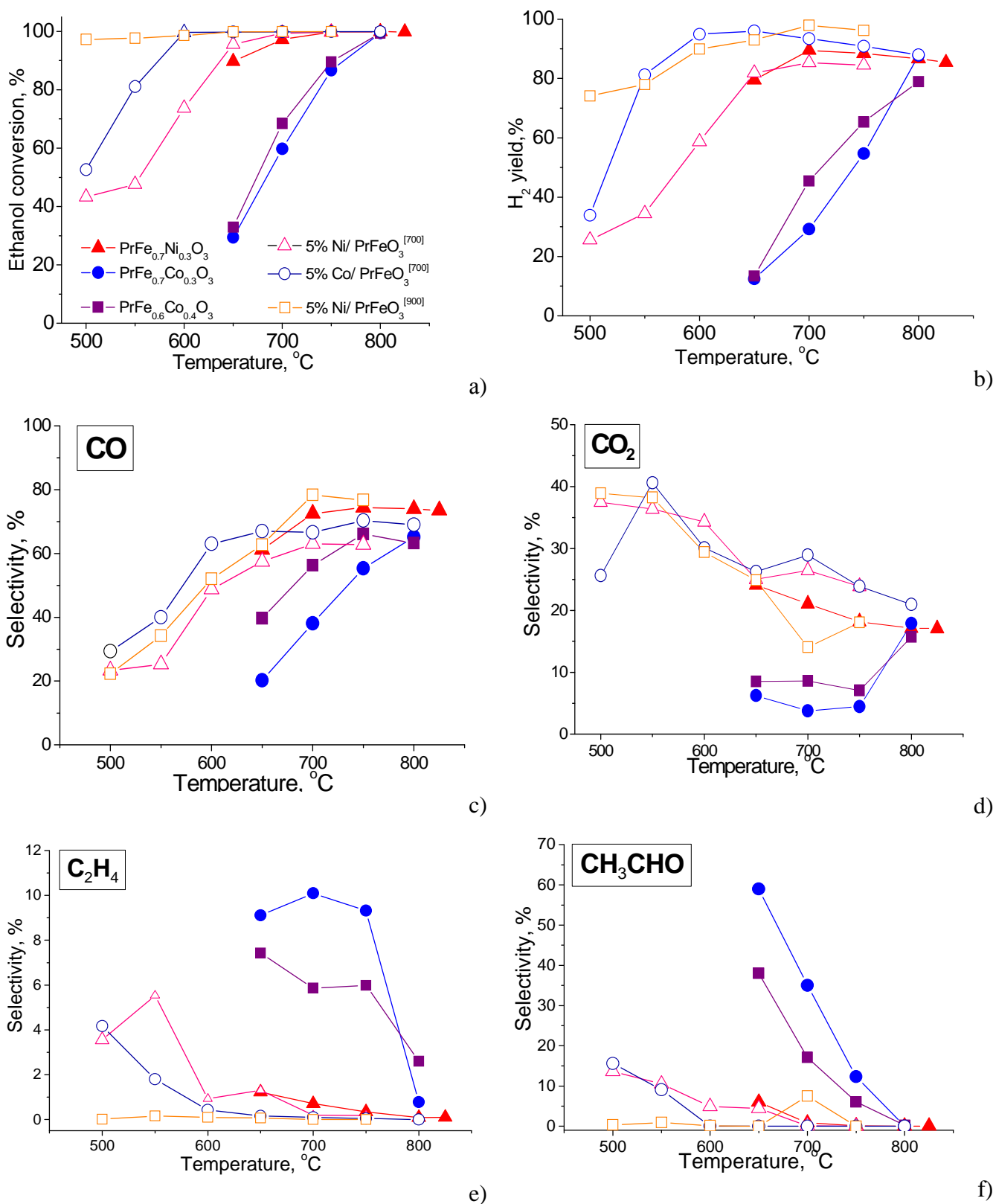


**Figure 3.2.5.** Temperature dependences of ethanol conversion, hydrogen yield, and selectivities for main products for the catalysts with different active metal (Ni/Co) and synthesis method (massive/supported) in steam reforming of ethanol.

### 3.2.3. Effect of the catalyst's composition and synthesis method on stability in ethanol steam reforming

Important information on the catalyst's stability and the active sites evolution can be obtained by studying the catalyst samples in and after long-term testing at a constant temperature. Figure 3.2.6, a) shows the dependence of the ethanol conversion on the time-on-stream for the perovskite-based catalyst in a standard reaction mixture at 650 ° for 6 hours. As can be seen from the graph, the Ni-based catalysts exhibit relatively stable catalytic activity in the tests, especially the PrFe<sub>0.6</sub>Ni<sub>0.3</sub>O<sub>3</sub> one.

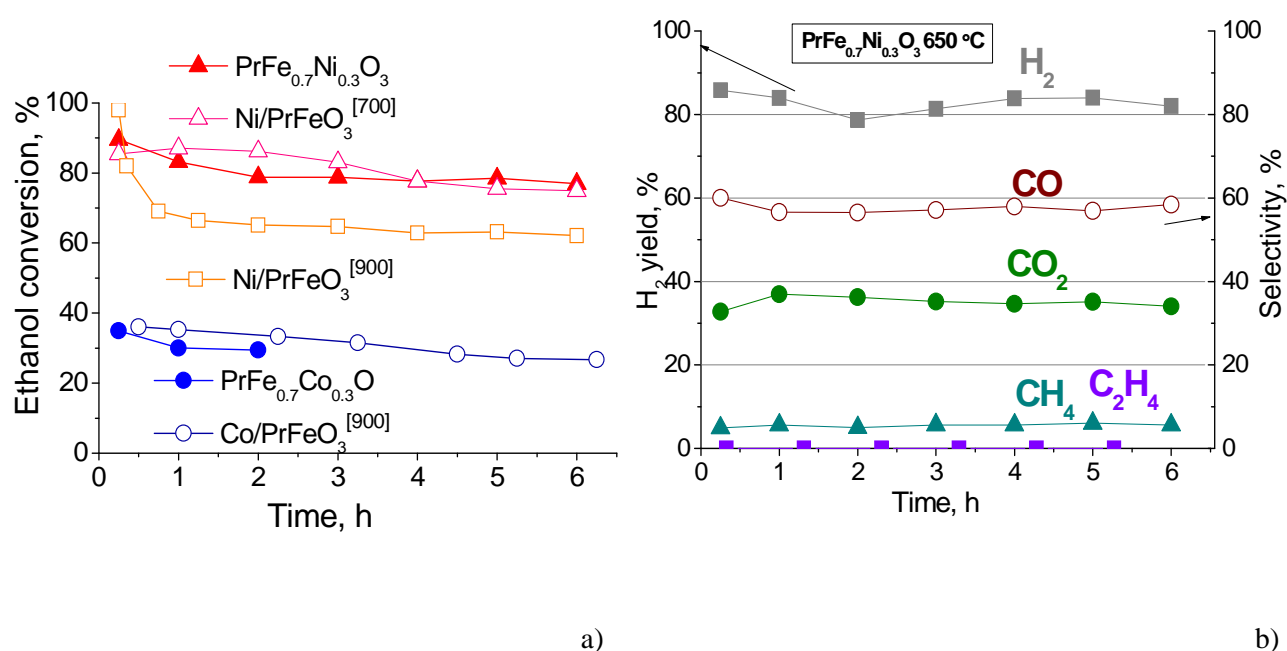


**Figure 3.2.6.** Results of the long-term steam reforming of ethanol tests at 650 °C: **a)** ethanol conversion for the catalysts with different active metal (Ni/Co) and synthesis method (massive/supported); **b)** hydrogen yield and products selectivities for the PrFe<sub>0.6</sub>Ni<sub>0.3</sub>O<sub>3</sub> catalyst

X-ray diffraction analysis of this catalyst after reaction, as well as results for all perovskites-based samples LnFe<sub>1-x-y</sub>Ni<sub>x</sub>M<sub>y</sub>O<sub>3</sub>, shows a partial decomposition of the perovskites precursor with the formation of the Ni-Fe (Ru) alloy particles and lanthanides oxides [269]. The resulting highly disperse alloy particles are less susceptible to carbonization and provide a high stability to sintering during the steam reforming reaction, which was confirmed by the TEM method. For example, in Figure 3.2.7, above, and Figure 3.2.8, a), electron micrographs for the most stable samples of PrFe<sub>0.7</sub>Ni<sub>0.3</sub>O<sub>3</sub> and PrFe<sub>0.6</sub>Ni<sub>0.3</sub>Ru<sub>0.1</sub>O<sub>3</sub> are shown, respectively.

In the case of 5% Ni (Co)/PrFeO<sub>3</sub> samples obtained by impregnation, the Ni/Co metal particles tend to sintering both for PrFeO<sub>3</sub><sup>[900]</sup> and PrFeO<sub>3</sub><sup>[700]</sup> supports, the effect is more pronounced in the second case (Figure 3.2.7, bottom and 3.2.8, b).

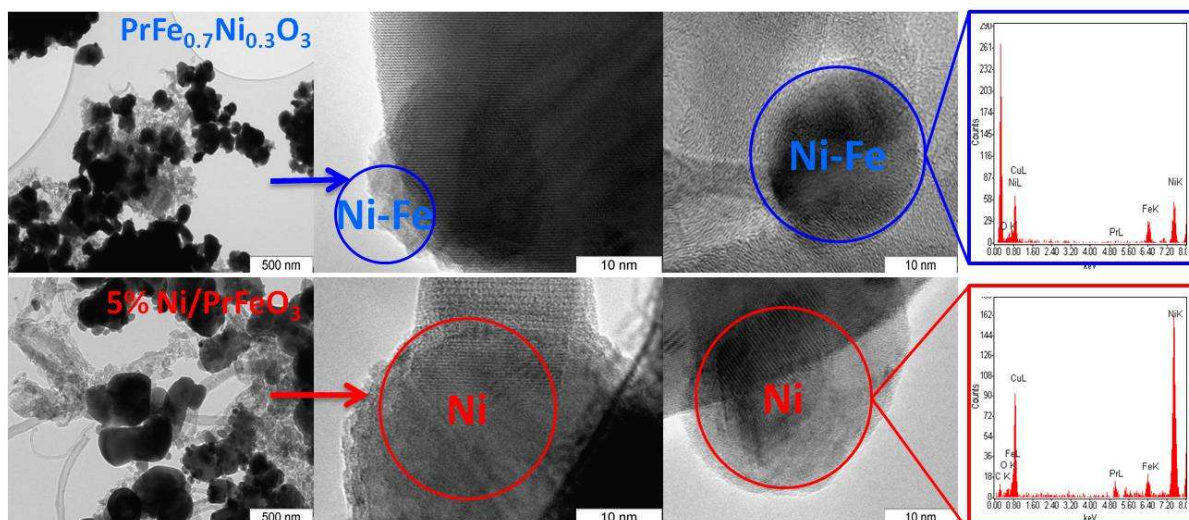
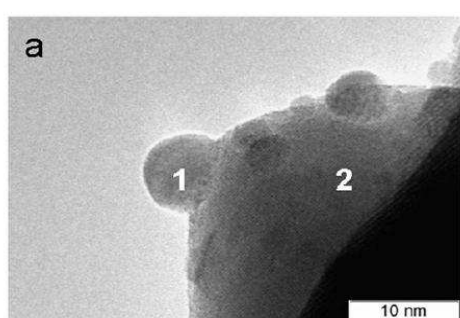
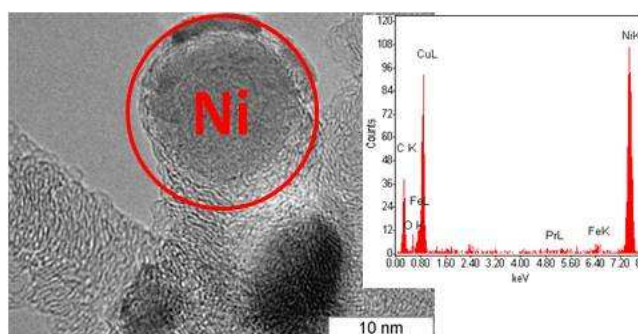


**Figure 3.2.7.** TEM images with EDX data for  $\text{PrFe}_{0.7}\text{Ni}_{0.3}\text{O}_3$  (top) and 5% Ni/ $\text{PrFeO}_3^{[900]}$  (bottom) samples after tests in ethanol steam reforming at 650 °C



a) atomic %

	Ru	Pr	Fe	Ni
1	46.48	40.03	3.24	10.24
2	7.38	83.17	6.65	2.8



a)

b)

**Figure 3.2.8.** TEM images with EDX data for a)  $\text{PrFe}_{0.6}\text{Ni}_{0.3}\text{Ru}_{0.1}\text{O}_3$  и б) 5% Ni/ $\text{PrFeO}_3^{[700]}$  after tests in ethanol steam reforming at 650 °C

### 3.2.4. Catalytic activity in glycerol steam/oxy-steam reforming

It is known that during the glycerol steam reforming reaction, a wide range of liquid by-product can be produced, which quantitative identification is difficult. In this regard, in order to compare the catalytic activity of various samples, the terms «conversion to gas phase»  $X_g$  and «productivity» for gas products were introduced. The productivity is calculated in units (mol/mol), where (mol) is the number of glycerol moles converted into gas products. The data on the glycerol conversion to gas products  $X_g$  and the distribution of productivities in the gaseous phase, obtained earlier [87] in blank experiment with a reactor filled with SiC, with the reaction mixture  $C_3H_8O_3: H_2O = 1:9$ , gas hourly space velocity of  $28000\text{ h}^{-1}$  and temperature  $650\text{ }^\circ\text{C}$  are shown in Figure 3.2.9.

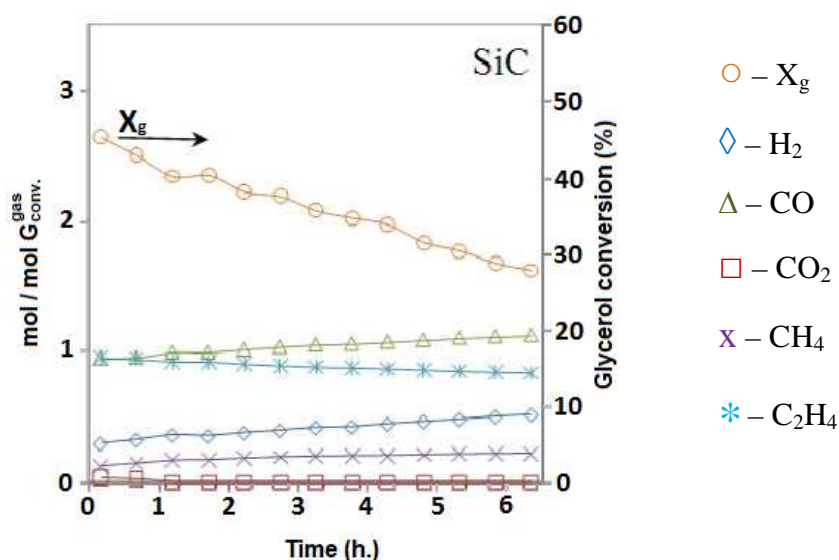


**Figure 3.2.9.** Glycerol conversion to gas  $X_g$  and productivities to the gaseous products in the blank experiment with the reactor filled with SiC ( $C_3H_8O_3: H_2O=1:9$ ,  $GHSV=28000\text{ h}^{-1}$ ,  $T=650\text{ }^\circ\text{C}$ )

To determine the optimal catalyst's pretreatment conditions, the comparative tests with preliminary reduction of the  $LnFe_{1-x-y}Ni_xM_yO_3$  precursors in hydrogen at two temperatures:  $500$  and  $800\text{ }^\circ\text{C}$  (Fig. 3.2.10, a) were carried out. It was shown that the reduction temperature of the initial perovskite affects the stability of the catalyst. At comparable high values of conversion to the gas phase for catalysts  $PrFe_{0.6}Ni_{0.3}Ru_{0.1}O_3^{[red. 500]}$  and  $PrFe_{0.6}Ni_{0.3}Ru_{0.1}O_3^{[red. 800]}$ , the initial hydrogen yield for the sample reduced at  $500\text{ }^\circ\text{C}$  are slightly lower. However, deactivation of the catalyst in this case is slower (Figure 3.2.10, a). Most likely, the decrease in the initial hydrogen productivity is associated with its spending on additional reduction of the catalyst by the reaction mixture. The

formation of metallic Ni-Fe alloy particles after the tests was shown for catalysts in both cases (Figure 3.2.10, b). Further catalytic tests were carried out with the reduction pretreatment at 500 °C.

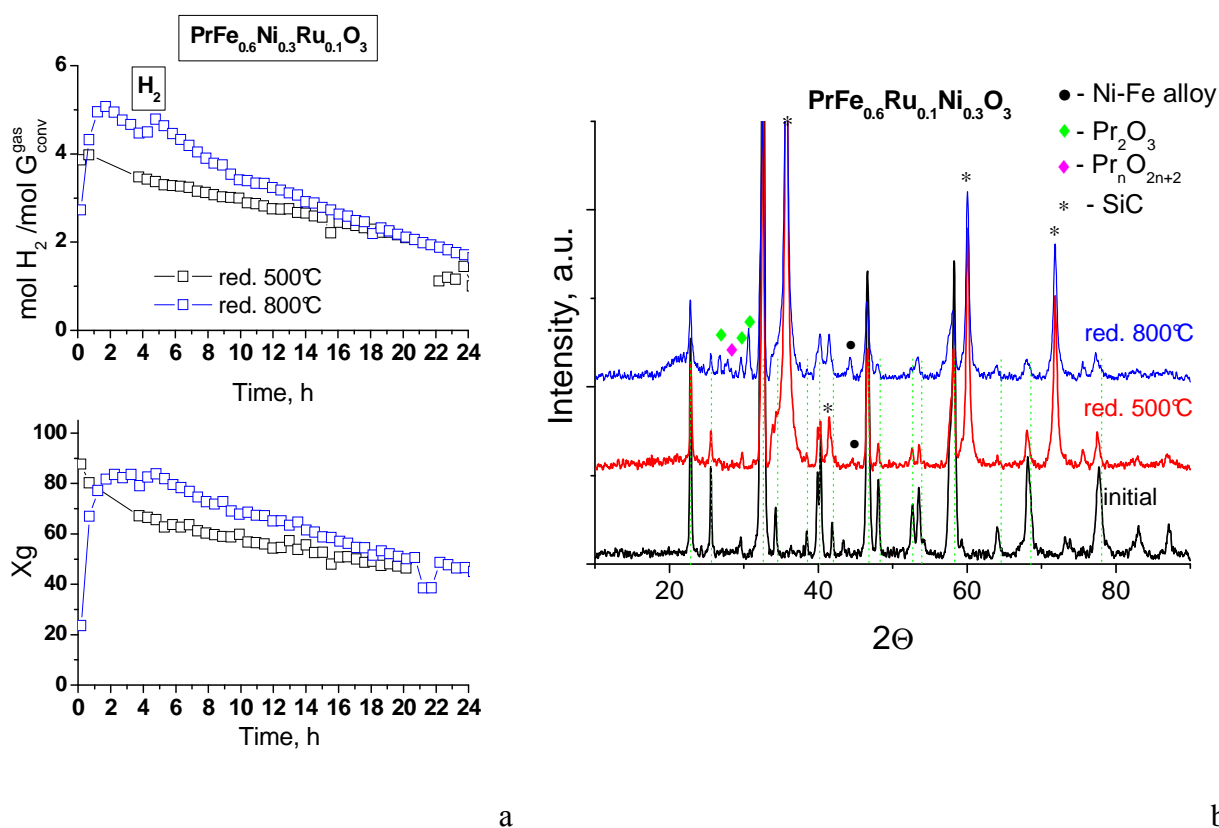


**Figure 3.2.10 a)** Hydrogen productivity and glycerol conversion to gas products  $X_g$  obtained for  $\text{PrFe}_{0.6}\text{Ni}_{0.3}\text{Ru}_{0.1}\text{O}_3$  reduced at 500 and 800 °C in GSR ( $\text{C}_3\text{H}_8\text{O}_3 : \text{H}_2\text{O} = 1:9$ ,  $\text{GHSV} = 28000 \text{ h}^{-1}$ ,  $T=650 \text{ °C}$ ); **b)** XRD patterns of  $\text{PrFe}_{0.6}\text{Ni}_{0.3}\text{Ru}_{0.1}\text{O}_3$ : initial and after GSR reaction with different pretreatment

Figures 3.2.11-3.2.12 depicts the data obtained in GSR reaction for all the catalysts tested. All nickel-containing catalysts show high activity in the glycerol steam reforming reaction, but tend to deactivate after 4-6 hours. A typical distribution of reaction gas products and glycerol conversion to the gas phase for these samples are shown in Figure 3.2.11. Thus, for samples  $\text{PrFe}_{0.7}\text{Ni}_{0.3}\text{O}_3$  and  $\text{La}_{0.7}\text{Pr}_{0.3}\text{Fe}_{0.7}\text{Ni}_{0.3}\text{O}_3$ , a maximum on the curves is observed probably due to perovskite additional reduction in the reaction mixture, followed by a rapid decrease in activity causing by carbonization. The high initial activity of the catalyst based on  $\text{PrFe}_{0.6}\text{Ni}_{0.3}\text{Ru}_{0.1}\text{O}_3$  can be explained by the presence of ruthenium that decreases perovskite reduction temperature below 300 °C, so the active phase formation occurs completely during pretreatment. In addition, the activity of this catalyst decreases gradually and slowly enough, which indicates its greater resistance to carbonization comparing with the non-ruthenium samples. According the Ln cation influence, for praseodymium-based catalysts, higher hydrogen yield and glycerol conversion to the gas phase are observed. The

H<sub>2</sub> and CO<sub>2</sub> productivity, at a close X<sub>g</sub> values, are higher for the sample based on PrFe<sub>0.6</sub>Ni<sub>0.3</sub>Ru<sub>0.1</sub>O<sub>3</sub>.

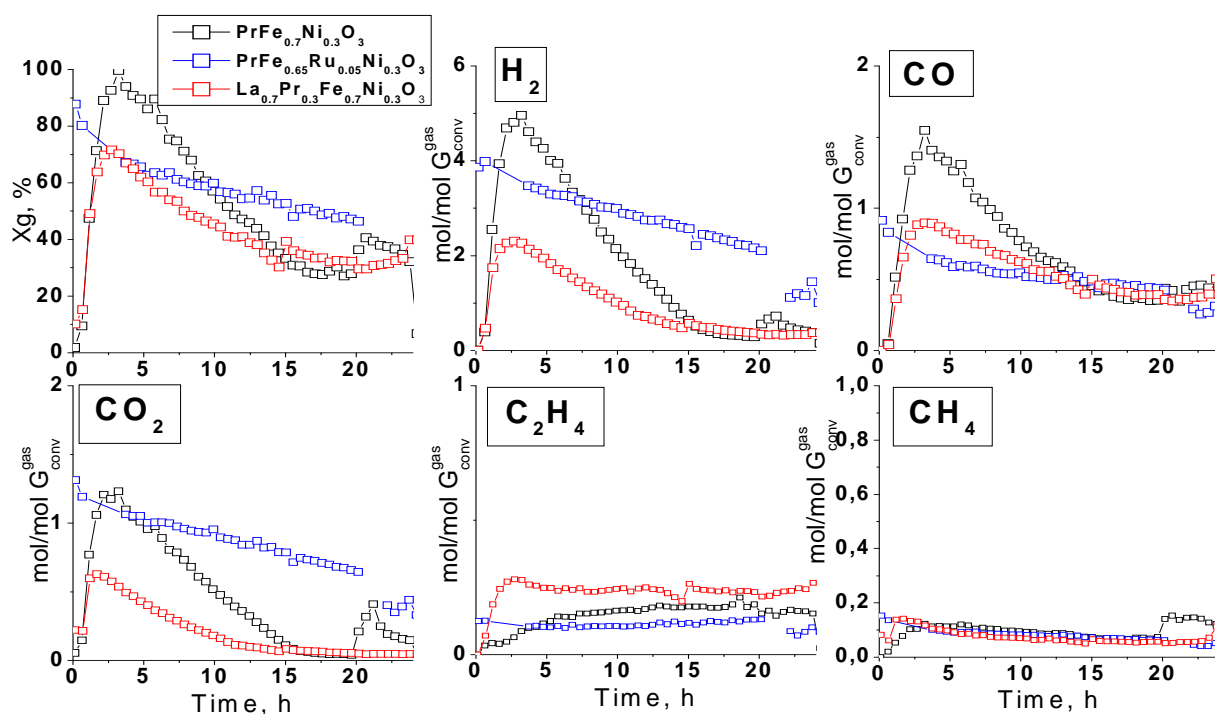


**Figure 3.2.11.** Glycerol conversion to gas X<sub>g</sub> and productivities to the gaseous products P<sub>i</sub> in the glycerol steam reforming reaction (C<sub>3</sub>H<sub>8</sub>O<sub>3</sub>: H<sub>2</sub>O=1:9, GHSV=28000 h<sup>-1</sup>, T=650 °C) obtained for PrFe<sub>0.7</sub>Ni<sub>0.3</sub>O<sub>3</sub>, PrFe<sub>0.6</sub>Ni<sub>0.3</sub>Ru<sub>0.1</sub>O<sub>3</sub> and La<sub>0.7</sub>Pr<sub>0.3</sub>Fe<sub>0.7</sub>Ni<sub>0.3</sub>O<sub>3</sub> samples

Catalytic tests for cobalt-based catalysts, the results are presented in Figure 3.2.12 for PrFe<sub>0.7</sub>Co<sub>0.3</sub>O<sub>3</sub>, shown their low activity in reactions of hydrogen formation. Despite the glycerol conversion X<sub>g</sub> exceeds 70%, the hydrogen productivity for cobalt-containing systems (even with the oxygen addition in GOSR) remains low (0.8 mol H<sub>2</sub>/mol G<sub>conv</sub><sup>gas</sup>), which corresponds to the value for the sample PrFeO<sub>3</sub> without active component (Figure 3.2.12). Most likely, this behavior can be explained by the difficulty of the cobalt reduction from the perovskites structure below 500-650 °C, according to H<sub>2</sub>-TPR data. Significant amount of ethylene in products for this sample also indicates a low selectivity of Co-based group of catalysts.



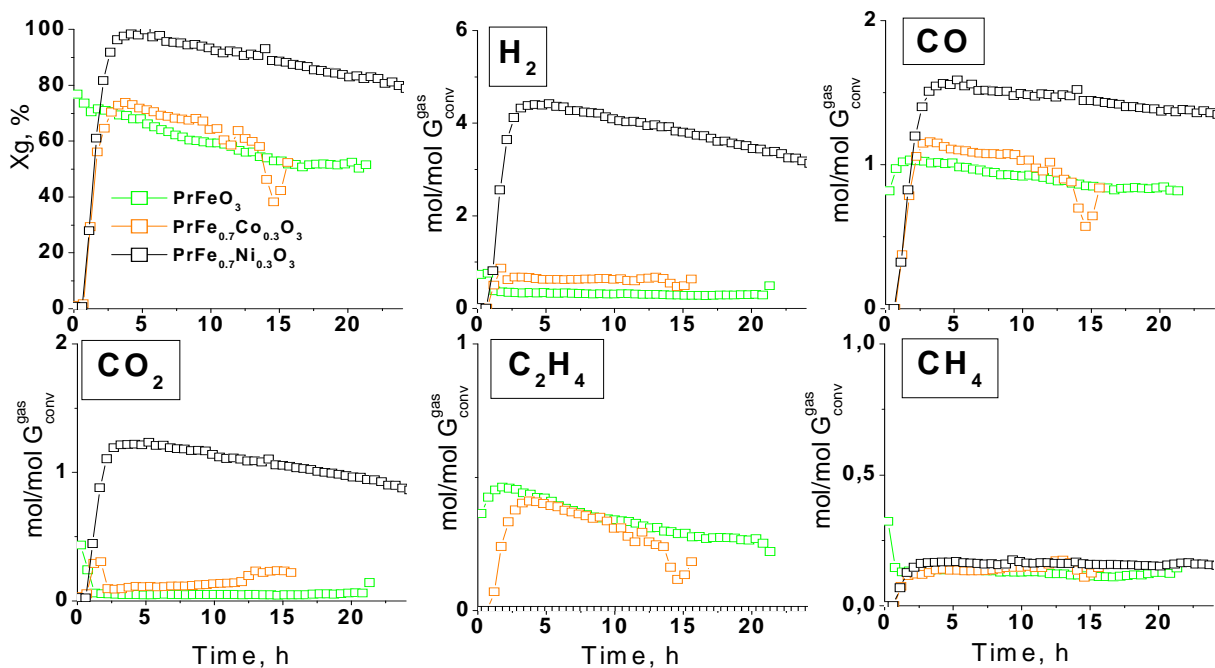


**Figure 3.2.12.** Glycerol conversion to gas  $X_g$  and productivities to the gaseous products  $P_i$  in the glycerol steam reforming reaction ( $C_3H_8O_3: H_2O=1:9$ ,  $GHSV=28000\text{ h}^{-1}$ ,  $T=650\text{ }^\circ\text{C}$ ) obtained for  $PrFeO_3$ ,  $PrFe_{0.7}Co_{0.3}O_3$  и  $PrFe_{0.7}Ni_{0.3}O_3$  samples

The comparative tests with an oxygen addition to the reaction mixture (GOSR) carried out for all the catalysts show that, in general, the activity decreases significantly slowly than that in the GSR case, without loss of productivities for  $H_2$  and  $CO$ . A comparison of the activity in these two reactions for the  $PrFe_{0.7}Ni_{0.3}O_3$  sample is shown in Figure 3.2.13. As it can be seen from the graphs, the maximum values of conversion close to 100 % both in GSR and GOSR cases are achieved approximately after 4 hours of reaction with the hydrogen productivity of 5 and 4.3 mol  $H_2$ /mol  $G_{conv}^{gas}$ , respectively. Significant increase in stability correlates with the absence of ethylene in the reaction products, and consistent with the results of temperature-programmed oxidation (TPO- $O_2$ ) carried out after the reactions show that the amount of carbon deposits is reduced several fold in the GOSR conditions.



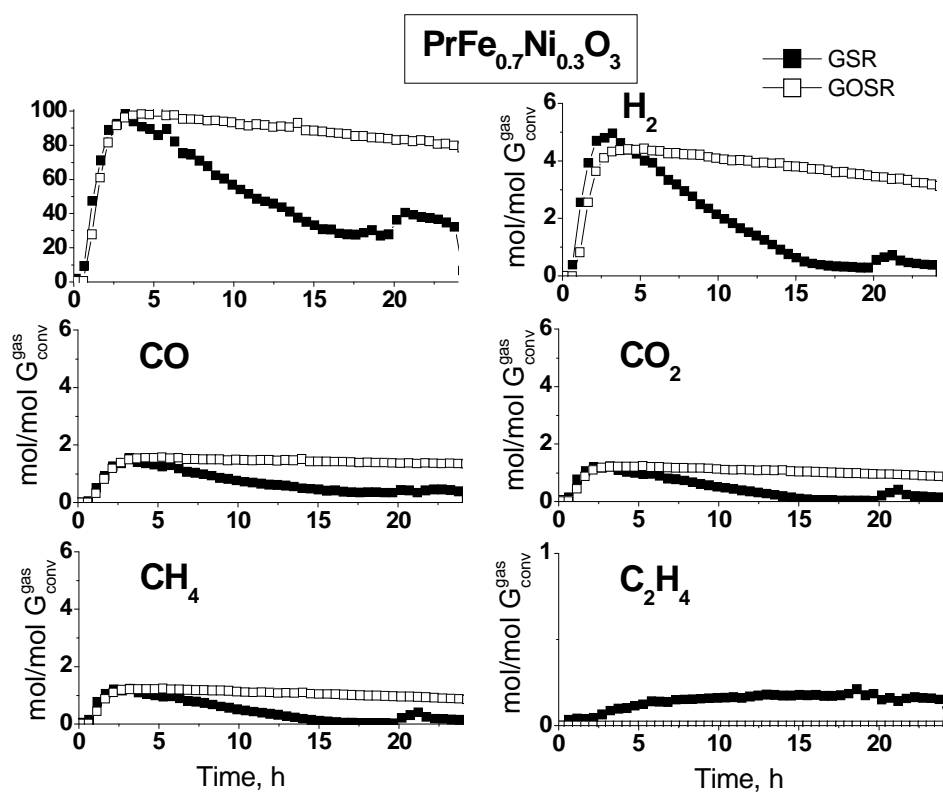


**Figure 3.2.13.** Glycerol conversion to gas  $X_g$  and productivities to the gaseous products  $P_i$  obtained for  $\text{PrFe}_{0.7}\text{Ni}_{0.3}\text{O}_3$  sample in glycerol steam reforming reaction ( $\text{C}_3\text{H}_8\text{O}_3:\text{H}_2\text{O}=1:9$ ,  $\text{GHSV}=28000\text{ h}^{-1}$ ,  $T=650\text{ }^\circ\text{C}$ ) and glycerol oxy-steam reforming reaction ( $\text{C}_3\text{H}_8\text{O}_3:\text{H}_2\text{O}:\text{O}_2 = 1:9:0.25$ ,  $\text{GHSV}=28000\text{ h}^{-1}$ ,  $T=650\text{ }^\circ\text{C}$ )

The TPO- $\text{O}_2$  data for the two most active catalysts  $\text{PrFe}_{0.7}\text{Ni}_{0.3}\text{O}_3$  and  $\text{PrFe}_{0.6}\text{Ni}_{0.3}\text{Ru}_{0.1}\text{O}_3$  after reaction for 24 hours are shown on Figure 3.2.14. Due to the high activity, the strong deactivation with a large amount of carbon deposits occurs for the  $\text{PrFe}_{0.7}\text{Ni}_{0.3}\text{O}_3$ . The presence of Ru reduces the formation of high-temperature stable carbon deposits. Addition of oxygen to the reaction medium allows one to reduce the formation of all forms of carbon deposits, which agrees with a slower decrease in activity for this reaction.

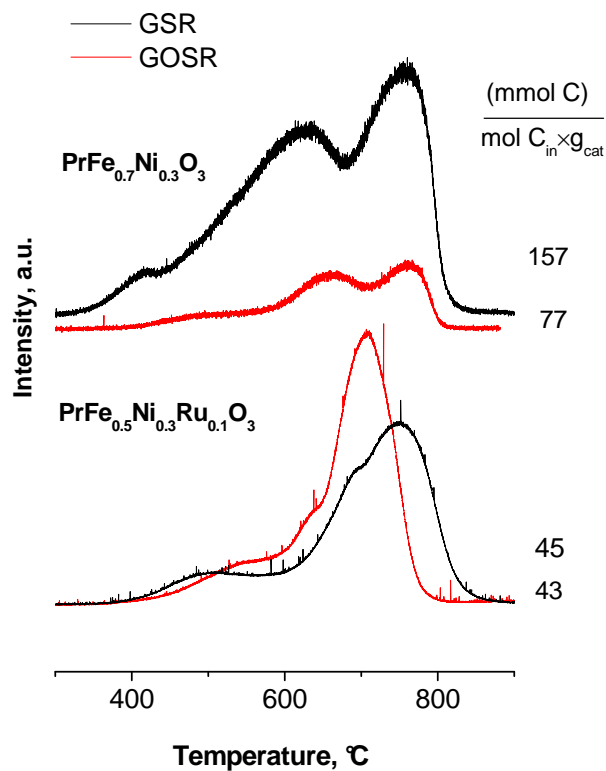


**Figure 3.2.14.** TPO-O<sub>2</sub> data after reaction of GSR and GOSR for PrFe<sub>0.7</sub>Ni<sub>0.3</sub>O<sub>3</sub> and PrFe<sub>0.6</sub>Ni<sub>0.3</sub>Ru<sub>0.1</sub>O<sub>3</sub> catalysts

Thus, in the massive perovskites-based family, the catalyst based on PrFe<sub>0.6</sub>Ni<sub>0.3</sub>Ru<sub>0.1</sub>O<sub>3</sub> is the most active and stable to carbonization in the reactions of steam and oxy-steam reforming of glycerol.

### 3.2.5. Conclusion to Section 3.2

According to the results of catalytic tests, all the  $\text{LnFe}_{1-x-y}\text{Ni}_x\text{M}_y\text{O}_3$  perovskites-based catalysts studied are active in the ethanol steam reforming, glycerol steam and oxy-steam reforming reactions. It is shown that the activity, selectivity and stability of the catalysts depend both on the nature of the lanthanide and the transition metal, and on the catalyst's precursor synthesis method:

- The most active and stable catalysts are the samples containing Pr and Ni. The presence of Ru reduces the formation of carbon deposits. The catalyst based on  $\text{PrFe}_{0.6}\text{Ni}_{0.3}\text{Ru}_{0.1}\text{O}_3$  is the most active and stable to carbonization in the reactions of ethanol steam reforming, steam and oxy-steam reforming of glycerol. For the glycerol steam reforming it was shown that the cobalt-based catalysts have low activity in reactions of hydrogen formation.
- Comparison of the catalytic activity of massive substituted  $\text{PrFe}_{0.6}\text{Ni}_{0.3}\text{Ru}_{0.1}\text{O}_3$  and impregnated 5%Ni(Co)/ $\text{PrFeO}_3$  catalysts shows that the impregnated catalysts are more active at low temperatures, which is explained by easier reduction of nickel. Nevertheless, the rapid deactivation for the impregnated ones is observed. The results both temperature-dependence and stability tests confirms the main hypothesis taken for this investigation: the precursor synthesis method determines the features of the active phase (dispersion, metal-support interaction) formed after reducing pretreatment, which is essential factor defining the stability of the catalysts. Using substituted perovskites  $\text{LnFe}_{1-x-y}\text{Ni}_x\text{M}_y\text{O}_3$  containing active metal in structure as precursors give not only the optimal composition of active metals and great red-ox properties but also a high dispersed well-distributed alloy metal particles with the strong metal-support interaction.
- Analysis of the catalytic data revealed that the main route for the ethanol steam reforming reaction in the presence of perovskite-based catalysts is the dehydrogenation of ethanol to form an intermediate, acetaldehyde, which contributes to the high stability of these samples to carbonization.
- Oxygen addition helps to stabilize catalytic performance in the oxy-steam reforming of glycerol without lose in hydrogen production.

## **CHAPTER 4. SUPPORTED CATALYST'S FAMILY $m\text{LnNi}_{0.9}\text{Ru}_{0.1}\text{O}_3/n\%\text{Mg-}\gamma\text{-Al}_2\text{O}_3$ : PHYSICOCHEMICAL PROPERTIES AND CATALYTIC ACTIVITY IN STEAM REFORMING OF ETHANOL AND STEAM/OXY-STEAM REFORMING OF GLYCEROL**

In order to increase the specific surface areas of the perovskite-like materials they were supported on modified  $\gamma\text{-Al}_2\text{O}_3$ . This chapter is devoted to the investigation of the supported  $m\text{LnNi}_{0.9}\text{Ru}_{0.1}\text{O}_3/n\text{Mg-}\gamma\text{-Al}_2\text{O}_3$  precursors prepared via the deposition of perovskite precursors from aqueous or organic solutions onto the modified support  $\text{Mg-}\gamma\text{-Al}_2\text{O}_3$ , and catalysts obtained upon their reduction. Physical-chemical properties and its relationship with the activity and stability in steam reforming of ethanol (ESR) as well as steam (GSR) and oxy-steam (GOSR) reforming of glycerol are considered in a three main sections.

In the first section, the effect of the magnesium introduction method, its content and perovskite composition on the structural and textural properties of the oxides synthesized was studied using BET, XRD and TEM methods. Additionally, the surface properties were investigated in details using XPS, UV-Vis spectroscopy and IR spectroscopy of adsorbed CO. Reducibility of the precursors was explored by the TPR- $\text{H}_2$  method.

The second section describes the catalytic activity of preliminary reduced  $m\text{LnNi}_{0.9}\text{Ru}_{0.1}\text{O}_3/n\text{Mg-}\gamma\text{-Al}_2\text{O}_3$  samples in the steam reforming of ethanol reaction in the temperature range of 650-800 °C and at the constant  $T = 650$  °C. The third section contains results of the catalytic tests of preliminary reduced the samples in the steam and oxy-steam reforming of glycerol reactions at the constant  $T = 650$  °C during 24 hours. The main conclusions about the effect of acidic properties of the support surface, the state of active components and supporting oxide's composition on the activity and stability in the reactions studied were postulated.

#### 4.1. Structural and textural properties of initial supports and catalysts

Supported catalysts with the general formula  $mLnNi_{0.9}Ru_{0.1}O_3/n\%Mg-\gamma-Al_2O_3$  ( $Ln = La, Pr$ ,  $m = 10; 20$ ,  $n = 6; 10; 15$ ) were synthesized via the deposition of perovskite precursors from aqueous and organic solutions onto the modified support [ $Mg-\gamma-Al_2O_3$ ].

**Table 4.1.1.** Synthesis method, specific surface area and spinel lattice parameter of supports  $n\%Mg-\gamma-Al_2O_3$  and catalysts based on it

Composition	Synthesis method	SSA, $m^2/g$	a, Å
$\gamma-Al_2O_3$	Disperal→500°C	177	7.917
6%Mg- $\gamma-Al_2O_3^D$	incipient wetness impregnation of Disperal	155	7.981
6%Mg- $\gamma-Al_2O_3$	incipient wetness impregnation of $\gamma-Al_2O_3$	133	7.971
10%Mg- $\gamma-Al_2O_3$	incipient wetness impregnation of $\gamma-Al_2O_3$	127	7.990
10%Mg- $\gamma-Al_2O_3^P$	deposition from organic precursors	191	7.935
15%Mg- $\gamma-Al_2O_3$	incipient wetness impregnation of $\gamma-Al_2O_3$	113	7.995
$MgAl_2O_4$	Pechini	69	8.089
$Mg_{0.5}Ni_{0.5}Al_2O_4$	Pechini	121	8.065
10% $LaNi_{0.9}Ru_{0.1}O_3$ /[ $\gamma-Al_2O_3$ ]	incipient wetness impregnation	138	-
10% $LaNi_{0.9}Ru_{0.1}O_3$ /[6%Mg- $\gamma-Al_2O_3$ ]	incipient wetness impregnation	110	-
10% $LaNi_{0.9}Ru_{0.1}O_3$ /[6%Mg- $\gamma-Al_2O_3^D$ ]	incipient wetness impregnation	106	7.985
10% $LaNi_{0.9}Ru_{0.1}O_3$ /[10%Mg- $\gamma-Al_2O_3$ ]	incipient wetness impregnation	77	8.018
10% $PrNi_{0.9}Ru_{0.1}O_3$ /[6%Mg- $\gamma-Al_2O_3$ ]	incipient wetness impregnation	119	-
10% $PrNi_{0.9}Ru_{0.1}O_3$ /[10%Mg- $\gamma-Al_2O_3$ ]	incipient wetness impregnation	96	8.014
10% $PrNi_{0.9}Ru_{0.1}O_3$ /[10%Mg- $\gamma-Al_2O_3^P$ ]	incipient wetness impregnation	112	7.982
10% $PrNi_{0.9}Ru_{0.1}O_3$ /[15%Mg- $\gamma-Al_2O_3$ ]	incipient wetness impregnation	81	8.025
10% $PrNi_{0.9}Ru_{0.1}O_3$ /[ $MgAl_2O_4$ ]	incipient wetness impregnation	53	-
20% $PrNi_{0.9}Ru_{0.1}O_3$ /[10%Mg- $\gamma-Al_2O_3$ ]	incipient wetness impregnation	55	8.018

Data on the composition and synthesis method as well as some structural and textural characteristics of the samples obtained are listed in Table 4.1.1. The introduction of magnesium from an aqueous solution of nitrate into  $\gamma-Al_2O_3$  with the initial specific surface area of  $180 m^2/g$  decreases it to  $110-130 m^2/g$ , whereas in the case of a polymerized precursor synthesized by the

Pechini method, the specific surface area of 10%Mg- $\gamma$ -Al<sub>2</sub>O<sub>3</sub><sup>P</sup> increases to 190 m<sup>2</sup>/g. Specific surface area of the catalysts with the supported active component LnNi<sub>0.9</sub>Ru<sub>0.1</sub>O<sub>3</sub> depends on its content and is equal to 50-110 m<sup>2</sup>/g.

#### 4.1.1. Effect of magnesium content and its introduction method on the support properties

According to the goals of the work, it was preferable to obtain the [Mg- $\gamma$ -Al<sub>2</sub>O<sub>3</sub>] support with predominantly surface distribution of magnesium in order to block the  $\gamma$ -Al<sub>2</sub>O<sub>3</sub> acid sites. To determine the optimal method corresponding to the specified goal, the support was modified by different techniques (Figure 4.1.1): impregnation of the formed gamma aluminum oxide with aqueous (Mg- $\gamma$ -Al<sub>2</sub>O<sub>3</sub>) or organic (Mg- $\gamma$ -Al<sub>2</sub>O<sub>3</sub><sup>P</sup>) solution of magnesium nitrate, and introduction of magnesium by impregnation from an aqueous solution at the aluminum hydroxide (Mg- $\gamma$ -Al<sub>2</sub>O<sub>3</sub><sup>D</sup>) step. MgAl<sub>2</sub>O<sub>4</sub> spinel was also synthesized by the polymerized precursors (Pechini) method from Mg and Al nitrates. Details of the synthesis methods are reported in Chapter 2.

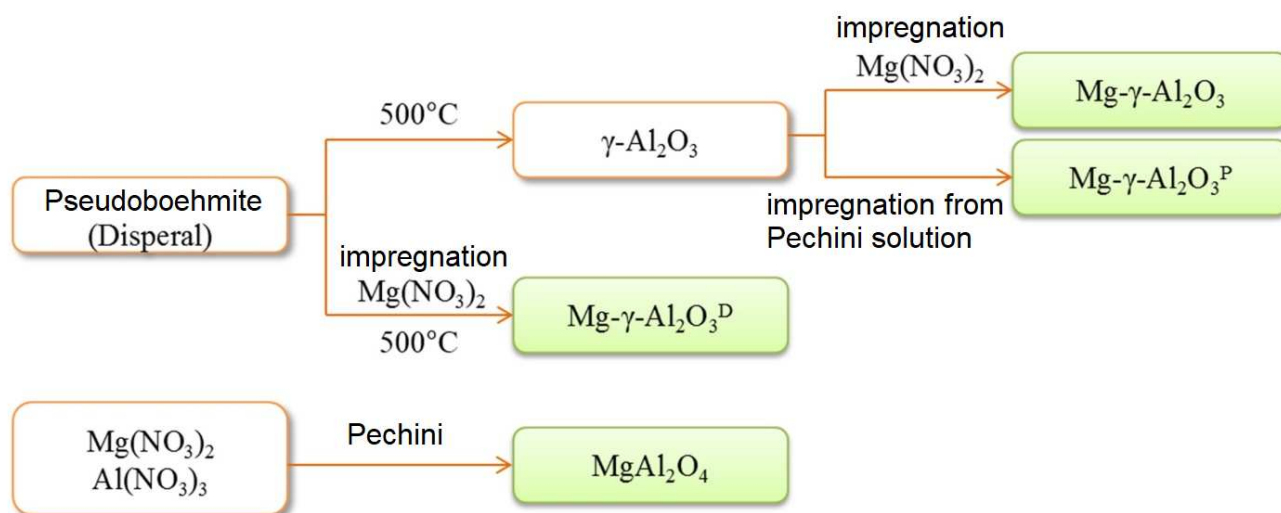


**Figure 4.1.1.** A scheme of the methods used to modify the support

XRD data on the structure of initial supports, particularly the lattice parameters calculated from the shift of the spinel phase peaks, are displayed on Figures 4.1.2-4.1.3 and listed in Table 4.1.1. According to XRD data, the initial  $\gamma$ -Al<sub>2</sub>O<sub>3</sub> has the cubic spinel structure [JCPDF 47-1308]. For all the studied samples, the addition of magnesium shifts the peaks on diffraction patterns toward lower angles, which indicates an increase in the lattice parameter of the spinel structure due to diffusion of Mg<sup>2+</sup> into the crystal lattice of  $\gamma$ -Al<sub>2</sub>O<sub>3</sub> [158]. The strength of magnesium-support interaction depends on both the magnesium content and the method of its introduction.

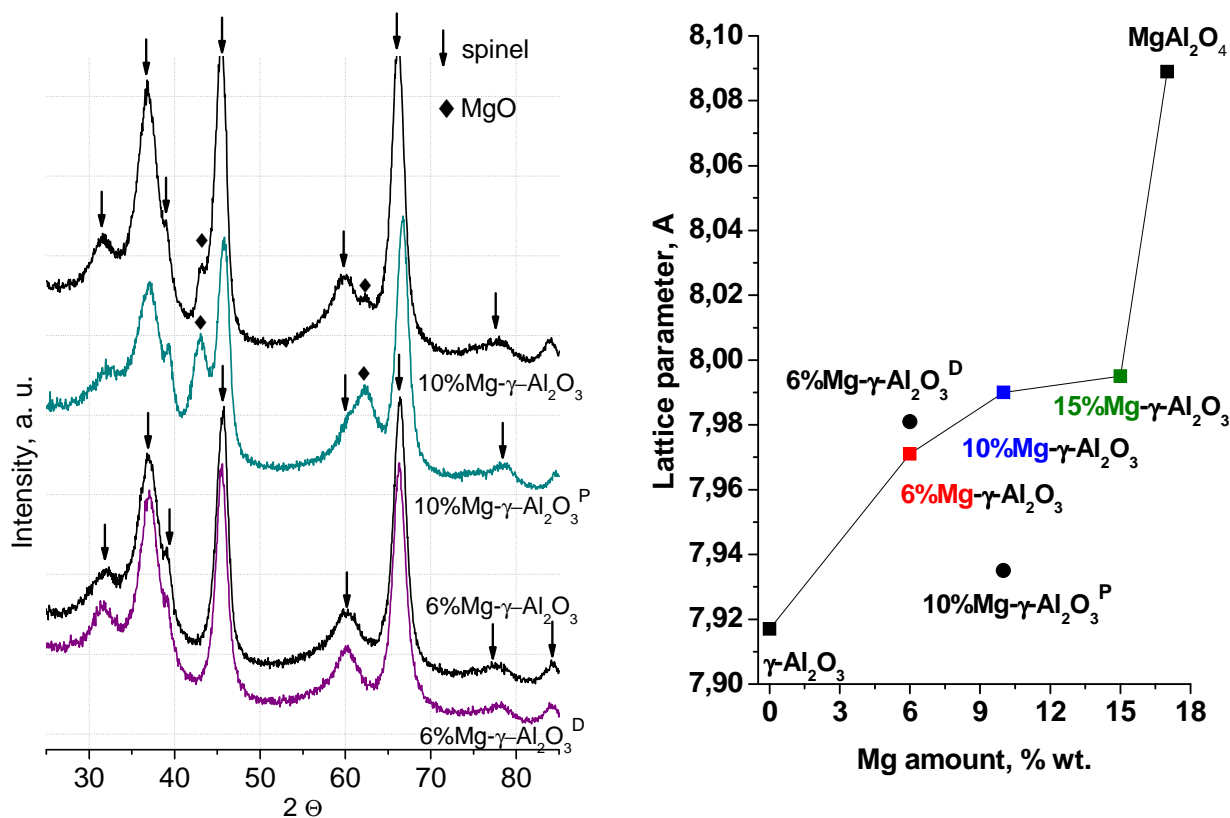


**Figure 4.1.2. a)** X-ray diffraction patterns of nMg- $\gamma$ - $\text{Al}_2\text{O}_3$  supports synthesized by different methods; **b)** The dependence of the spinel lattice parameter on magnesium content and introduction method for n%Mg- $\gamma$ - $\text{Al}_2\text{O}_3$  supports

Figure 4.1.2 a (bottom) displays the diffraction patterns of 6%Mg- $\gamma$ - $\text{Al}_2\text{O}_3$  and 6%Mg- $\gamma$ - $\text{Al}_2\text{O}_3^{\text{D}}$  samples. A comparison showed a more pronounced increase in the lattice parameter in the case of magnesium introduction at the 6%Mg- $\gamma$ - $\text{Al}_2\text{O}_3^{\text{D}}$  hydroxide step (Figure 4.1.2 b), which may indicate a stronger interaction of Mg with the oxide and its uniform distribution over the volume.

**Table 4.1.2.** Surface composition of 6%Mg- $\gamma$ - $\text{Al}_2\text{O}_3$  and 6%Mg- $\gamma$ - $\text{Al}_2\text{O}_3^{\text{D}}$  supports revealed by XPS

Composition	Elemental composition, % at.		
	Al	Mg	Mg/Al
6%Mg- $\gamma$ - $\text{Al}_2\text{O}_3^{\text{D}}$	16	1.1	0.06
6%Mg- $\gamma$ - $\text{Al}_2\text{O}_3$	18	1.6	0.09

For the 6%Mg- $\gamma$ - $\text{Al}_2\text{O}_3$  sample synthesized by impregnation of  $\gamma$ - $\text{Al}_2\text{O}_3$ , predominantly surface distribution of magnesium can be assumed. The surface enrichment with magnesium in the case of this sample was confirmed by XPS (Table 4.1.2).

A comparison of 10%Mg- $\gamma$ -Al<sub>2</sub>O<sub>3</sub> and 10%Mg- $\gamma$ -Al<sub>2</sub>O<sub>3</sub><sup>P</sup> (Figure 4.1.2 a, above) revealed a weak magnesium-support interaction in the second case. Diffraction patterns of the 10%Mg- $\gamma$ -Al<sub>2</sub>O<sub>3</sub> sample, which was obtained by impregnation from an aqueous solution, show weak reflections from the MgO phase and an increase in the lattice parameter of  $\gamma$ -Al<sub>2</sub>O<sub>3</sub>, whereas in the case of 10%Mg- $\gamma$ -Al<sub>2</sub>O<sub>3</sub><sup>P</sup> sample prepared via deposition by the Pechini method, magnesium resides mostly in the individual oxide: strong reflections from the MgO phase are observed, and the lattice parameter of spinel is close to that of  $\gamma$ -Al<sub>2</sub>O<sub>3</sub>.

For the sample synthesized from magnesium and aluminum nitrates according to the spinel stoichiometry, 17 wt.% Mg, the corresponding structure was obtained – MgAl<sub>2</sub>O<sub>4</sub> [JCPDF 21-1152] with the lattice parameter  $a(\text{MgAl}_2\text{O}_4) = 8.089 \text{ \AA}$ , which is close to the reference data. The lattice parameter of MgAl<sub>2</sub>O<sub>4</sub> spinel is much higher as compared to the Mg/Al<sub>2</sub>O<sub>3</sub> solid solution and corresponds to a uniform distribution of magnesium in the bulk of the mixed oxide. Thus, *the impregnation of the formed gamma aluminum oxide with an aqueous solution of magnesium nitrate* makes it possible to obtain supports with predominant distribution of magnesium on the support surface; therefore, this method was chosen as *the best one for the synthesis of catalyst supports*.

The effect of magnesium content on the structural properties of the samples prepared by impregnation was studied for three concentrations: 6, 10 and 15 wt.% Mg. Investigation of the phase composition of the synthesized supports demonstrated that the lattice parameter increases nonlinearly with increasing the magnesium content (Figure 4.1.2 b).

In the case of 6%Mg- $\gamma$ -Al<sub>2</sub>O<sub>3</sub>, only the spinel peaks are observed on the diffraction pattern (Figure 4.1.3). This testifies to incorporation of magnesium into the structure of initial  $\gamma$ -Al<sub>2</sub>O<sub>3</sub>, which is accompanied by an increase in the lattice parameter of alumina (Figure 4.1.2 b). As the amount of magnesium grows, an increase in the lattice parameter becomes less pronounced. Therewith, for the sample with magnesium content of 10 wt.%, low-intensity peaks appear on the diffraction patterns in the region of 43 and 62.5°; these peaks correspond to trace amounts of the individual MgO oxide, the intensity increases when magnesium content reaches 15%. The results obtained are supported by the literature data. For example, the authors in [158] revealed a limit for magnesium intercalation into the formed alumina structure. This limit depends on the properties of initial alumina and can vary from 8 wt.% Mg (corresponds to the MgAl<sub>2</sub>O<sub>4</sub> surface monolayer) to 12 wt.% Mg.



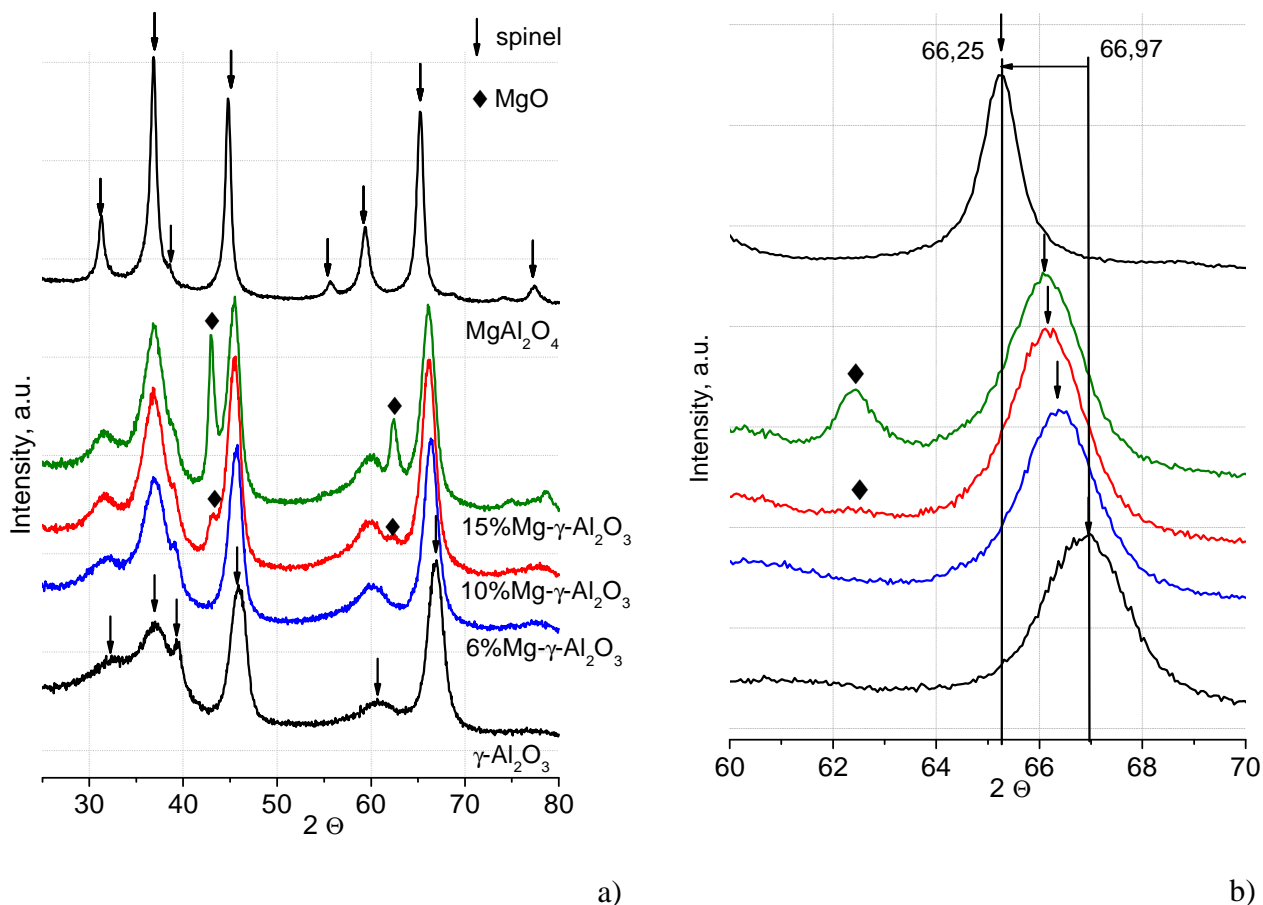
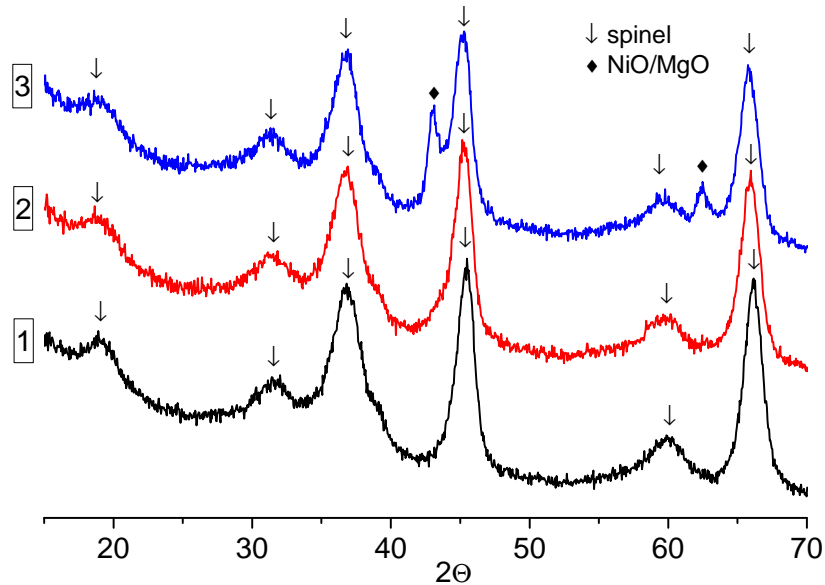


**Figure 4.1.3.** X-ray diffraction patterns of  $n\text{Mg-}\gamma\text{-Al}_2\text{O}_3$  supports for  $2\theta$  **a)**  $25\text{-}80^\circ$  and **b)**  $60\text{-}70^\circ$ .

#### 4.1.2. Effect of magnesium content on the nickel state in the $m\text{LnNi}_{0.9}\text{Ru}_{0.1}\text{O}_3/n\%\text{Mg-}\gamma\text{-Al}_2\text{O}_3$ catalysts

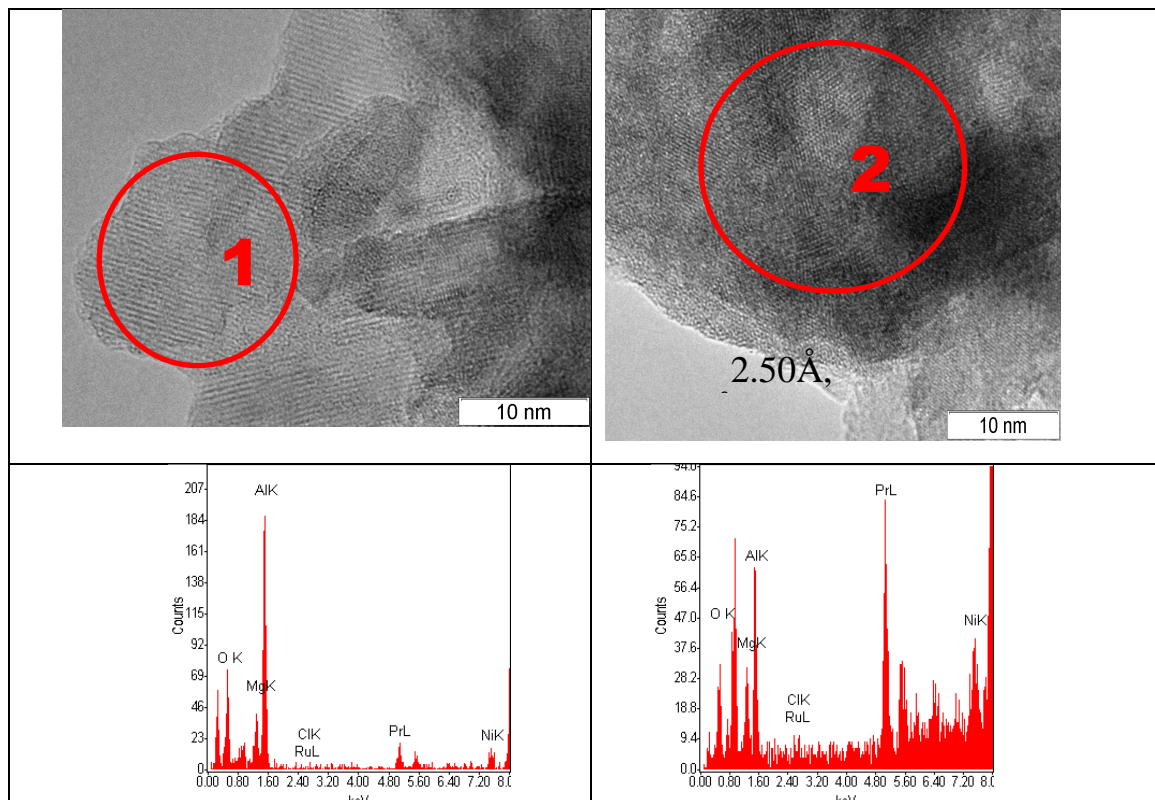
The XRD study of  $10\% \text{LnNi}_{0.9}\text{Ru}_{0.1}\text{O}_3/[n\%\text{Mg-}\gamma\text{-Al}_2\text{O}_3]$  catalysts showed that the diffraction patterns obtained for all the tested samples are identical to those of the  $n\text{Mg-}\gamma\text{-Al}_2\text{O}_3$  support before deposition. As an example, Figure 4.1.4 displays the diffraction patterns of praseodymium-containing  $10\%\text{PrNi}_{0.9}\text{Ru}_{0.1}\text{O}_3/n\%\text{Mg-}\gamma\text{-Al}_2\text{O}_3$  samples with different magnesium content. In all cases, deposition of the  $\text{LnNi}_{0.9}\text{Ru}_{0.1}\text{O}_3$  active component produces a more pronounced shift of the spinel phase peaks, which corresponds to a further increase in the lattice parameter of  $\gamma\text{-Al}_2\text{O}_3$  spinel (Table 4.1.1) due to Ni intercalation into its structure with the formation of  $\text{NiAl}_2\text{O}_4$ . The absence of reflections from praseodymium oxide, ruthenium and perovskite on the diffraction patterns indicates that these elements are in a highly disperse phases and cannot be identified by this method. In this connection, structural properties of the obtained systems were studied by TEM and UV-Vis.

TEM data together with the EDX spectra show that the 10% $\text{LnNi}_{0.9}\text{Ru}_{0.1}\text{O}_3/[\text{n}\%\text{Mg-}\gamma\text{-Al}_2\text{O}_3]$  samples contain not only the support phases ( $\text{MgAl}_2\text{O}_4$  and  $\text{MgO}$ ) but also phases of individual Pr and La oxides; nickel presents in the  $\text{MgO-NiO}$  mixed oxide and  $\text{Ni}(\text{Mg})\text{Al}_2\text{O}_4$  spinel phases.



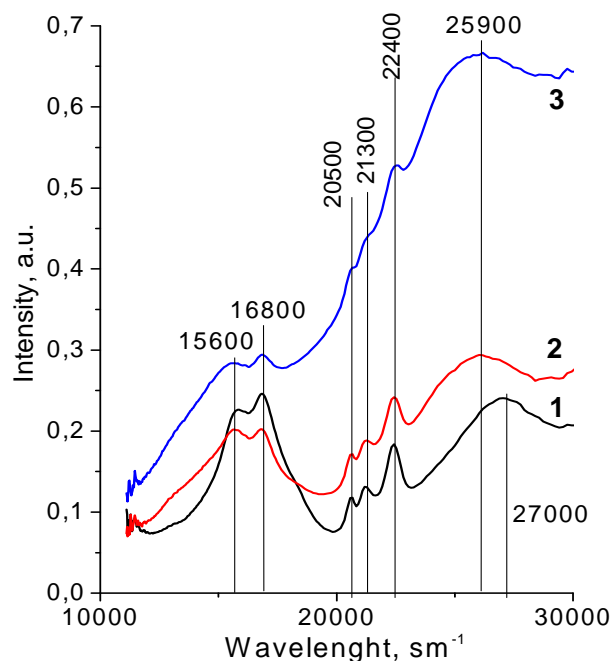
**Figure 4.1.4.** X-ray diffraction patterns of 10%  $\text{PrNi}_{0.9}\text{Ru}_{0.1}\text{O}_3/ \text{n}\% \text{Mg-}\gamma\text{-Al}_2\text{O}_3$  samples: 1)  $n = 6\%$ , 2)  $n = 10\%$ , and 3)  $n = 15\%$

Figure 4.1.5 displays electron microscopy images of the 20% $\text{PrNi}_{0.9}\text{Ru}_{0.1}\text{O}_3/[\text{10}\%\text{Mg-}\gamma\text{-Al}_2\text{O}_3]$  sample with an increased perovskite content; for this sample, the formation of the perovskite-like phase with the  $\text{A}_2\text{BO}_4$  structure and interplanar distances close to those of  $\text{Pr}_2\text{NiO}_4$  was demonstrated. Taking into account the absence of reflections from ruthenium on the diffraction patterns and the absence of individual ruthenium particles on TEM images, it can be supposed that ruthenium enters the structure of  $\text{Pr}_2\text{Ni}_{1-x}\text{Ru}_x\text{O}_4$  perovskite forming on the support surface.



**Figure 4.1.5.** TEM images and EDX spectra for the 20%PrNi<sub>0.9</sub>Ru<sub>0.1</sub>O<sub>3</sub>/[10%Mg- $\gamma$ -Al<sub>2</sub>O<sub>3</sub>] sample. Left – MgAl<sub>2</sub>O<sub>4</sub> spinel, right – Pr<sub>2</sub>Ni<sub>1-x</sub>Ru<sub>x</sub>O<sub>4</sub> perovskite

Additional information on the state of nickel in the samples can be obtained by ultraviolet–visible spectroscopy (UV-Vis). Figure 4.1.6 displays the UV-Vis spectra for 10%PrNi<sub>0.9</sub>Ru<sub>0.1</sub>O<sub>3</sub>/n%Mg- $\gamma$ -Al<sub>2</sub>O<sub>3</sub> samples with different magnesium content; three groups of absorption bands are observed on the spectra: 1) 15600 and 16800 cm<sup>-1</sup>, 2) 20500, 21300 and 22500 cm<sup>-1</sup>, and 3) 25900 and 27000 cm<sup>-1</sup>. According to the literature data, a.b. at 15600 and 16800 cm<sup>-1</sup> correspond to tetrahedrally coordinated nickel cations (Ni<sup>2+</sup><sub>Td</sub>), while a.b. at 25900 and 27000 cm<sup>-1</sup> – to octahedrally coordinated ones (Ni<sup>2+</sup><sub>Oh</sub>) [270]. The bands of the second group are caused by the f-f transitions of Pr<sup>3+</sup> cations [271]. Supposedly, for the PrRu<sub>0.1</sub>Ni<sub>0.9</sub>O<sub>3</sub>/6%Mg- $\gamma$ -Al<sub>2</sub>O<sub>3</sub> sample, the bands at 15600 and 16800 cm<sup>-1</sup> are caused by the d-d transitions of Ni<sup>2+</sup><sub>Td</sub> cations, while a.b. at 27000 cm<sup>-1</sup> – by Ni<sup>2+</sup><sub>Oh</sub> entering the composition of NiAl<sub>2</sub>O<sub>4</sub> spinel. As magnesium concentration is raised to  $\geq 10\%$ , intensity of the Ni<sup>2+</sup><sub>Td</sub> band decreases, intensity of the band in the region of 26000 cm<sup>-1</sup> increases, and a shoulder appears at 13100 cm<sup>-1</sup>. The indicated bands can be caused by the d-d transitions of Ni<sup>2+</sup><sub>Oh</sub> cations in NiO or in a NiO-MgO solid solution [271], which agree with the XRD data.



**Figure 4.1.6.** UV-Vis spectra for 10%PrNi<sub>0.9</sub>Ru<sub>0.1</sub>O<sub>3</sub>/n%Mg- $\gamma$ -Al<sub>2</sub>O<sub>3</sub> catalysts: 1) 6%Mg, 2) 10% Mg, and 3) 15% Mg.

Thus, *the state of nickel depends on magnesium concentration in the support*: at a low magnesium concentration nickel interacts mostly with  $\gamma$ -Al<sub>2</sub>O<sub>3</sub> to yield Ni<sub>x</sub>(Mg<sub>1-x</sub>)Al<sub>2</sub>O<sub>4</sub>, whereas an increased content of magnesium, when MgO is present in the initial support, leads to the formation of a NiO-MgO solid solution.

#### **4.1.3. Surface composition of the supports and initial catalysts**

XPS data on the surface composition of some supports and catalysts are listed in Table 4.1.3. The data obtained indicate that at equal magnesium content, its surface concentration is higher for the sample prepared by impregnation of  $\gamma$ -Al<sub>2</sub>O<sub>3</sub> in comparison with the sample obtained by impregnation at the aluminum hydroxide step. The surface concentration of nickel increases with the surface concentration of magnesium; this is accompanied by the formation of a NiO-MgO solid solution, which content increases when magnesium content in the support is raised above 10 wt.%.

**Table 4.1.3.** Surface composition of some supports and 10%LnNi<sub>0.9</sub>Ru<sub>0.1</sub>O<sub>3</sub>/6-10%Mg- $\gamma$ -Al<sub>2</sub>O<sub>3</sub> catalysts

Composition	Elemental composition, % at.						
	Al	Mg	Ni	La/Pr	Mg/Al	Ni/Al	Ni/La(Pr)
6%Mg- $\gamma$ -Al <sub>2</sub> O <sub>3</sub> <sup>D</sup>	16	1.1	0.00	0.00	0.06	-	-
6%Mg- $\gamma$ -Al <sub>2</sub> O <sub>3</sub>	18	1.6	0.00	0.00	0.09	-	-
10%LaRuNi/6%Mg- $\gamma$ Al <sub>2</sub> O <sub>3</sub> <sup>D</sup>	15	1.0	0.72	1.82	0.06	0.048	0.40
10%LaRuNi/6%Mg- $\gamma$ Al <sub>2</sub> O <sub>3</sub>	15	1.3	1.13	2.06	0.09	0.075	0.55
10%PrRuNi/6%Mg- $\gamma$ Al <sub>2</sub> O <sub>3</sub>	16	0.87	0.84	2.4	0.05	0.053	0.36
10%PrRuNi/10%Mg- $\gamma$ Al <sub>2</sub> O <sub>3</sub>	16	1.6	1.0	3.0	0.1	0.063	0.34

The Ni<sup>2p</sup> XPS spectra displayed on Figure 4.1.7 demonstrate that nickel in the studied samples has different states, which agree with the UV-Vis data.

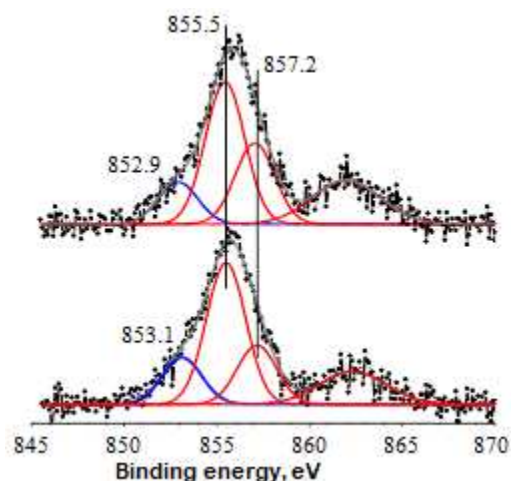


**Figure 4.1.7.** Ni<sup>2p</sup> XPS spectra of 10%PrRuNi/6%Mg- $\gamma$ Al<sub>2</sub>O<sub>3</sub> (bottom) and 10%PrRuNi/10%Mg- $\gamma$ Al<sub>2</sub>O<sub>3</sub> (above)

The binding energy of the most intensive peak at 855.5 eV corresponds to divalent nickel. However, this state is not the NiO oxide, which is characterized by splitting of the main peak of the Ni<sup>2p</sup> line with the maxima at 854 and 855.5 eV and by the presence of an intensive shake-up satellite with the binding energy 861 eV [272].

The absence of the main peak splitting and the decreased intensity of the satellite indicate that Ni<sup>2+</sup> ions interact with the oxide matrix. Besides, an additional state with the binding energy 852.9-853.1 eV is present in the Ni<sup>2p</sup> spectra, which corresponds to the reduced nickel that can form due to reduction of highly disperse clusters upon measuring the XPS spectra.

#### 4.1.4. Effect of magnesium content on the surface acidity of supports and catalysts

Data on the surface acidity of supports and related catalysts obtained by IR spectroscopy of adsorbed CO are displayed on Figures 4.1.8-4.1.9. These data confirm that the surface acidity decreases with increasing the surface concentration of magnesium, and deposition of the active components leads to its further decrease.

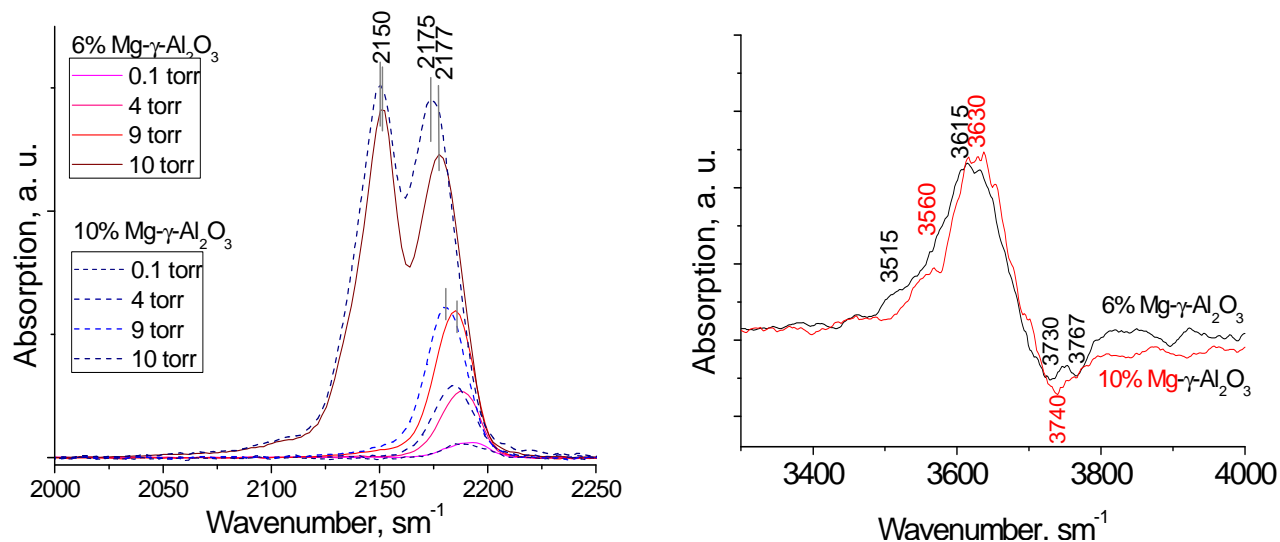


**Figure 4.1.8.** Data on IR spectroscopy of CO adsorbed for 6% Mg- $\gamma$ -Al<sub>2</sub>O<sub>3</sub> and 10% Mg- $\gamma$ -Al<sub>2</sub>O<sub>3</sub> supports after pretreatment in hydrogen:  
a) IR spectra of CO adsorbed at 77 K and CO pressure of 0.1 – 10 Torr;  
b) The difference IR spectrum of CO adsorbed at 77 K and CO pressure of 10 Torr

The spectra of 6% Mg- $\gamma$ -Al<sub>2</sub>O<sub>3</sub> and 10% Mg- $\gamma$ -Al<sub>2</sub>O<sub>3</sub> supports (Figure 4.1.8) at a CO pressure of 0.1 Torr show a low-intensity shoulder in the adsorption region of 2192 and 2189 cm<sup>-1</sup>; as the pressure is raised, the position of the shoulder shifts to 2177 and 2175 cm<sup>-1</sup>, respectively, which is accompanied by an increase in intensity of the peaks. The absorption band in this region corresponds to the CO complex with Lewis acid sites of alumina – Al<sup>3+</sup> anions. The band at 2150 cm<sup>-1</sup> can be attributed to CO adsorption on OH groups or Mg<sup>2+</sup> cations.

The strength of the surface Brønsted acidity correlates with the shift of the band of OH groups upon CO adsorption. Stretching vibrations of hydroxyl groups on the  $\gamma$ -Al<sub>2</sub>O<sub>3</sub> surface are observed in the region of 3570 – 3770 cm<sup>-1</sup>. A more pronounced low-frequency shift indicates a higher acidity of the OH group (therewith, the negative peaks observed in the difference spectrum correspond to positions of the initial OH groups).

For 6% Mg- $\gamma$ -Al<sub>2</sub>O<sub>3</sub> and 10% Mg- $\gamma$ -Al<sub>2</sub>O<sub>3</sub> supports, the bands at 3570, 3620 and 3650 cm<sup>-1</sup> (Fig. 4.1.8 b), which are typical of CO adsorption on OH groups with different acidity, appear in the

region of stretching vibrations of hydroxyl groups at a CO pressure of 10 Torr. The high-frequency shift of the peaks observed for the 10%Mg- $\gamma$ -Al<sub>2</sub>O<sub>3</sub> sample indicates a decrease in the acidity of such sites.

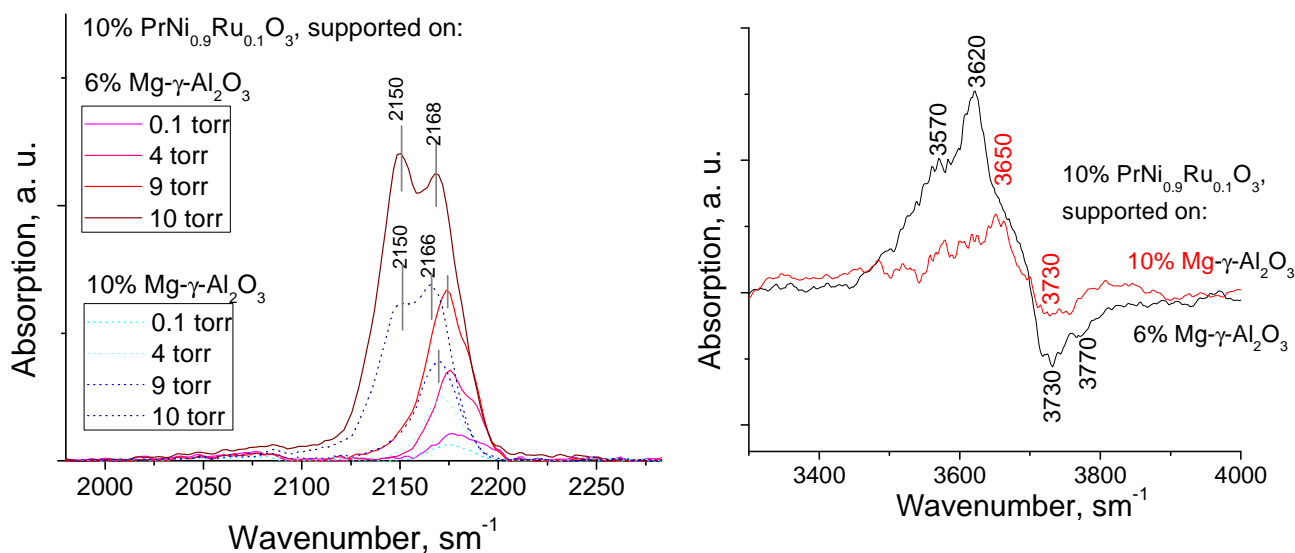


**Figure 4.1.9.** Data on IR adsorption of CO for 10%PrNi<sub>0.9</sub>Ru<sub>0.1</sub>O<sub>3</sub>/[6%Mg- $\gamma$ -Al<sub>2</sub>O<sub>3</sub>] and 10%PrNi<sub>0.9</sub>Ru<sub>0.1</sub>O<sub>3</sub>/[10%Mg- $\gamma$ -Al<sub>2</sub>O<sub>3</sub>] catalysts after pretreatment in hydrogen:  
a) IR spectra of CO adsorbed at 77 K and CO pressure of 0.1 – 10 Torr;  
b) The difference IR spectrum of CO adsorbed at 77 K and CO pressure of 10 Torr

Figure 4.1.9 displays IR spectra of CO adsorbed at 77 K on 10%PrNi<sub>0.9</sub>Ru<sub>0.1</sub>O<sub>3</sub>/10%Mg-Al<sub>2</sub>O<sub>3</sub> catalysts after hydrogen pretreatment at CO pressure 0.1 – 10 Torr. Similar spectra were obtained for other samples. In the spectrum of 10% PrNi<sub>0.9</sub>Ru<sub>0.1</sub>O<sub>3</sub>/10%Mg- $\gamma$ -Al<sub>2</sub>O<sub>3</sub>, the band at 2150 cm<sup>-1</sup> can be assigned to CO adsorption on both the OH groups and praseodymium or Mg<sup>2+</sup> cations; the bands at 2165-2190 cm<sup>-1</sup> correspond to CO adsorption on Al<sup>3+</sup> cations (Lewis sites); and the band at 2085 cm<sup>-1</sup> is typical of linear CO complexes with metallic Ni or Ru.

For the studied catalysts, the shift of absorption bands in the region of 3570 – 3730 cm<sup>-1</sup> (Figure 4.1.9 b), which are typical of CO complexes adsorbed on OH groups of alumina, indicates a further decrease in acidity as compared to the supports. Such a shift was most pronounced for the 10%PrNi<sub>0.9</sub>Ru<sub>0.1</sub>O<sub>3</sub>/10%Mg-Al<sub>2</sub>O<sub>3</sub> catalyst. Overall, the analysis of the shift of these bands and proton affinity of the corresponding OH groups (Table 4.1.4) showed that an increase in Mg concentration in the tested catalysts decreases the amount and strength of surface acid sites.

**Table 4.1.4.** Position, shift and proton affinity (PA) of a.b. for CO complexes adsorbed on OH groups

Sample	$N_{OH}, cm^{-1}$	$\Delta\nu_{OH}, cm^{-1}$	PA, kJ/mol
6% Mg- $\gamma$ -Al <sub>2</sub> O <sub>3</sub>	3730	215	1223
	3770	155	1285
10% PrRu <sub>0.1</sub> Ni <sub>0.9</sub> O <sub>3</sub> /6% Mg- $\gamma$ -Al <sub>2</sub> O <sub>3</sub>	3730	160	1280
	3770	150	1292
10% Mg- $\gamma$ -Al <sub>2</sub> O <sub>3</sub>	3730	170	1268
	3770	140	1305
10% PrRu <sub>0.1</sub> Ni <sub>0.9</sub> O <sub>3</sub> /10% Mg- $\gamma$ -Al <sub>2</sub> O <sub>3</sub>	3730	80	1413

#### 4.1.5. Effect of magnesium content and its introduction method on the nickel reducibility from the catalyst precursors

Typical TPR-H<sub>2</sub> spectra of LnNi<sub>0.9</sub>Ru<sub>0.1</sub>O<sub>3</sub>/0-15% Mg- $\gamma$ -Al<sub>2</sub>O<sub>3</sub> samples are displayed on Figure 4.1.10. In all cases, the spectra have a high-temperature peak above 600°C and a series of broad low-intensity lines in the low-temperature region; therewith, the profile of the spectra and positions of the peaks depend on magnesium concentration and its introduction method and are weakly dependent on the nature of a rare-earth element. The spectra of 10% LaNi<sub>0.9</sub>Ru<sub>0.1</sub>O<sub>3</sub>/[ $\gamma$ -Al<sub>2</sub>O<sub>3</sub>] without magnesium and 10% LaNi<sub>0.9</sub>Ru<sub>0.1</sub>O<sub>3</sub>/[6% Mg- $\gamma$ -Al<sub>2</sub>O<sub>3</sub><sup>D</sup>], which was obtained by impregnation of the initial aluminum hydroxide, are identical: a broad low-temperature shoulder below 400°C may correspond to the reduction of highly disperse NiO clusters. The high-temperature peak at 840-850°C corresponds to the reduction of NiAl<sub>2</sub>O<sub>4</sub>.

Spectra of the LaNi<sub>0.9</sub>Ru<sub>0.1</sub>O<sub>3</sub>/[6% Mg- $\gamma$ -Al<sub>2</sub>O<sub>3</sub>] and LaNi<sub>0.9</sub>Ru<sub>0.1</sub>O<sub>3</sub>/[10% Mg- $\gamma$ -Al<sub>2</sub>O<sub>3</sub>] samples, which were prepared by impregnation of the formed  $\gamma$ -Al<sub>2</sub>O<sub>3</sub> with aqueous solutions where magnesium concentration was equal to 6 and 10 wt. %, have a more complicated profile. This is caused by the appearance of a new nickel state related to the formation of a NiO-MgO solid solution, as was shown by XRD, UV-Vis and XPS. The spectrum of the 10% PrNi<sub>0.9</sub>Ru<sub>0.1</sub>O<sub>3</sub>/[10% Mg- $\gamma$ -Al<sub>2</sub>O<sub>3</sub><sup>P</sup>] sample, which was obtained by magnesium deposition on  $\gamma$ -Al<sub>2</sub>O<sub>3</sub> from a polymeric organic solution, contains a low-temperature peak at 270°C, which corresponds to the reduction of highly disperse particles of Ni and Ru oxides that are weakly bound to the support surface. For all the samples, the main peak located in the temperature range of 740-860°C corresponds to nickel reduction from the spinel structure.



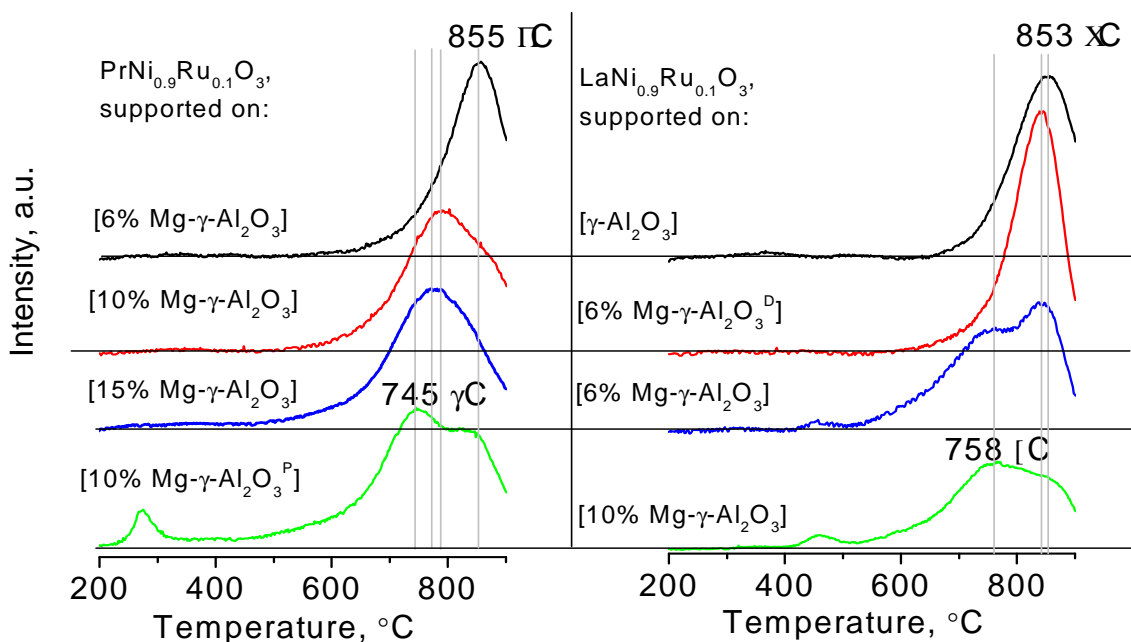


**Figure 4.1.10.** TPR-H<sub>2</sub> spectra for LnNi<sub>0.9</sub>Ru<sub>0.1</sub>O<sub>3</sub>/0-15%Mg- $\gamma$ -Al<sub>2</sub>O<sub>3</sub> samples

As the Mg content is increased, this peak shifts toward low temperatures for both the lanthanum and praseodymium samples.

Such a behavior was observed in [157, 167, 169, 176] and corresponds to an easier reduction of nickel from the Ni<sub>x</sub>Mg<sub>1-x</sub>Al<sub>2</sub>O<sub>4</sub> mixed spinel phase as compared to NiAl<sub>2</sub>O<sub>4</sub>. An increase in the perovskite content to 20 wt.% produces four peaks on the reduction curve (Fig. 4.1.11), which correspond to four states of nickel in the oxide. The low-temperature peak at 250 °C corresponds to the reduction of highly disperse ruthenium oxides, and a weak shoulder in the region of 410 °C can be assigned to nickel reduction from the individual oxide. Taking into account TEM and UV-Vis data, a broad peak with the maxima at 700 and 832 °C corresponds to nickel reduction from NiO-MgO, Ni<sub>x</sub>Mg<sub>1-x</sub>Al<sub>2</sub>O<sub>4</sub> and the perovskite-like Pr<sub>2</sub>NiO<sub>4</sub> phase.

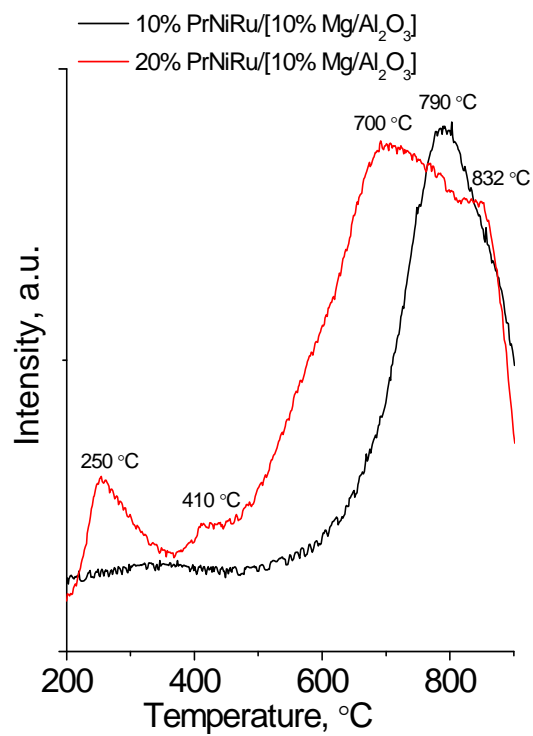


**Figure 4.1.11.** TPR-H<sub>2</sub> spectra for mPrNi<sub>0.9</sub>Ru<sub>0.1</sub>O<sub>3</sub>/n% Mg-γ-Al<sub>2</sub>O<sub>3</sub> samples: the effect of m - percentage of the perovskite supported

#### 4.1.6. Conclusion to Section 4.1

The properties of the supported complex oxides with the general formula  $m\text{LnNi}_{0.9}\text{Ru}_{0.1}\text{O}_3/n\text{Mg-}\gamma\text{-Al}_2\text{O}_3$  (Ln = Pr, La) were synthesized and studied using a physicochemical method's complex (BET, XRD, TEM with EDX, XPS, UV-Vis, IR-spectroscopy of adsorbed CO and TPR-H<sub>2</sub>). The shortcut of the results obtained is as follows:

- The average SSA of all samples obtained is about 100-120 m<sup>2</sup>/g.
- The samples are oxides with a spinel structure with increased lattice parameters due to the partial incorporation of magnesium and nickel cations into the lattice.
- Among the several methods of the supports modification with Mg, the impregnation of the formed gamma aluminum oxide with an aqueous solution of magnesium nitrate makes it possible to obtain supports with predominant distribution of magnesium on the support surface; therefore, this method was chosen as the best one for the synthesis of catalyst supports. For samples obtained by this method, an increase in the Mg content  $\geq 10\%$  leads to the formation of a phase of MgO, with the amount increases with increasing the Mg content to 15%. The study of these supports by the IR spectroscopy of adsorbed CO shows a decrease in the acidity of the surface with an increase in the surface concentration of magnesium.
- It was shown that, Mg concentration affects the interaction of nickel with the support: at  $n = 6\%$ , nickel is predominantly incorporated into the  $\gamma\text{-Al}_2\text{O}_3$  to form spinel  $\text{Ni}_x(\text{Mg}_{1-x})\text{Al}_2\text{O}_4$ ; at  $n \geq 10\%$ , a solid solution of NiO-MgO is additionally formed. With a 20% perovskites content, some of the nickel shown to be part of the superficial perovskite-like structures  $\text{PrNi}_x\text{Ru}_{1-x}\text{O}_3$  и  $\text{Pr}_2\text{Ni}_x\text{Ru}_{1-x}\text{O}_4$ .
- The effect of the magnesium introduction method, its content and perovskite composition on the formation of the active phase of metallic nickel in the process of reduction treatment is established. According to the results of TPR-H<sub>2</sub>, the decrease in the reduction temperature of the catalysts occurs with an increase in the Mg surface concentration (the optimal one is achieved using impregnation of the  $\gamma\text{-Al}_2\text{O}_3$  formed with an aqueous solution of magnesium nitrate, the Mg amount of 10-15% wt). Such a behavior corresponds to an easier reduction of nickel from the  $\text{Ni}_x\text{Mg}_{1-x}\text{Al}_2\text{O}_4$  mixed spinel phase in the samples with  $n \geq 10\%$  wt., as compared to  $\text{NiAl}_2\text{O}_4$  phase inherent in samples with a magnesium content below 6 % wt. An increase in the perovskite content to 20 wt. % make more pronounced the high-temperature broad peak with the maxima at 700 and 832 °C corresponds to nickel reduction from NiO-MgO,  $\text{Ni}_x\text{Mg}_{1-x}\text{Al}_2\text{O}_4$  and perovskite-like  $\text{PrNi}_x\text{Ru}_{1-x}\text{O}_3$  phase, which are the preferable phases to reduced from to obtain a high-dispersed metal particles with strong Me-Support interaction.

## 4.2. Catalytic activity in steam reforming of ethanol

The catalytic activity of the series of samples was studied at 500-800 °C using catalysts with the grain size of 0.25-0.5 mm under conditions corresponding to the blank run, which was described in Section 3.2.2. The study showed that magnesium content and its introduction method as well as the composition and amount of the deposited perovskite determine the catalytic behavior of the systems produced.

### 1) Effect of magnesium introduction method

A similar catalytic behavior was observed for samples with unmodified  $\gamma$ -Al<sub>2</sub>O<sub>3</sub> support and with supports modified by the methods which, according to physicochemical studies, do not ensure a complete surface coverage with magnesium (Mg- $\gamma$ -Al<sub>2</sub>O<sub>3</sub><sup>D</sup> and Mg- $\gamma$ -Al<sub>2</sub>O<sub>3</sub><sup>P</sup>).

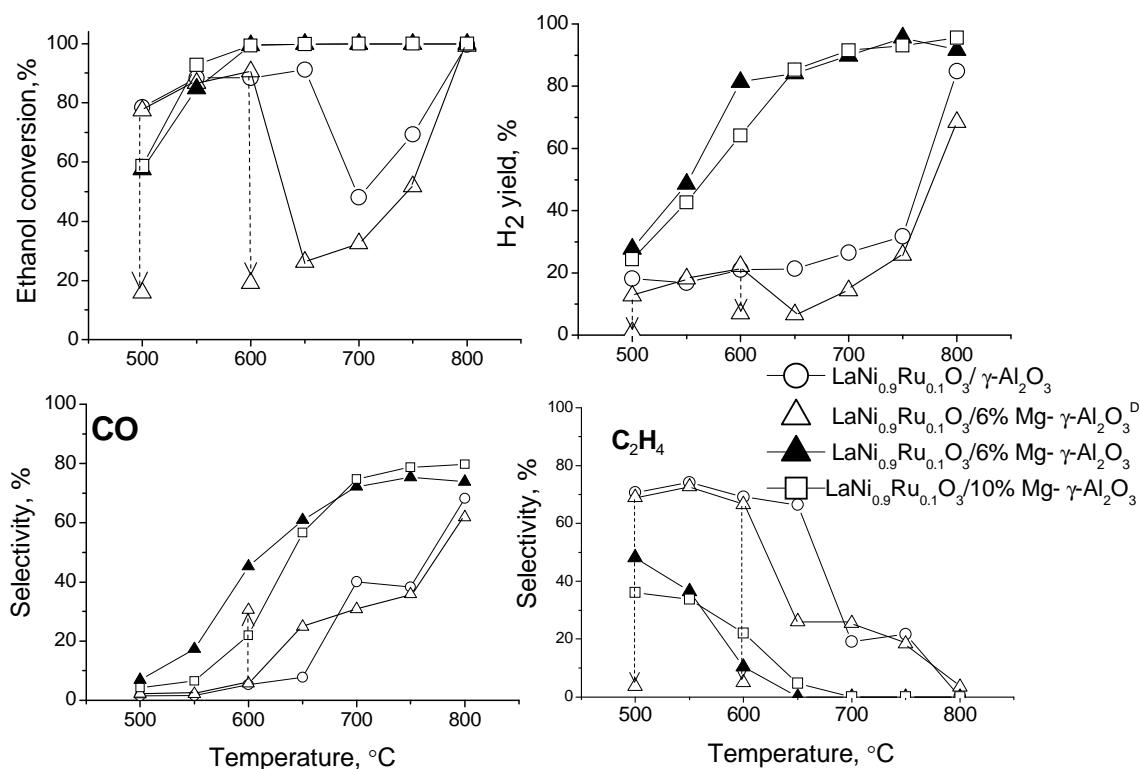
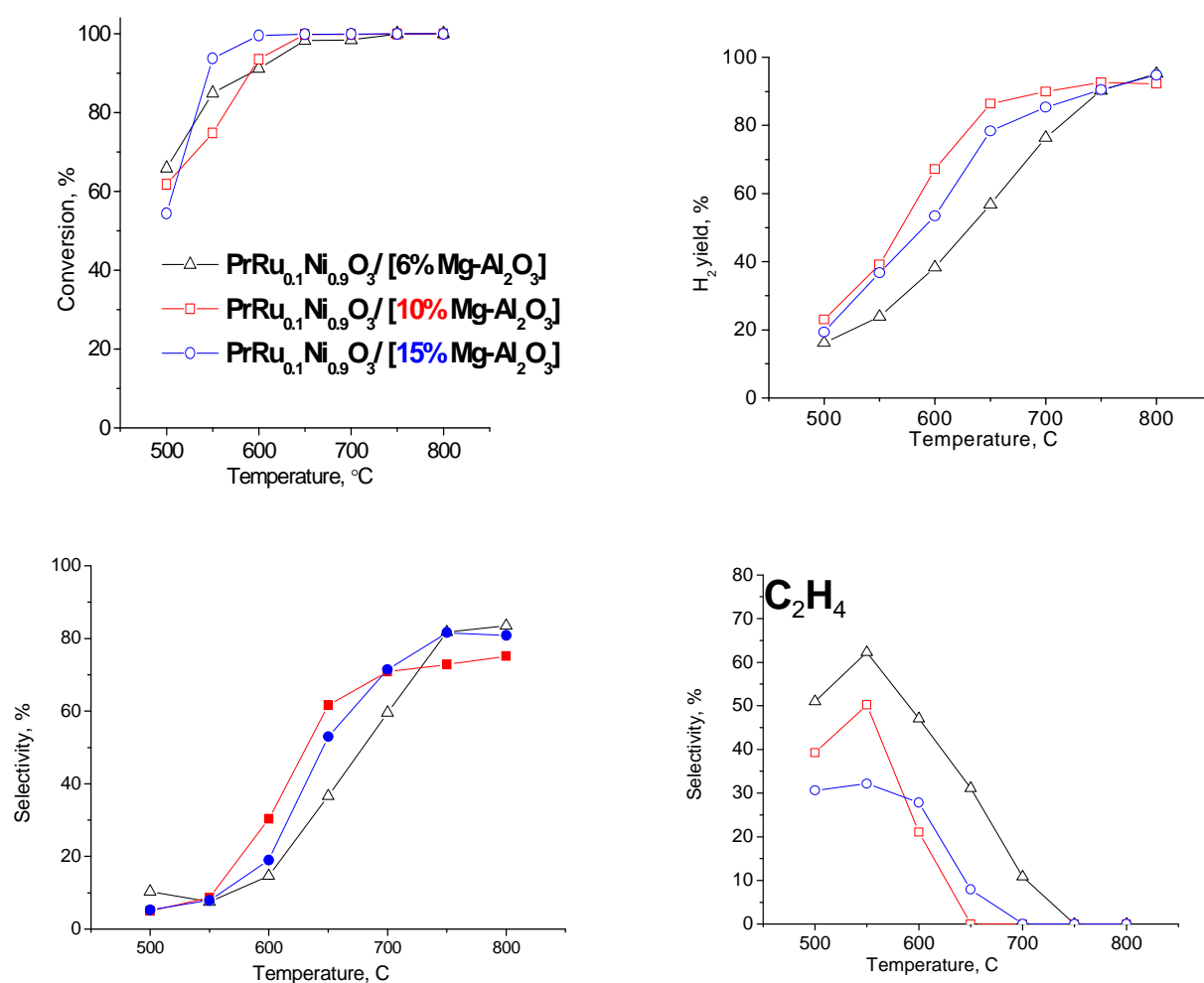


Figure 4.2.1. The effect of Mg concentration and its introduction method on the activity and selectivity of LaNi<sub>0.9</sub>Ru<sub>0.1</sub>O<sub>3</sub>/6-10% Mg- $\gamma$ Al<sub>2</sub>O<sub>3</sub> catalysts in steam reforming of ethanol. Catalyst grain size 0.25-0.5 mm, contact time 0.07 s, H<sub>2</sub>O:EtOH = 4

These samples demonstrate a low selectivity for hydrogen in the temperature range of 500-750 °C, and the observed > 80% conversion of ethanol at the indicated temperatures was

accompanied by a high yield of ethylene (70%). This regularity was established for lanthanum-containing samples 10%LaNi<sub>0.9</sub>Ru<sub>0.1</sub>O<sub>3</sub>/[ $\gamma$ -Al<sub>2</sub>O<sub>3</sub>] without magnesium and for 10%LaNi<sub>0.9</sub>Ru<sub>0.1</sub>O<sub>3</sub>/[6%Mg- $\gamma$ -Al<sub>2</sub>O<sub>3</sub><sup>D</sup>] on the support obtained by magnesium introduction at the aluminum hydroxide step (Figure 4.2.1). A comparison with the 10%LaNi<sub>0.9</sub>Ru<sub>0.1</sub>O<sub>3</sub>/[6%Mg- $\gamma$ -Al<sub>2</sub>O<sub>3</sub>] sample obtained by impregnation of  $\gamma$ -Al<sub>2</sub>O<sub>3</sub> with magnesium revealed a substantial enhancement of catalytic properties after magnesium introduction by this method: 100% conversion of ethanol for this sample was reached already at 600 °C, the yield of hydrogen was close to the thermodynamic limit over the entire temperature range, and the yield of ethylene at the indicated temperature did not exceed 10%.



**Figure 4.2.2.** Temperature dependences of ethanol conversion, hydrogen yield, and selectivities for CO and C<sub>2</sub>H<sub>4</sub> for praseodymium-containing catalysts with different magnesium content. Catalyst grain size 0.25-0.5 mm, contact time 0.07 s, H<sub>2</sub>O:EtOH = 4

On Figure 4.2.2, catalysts with different supports are compared using on an example of praseodymium-containing samples. The high selectivity for ethylene and methane and low

hydrogen yield in the case of magnesium deposited from an organic precursor for the 10%PrNi<sub>0.9</sub>Ru<sub>0.1</sub>O<sub>3</sub>/[10%Mg- $\gamma$ -Al<sub>2</sub>O<sub>3</sub><sup>P</sup>] sample agree with XRD and UV-Vis data indicating a weak interaction between MgO and Al<sub>2</sub>O<sub>3</sub>. Therewith, comparable data were obtained for catalysts 10%PrNi<sub>0.9</sub>Ru<sub>0.1</sub>O<sub>3</sub>/[10%Mg- $\gamma$ -Al<sub>2</sub>O<sub>3</sub>] and 10%PrNi<sub>0.9</sub>Ru<sub>0.1</sub>O<sub>3</sub>/[MgAl<sub>2</sub>O<sub>3</sub>] (magnesium content 17 wt.%).

The results obtained in the study corroborate the literature data and testify that dehydration process of the steam reforming intermediates proceeds on the alumina surface. A higher surface concentration of magnesium in the samples leads to decrease in the concentration of acid Lewis sites responsible for the formation of strongly bound ethoxy species – carbon precursors, which is confirmed by a decrease in selectivity for ethylene with increasing the surface concentration of magnesium.

## 2) Effect of magnesium content

An increase in magnesium content in the catalyst also decreases the selectivity for ethylene at temperatures below 600 °C for both La- and Pr-containing catalysts. Data on ethanol conversion, hydrogen yield, and selectivities for CO and C<sub>2</sub>H<sub>4</sub> obtained for praseodymium-based samples are displayed on Figure 4.2.2. For these compositions, a decrease in the selectivity for ethylene correlates with a decrease in the surface acidity calculated from IR spectroscopy of adsorbed CO (Table 4.2).

**Table 4.2.** Selectivity for C<sub>2</sub>H<sub>4</sub> and proton affinity (PA) (from IR data about CO adsorption\* on hydroxyl groups – a.b. 3730 cm<sup>-1</sup>) versus magnesium content for catalysts 10%PrNi<sub>0.9</sub>Ru<sub>0.1</sub>O<sub>3</sub>/n% Mg- $\gamma$ Al<sub>2</sub>O<sub>3</sub>, n = 6, 10

	Catalyst	
	PrNi <sub>0.9</sub> Ru <sub>0.1</sub> O <sub>3</sub> /6% Mg- $\gamma$ Al <sub>2</sub> O <sub>3</sub>	PrNi <sub>0.9</sub> Ru <sub>0.1</sub> O <sub>3</sub> /10% Mg- $\gamma$ Al <sub>2</sub> O <sub>3</sub>
PA, kJ/mol	1280	1413
Selectivity in C <sub>2</sub> H <sub>4</sub> , %		
500°C	50	40
550°C	62	50

\*CO was adsorbed on the catalysts that were reduced in a mixture of 5%H<sub>2</sub> in He at 400 °C.

Measurements of the catalytic activity of lanthanum-containing samples 10%LaNi<sub>0.9</sub>Ru<sub>0.1</sub>O<sub>3</sub>/[nMg- $\gamma$ -Al<sub>2</sub>O<sub>3</sub>] with different magnesium content in ethanol steam reforming showed that the hydrogen yield and selectivities for CO and CO<sub>2</sub> are much lower for the catalysts supported on  $\gamma$ -Al<sub>2</sub>O<sub>3</sub> and 6%Mg- $\gamma$ -Al<sub>2</sub>O<sub>3</sub><sup>D</sup> with a low surface content of magnesium as compared

to other compositions. At the same time, selectivity for ethylene decreases with increasing the surface content of magnesium, which is caused by a decrease in the concentration of acid Lewis sites on the support surface (Figure 4.2.2).

*In situ* IR spectroscopy study of the surface complexes and gaseous products formed via the interaction of ethanol and ethanol-water mixture with the catalyst surface showed that an increase in magnesium concentration facilitates the preferential formation of weakly bound monodentate ethoxy groups with a high reactivity [273].

### 3) Effect of the nature of a rare-earth element

When magnesium content in the catalyst exceeds 10 wt.%, nickel-containing catalysts based on lanthanum and praseodymium exhibit identical activity (Figures 4.2.1 and 4.2.2). High ethanol conversions for the samples are reached already at 600 °C; therewith, the high yields of hydrogen and CO as well as the low selectivity for by-products are retained.

### 4.3. Catalytic activity in steam/oxy-steam reforming of glycerol

As for the massive catalysts (Section 3.2.4), the data on the glycerol conversion to gas products  $X_g$  and the distribution of productivities in the gaseous phase were obtained for the following parameters: the reaction mixture  $C_3H_8O_3:H_2O = 1:9$ , gas hourly space velocity of  $28000\text{ h}^{-1}$  and temperature  $650\text{ }^\circ\text{C}$ .

First of all, it should be noted that the catalysts with unmodified  $\gamma\text{-Al}_2\text{O}_3$  and with 6%Mg- $\gamma\text{-Al}_2\text{O}_3^D$  support, which are ones where a uniform surface coverage with magnesium was not obtained, are inefficient toward steam reforming of glycerol.

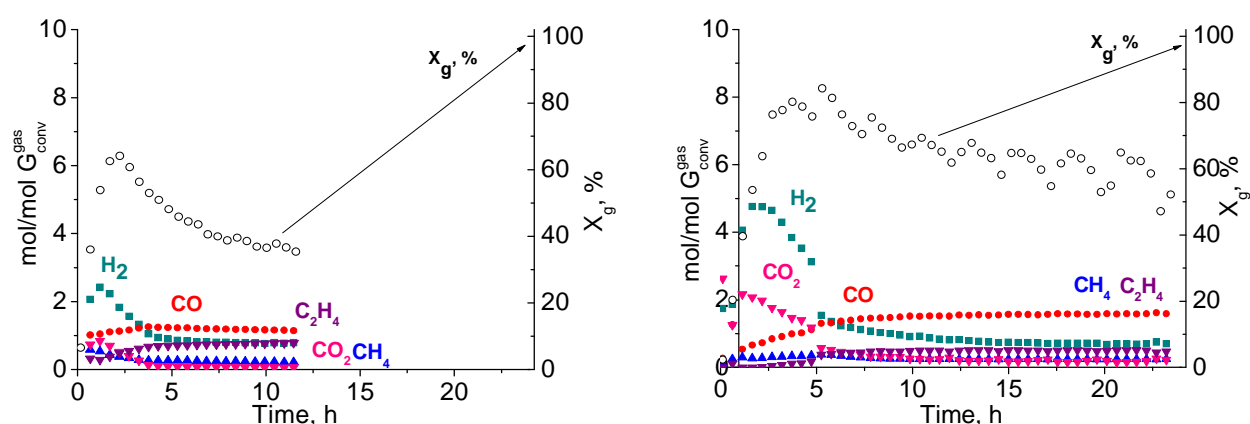


**Figure 4.3.1.** Glycerol conversion to gas  $X_g$  and productivities to the gaseous products  $P_i$  for the 10%LaNi<sub>0.9</sub>Ru<sub>0.1</sub>O<sub>3</sub>/[6%Mg- $\gamma$ -Al<sub>2</sub>O<sub>3</sub><sup>D</sup>] sample in a) GSR ( $C_3H_8O_3:H_2O=1:9$ , GHSV= $28000\text{ h}^{-1}$ ,  $T=650\text{ }^\circ\text{C}$ ) and b) GOSR ( $C_3H_8O_3:H_2O:O_2 = 1:9:0.25$ , GHSV= $28000\text{ h}^{-1}$ ,  $T=650\text{ }^\circ\text{C}$ ) reactions

As an example, Figure 4.3.1 displays data for the 10%LaNi<sub>0.9</sub>Ru<sub>0.1</sub>O<sub>3</sub>/[6%Mg- $\gamma$ -Al<sub>2</sub>O<sub>3</sub><sup>D</sup>] sample. A minor increase in the hydrogen productivity in the first hours of the reaction indicates a non-zero initial activity of the catalyst. Nevertheless, after 4 hours of the reaction, hydrogen productivity reaches a constant value of  $0.8\text{ mol H}_2/\text{mol glycerol}$ , does not change until experiment termination and corresponds to the gas-phase non-catalytic reaction. Thus, fast deactivation is observed for these samples, which is related to the involvement of surface acid sites in the formation of carbon, which blocks active metal sites. The oxygen addition to the reaction mixture (Figure 4.3.1, b) substantially enhances the glycerol conversion due to increasing the selectivity for CO; however, the yield of hydrogen attains a maximum of  $3.5\text{ mol H}_2/\text{mol glycerol}$  after 3 hours of the reaction and drops to  $0.8\text{ mol H}_2/\text{mol glycerol}$  already after 7 hours of the reaction.

In this connection, the reaction was carried out with the most promising supported catalysts whose supports were modified by impregnation of the formed alumina from an aqueous solution. In



general, stability is determined mostly by magnesium content and method of its introduction, while selectivity for hydrogen and by-products as well as conversion – by the perovskite composition.

### 1. Effect of magnesium content

Figure 4.3.2 displays productivities for main products and glycerol conversion to gas for the praseodymium-containing series of catalysts  $10\% \text{PrNi}_{0.9}\text{Ru}_{0.1}\text{O}_3/[\text{n}\% \text{Mg}-\gamma\text{-Al}_2\text{O}_3]$  with different magnesium content versus the reaction time.

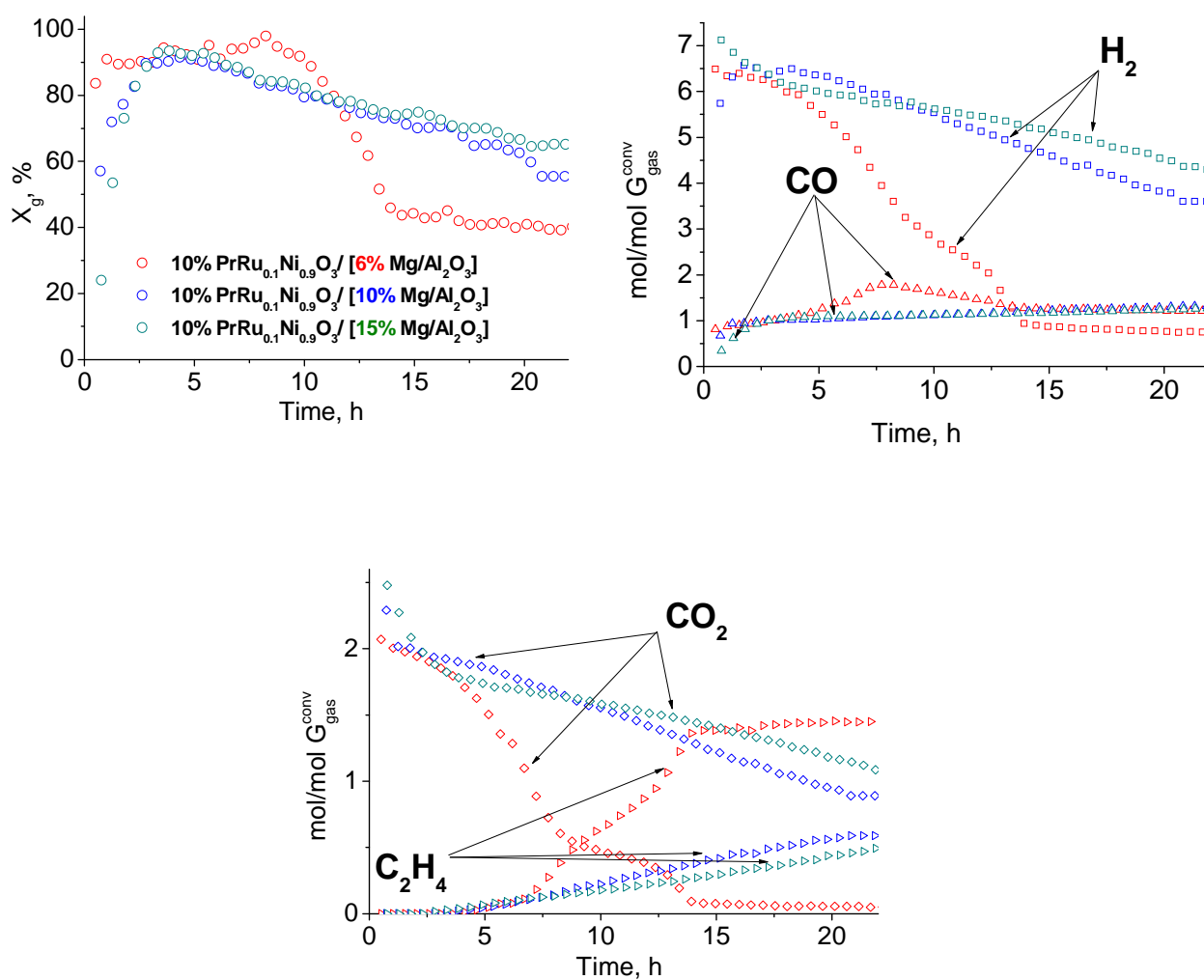


**Figure 4.3.2** Glycerol conversion to gas  $X_g$  and productivities to the gaseous products  $P_i$  in the glycerol steam reforming reaction ( $\text{C}_3\text{H}_8\text{O}_3: \text{H}_2\text{O}=1:9$ ,  $\text{GHSV}=28000 \text{ h}^{-1}$ ,  $T=650 \text{ }^\circ\text{C}$ ) obtained for  $10\% \text{PrNi}_{0.9}\text{Ru}_{0.1}\text{O}_3/[\text{n}\% \text{Mg}-\gamma\text{-Al}_2\text{O}_3]$  samples with different magnesium content in the support

The maximum activity of these catalysts was reached after five hours of the reaction, with the maximum yield of hydrogen corresponds to the thermodynamic limit (6.2 mol  $\text{H}_2$ /mol glycerol). The deactivation rate after five hours of the reaction depends on magnesium content in the samples.

For the sample with the 6 wt.% magnesium content the most rapid decrease in the hydrogen productivity was observed. High value of glycerol conversion is provided by the ethylene formation that becomes a main reaction product.

Influence of the rare-earth element nature is much more pronounced in the catalytic behavior of the deposited perovskites family in the steam reforming reaction of glycerol comparing with the ethanol one. Other things being equal, glycerol conversion is higher for Pr-containing catalysts. Figure 4.3.3 illustrates a comparison of the catalytic behavior of 10%LaNi<sub>0.9</sub>Ru<sub>0.1</sub>O<sub>3</sub>/[10%Mg-γ-Al<sub>2</sub>O<sub>3</sub>] and 10%PrNi<sub>0.9</sub>Ru<sub>0.1</sub>O<sub>3</sub>/[10%Mg-γ-Al<sub>2</sub>O<sub>3</sub>] samples.

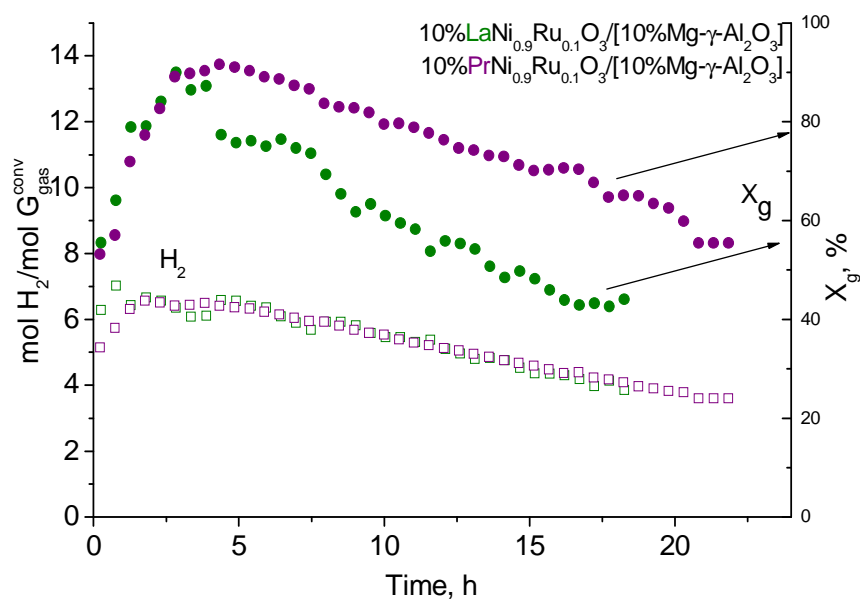


**Figure 4.3.3.** Glycerol conversion to gas X<sub>g</sub> and H<sub>2</sub> productivity in the glycerol steam reforming reaction (C<sub>3</sub>H<sub>8</sub>O<sub>3</sub>: H<sub>2</sub>O=1:9, GHSV=28000 h<sup>-1</sup>, T=650 °C) obtained for 10%LnNi<sub>0.9</sub>Ru<sub>0.1</sub>O<sub>3</sub>/[n%Mg-γ-Al<sub>2</sub>O<sub>3</sub>] (Ln = La, Pr) samples with different Ln cation

An increasing of the perovskites amount in the catalyst up to 20% does not lead to a significant improvement in the activity but slightly improve the stability after 8 hours of reaction run (Figure 4.3.4). For the 20% sample, hydrogen productivity shows only a minor decrease with time and after 20 hours of the reaction is equal to 5 mol H<sub>2</sub>/mol glycerol (80% of the thermodynamic limit).

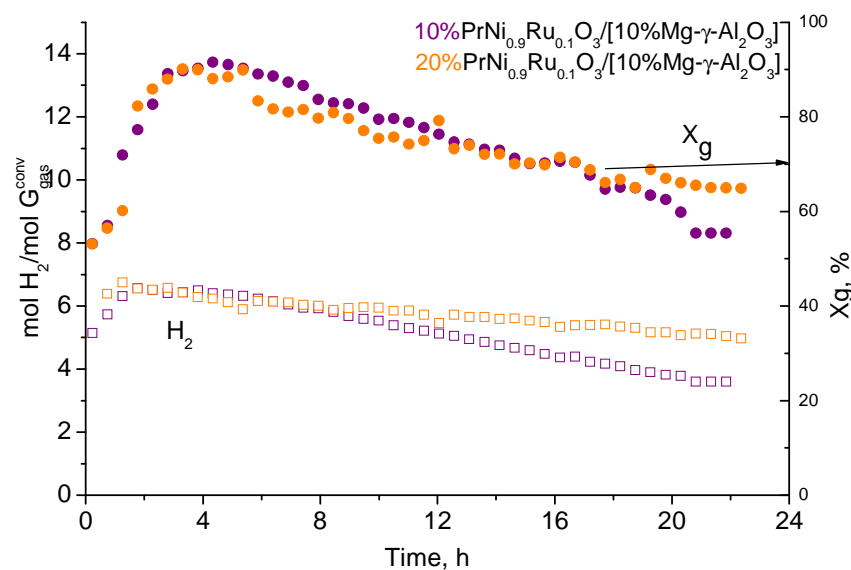


**Figure 4.3.4.** Glycerol conversion to gas  $X_g$  and  $H_2$  productivity in the glycerol steam reforming reaction ( $C_3H_8O_3: H_2O=1:9$ ,  $GHSV=28000\text{ h}^{-1}$ ,  $T=650\text{ }^\circ\text{C}$ ) obtained for samples with different perovskites amount

The oxygen addition to the reaction mixture substantially improves stability of the catalysts and maintains the high yield of hydrogen. Figure 4.3.5 displays the time dependences of productivity for hydrogen and ethanol conversion for the  $10\%PrNi_{0.9}Ru_{0.1}O_3/[15\%Mg-\gamma-Al_2O_3]$  catalyst, which is most stable in GSR.

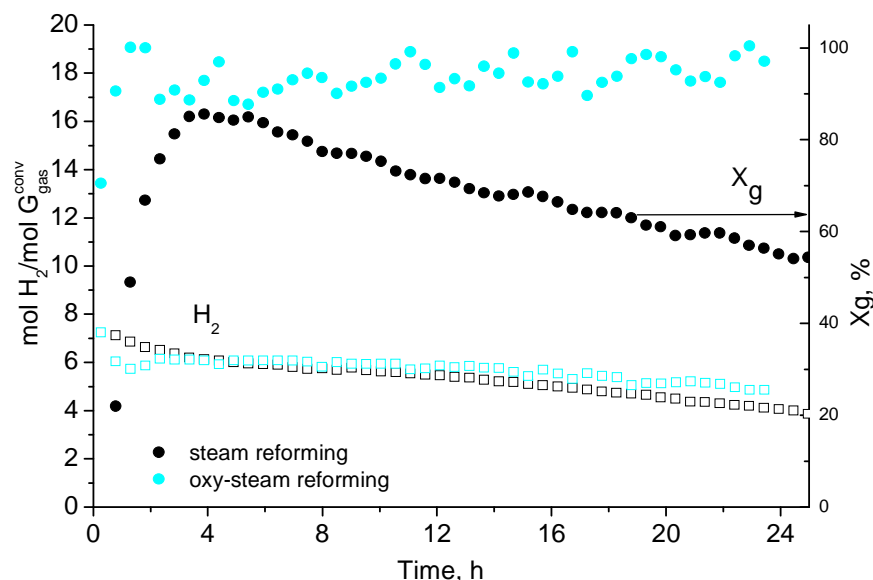


**Figure 4.3.5.** Glycerol conversion to gas  $X_g$  and productivities to the gaseous products  $P_i$  for the  $10\%PrNi_{0.9}Ru_{0.1}O_3/[15\%Mg-\gamma-Al_2O_3]$  sample in a) GSR ( $C_3H_8O_3: H_2O=1:9$ ,  $GHSV=28000\text{ h}^{-1}$ ,  $T=650\text{ }^\circ\text{C}$ ) and b) GOSR ( $C_3H_8O_3:H_2O:O_2 = 1:9:0.25$ ,  $GHSV=28000\text{ h}^{-1}$ ,  $T=650\text{ }^\circ\text{C}$ ) reactions

#### 4.4. Conclusion to Chapter 4

The effect of magnesium content and method of its introduction, as well as composition and amount of the deposited perovskite precursor on the activity, stability and selectivity of the catalysts in steam reforming of ethanol, steam and steam-oxygen reforming of glycerol was revealed. The catalytic testing showed that all the tested catalysts are active in the studied reactions. It was demonstrated that activity, selectivity and stability of the catalysts depend on the nature of lanthanide and transition metals, Mg amount and methods used for catalyst synthesis and modification.

- The results obtained in the study corroborate the literature data and testify that dehydration process of the steam reforming intermediates with the double C=C-bonded compounds formation proceeds on the alumina surface. The increasing of the Mg amount from 6 to 15 % wt. for the samples obtained via impregnation of the formed gamma aluminum oxide with an aqueous solution of magnesium nitrate makes it possible to obtain supports with predominant distribution of magnesium on the support surface providing a sufficient Mg surface concentration. This leads to decrease in the surface acidity calculated from IR spectroscopy of adsorbed CO decreasing the selectivity for ethylene at temperatures below 600 °C for both La- and Pr-containing catalysts in the ESR and GSR reactions.
- For the ESR reaction when magnesium content in the catalyst exceeds 10 wt.%, nickel-containing catalysts based on lanthanum and praseodymium exhibit identical activity. High ethanol conversions for the samples are reached already at 600 °C; therewith, the high yields of hydrogen and CO as well as the low selectivity for by-products are retained. In case of GSR reaction, the influence of the rare-earth element nature is much more pronounced: other things being equal, glycerol conversion is higher for Pr-containing catalysts.
- The most active and stable catalysts in both reactions are the samples containing Pr and Ni and 10-15 % Mg amount:  $10\% \text{PrNi}_{0.9}\text{Ru}_{0.1}\text{O}_3 / [10-15\% \text{Mg}-\gamma\text{-Al}_2\text{O}_3]$ .
- It was shown that the addition of oxygen to the reaction medium decreases the formation of all forms of carbon deposits.

**CHAPTER 5. STRUCTURED CATALYTIC SYSTEMS  $\text{LaNi}_{0.9}\text{Ru}_{0.1}\text{O}_3/\text{nMg-}\gamma\text{-Al}_2\text{O}_3$   
DEPOSITED ON DIFFERENT FOAM SUPPORTS: ASSESSMENT OF CATALYTIC  
PROPERTIES AND STABILITY IN STEAM AND OXY-STEAM REFORMING OF  
ETHANOL IN CONCENTRATED MIXTURES**

In order to increase further the specific surface areas of the prepared catalytic materials supported on modified  $\text{Mg-}\gamma\text{-Al}_2\text{O}_3$  and to test the possibility of their potential application in the industrial fuel cells the structured foam-like platelets were used as a structure-forming framework. This chapter is devoted to the investigation of the  $10\%\text{LaNi}_{0.9}\text{Ru}_{0.1}\text{O}_3/6\%\text{Mg-}\gamma\text{-Al}_2\text{O}_3$  catalysts supported on different porous foam supports prepared via deposition from the catalyst's organic suspension followed by calcination at  $900\text{ }^\circ\text{C}$ . Activity of catalysts and estimation of their stability in steam and oxy-steam reforming of ethanol reactions in a pilot reactor in concentrated mixtures were studied.

**5.1. Structural and textural properties of initial supports and catalysts**

The only one catalyst with the composition of  $10\%\text{LaNi}_{0.9}\text{Ru}_{0.1}\text{O}_3/6\%\text{Mg-}\gamma\text{-Al}_2\text{O}_3$  was chosen for this study. It was supported on porous platelets made of the Ni-Al alloy, Ni-Al-SiC and Ni-Al-SiC/corundum ceramics by the method described in the Chapter 2.1.4, 10%wt. of the active component was added finally to an initial platelet. Some characteristics of the initial foams are listed in the Table 5.1.

**Table 5.1** Main characteristics of structured substrates

№	Chemical composition, wt.%	Density, g/cm <sup>3</sup>	Pore size/porosity	Heat conductivity, Wm <sup>-1</sup> K <sup>-1</sup>	Shape and size, mm
1	Ni-Al alloy, Al 10%	2.5	60 ppi/65.6%	9.8	35 × 35 × 1
2	SiC 40%; Al <sub>2</sub> O <sub>3</sub> -SiO <sub>2</sub> rest	0.5	30 ppi/75.5%	3.5	38 × 38 × 5
3	a-Al <sub>2</sub> O <sub>3</sub> 45%; Al <sub>2</sub> O <sub>3</sub> -SiO <sub>2</sub> rest	0.6	30 ppi/78.6%	1.7	38 × 38 × 5

The data is given for pure structured foams without supported perovskite precursors. The most dense foam and probably the most robust in the technical use is the metallic Ni-Al alloy. It possesses the highest heat conductivity  $9.8\text{ Wm}^{-1}\text{K}^{-1}$  which makes this foam very convenient for use as a support in exothermic reactions, as steam reforming of oxygenates are, where could be a problem of the fast heat evacuation. The method of the Ni-Al alloy plate's synthesis provides passivation of the nickel surface, preventing its participation in the reaction or oxidation process.

The SEM pictures of the wall section for the platelet as prepared and calcined in air at 900 °C proves the stability to oxidation due to the Ni-Al alloy surface layer (Fig. 5.1. b).

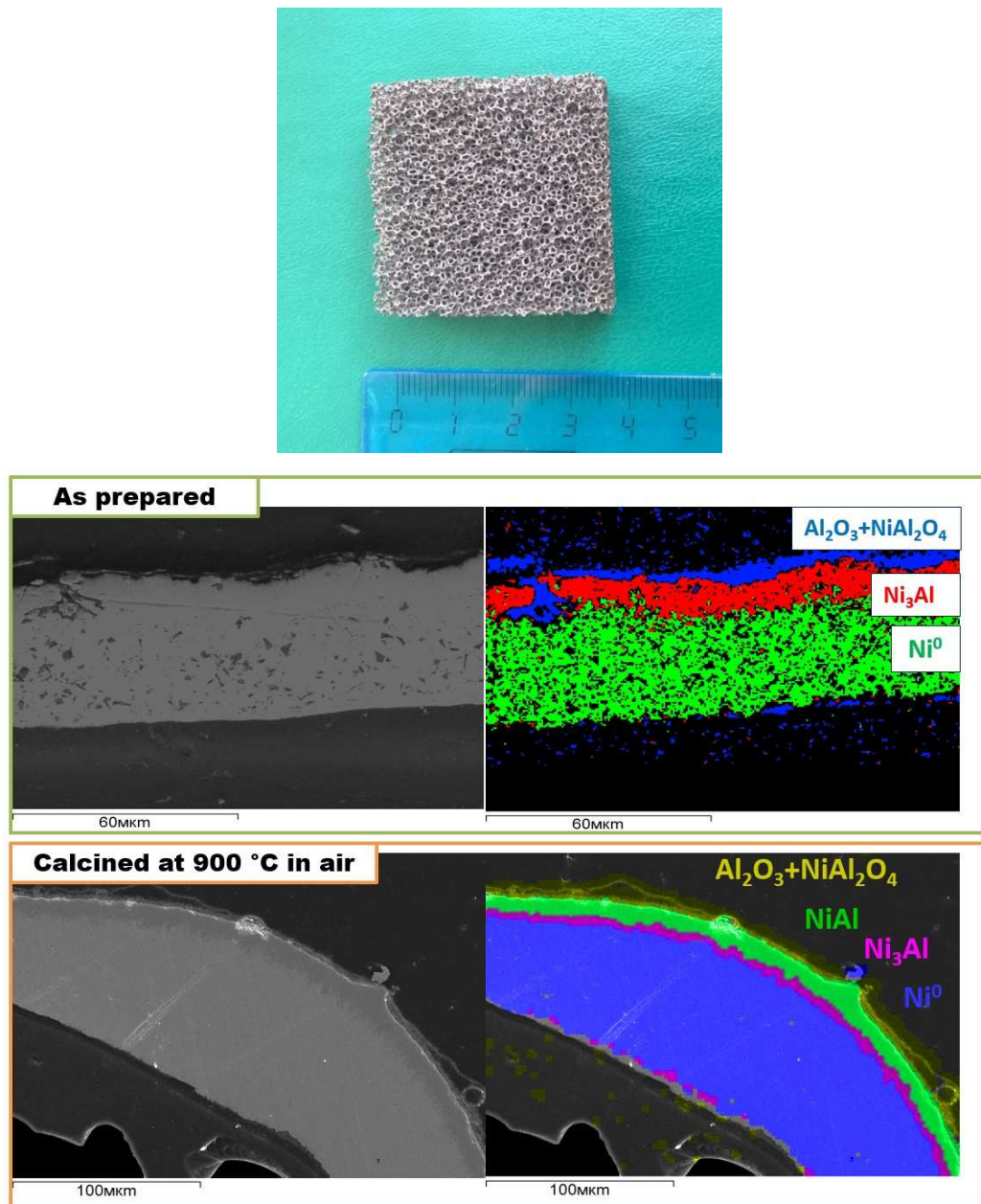


**Figure 5.1.** – a. – The photography of Ni-Al foam, b - SEM pictures with EDX analysis of the wall section: as prepared (top) and calcined at 900°C (bottom)

From the other side other structured supports (SiC- and  $\text{Al}_2\text{O}_3$ -based) have bigger porosity that can be a positive factor for lower diffusion limitations and thus more effective heat evacuation with the gas flow. After the deposition of the active component on the three structured supports the platelet's surfaces were evenly covered with the catalysts without blocking the pores, which was noticeable in the SEM pictures for these structured systems.

## 5.2. Catalytic activity in steam/oxy-steam reforming of ethanol

The activity of the 10%LaNi<sub>0.9</sub>Ru<sub>0.1</sub>O<sub>3</sub>/6%Mg- $\gamma$ -Al<sub>2</sub>O<sub>3</sub> catalyst supported on porous platelets was studied in steam and oxy-steam reforming of ethanol in concentrated mixtures at a temperature of 850 °C, contact time 1 s, and different compositions of the reaction mixture:

<u>Ethanol oxy-steam reforming (EOSR)</u>	29% C <sub>2</sub> H <sub>5</sub> OH + 57% H <sub>2</sub> O + 3% O <sub>2</sub> + 10% N <sub>2</sub> ;
<u>Ethanol steam reforming (ESR)</u>	30% C <sub>2</sub> H <sub>5</sub> OH + 60% H <sub>2</sub> O + 10% N <sub>2</sub> .

For all the catalysts studied, conversion of ethanol was 100% under the indicated conditions. Figure 5.2 (a) displays comparative data on H<sub>2</sub> and CO concentrations in the reaction products of ethanol steam-oxygen reforming for three different supports.

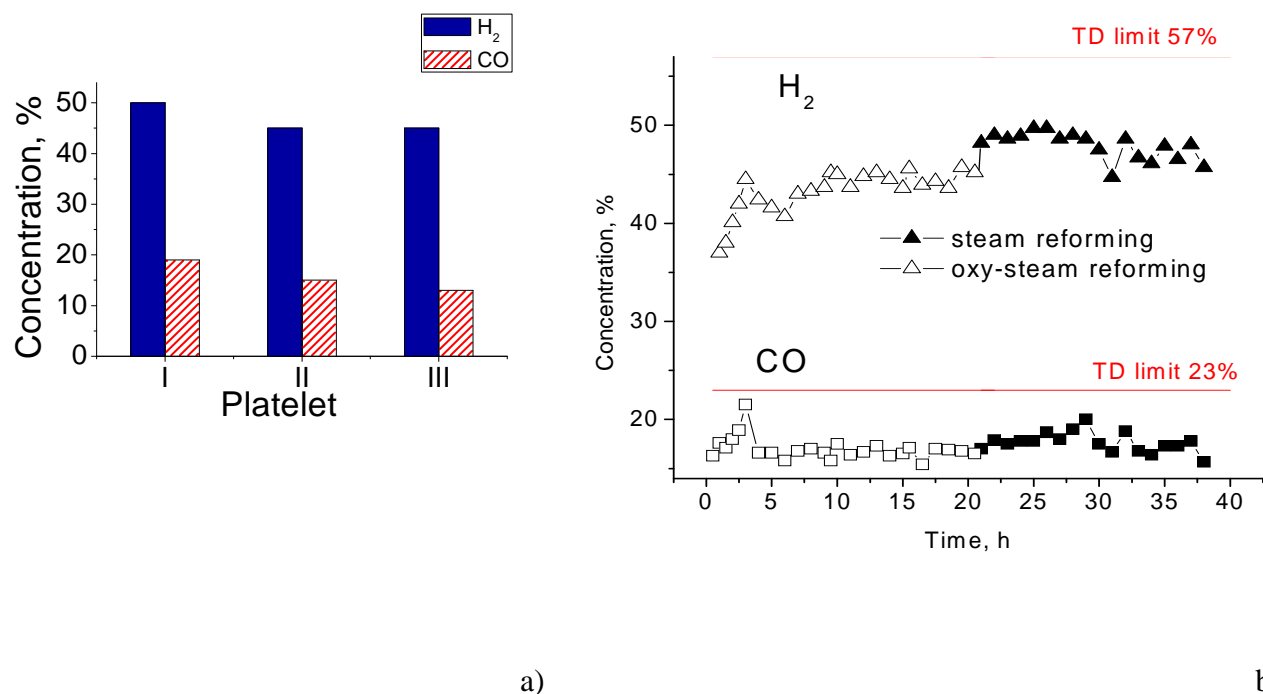


**Figure 5.2. a** – H<sub>2</sub> and CO concentrations in the EOSR products for the 10%LaNi<sub>0.9</sub>Ru<sub>0.1</sub>O<sub>3</sub>/6%Mg- $\gamma$ -Al<sub>2</sub>O<sub>3</sub> catalyst supported on (I) Ni-Al, (II) SiC/Al-Si-O and (III) corundum/Al-Si-O foam supports. **b** – H<sub>2</sub> and CO concentrations in the reaction products during stability testing performed consecutively for EOSR and ESR reactions using the 10%LaNi<sub>0.9</sub>Ru<sub>0.1</sub>O<sub>3</sub>/6%Mg- $\gamma$ -Al<sub>2</sub>O<sub>3</sub> catalyst with the Ni-Al foam support

As it can be seen on the plot, the highest concentrations of hydrogen and carbon monoxide were 49 and 27 %, respectively; as expected they were obtained for the sample with the Ni-Al foam support. Its high activity was caused by a higher thermal conductivity, which ensures an efficient heat transfer along the catalytic bed. The lower hydrogen and CO concentrations in other two samples may be caused by collateral reactions that could be favored in these conditions – long



contact time, not-effective products and heat evacuation that cause the adsorption of produced  $H_2$  and CO on the catalyst surface and their further oxidation. In a Figure 5.3., the SEM pictures of the catalysts used are given. The well-preserved structure and the absence of filamentous carbon are clearly visible.

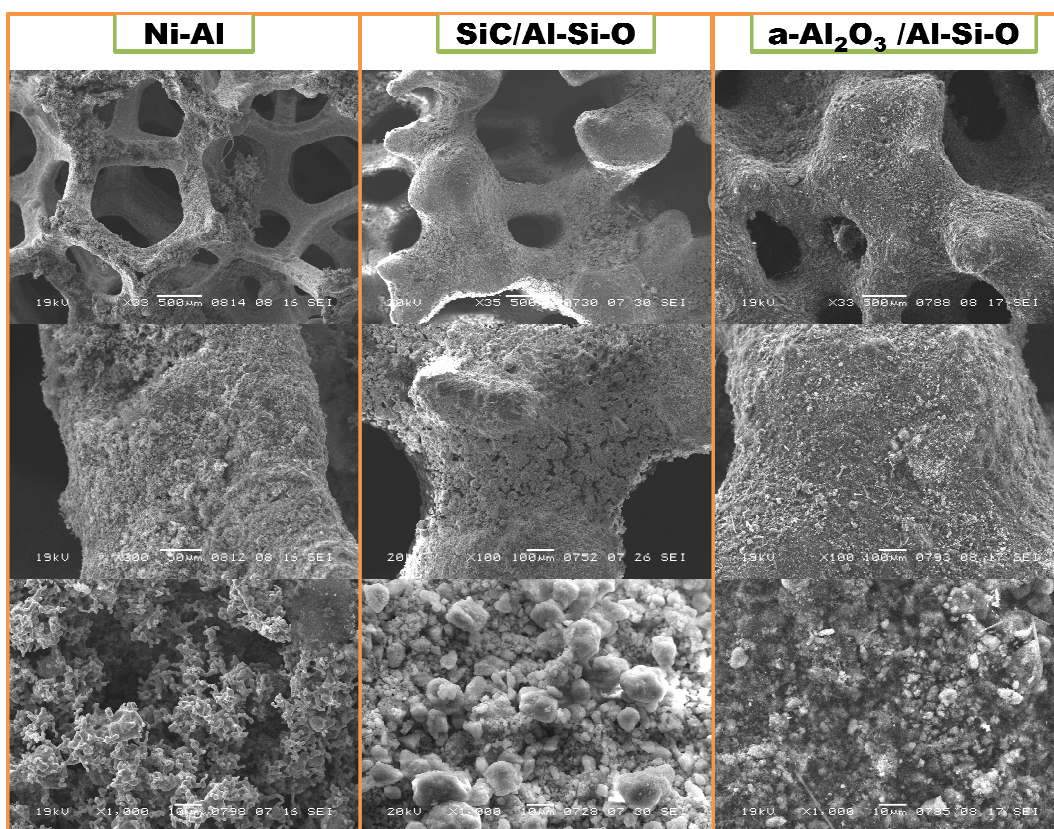


**Figure 5.3.** SEM pictures of the structured catalysts based on  $10\%LaNi_{0.9}Ru_{0.1}O_3/6\%Mg-\gamma-Al_2O_3$  supported on (I) Ni-Al, (II) SiC/Al-Si-O and (III)  $\alpha-Al_2O_3/Al-Si-O$  foam supports after EOSR reaction

Stability testing of the catalyst [ $10\%LaNi_{0.9}Ru_{0.1}O_3/6\%Mg-\gamma-Al_2O_3/Ni-Al$  foam support] in EOSR and ESR reactions, which were performed consecutively on the same platelet, shows that the catalyst does not lose its activity for 40 hours of operation in concentrated mixtures (Figure 5.2 b).

The data obtained for the supported catalysts (the second family from the Chapter IV), revealing that the Pr-based samples are more active than La-based ones, allow us to expect the even better activity and stability of the structured catalysts using the  $PrNi_{0.9}Ru_{0.1}O_3/Mg-\gamma-Al_2O_3$  composition; research in this direction is planned and will be the further direction of these systems' improvement. The results obtained give a very promising expectation, that the catalysts based on  $LnNi_{0.9}Ru_{0.1}O_3/Mg-\gamma-Al_2O_3$  on the structured supports proposed in the work can be employed to develop highly efficient reactors for the production of hydrogen and syngas as well as medium-temperature fuel cells.



## CHAPTER 6. MAIN CONCLUSIONS

The purpose of the work was to find the active and stable cost-effective metal-oxide catalysts for the promising process of steam reforming of biomass-derived oxygenates as ethanol and glycerol. According to the literature data analysis, the main points to be solved were determined. The general one was using as an active component relatively cheap transition metals instead of precious ones. Among others, Ni and Co were chosen. To overcome the most severe obstacle inherent to these catalysts' group – intensive carbonization during the reaction causing fast deactivation – several approaches were implemented.

1. The metal particles have to be as small as possible with the strong metal-support interaction to prevent its sintering and enlargement under reaction medium. In this work, it was supposed to achieve this goal through the use of the Ni(Co)-containing mixed oxides as precursors that can be activated by reduction with the partial emerge of the cations needed from the structure to form high-dispersed well-distributed metal nanoparticles on the surface of remaining oxide. Moreover, rare-earth elements in the composition can help to enhance the catalysts stability helping to oxidize the coke precursors. Ni(Co) dispersed particles can be additionally stabilized by Ni-Fe(Ru) alloy formation possessing strong interaction with the oxide remaining and in case of mixed oxides doped with transition (Fe) or precious (Ru) metals.

In this regard, the *first catalysts' family based on perovskites with the general formula  $\text{LnFe}_{1-x-y}\text{M}_x\text{Ru}_y\text{O}_3$*  (Ln = Pr, La, M= Ni, Co,  $x = 0.3; 0.4$   $y = 0; 0.1$ ) was synthesized by the modified Pechini method and its both physical-chemical and catalytic properties were studied. To identify the effect of perovskite precursor's synthesis method on the activity and selectivity of the catalysts, a series of 5% Co(Ni)/PrFeO<sub>3</sub> comparison catalysts were prepared by impregnating the perovskite PrFeO<sub>3</sub> with the Ni(Co) nitrates solution.

The results of the textural and structural properties studies of the samples were analyzed in details. It was shown, that by the modified Pechini method from organic polymer solution followed by calcinations at 700-900 °C, a single-phase perovskites  $\text{LnFe}_{1-x-y}\text{M}_x\text{Ru}_y\text{O}_3$  (Ln = La, Pr, M = Ni, Co) of the orthorhombic structure are formed for the parameters:  $x \leq 0.3$  for Ni,  $x \leq 0.4$  for Co;  $y = 0-0.1$ . In the case of 5% M/PrFeO<sub>3</sub> samples obtained by impregnation, Ni(Co) are not included in the perovskite structure and are present as individual oxides of NiO or Co<sub>3</sub>O<sub>4</sub> on the PrFeO<sub>3</sub> surface. The investigation of surface characteristics shows that average SSA of all samples obtained is about 4-10 m<sup>2</sup>/g, which are typical values for perovskites of this composition. The TPR-H<sub>2</sub> studies showed that the reducibility of individual perovskite depends on its composition and doping cations, but in general for all perovskites the same reduction tendency is observed: up to 500°C in

hydrogen flow the structure remains stable (according to TPR-H<sub>2</sub> data up to 100% of Ni<sup>3+</sup>(Co<sup>3+</sup>) reduced to Ni<sup>2+</sup>(Co<sup>2+</sup>) within the perovskite structure). Further increasing of temperature up to 800 °C leads to a Ni(Co) and Fe metallic particles partially emerge from the perovskite and stabilized on the surface of oxide with simultaneous formation of Pr oxides phases. Perovskite reducibility depends both on the nature of the lanthanide and transition metal: Pr-containing samples are reduced more easily than La-containing, and Ni-containing are reduced more easily than Co-containing.

Tests in the steam reforming of ethanol reaction in the temperature range 600 - 850 °C of the catalysts preliminarily reduced in hydrogen at 800 °C show that for all LnFe<sub>1-x-y</sub>M<sub>x</sub>Ru<sub>y</sub>O<sub>3</sub> samples similar dependencies are observed - high values of ethanol conversion are observed already at 700 °C, and the main reaction products are H<sub>2</sub>, CO and CO<sub>2</sub>. The samples containing Pr exhibit higher activity and stability than the La-containing due to the high red-ox activity of the praseodymium, which promotes the oxidation of coke precursors. The activity of samples based on Co is much lower than for Ni-containing analogs over the entire temperature range. At the same time, a high yield of acetaldehyde and ethylene indicates a low rate of conversion of these intermediates to the target products. The results obtained are consistent with the difficulty of reducing Co from the perovskite structure shown by the TPR-H<sub>2</sub> method. Comparison of the activity of catalysts based on LnFe<sub>1-x-y</sub>M<sub>x</sub>Ru<sub>y</sub>O<sub>3</sub> and 5% Co(Ni)/PrFeO<sub>3</sub> shows that the supported 5% Co(Ni)/PrFeO<sub>3</sub> are more active at T ≤ 700 °C, which is due to an easier reduction of nickel/cobalt, according to the TPR-H<sub>2</sub> data. However, the tests of these samples at a constant temperature of 650 °C for 7 hours showed rapid deactivation in the case of 5% Co (Ni)/PrFeO<sub>3</sub>, and TEM images of the catalysts after the reaction indicate a significant sintering of the metal particles for the impregnated samples. Thus, the catalysts based on substituted ferrites LnFe<sub>1-x-y</sub>M<sub>x</sub>Ru<sub>y</sub>O<sub>3</sub> demonstrate greater resistance to sintering of metal particles and carbonization as a result of strong interaction of metal particles with the support and dilution of nickel ensembles due to the formation of a Ni-Fe(Ru) alloy. Analysis of the catalytic data revealed that the main route for the ethanol steam reforming reaction in the presence of perovskite-based catalysts is the dehydrogenation of ethanol to form an intermediate, acetaldehyde, which contributes to the high stability of these samples to carbonization

The LnFe<sub>1-x-y</sub>M<sub>x</sub>Ru<sub>y</sub>O<sub>3</sub> catalysts were reduced in hydrogen at 500 °C and tested as well in the steam reforming of glycerol reaction at 650 °C. For samples based on nickel PrFe<sub>0.7</sub>Ni<sub>0.3</sub>O<sub>3</sub>, La<sub>0.7</sub>Pr<sub>0.3</sub>Fe<sub>0.7</sub>Ni<sub>0.3</sub>O<sub>3</sub>, PrFe<sub>0.6</sub>Ni<sub>0.3</sub>Ru<sub>0.1</sub>O<sub>3</sub>, it was shown that the character of the change in the conversion level and hydrogen yield in time depends on the materials' composition. Thus, for samples PrFe<sub>0.7</sub>Ni<sub>0.3</sub>O<sub>3</sub> and La<sub>0.7</sub>Pr<sub>0.3</sub>Fe<sub>0.7</sub>Ni<sub>0.3</sub>O<sub>3</sub>, a maximum on the curves is observed probably due to perovskite additional reduction in the reaction mixture, followed by a rapid decrease in

activity caused by carbon deposit. The high initial activity of the catalyst based on  $\text{PrFe}_{0.6}\text{Ni}_{0.3}\text{Ru}_{0.1}\text{O}_3$  can be explained by the presence of ruthenium that decreases perovskite reduction temperature below 300 °C, so the active phase formation occurs completely during pretreatment. In addition, the activity of this catalyst decreases gradually and slowly enough, which indicates its greater resistance to coking comparing with the non-ruthenium samples. According the Ln cation influence, for praseodymium-based catalysts, higher hydrogen yield and glycerol conversion to the gas phase are observed. The  $\text{H}_2$  and  $\text{CO}_2$  productivity, at a close  $X_g$  values, are higher for the sample based on  $\text{PrFe}_{0.6}\text{Ni}_{0.3}\text{Ru}_{0.1}\text{O}_3$ . Tests of catalysts based on cobalt showed that they exhibit low activity in reactions leading to the formation of hydrogen: despite the conversion of glycerol to the gas phase  $X_g$  of 70%, the hydrogen productivity for cobalt-containing systems even with the addition of oxygen (GOSR) remains low (0.8 mol  $\text{H}_2$ /mol  $G_{conv}^{gas}$ ), which corresponds to the value for the sample  $\text{PrFeO}_3$  without presence of any active metal.

Summarizing all the data obtained for the first family, it was shown that perovskite-based catalysts  $\text{LnFe}_{1-x-y}\text{M}_x\text{Ru}_y\text{O}_3$  with optimized composition – praseodymium-, nickel- and ruthenium-based - exhibit high activity and stability in both reactions studied. Nevertheless, with satisfactory stability in the steam reforming of ethanol, such compositions deactivates significantly in the steam reforming of glycerol reaction, even most effective  $\text{PrFe}_{0.6}\text{Ni}_{0.3}\text{Ru}_{0.1}\text{O}_3$  ruthenium doped one. In this connection, there was a need to further improve the properties of precursor materials.

2. First of all, it was necessary to increase the specific surface areas of the catalysts, additionally reduce as much as possible the content of a fairly expensive rare-earth elements. It was proposed to achieve this property by using an alumina-based support for perovskite with a high specific surface area. Widespread in industry inexpensive high SSA support  $\gamma\text{-Al}_2\text{O}_3$  is also well-known as an oxide with the acidic properties. Being used as a catalyst for oxygenates' steam reforming reaction, it will dramatically suppresses stability by initiation of the dehydration reaction with the carbon deposits rapid accumulation. In this connection, it is necessary to decrease the surface acidity; well-studied method of the surface modification with alkaline-earth element Mg was chosen. There were several issues to overcome; first of all, the synthesis of the systems that combine several structural types in one is a nontrivial task, poorly lit in a literature. Moreover, for the active metal used (nickel), the possibility of existence in both the applied component and the carrier phases complicates the preparation of a catalyst with controlled properties.

In this regard, the *second catalysts' family based on supported catalysts with the general formula  $m\text{LnNi}_{0.9}\text{Ru}_{0.1}\text{O}_3/n\%\text{Mg-}\gamma\text{-Al}_2\text{O}_3$*  (Ln = La, Pr, m = 10; 20, n = 6; 10; 15) was synthesized and studied. Supported catalysts  $m\text{LnNi}_{0.9}\text{Ru}_{0.1}\text{O}_3/n\%\text{Mg-}\gamma\text{-Al}_2\text{O}_3$  (Ln = La, Pr, m = 10; 20, n = 6; 10; 15) were synthesized via the deposition of perovskite precursors from aqueous or organic

solutions onto the modified support [Mg- $\gamma$ -Al<sub>2</sub>O<sub>3</sub>]. The investigation of surface characteristics shows that average SSA of all samples obtained is about 80-110 m<sup>2</sup>/g, which tenfold higher than that for massive perovskites one.

Using a set of methods, it was shown that during the synthesis of the supported mLnNi<sub>0.9</sub>Ru<sub>0.1</sub>O<sub>3</sub>/n%Mg- $\gamma$ -Al<sub>2</sub>O<sub>3</sub> samples the introduction of magnesium and nickel in the  $\gamma$ -Al<sub>2</sub>O<sub>3</sub> support occurs. Studies aimed at elucidating the effect of the Mg introduction method into the support and its content have shown that the impregnation of the formed gamma aluminum oxide with an aqueous solution of magnesium nitrate makes it possible to obtain supports with predominant distribution of magnesium on the support surface; therefore, this method was chosen as the best one for the synthesis of the catalysts' supports. For samples obtained by this method, an increase in the Mg content  $\geq$  10% leads to the formation of a phase of MgO (the amount of MgO phase is increased with the increases in the Mg content to 15%). The study of these supports by the IR spectroscopy of adsorbed CO shows a decrease in the acidity of the surface with an increase in the surface concentration of magnesium. Furthermore, the Mg introduction not only reduces the acidity of  $\gamma$ -Al<sub>2</sub>O<sub>3</sub> but its concentration affects the interaction of nickel with the support: at n = 6%, nickel is predominantly incorporated into the  $\gamma$ -Al<sub>2</sub>O<sub>3</sub> to form spinel Ni<sub>x</sub>(Mg<sub>1-x</sub>)Al<sub>2</sub>O<sub>4</sub>; at n  $\geq$  10%, a solid solution of NiO-MgO is additionally formed. With a 20% perovskites content, some of the nickel shown to be a part of the superficial perovskite-like structures PrNi<sub>x</sub>Ru<sub>1-x</sub>O<sub>3</sub> and Pr<sub>2</sub>Ni<sub>x</sub>Ru<sub>1-x</sub>O<sub>4</sub>.

The TPR-H<sub>2</sub> studies showed that the reduction of mLnNi<sub>0.9</sub>Ru<sub>0.1</sub>O<sub>3</sub>/n%Mg- $\gamma$ -Al<sub>2</sub>O<sub>3</sub> samples with the formation of highly dispersed metallic Ni particles and the Ni-Ru alloy is determined by the degree of nickel interaction with the support, which depends on the concentration of magnesium and perovskite: its increase leads to a facilitation of Ni reduction from the oxide. Such a behavior corresponds to an easier reduction of nickel from the Ni<sub>x</sub>Mg<sub>1-x</sub>Al<sub>2</sub>O<sub>4</sub> mixed spinel phase in the samples with n  $\geq$  10% wt., as compared to NiAl<sub>2</sub>O<sub>4</sub> phase inherent in samples with a magnesium content below 6 % wt. An increase in the perovskite content to 20 wt. % make more pronounced the high-temperature broad peak with the maxima at 700 and 832 °C corresponds to nickel reduction from NiO-MgO, Ni<sub>x</sub>Mg<sub>1-x</sub>Al<sub>2</sub>O<sub>4</sub> and perovskite-like PrNi<sub>x</sub>Ru<sub>1-x</sub>O<sub>3</sub> phase, which are the preferable phases to reduced from to obtain a high-dispersed metal particles with strong Me-Support interaction.

Tests in the steam reforming of ethanol reaction in the temperature range 600 - 850 °C of the catalysts preliminarily reduced in hydrogen at 500 °C show that the surface acidity of the support is the essential parameter affect the catalytic properties of the mLnNi<sub>0.9</sub>Ru<sub>0.1</sub>O<sub>3</sub>/n%Mg- $\gamma$ -Al<sub>2</sub>O<sub>3</sub> family. The samples with the insufficient Mg surface concentration demonstrate a low selectivity

for hydrogen in the temperature range of 500-750 °C, and the observed > 80% conversion of ethanol at the temperatures indicated was accompanied by a high yield of ethylene (70%). An increase in magnesium content in the catalyst decreases the selectivity for ethylene at temperatures below 600 °C for both La- and Pr-containing catalysts; for these compositions, such a decrease correlates with a decrease in the surface acidity calculated from IR spectroscopy of adsorbed CO. When magnesium content in the catalyst exceeds 10 % wt., nickel-containing catalysts based on lanthanum and praseodymium exhibit identical catalytic behavior. High ethanol conversions for the samples are reached already at 600 °C; therewith, the high yields of hydrogen and CO as well as the low selectivity for by-products are retained.

As for the massive catalysts, the steam reforming of glycerol studies were also performed. Data on the glycerol conversion to gas products  $X_g$  and the distribution of productivities in the gaseous phase were obtained for the following parameters: the reaction mixture  $C_3H_8O_3: H_2O = 1:9$ , gas hourly space velocity of  $28000\text{ h}^{-1}$  and temperature 650 °C.

It was shown, that surface acidity of the support, as well as the composition and amount of the perovskite deposited determine the catalytic behavior of the systems produced. The catalysts where a uniform surface coverage with magnesium was not achieved are inefficient toward steam reforming of glycerol at all (the hydrogen productivity was 0.8 mol  $H_2$ /mol glycerol), or, in case of sample with the 6 wt. % magnesium, demonstrate an abrupt decrease in the hydrogen productivity after 8 hours of reaction. For the samples with the Mg amount  $\geq 10\%$  wt, the influence of the rare-earth element nature is much more pronounced in case of GSR reaction comparing with the ESR one: other things being equal, glycerol conversion is higher for Pr-containing catalysts. The maximum activity of these 10%PrNi<sub>0.9</sub>Ru<sub>0.1</sub>O<sub>3</sub>/10-15%Mg- $\gamma$ -Al<sub>2</sub>O<sub>3</sub> catalysts was reached after five hours of the reaction, with the maximum yield of hydrogen corresponds to the thermodynamic limit (6.2 mol  $H_2$ /mol glycerol). An increasing of the perovskites amount in the catalyst up to 20% does not lead to a significant improvement in the activity but slightly improve the stability after 8 hours of reaction run. For the 20% sample, hydrogen productivity shows only a minor decrease with time and after 20 hours of the reaction is equal to 5 mol  $H_2$ /mol glycerol (80% of the thermodynamic limit). It was also shown that the oxygen addition to the reaction mixture substantially improves stability of the catalysts and maintains the high yield of hydrogen.

Summarizing, it is shown that the catalysts of the optimal composition 10-20% PrNi<sub>0.9</sub>Ru<sub>0.1</sub>O<sub>3</sub>/10%Mg- $\gamma$ -Al<sub>2</sub>O<sub>3</sub> provide the greatest yield of hydrogen (~ 90%) and stability for 8-20 hours in the both reactions studied at the T = 650 °C.

3. To elucidate the thermal compatibility and activity of *structured catalysts based on porous supports* in a pilot reactor under conditions close to industrial ones, the catalyst

LaNi<sub>0.9</sub>Ru<sub>0.1</sub>O<sub>3</sub>/6%Mg- $\gamma$ -Al<sub>2</sub>O<sub>3</sub> that showed average results in a steam reforming reactions was supported on three types of porous metallic or metallic-ceramic substrates by slip casting slurries in isopropanol with addition of polyvinyl butyral followed by drying and calcination under air at 700 °C for 2 h.

The high activity of the catalysts based on structured macroporous Ni-Al, SiC/Al-Si-O and Ni-Al-SiC/ $\alpha$ -Al<sub>2</sub>O<sub>3</sub> carrier was demonstrated in the steam reforming reaction of ethanol in a pilot reactor. The structured catalyst based on the metal Ni-Al platelet provides the yield of hydrogen 80-87% of oxy-steam and steam reforming of ethanol in the concentrated mixtures (ethanol concentration of 30%) in a pilot reactor for 40 hours (T = 850 °C, contact time 1s).

It can be concluded that the catalysts investigated with the optimized compositions from both first  $LnFe_{1-x-y}M_xRu_yO_3$  and second  $mLnNi_{0.9}Ru_{0.1}O_3/n\%Mg-\gamma-Al_2O_3$  families are very promising catalyst for the steam reforming of oxygenates. The revealed dependences of the catalytic properties on the chemical composition, textural and acidic properties of the materials can be used for further studies aimed to improve the catalysts for reforming of oxygenates. The catalysts based on LaNi<sub>0.9</sub>Ru<sub>0.1</sub>O<sub>3</sub>/Mg- $\gamma$ -Al<sub>2</sub>O<sub>3</sub> on the structured supports proposed in the work can be employed to develop highly efficient reactors for the production of hydrogen and syngas as well as medium-temperature fuel cells. The data obtained for the supported catalysts, revealing that the Pr-based samples are more active than La- ones allow us to expect the even better stability of the structured catalysts using the PrNi<sub>0.9</sub>Ru<sub>0.1</sub>O<sub>3</sub>/Mg- $\gamma$ -Al<sub>2</sub>O<sub>3</sub> composition; this assumption requires a further investigation. Data on the stability of structured samples with the foam-metallic Ni-Al support obtained in a pilot reactor for 40 h confirm that such systems are promising for introducing the processes of biofuels to syngas and hydrogen transformation into the modern power industry.

## List of publications and presentations on the subject of the thesis

### List of publications

1. Ni(Co)-Containing Catalysts Based on Perovskite-Like Ferrites for Steam Reforming of Ethanol, Arapova M. V., Pavlova S. N., Rogov V. A., Krieger T. A., Ishchenko A.V., Roger A.-C. // *Catalysis for Sustainable Energy*.-V.1.-2014.-P. 10-20. DOI: 10.2478/cse-2014-0002
2. Hydrogen and syngas production via ethanol steam reforming over supported nickelates, Arapova M. V., Pavlova S. N., Larina T. V., Glazneva T.S., Rogov V. A., Krieger T. A., Sadykov V. A., Smorygo O., Parkhomenko K., Roger A.-C. // *Materials and Technologies for Energy Efficiency* / Ed. A. Mendes-Vilas. - Boca Raton, USA: Brown Walker Press, 2015. - P. 131-135. ISBN 1627345590.
3. Perovskite-based Catalysts for Transformation of Natural Gas and Oxygenates into Syngas, Sadykov V. A., Pavlova S. N., Alikina G. M., Sazonova N. N., Mezentseva N. V., Arapova M. V., Rogov V. A., Krieger T. A., Ishchenko A. V., Gulyaev R. V., Zadesenets A. V., Roger A. C., Chan-Thaw C. E., Smorygo O. L. // *Perovskite: Crystallography, Chemistry and Catalytic Performance* / Eds.: J. Zhang, H. Li. – InTech.Nova Science publishers – 2013. – P. 1-58. ISBN 978-1-62417-800-9.
4. Mechanism of ethanol steam reforming over Pt/(Ni+Ru)-promoted oxides by FTIRS in situ, Sadykov V. A., Chub O., Chesalov Yu., Mezentseva N., Pavlova S. N., Arapova M. V., Rogov V.A., Simonov M.N., Roger A.-C., Parkhomenko K., Van Veen A. C. // *Topics in Catalysis*. V. – 59. 2016. – P. - 1332–1342. DOI: 10.1007/s11244-016-0659-y
5. Structured nanocomposite catalysts of biofuels transformation into syngas and hydrogen: Design and performance, Sadykov V., Mezentseva N., Simonov M., Smal E., Arapova M., Pavlova S., Fedorova Y., Chub O., Bobrova L., Kuzmin V., Ishchenko A., Krieger T., Roger A.-C., Parkhomenko K., Mirodatos C., Smorygo O., Ross J. // *International Journal of Hydrogen Energy*.– V. 40. – I. 24. -2015. – P. 7511-7522. DOI: 10.1016/j.ijhydene.2014.11.151
6. Structured Catalysts for Biofuels Transformation into Syngas with Active Components Based on Perovskite and Spinel Oxides Supported on Mg-Doped Alumina, Sadykov V., Pavlova S., Smal E., Arapova M., Simonov M., Mezentseva N., Rogov V., Glazneva T., Lukashevich A., Roger A.-C., Parkhomenko K., van Veen A., Smorygo O // *Catalysis Today*. - V. 293-294. - 2017. - P. 176-185. DOI: 10.1016/j.cattod.2017.05.055

### List of presentations

1. Pavlova S., Arapova M., Alikina G., Rogov V., Krieger T., Sadykov V., Roger A.-C., Chan – Thaw C. E., «Hydrogen and syngas production by steam reforming of ethanol using LnFeNiMO<sub>3</sub> (M=Co, Mn, Ru) perovskites as catalyst precursors», 11th European Congress on Catalysis– EuropaCat-XI, Lyon, France, 2013, P.585.
2. Pavlova S., Arapova M., Alikina G., Rogov V., Krieger T., Sadykov V., Roger A.-C. «Steam reforming of ethanol for hydrogen and syngas production over perovskite-type Ni(Co, Ru) ferrites

as catalyst precursors», The Seventh Tokyo Conference on Advanced Catalytic Science and Technology - TOCAT7, Kyoto, Japan, 2014, Poster O-A22 (19).

3. Arapova M. V., Pavlova S. N., Larina T. V., Rogov V. A., Krieger T. A., Sadykov V. A., Smorygo O., Parkhomenko K., Roger A.-C., «Hydrogen and syngas production via ethanol steam reforming over supported ferrites-nikelates», Energy&Materials, Research Conference - EMR2015 Madrid, Spain, 2015, P.138.

4. Sadykov V., Arapova M., Smal E., Pavlova S., Roger A.-C., van Veen A., «Nanocomposite catalysts of biofuels transformation into syngas: design and performance», 6<sup>th</sup> Annual Global Congress of Catalysis, Xian, China, 2015, P.45.

5. M. Arapova, S. Pavlova, V. Sadykov, K. Parkhomenko, A.-C.Roger., «Perovskite-based catalysts for steam/autothermal reforming of bioethanol», GDRI French – Russian Meeting, «Catalytic transformation of biomass into valuable products», Strasbourg, France, 15-17.07.2015, oral presentation

6. M. Arapova, S. Pavlova, T. Larina, V. Rogov, T. Krieger, V. Sadykov, T. Glazneva, O. Smorygo, K. Parkhomenko, A.-C. Roger., «Hydrogen production via ethanol steam reforming over supported nikelates: from powders to structured catalysts», 12th European Congress on Catalysis – EuropaCat-XI, Kazan, Russia, 30 August – 4 September, 2015, poster

7. Arapova M.V., Pavlova S.N., Parkhomenko K.V., Glasneva T.S., Larina T.V., Rogov V.A., Krieger T.A., Sadykov V.A., Roger A.-C., «Hydrogen production via steam reforming of bio-oil's light components – ethanol and glycerol – over supported nickelates», 4th International School-Conference on Catalysis for Young Scientists "CATALYST DESIGN. From Molecular to Industrial level", 5-6 September, Kazan, Russia, oral presentation

8. Arapova M., Pavlova S., Parkhomenko K., Glasneva T., Larina T., Sadykov V., Roger A.-C., Smorygo O., “Steam reforming of ethanol and glycerol over functionally graded nickelate-based catalysts: from grain to structured catalysts”, FCCat, the 1st French Conference on Catalysis, 23-27 May, Frejus, France, poster

9. M. Arapova, K. Parkhomenko, A.-C. Roger, S. Pavlova and V. Sadykov, “Perovskite-like nicketales for hydrogen production via sream reforming of oxygenates”, 2nd EFCATS-CNRS European Summer School on Catalyst Preparation: Fundamental Concepts and Industrial Requirements”, 12-17 June, Ardeche, France, poster

10. Pavlova S., Arapova M., Alikina G., Rogov V., Krieger T., Sadykov V., Roger A.-C. Steam reforming of ethanol for hydrogen and syngas production over perovskite-type Ni(Co, Ru) ferrites as catalyst precursors // The Seventh Tokyo Conference on Advanced Catalytic Science and Technology (TOCAT7). – 2014. - Kyoto, Japan. – P. O-A22 (19).



## References

- [1] World Energy Outlook, МЭА, 2009 // <http://www.worldenergyoutlook.org/media/weowebiste/2009/WEO2009.pdf>
- [2] Russian Energy Agency, FGBU REA Ministry of Energy of the Russian Federation, Bioenergy of Russia in the 21st Century, Moscow, 2012.
- [3] International energy agency technical report, 2013 key world energy. Statistics. 2013. // [publications/freepublications/publication/KeyWorld2013\\_FINAL\\_WEB.pdf](http://publications/freepublications/publication/KeyWorld2013_FINAL_WEB.pdf)
- [4] Vamvuka D. Bio-oil, solid and gaseous biofuels from biomass pyrolysis processes—An overview // International Journal of Energy Research. – 2011. – V. 35. – P. 835–862.
- [5] Ben-Iwo J., Manovic V., Longhurst P. Biomass resources and biofuels potential for the production of transportation fuels in Nigeria // Renewable and Sustainable Energy Reviews. – 2016. – V. 63. – P. 172–192.
- [6] Florez-Orrego D., Silva J.A.M., de Oliveira S. Exergy and environmental comparison of the end use of vehicle fuels: the Brazilian case // Energ Convers Manag. – 2015. – V. 100. – P. 220–31.
- [7] Carlos R., Khang D. Characterization of biomass energy projects in Southeast Asia // Biomass and Bioenergy. – 2008. – V. 32. – P. 525-532.
- [8] Panwar N.L., Kaushik S.C., Kothari S. Role of renewable energy sources in environmental protection: A review // Renewable and Sustainable Energy Reviews.–2011.– V. 15. – P. 1513-1524.
- [9] van Eijck J., Batidzirai B., Faaij A. Current and future economic performance of first and second generation biofuels in developing countries // Applied Energy.–2014.–V. 135. – P. 115–141.
- [10] Report «Energy and sustainable development in Russia» // [www.undp.ru/documents/NHDR\\_2009\\_Russian.pdf](http://www.undp.ru/documents/NHDR_2009_Russian.pdf)
- [11] The decree of the President of the Russian Federation from 04.06.2008 N 889 "About some measures on increase of power and ecological efficiency of the Russian economy "
- [12] Dodds P.E., Staffell L., Hawkes A.D., Li F., Grunewald P., McDowall W. et al. Hydrogen and fuel cell technologies for heating: a review // International Journal of Hydrogen Energy. – 2015. – V. 40. – P. 2065–2083.
- [13] Momirlan M, Veziroglu T. The properties of hydrogen as fuel tomorrow in sustainable energy system for a cleaner planet // International Journal of Hydrogen Energy.–2005.–V. 30.– P. 795–802.
- [14] Haryanto A, Fernando S, Murali N, Adhikari S. Current status of hydrogen production techniques by steam reforming of ethanol: a review // Energy Fuels.–2005.– V. 19. – P. 2098–2106.
- [15] Balat M. Potential importance of hydrogen as a future solution to environmental and transportation problems // International Journal of Hydrogen Energy.–2008.– V. 33.–P. 4013– 4029.
- [16] da Silva Veras T., Mozer T. S., da Costa Rubim D., dos Santos M., da Silva Cesar A. Hydrogen: Trends, production and characterization of the main process worldwide // International Journal of Hydrogen Energy. – 2017. –V. 42. – P. 2018-2033.

- [17] International Energy Agency. Technology roadmap: hydrogen and fuel cells, Paris, 2015.
- [18] Ewan B.C.R., Allen R.W.K. A figure of merit assessment of the routes to hydrogen // *International Journal of Hydrogen Energy*. – 2005. – V. 30. P. 809 – 819.
- [19] Bae J., Lee S., Kim S., Oh J., Choi S., Bae M., Kang I., Katikaneni S. P. Liquid fuel processing for hydrogen production: A review // *International Journal of Hydrogen Energy*. – 2016. – V. 41. – P. 19990-20022.
- [20] Lopez E., Divins N. J., Anzola A., Schbib S., Borio D., Llorca J. Ethanol steam reforming for hydrogen generation over structured catalysts // *International Journal of Hydrogen Energy*. – 2013. – V. 38. – I. 11. P. 4418–4428.
- [21] Gonzalez-Gil R., Herrera C., Larrubia M.A., Marino F., Laborde M., Alemany L.J. Hydrogen production by ethanol steam reforming over multimetallic RhCeNi/Al<sub>2</sub>O<sub>3</sub> structured catalyst. Pilot-scale study // *International Journal of Hydrogen Energy*. – 2016. – V. 41. – P. 16786-16796.
- [22] Chen K., Zhang L., Gholizadeh M., Ai N., Mahmudul Hasan M.D., Mourant D., Li C.-Z., Jiang S. P. Feasibility of tubular solid oxide fuel cells directly running on liquid biofuels // *Chemical Engineering Science*. – 2016. – V. 154. P. 108-118.
- [23] Thanomjit C., Patcharavorachot Y., Ponpesh P., Arpornwichanop A. Thermodynamic analysis of solid oxide fuel cell system using different ethanol reforming processes // *International Journal of Hydrogen Energy*. – 2015. V. 40. – P. 6950–6958.
- [24] Badwal S.P.S., Giddey S., Kulkarni A., Goel J., Basu S. Direct ethanol fuel cells for transport and stationary applications – A comprehensive review // *Applied Energy*. – 2015. V.145.–P. 80–103.
- [25] Rossetti I., Compagnoni M., Torli M., Process simulation and optimization of H<sub>2</sub> production from ethanol steam reforming and its use in fuel cells. 2. Process analysis and optimization // *Chemical Engineering Journal*. – 2015. – V. 281. - P. 1036–1044.
- [26] Fierro V., Akdim O., Mirodatos C., On-board hydrogen production in a hybrid electric vehicle by bio-ethanol oxidative steam reforming over Ni and noble metal based catalysts // *Green Chemistry* – 2003. – V. 5. P. 20–24.
- [27] <http://h2usa.org/fuel-cell-electric-vehicles>
- [28] Kirillov V.A., Meshcheryakov V.D., Sobyenin V.A., Belyaev V.D., Amosov Y.I., Kuzin N.A., et al. Bioethanol as a promising fuel for fuel cell power plants // *Theoretical Foundations of Chemical Engineering*. – 2008. – V. 42. - P. 1–11.
- [29] de Bruijn F. The current status of fuel cell technology for mobile and stationary applications // *Green Chemistry*. – 2005. - V. 7. – P. 132–50.
- [30] Molino A., Chianese S., Musmarra D. Biomass gasification technology: The state of the art overview // *Journal of Energy Chemistry*. – 2016. –V. 25. – P. 10–25.
- [31] Din Z.U., Zainal Z.A. Biomass integrated gasification – SOFC systems: Technology overview // *Renewable and Sustainable Energy Reviews*. – 2016. – V. 53. – P. 1356–1376.
- [32] Hamelinck C.N., Suurs R.A.A., Faaij A.P.C. International bioenergy transport costs and energy balance // *Biomass and Bioenergy*. – 2005. – V. 29. – P. 114–134.

- [33] Bridgwater A.V. Review of fast pyrolysis of biomass and product upgrading // Biomass and bioenergy. – 2012. – V. 38. – P. 68-94.
- [34] Vamvuka D. Bio-oil, solid and gaseous biofuels from biomass pyrolysis processes — An overview // International Journal of Energy Research. – 2011. – V. 35. – P. 835–862.
- [35] Kan T., Strezov V., Evans T.J. Lignocellulosic biomass pyrolysis: A review of product properties and effects of pyrolysis parameters // Renewable and Sustainable Energy Reviews. – 2016. – V. 57. – P. 1126–1140.
- [36] Bioenergy Annual Report, МЭА, 2010 // <http://www.ieabioenergy.com/LibItem.aspx?id=6780>
- [37] Russian Energy Agency, Development of the biofuel market in the world and in the Russian Federation, Moscow, 2012
- [38] Mirzoev V., Puschik E. Fuel and Ethanol - World Prospects // Journal of International Bioenergetics. – 2010.
- [39] Huber G.W., Iborra S.; Corma A.C. Synthesis of transportation fuels from biomass: chemistry, catalysts, and engineering // Chemical Reviews. – 2006. – V. 106. – P. 4044.
- [40] Ayoub M., Abdullah A.Z. Critical review on the current scenario and significance of crude glycerol resulting from biodiesel industry towards more sustainable renewable energy industry // Renewable and Sustainable Energy Reviews. – 2012. – V. 16. – P. 2671– 2686.
- [41] Tan H.W., Abdul Aziz A.R., Aroua M.K. Glycerol production and its applications as a raw material: A review // Renewable and Sustainable Energy Reviews. – 2013. – V. 27. – P. 118–127.
- [42] Quispe C.A.G., Coronado C.J.R., Carvalho Jr.J.A. Glycerol: Production, consumption, prices, characterization and new trends in combustion // Renewable and Sustainable Energy Reviews. – 2013. – V. 27. – P. 475–493.
- [43] Robert H. Heterogeneous Catalysis // Catalysis Handbook of Green Chemistry. – V. 2. – P. 96.
- [44] Chattanathan S.A., Adhikari S., Abdoulmoumine N. A review on current status of hydrogen production from bio-oil // Renewable and Sustainable Energy Reviews. – 2012. – V. 16. – I. 5. – P. 2366–2372.
- [45] Li D., Li X., Gong J. Catalytic Reforming of Oxygenates: State of the Art and Future Prospects // Chemical Reviews. – 2016. – V. 116 (19). – P. 11529–11653.
- [46] Cai W., Wang F., Zhan E., Van Veen A.C., Mirodatos C., Shen W. Hydrogen production from ethanol over Ir/CeO<sub>2</sub> catalysts: A comparative study of steam reforming, partial oxidation and oxidative steam reforming // Journal of Catalysis. – 2008. – V.257. – P. 96–107.
- [47] de Lima S.M., da Cruz I. O., Jacobs G., Davis B. H., Mattos L. V., Noronha F. B. Steam reforming, partial oxidation, and oxidative steam reforming of ethanol over Pt/CeZrO<sub>2</sub> catalyst // Journal of Catalysis. – 2008. – V.257. – P. 356–368.
- [48] Pirez C., Fang W., Capron M., Paul S., Jobic H., Dumeignil F., Jalowiecki-Duhamel L. Steam reforming, partial oxidation and oxidative steam reforming for hydrogen production from ethanol over cerium nickel based oxyhydride catalyst // Applied Catalysis A: General. – 2016. – V.518. – P. 78-86.

- [49] Sun S., Yan W., Sun P., Chen J. Thermodynamic analysis of ethanol reforming for hydrogen production // *Energy*. – 2012. – V. 44. – P. 911-924.
- [50] Wang W., Wang Y. Thermodynamic analysis of hydrogen production via partial oxidation of ethanol // *International Journal of Hydrogen Energy*. – 2008. – V.33. – P. 5035–5044.
- [51] Cavallaro S., Chiodo V., Vita A., Freni S. Hydrogen production by auto-thermal reforming of ethanol on Rh/Al<sub>2</sub>O<sub>3</sub> catalyst // *Journal of Power Sources*. – 2003. – V. 123. – P. 10–16.
- [52] Trane R., Dahl S., Skjoth-Rasmussen M.S., Jensen A.D. Catalytic steam reforming of bio-oil // *International Journal of Hydrogen Energy*. – 2012. – V. 37. – P. 6447-6472.
- [53] Wang S., Song X., Wang Q., Liu G., Lu H. Thermodynamic evaluation of glycerol autothermal reforming in membrane reactors // *International Journal of Hydrogen Energy*. – 2016. – V. 41. – P. 17864-17870.
- [54] Mondal T., Pant K. K., Dalai A. K. Oxidative and non-oxidative steam reforming of crude bio-ethanol for hydrogen production over Rh promoted Ni/CeO<sub>2</sub>-ZrO<sub>2</sub> catalyst // *Applied Catalysis A: General*. – 2015. – V. 499. – P. 19–31.
- [55] Baruah R., Dixit M., Basarkar P., Parikh D., Bhargav A. Advances in ethanol autothermal reforming // *Renewable and Sustainable Energy Reviews*. – 2015. – V. 51. – P. 1345–1353.
- [56] Liu Y., Farrauto R., Lawal A. Autothermal reforming of glycerol in a dual layer monolith catalyst // *Chemical Engineering Science*. – 2013. – V. 89. – P. 31–39.
- [57] Hajjaji N., Baccar I., Pons M.-N. Energy and exergy analysis as tools for optimization of hydrogen production by glycerol autothermal reforming // *Renewable Energy*. – 2014. – V. 71. – P. 368-380.
- [58] Voldsund M., Jordal K., Anantharaman R. Hydrogen production with CO<sub>2</sub> capture // *International Journal of Hydrogen Energy*. – 2016. – V. 41. – P. 4969-4992.
- [59] Leal A.L., Soria M.A., Madeira L.M. Autothermal reforming of impure glycerol for H<sub>2</sub> production: Thermodynamic study including in situ CO<sub>2</sub> and/or H<sub>2</sub> separation // *International Journal of Hydrogen Energy*. – 2016. – V. 41. – P. 2607-2620.
- [60] Basagiannis A.C., Verykios X.E. Influence of the carrier on steam reforming of acetic acid over Ru-based catalysts // *Applied Catalysis B: Environmental*. – 2008. – V. 82. – P. 77–88.
- [61] Ni M., Leung D.Y.C., Leung M.K.H. A review on reforming bio-ethanol for hydrogen production // *International Journal of Hydrogen Energy*. – 2007. – V. 32. – P. 3238 – 3247.
- [62] Vaidya P.D., Rodrigues A.E. Review: Insight into steam reforming of ethanol to produce hydrogen for fuel cells // *Chemical Engineering Journal*. – 2006. – V. 117. – P. 39–49.
- [63] de la Piscina P.R., Homs N. Use of biofuels to produce hydrogen (reformation processes) // *Chemical Society Reviews*. – 2008. – V. 37, – P. 2459.
- [64] Mattos, L.V., Jacobs G., Davis B.H., Noronha F.B. Production of Hydrogen from Ethanol: Review of Reaction Mechanism and Catalyst Deactivation // *Chemical. Reviews*. – 2012. – V. 112. – P. 4094-4123.

- [65] Zanchet D., Santos J.B.O., Damyanova S., Gallo J.M.R., Bueno C., Toward J.M. Understanding Metal-Catalyzed Ethanol Reforming // ACS Catalysis. – 2015. – V. 5. – P. 3841-3863.
- [66] Hou T.S., Chen Y., Wang D., Cai W. Hydrogen Production from Ethanol Reforming: Catalysts and Reaction Mechanism // Renewable & Sustainable Energy Reviews. – 2015. – V. 44. – P. 132-148.
- [67] Rabenstein G., Hacker V.J. Hydrogen for fuel cells from ethanol by steam-reforming, partial-oxidation and combined auto-thermal reforming: A thermodynamic analysis // Power Sources. – 2008. – V. 185. – P. 1293-1304.
- [68] Li J., Yu H., Yang G., Peng F., Xie D., Wang H., et al. Steam reforming of oxygenate fuels for hydrogen production: a thermodynamic study // Energy Fuels. – 2011. – V. 25. – P. 2643–2650.
- [69] Diaz A. F., Gracia F. Steam reforming of ethanol for hydrogen production: thermodynamic analysis including different carbon deposits representation // Chemical Engineering Journal. – 2010. – V. 165. – P. 649–657.
- [70] Aupretre F., Descorme C., Duprez D. Hydrogen production for fuel cells from the catalytic ethanol steam reforming // Topics in Catalysis. – 2004. – V. 30/31. – N. 1–4. – P. 487-492.
- [71] Barattini L., Ramis G., Resini C., Busca G., Sisani M., Costantino U. Reaction path of ethanol and acetic acid steam reforming over Ni–Zn–Al catalysts. Flow reactor studies // Chemical Engineering Journal. – 2009. – V. 153. – P. 43–49.
- [72] Aupretre F., Descorme C., Duprez D. Bio-ethanol catalytic steam reforming over supported metal catalyst // Catalysis Communications. – 2002. – V. 3. – P. 263–267.
- [73] Jacobs G., Keogh R. A., Davis B. H. Steam reforming of ethanol over Pt/ceria with co-fed hydrogen // Journal of Catalysis. – 2007. – V. 245. – P. 326–337.
- [74] Busca G., Montanari T., Resini C., Ramis G., Costantino U. Hydrogen from alcohols: IR and flow reactor studies // Catalysis Today. – 2009. – V. 143. – P. 2–8.
- [75] Vicente J., Montero C., Erena J., Azkoiti M.J., Bilbao J., Gayubo A.G. Coke deactivation of Ni and Co catalysts in ethanol steam reforming at mild temperatures in a fluidized bed reactor // International Journal of Hydrogen Energy. – 2014. – V. 39. – P. 12586-12596.
- [76] Silva J.M., Soria M.A., Madeira L.M. Challenges and strategies for optimization of glycerol steam reforming process // Renewable and Sustainable Energy Reviews. – 2015. – V. 42. – P. 1187–1213.
- [77] Avasthi K.S., Reddy R.N., Patel S. Challenges in the production of hydrogen from glycerol-a biodiesel byproduct via steam reforming process // Procedia Engineering. – 2013. – V. 51. – P. 423–429.
- [78] Lin Y.C. Catalytic valorization of glycerol to hydrogen and syngas // International Journal of Hydrogen Energy. – 2013. – V. 38. – P. 2678–2700.

- [79] Schwengber C. A., Alves H.J., Schaffner R.A., Alves da Silva F., Sequinel R., Rossato V.B., Ferracin R.J. Overview of glycerol reforming for hydrogen production // *Renewable and Sustainable Energy Reviews*. – 2016. – V. 58. – P. 259–266.
- [80] Papageridis K.N., Siakavelas G., Charisiou N. D., Avraam D. G., Tzounis L., Kousi K., Goula M.A. Comparative study of Ni, Co, Cu supported on  $\gamma$ -alumina catalysts for hydrogen production via the glycerol steam reforming reaction // *Fuel Processing Technology*. – 2016. – V. 152. – P. 156–175.
- [81] Chai S.H., Wang H.P., Liang Y., Xu B.Q. Sustainable production of acrolein: gasphase dehydration of glycerol over Nb<sub>2</sub>O<sub>5</sub> catalyst // *Journal of Catalysis*. – 2007. – V. 250. – P. 342–349.
- [82] Corma A., Huber G.H., Sauvanaud L., O'Connor P. Biomass to chemicals: catalytic conversion of glycerol/water mixtures into acrolein, reaction network // *Journal of Catalysis*. – 2008. – V. 257. – P. 163–171.
- [83] Iriondo A., Barrio V.L., Cambra J.F., Arias P.L., Guemez M.B., Sanchez-Sanchez M.C., Navarro R.M., Fierro J.L.G. Glycerol steam reforming over Ni catalysts supported on ceria and ceria-promoted alumina // *International Journal of Hydrogen Energy*. – 2010. – V. 35. – P. 11622–11633.
- [84] Adhikari S., Fernando S., Gwaltney S.R., Filip S.D., Mark B.R., Steele P.H., Haryanto A. Current Status of Hydrogen Production Techniques by Steam Reforming of Ethanol: A Review // *International Journal of Hydrogen Energy*. – 2007. – V. 32. – P. 2875–2880.
- [85] Chen H., Ding Y., Cong N.T., Dou B., Dupont V., Ghadiri M., Williams P.T. A comparative study on hydrogen production from steam-glycerol reforming: thermodynamics and experimental // *Renewable Energy*. – 2011. – V. 36. – P. 779–788.
- [86] Rossi C.C.R.S., Alonso C.G., Antunes O.A.C., Guirardello R., Cardozo-Filho L. Thermodynamic analysis of steam reforming of ethanol and glycerine for hydrogen production // *International Journal of Hydrogen Energy*. – 2009. – V. 34. – P. 323–332.
- [87] Arago Marin M. C. Valorisation du glycerol par vaporeformage catalitique pour la production d'hydrogene // PhD thesis, University of Strasbourg, Strasbourg, France, 2011.
- [88] Wang H., Wang X., Li M., Li S., Wang S., Ma X. // *International Journal of Hydrogen Energy*. – 2009. – V. 34. – P. 5683–5690.
- [89] Silva J. M., Soria M.A., Madeira L. M. Steam reforming of glycerol for hydrogen production: Modeling study // *International Journal of Hydrogen Energy*. – 2016. – V. 41. – P. 1408–1418.
- [90] Song D.Y., Wang C., Chen H., Xu Y. Hydrogen production from catalytic steam reforming of biodiesel byproduct glycerol: issues and challenges // *Renewable and Sustainable Energy Reviews*. – 2014. – V. 30. – P. 950–960.
- [91] Bobadilla L.F., Penkova A., Romero-Sarria F., Centeno M.A., Odriozola J.A. Influence of the acid-base properties over NiSn/MgO–Al<sub>2</sub>O<sub>3</sub> catalysts in the hydrogen production from glycerol steam reforming // *International Journal of Hydrogen Energy*. – 2014. – V. 39. – P. 5704–5712.

- [92] Franchini C.A., Aranzuez W., de Farias A.M.D., Pecchi G., Fraga M.A. Ce-substituted  $\text{LaNiO}_3$  mixed oxides as catalyst precursors for glycerol steam reforming // *Applied Catalysis B Environmental*. – 2014. – V. 147. – P. 193–202.
- [93] Cortright R.D., Davda R.R., Dumesic J.A. Hydrogen from catalytic reforming of biomass-derived hydrocarbons in liquid water // *Nature*. – 2002. – V. 418. – P. 964–967.
- [94] Pompeo F., Santori G., Nichio N.N. Hydrogen and/or syngas from steam reforming of glycerol. Study of platinum catalysts // *International Journal of Hydrogen Energy*. – 2010. – V. 35. – P. 8912–8920.
- [95] de Borcx P.K., Kock A.J.H.M., Boellaard E., Klop W., Geus J.W. The Formation of Filamentous Carbon on iron and Nickel Catalysts // *Journal of Catalysis*. – 1985. – V. 96. – P. 454–467.
- [96] Vaidya P.D., Rodrigues A.E. Glycerol Reforming for Hydrogen Production: A Review // *Chemical Engineering and Technology*. – 2009. – V. 32. – P. 1463–1469.
- [97] Tran N.H., Kannangara G.S.K. Conversion of Glycerol to Hydrogen Rich Gas // *Chemical Society Reviews*. – 2013. – V. 42. – P. 9454–9479.
- [98] Zhong Z., Ang H., Choong C., Chen L., Huang L., Lin J. The role of acidic sites and the catalytic reaction pathways on the Rh/ZrO<sub>2</sub> catalysts for ethanol steam reforming // *Physical Chemistry Chemical Physics*. – 2009. – V. 11. – P. 872–80.
- [99] González V.O.A., Reyes H.J.A., Wang J.A., Chen L.F. Hydrogen production over Rh/Ce-MCM-41 catalysts via ethanol steam reforming // *International Journal of Hydrogen Energy*. – 2013. – V. 38. – P. 13914–25.
- [100] Coronel L., Múnera J.F., Tarditi A.M., Moreno M.S., Cornaglia L.M. Hydrogen production by ethanol steam reforming over Rh nanoparticles supported on lanthana/silica systems // *Applied Catalysis: B*. – 2014. – V. 160–161. – P. 254–66.
- [101] Chiodo V., Freni S., Galvagno A., Mondello N., Frusteri F. Catalytic features of Rh and Ni supported catalysts in the steam reforming of glycerol to produce hydrogen // *Applied Catalysis A: General*. – 2010. – V. 381. – I. 1–2. – P. 1–7.
- [102] de Rezende S.M., Franchini C.A., Dieuzeide M.L., de Farias A.M.D., Amadeo N., Fraga M.A. Glycerol steam reforming over layered double hydroxide-supported Pt catalysts // *Chemical Engineering Journal*. – 2015. – V. 272. – P. 108–118.
- [103] Panagiotopoulou P., Verykios X.E. Mechanistic aspects of the low temperature steam reforming of ethanol over supported Pt catalysts // *International Journal of Hydrogen Energy*. – 2012. – V. 37. – P. 16333–16345.
- [104] Sad M.E., Duarte H.A., Vignatti Ch., Padro C.L., Aspesteguia C.R. Steam reforming of glycerol: Hydrogen production optimization // *International Journal of Hydrogen Energy*. – 2015. – V. 40. – P. 6097–6106.

- [105] Galvita V., Belyaev V., Semikolenov V., Tsiakaras P., Frumin A., Sobyenin V. Ethanol decomposition over Pd-based catalyst in the presence of steam // *Reaction Kinetics and Catalysis Letters*. – 2002. – V. 76(2). – P. 343-351.
- [106] Breen J., Burch R., Coleman H. Metal-catalysed steam reforming of ethanol in the production of hydrogen for fuel cell applications // *Applied Catalysis: B Environmental*. – 2002. – V. 39(1). – P. 65-74.
- [107] Goula M.A., Kontou S.K., Tsiakaras P.E. Hydrogen Production by Ethanol Steam Reforming over a Commercial Pd/ $\gamma$ -Al<sub>2</sub>O<sub>3</sub> Catalyst // *Applied Catalysis*. – 2004. – V. 49. – P. 135-144.
- [108] Wang Q., Guo L., Li X. Steam reforming of model compounds from bio-oil for hydrogen production over Pd/HZSM-5 catalyst // *Advanced Materials Research*. – 2012. – V. 550-553. – P. 558-562.
- [109] Gallo A., Pirovano C., Ferrini P., Marelli M., Psaro R., Santangelo S., Faggio G., Dal Santo V. Influence of reaction parameters on the activity of ruthenium based catalysts for glycerol steam reforming // *Applied Catalysis: B Environmental*. – 2012. – V. 121-122. – P. 40-49.
- [110] Kim J., Lee D. Glycerol steam reforming on supported Ru-based catalysts for hydrogen production for fuel cells // *International Journal of Hydrogen Energy*. – 2013. – V. 38. – P. 11853-11862.
- [111] Hirai T., Ikenaga N.O., Miyake T., Suzuki T. Production of hydrogen by steam reforming of glycerin on ruthenium catalyst // *Energy Fuel*. – 2005. – V. 19. – P. 1761-1762.
- [112] Yee A., Morrison S.J., Idriss H. The reactions of ethanol over M/CeO<sub>2</sub> catalysts: evidence of carbon-carbon bond dissociation at low temperatures over Rh/CeO<sub>2</sub>. // *Catalysis Today*. – 2000. – V. 63. – P. 327-335.
- [113] Sheng P.Y., Yee A., Bowmaker G.A., Idriss H. H<sub>2</sub> production from ethanol over Rh-Pt/CeO<sub>2</sub> catalysts: the role of Rh for the efficient dissociation of the carbon-carbon bond // *Journal of Catalysis*. – 2002. – V.208. – P. 393-403.
- [114] Crampton A.S., Rotzer M.D., Schweinberger F.F., Yoon B., Landman U., Heiz U. Ethylene hydrogenation on supported Ni, Pd and Pt nanoparticles: Catalyst activity, deactivation and the d-band model // *Journal of Catalysis*. – 2016. – V. 333. – P. 51-58.
- [115] Wang J.H., Lee C.S., Lin M.C. Mechanism of ethanol reforming: theoretical foundations // *Journal of Physical Chemistry*. – 2009. – V. 113. – P. 6681-6688.
- [116] Liguras D.K., Kondarides D.I., Verykios X.E. Production of hydrogen for fuel cells by steam reforming of ethanol over supported noble metal catalysts // *Applied Catalysis B: Environmental*. – 2003. – V. 43. – P. 345-354.
- [117] Aupretre F., Descorme C., Duprez D. Bio-ethanol catalytic steam reforming over supported metal catalysts // *Catalysis Communications*. – 2002. – V. 3. – P. 263-267.
- [118] Kugai J., Subramani V., Song C., Engelhard M.H., Chin Y.H. Effects of nanocrystalline CeO<sub>2</sub> supports on the properties and performance of Ni-Rh bimetallic catalyst for oxidative steam reforming of ethanol // *Journal of Catalysis*. – 2006. – V. 238. – P. 430-440.



- [119] Hu X., Lu G. Comparative study of alumina-supported transition metal catalysts for hydrogen generation by steam reforming of acetic acid // *Applied Catalysis B: Environmental*. – 2010. – V. 99. – P. 289–297.
- [120] Vicente J., Montero C., Erena J., Azkoiti M.J., Bilbao J., Gayubo A.G. Coke deactivation of Ni and Co catalysts in ethanol steam reforming at mild temperatures in a fluidized bed reactor // *International Journal of Hydrogen Energy*. – 2014. – V. 39. – P. 12586-12596.
- [121] Xing R., Lebarbier Dagle V., Flake M., Kovarik L., Albrecht K.O., Deshmane C., Dagle R.A. Steam reforming of fast pyrolysis-derived aqueous phase oxygenates over Co, Ni, and Rh metals supported on MgAl<sub>2</sub>O<sub>4</sub> // *Catalysis Today*. – 2016. – V. 269. – P. 166–174.
- [122] Song H., Zhang L., Watson R.B., Braden D., Ozkan U.S. Investigation of bio-ethanol steam reforming over cobalt-based catalysts // *Catalysis Today*. – 2007. – V. 129. – P. 346–354.
- [123] Cheng C.K., Foo S.Y., Adesina A.A. H<sub>2</sub>-rich synthesis gas production over Co/Al<sub>2</sub>O<sub>3</sub> catalyst via glycerol steam reforming // *Catalysis Communications*. – 2010. – V. 12. – P. 292–298.
- [124] de Avila C.N., Hori C.E., de Assis A.J. Thermodynamic assessment of hydrogen production and cobalt oxidation susceptibility under ethanol reforming conditions // *Energy* – 2011. – V. 36. – P. 4385-4395.
- [125] Rossetti I., Lasso J., Nichele V., Signoretto M., Finocchio E., Ramis G., Di Michele A. Silica and zirconia supported catalysts for the low-temperature ethanol steam reforming // *Applied Catalysis B: Environmental*. – 2014. – V. 150 – 151. – P. 257– 267.
- [126] Trane-Restrup R., Dahl S., Jensen A.D. Steam reforming of ethanol: Effects of support and additives on Ni-based catalysts // *International Journal of Hydrogen Energy*. – 2013. – V. 38. – P. 15105-15118.
- [127] Manukyan K.V., Cross A.J., Yeghishyan A.V., Rouvimov S., Miller J.J., Mukasyan A.S., Wolf E.E. Highly stable Ni–Al<sub>2</sub>O<sub>3</sub> catalyst prepared from a Ni–Al layered double hydroxide for ethanol decomposition toward hydrogen // *Applied Catalysis A: General*. – 2015. – V. 508. – P. 37–44.
- [128] Montero C., Ochoa A., Castano P., Bilbao J.R., Gayubo A.G. Monitoring NiO and coke evolution during the deactivation of a Ni/La<sub>2</sub>O<sub>3</sub>– $\alpha$ Al<sub>2</sub>O<sub>3</sub> catalyst in ethanol steam reforming in a fluidized bed // *Journal of Catalysis*. – 2015. – V. 331. – P. 181–192.
- [129] Trimm D.L. Coke formation and minimisation during steam reforming reactions // *Catalysis Today*. – 1997. – V. 37. – P. 233–238.
- [130] Rostrup-Nielsen J.R. Sulfur-passivated nickel catalysts for carbon-free steam reforming of methane // *Journal of Catalysis*. – 1984. – V. 85. – P. 31–43.
- [131] Duprez D., Demicheli M.C., Marecot P., Barbier J., Ferretti O.A., Ponzi E.N. Deactivation of Steam-Reforming Model Catalysts by Coke Formation I. Kinetics of the Formation of Filamentous Carbon in the Hydrogenolysis of Cyclopentane on Ni/Al<sub>2</sub>O<sub>3</sub> Catalysts // *Journal of Catalysis*. – 1990. – V. 124. – P. 324-335.

- [132] Yan X., Liu C. Effect of the catalyst structure on the formation of carbon nanotubes over Ni/MgO catalyst // *Diamond & Related Materials*. – 2013. – V. 31. – P. 50–57.
- [133] Rossetti I., Biffi C., Bianchi C.L., Nichele V., Signoretto M., Menegazzo F., Finocchio E., Ramis G., Di Michele A. Ni/SiO<sub>2</sub> and Ni/ZrO<sub>2</sub> catalysts for the steam reforming of ethanol // *Applied Catalysis B: Environmental*. – 2012. – V. 117–118. – P. 384–396.
- [134] Rossetti I., Gallo A., Dal Santo V., Bianchi C.L., Nichele V., Signoretto M., Finocchio E., Ramis G., Garbarino G., Di Michele A. Nickel Catalysts Supported Over TiO<sub>2</sub>, SiO<sub>2</sub> and ZrO<sub>2</sub> for the Steam Reforming of Glycerol // *ChemCatChem Catalysis*. – 2013. – V. 5. – P. 294.
- [135] Krалева E., Sokolov S., Schneider M., Ehrich H. Support effects on the properties of Co and Ni catalysts for the hydrogen production from bio-ethanol partial oxidation // *International Journal of Hydrogen Energy*. – 2013. – V. 38. – P. 4380-4388.
- [136] Nichele V., Signoretto M., Pinna F., Menegazzo F., Rossetti I., Cruciani G., Cerrato G., Di Michele A. Ni/ZrO<sub>2</sub> catalysts in ethanol steam reforming: Inhibition of coke formation by CaO-doping // *Applied Catalysis B: Environmental*. – 2014. – V. 150–151. – P. 12–20.
- [137] Dieuzeidea M.L., Jobbagyb M., Amadeo N. Glycerol steam reforming over Ni/ $\gamma$ -Al<sub>2</sub>O<sub>3</sub> catalysts, modified with Mg(II). Effect of Mg (II) content // *Catalysis Today*. – 2013. – V. 213. – P. 50– 57.
- [138] Natesakhawat S., Oktar O., Ozkan U.S. Effect of lanthanide promotion on catalytic performance of sol–gel Ni/Al<sub>2</sub>O<sub>3</sub> catalysts in steam reforming of propane // *Journal of Molecular Catalysis A: Chemical*. – 2005. – V. 241. – P. 133–146.
- [139] Zhang J., Xu H., Jin X., Ge Q., Li W. Characterizations and activities of the nano-sized Ni/Al<sub>2</sub>O<sub>3</sub> and Ni/La–Al<sub>2</sub>O<sub>3</sub> catalysts for NH<sub>3</sub> decomposition // *Applied Catalysis A: General*. – 2005. – V. 290. – P. 87–96.
- [140] Benggaard H.S., et al. Steam reforming and graphite formation on Ni catalysts // *J. Catal.* – 2002. – V. 209. – P. 365–384.
- [141] Libby W.F. Promising catalyst for auto exhaust // *Science*. – 1971. – V. 171. – P. 499.
- [142] Andonova S., de Avila C.N., Arishtirova K., Bueno J.M.C., Damyanova S. Structure and redox properties of Co promoted Ni/Al<sub>2</sub>O<sub>3</sub> catalysts for oxidative steam reforming of ethanol // *Applied Catalysis B: Environmental*. – 2011. – V. 105. – P. 346–360.
- [143] Zhang F., Wang N., Yang L., Li M., Huang L. Ni-Co bimetallic MgO-based catalysts for hydrogen production via steam reforming of acetic acid from bio-oil // *International Journal of Hydrogen Energy*. – 2014. – V. 39. – P. 18688-18694.
- [144] Huang S.C., Lin C.H., Wang J.H. Trends of water gas shift reaction on close-packed transition metal surfaces // *The Journal of Physical Chemistry C*. – 2010. – V. 114. – P. 9826–9834.
- [145] Ando Y., Matsuoka K. Role of Fe in Co-Fe particle catalysts for suppressing CH<sub>4</sub> production during ethanol steam reforming for hydrogen production // *International Journal of Hydrogen Energy*. – 2016. – V. 41. – P. 12862-12868.

- [146] Özkan G., Gök S., Özkan G. Active carbon-supported Ni, Ni/Cu and Ni/Cu/Pd catalysed steam reforming of ethanol for the production of hydrogen // *Chemical Engineering Journal*. – 2011. – V. 171. – P. 1270–1275.
- [147] Soyal-Baltacıoğlu F., Erhan Aksoylu A., Önsan I., Steam reforming of ethanol over Pt–Ni Catalysts // *Catalysis Today*. – 2008. – V. 138. – P. 183–186.
- [148] Youn M.H., Seo J.G., Kim P., Song I.K. Role and effect of molybdenum on the performance of Ni-Mo/ $\gamma$ -Al<sub>2</sub>O<sub>3</sub> catalysts in the hydrogen production by auto-thermal reforming of ethanol // *Journal of Molecular Catalysis A: Chemical*. – 2007. – V. 261. – P. 276–281.
- [149] Malaibari Z.O., Amin A., Croiset E., Epling W. Performance characteristics of Mo-Ni/Al<sub>2</sub>O<sub>3</sub> catalysts in LPG oxidative steam reforming for hydrogen production // *International Journal of Hydrogen Energy*. – 2014. – V. 39. – P. 10061-10073.
- [150] Grzegorzczak W., Denis A., Borowiecki T. Studies of the molybdenum migration from Ni/Mo catalysts in the presence of steam // *Catalysis Communications*. – 2002. – V. 3. – P. 293–297.
- [151] Borowiecki T., Machocki A., Delmon B., Froment G.F. The effect of the molybdenum promoter on the coking induction time of the catalysts in the hydrocarbons steam reforming // *Catalyst Deactivation* / Eds. B. Delmon and G.F. Froment. - Elsevier Science B.V. – 1999.
- [152] Carrero A., Calles J.A., Vizcaino A.J. Effect of Mg and Ca addition on coke deposition over Cu–Ni/SiO<sub>2</sub> catalysts for ethanol steam reforming // *Chemical Engineering Journal*. – 2010. – V. 163. – P. 395–402.
- [153] Espinos J.P., Gonzalez-Eliphe A. R., Caballero A., Garcia J., Munuera G. The State of Nickel in Ni/SiO<sub>2</sub> and Ni/TiO<sub>2</sub>-Calcined Catalysts // *Journal of Catalysis*. – 1992. – V. 136. – P. 415–422.
- [154] Soares R.R., Simonetti D.A., Dumesic J.A. Glycerol as a Source for Fuels and Chemicals by Low-Temperature Catalytic Processing // *Angewandte Chemie International*. – 2006. – V. 45. – P. 3982-3985.
- [155] Manukyan K.V., Cross A.J., Yeghishyan A.V., Rouvimov S., Miller J.J., Mukasyan A.S., Wolf E.E. Highly stable Ni–Al<sub>2</sub>O<sub>3</sub> catalyst prepared from a Ni–Al layered double hydroxide for ethanol decomposition toward hydrogen // *Applied Catalysis A: General*. – 2015. – V. 508. – P. 37–44.
- [156] Vizcaino A.J., Carrero A., Calles J.A. Comparison of ethanol steam reforming using Co and Ni catalysts supported on SBA-15 modified by Ca and Mg // *Fuel Processing Technology*. – 2016. – V. 146. – P. 99–109.
- [157] Jabbour K., Massiani P., Davidson A., Casale S., El Hassan N. Ordered mesoporous “one-pot” synthesized Ni-Mg(Ca)-Al<sub>2</sub>O<sub>3</sub> as effective and remarkably stable catalysts for combined steam and dry reforming of methane (CSDRM) // *Applied Catalysis B: Environmental*. – 2017. – V. 201. – P. 527–542.
- [158] Penkova A., Bobadilla L.F., Romero-Sarria F., Centeno M.A., Odriozola J.A. Pyridine adsorption on NiSn/MgO–Al<sub>2</sub>O<sub>3</sub>: An FTIR spectroscopic study of surface acidity // *Applied Surface Science*. – 2014. – V. 317. – P. 241–251.

- [159] Song J.H., Han S.J., Yoo J., Park S., Kim D.H., Song I.K. Hydrogen production by steam reforming of ethanol over Ni-Sr-Al<sub>2</sub>O<sub>3</sub>-ZrO<sub>2</sub> aerogel catalyst // *Journal of Molecular Catalysis A: Chemical*. – 2016. – V. 424. – P. 342–350.
- [160] Garbarino G., Campodonico S., Perez A.R., Carnasciali M.M., Riani P., Finocchio E., Busca G. Spectroscopic characterization of Ni/Al<sub>2</sub>O<sub>3</sub> catalytic materials for the steam reforming of renewable // *Applied Catalysis A: General*. – 2013. – V. 452. – P. 163–173.
- [161] Ravindra Reddy C., Bhat Y.S., Nagendrappa G., Jai Prakash B.S. Bronsted and Lewis acidity of modified montmorillonite clay catalysts determined by FT-IR spectroscopy // *Catalysis Today*. – 2009. – V. 141. – P. 157–160.
- [162] Maroto-Valiente A., Cerro-Alarcon M., Guerrero-Ruiz A., Rodriguez-Ramos I. Effect of the metal precursor on the surface site distribution of Al<sub>2</sub>O<sub>3</sub>-supported Ru catalysts: catalytic effects on the n-butane/H<sub>2</sub> test // *Applied Catalysis A: General*. – 2005. – V. 283. – P. 23–32.
- [163] Hadjiivanov K. Identification and Characterization of Surface Hydroxyl Groups by Infrared Spectroscopy // *Advances in Catalysis*. – 2014. – V. 57. – Ch. 2.
- [164] Vizcaino A.J., Arena P., Baronetti G., Carrero A., Calles J.A., Laborde M.A., Amadeo N. Ethanol steam reforming on Ni/Al<sub>2</sub>O<sub>3</sub> catalysts: Effect of Mg addition // *International Journal of Hydrogen Energy*. – 2008. – V. 33. – P. 3489 – 3492.
- [165] Elias K.F.M., Lucrédio A.F., Assaf E.M. Effect of CaO addition on acid properties of Ni–Ca/Al<sub>2</sub>O<sub>3</sub> catalysts applied to ethanol steam reforming // *International Journal of Hydrogen Energy*. – 2013. – V. 38. – P. 4407–4417.
- [166] Choong C., Huang L., Zhong Z., Lin J. Hong L., Chen L. Effect of calcium addition on catalytic ethanol steam reforming of Ni/Al<sub>2</sub>O<sub>3</sub>: acidity/basicity, water adsorption and catalytic activity // *Applied Catalysis A: General*. – 2011. – V. 407. – P. 155–162.
- [167] Aupretre F., Descorme C., Duprez D., Casanave D., Uzio D. Ethanol steam reforming over Mg<sub>x</sub>Ni<sub>1-x</sub>Al<sub>2</sub>O<sub>3</sub> spinel oxide-supported Rh catalysts // *Journal of Catalysis*. – 2005. – V. 233. – P. 464–477.
- [168] Freni S., Cavallaro S., Mondello N., Spadaro L., Frusteri F. Steam reforming of ethanol on Ni/MgO catalysts: H<sub>2</sub> production for MCFC // *Journal of Power Sources*. – 2002. – V. 108. – P. 53–57.
- [169] Penkova A., Bobadilla L., Ivanova S., Dominguez M.I., Romero-Sarria F., Roger A.C., Centeno M.A., Odriozola J.A. Hydrogen production by methanol steam reforming on NiSn/MgO–Al<sub>2</sub>O<sub>3</sub> catalysts: The role of MgO addition // *Applied Catalysis A: General*. – 2011. – V. 392. – P. 184–191.
- [170] Lisboa J. da S., Santos D., Passos F., Noronha F. Influence of the addition of promoters to steam reforming catalysts // *Catalysis Today*. – 2005. – V. 101. – P. 15–21.
- [171] Hu X., Lu G. Inhibition of methane formation in steam reforming reactions through modification of Ni catalyst and the reactants // *Green Chemistry*. – 2009. – V. 11. – P. 724–732.

- [172] Greluk M., Słowik G., Rotko M., Machocki A. Steam reforming and oxidative steam reforming of ethanol over PtKCo/CeO<sub>2</sub> catalyst // *Fuel*. – 2016. – V. 183. – P. 518–530.
- [173] Llorca J., Homs N., Sales J., Fierro J.L., Piscina P.R. Effect of sodium addition on the performance of Co–ZnO-based catalysts for hydrogen production from bioethanol // *Journal of Catalysis*. – 2004. – V. 222. – P. 470–480.
- [174] Yurdakul M., Ayas N., Bizkarra K., El Doukkali M., Cambra J.F. Preparation of Ni-based catalysts to produce hydrogen from glycerol by steam reforming process // *International Journal of Hydrogen Energy*. – 2016. – V. 41. – P. 8084-8091.
- [175] Calles J.A., Carrero A., Vizcaino A.J. Ce and La modification of mesoporous Cu–Ni/SBA-15 catalysts for hydrogen production through ethanol steam reforming // *Microporous and Mesoporous Materials*. – 2009. – V. 119. – P. 200–207.
- [176] Sánchez-Sánchez M.C., Navarro R.M., Fierro J.L.G. Ethanol steam reforming over Ni/M<sub>x</sub>O<sub>y</sub>–Al<sub>2</sub>O<sub>3</sub> (M = Ce, La, Zr and Mg) catalysts: influence of support on the hydrogen production // *International Journal of Hydrogen Energy*. – 2007. – V. 32. – P. 1462–1471.
- [177] Bednarczuk L., Ramirez de la Piscina P., Homs N. Efficient CO<sub>2</sub>-regeneration of Ni/Y<sub>2</sub>O<sub>3</sub>-La<sub>2</sub>O<sub>3</sub>-ZrO<sub>2</sub> systems used in the ethanol steam reforming for hydrogen production // *International Journal of Hydrogen Energy*. – 2016. – V. 41. – P. 19509-19517.
- [178] Osorio-Vargas P., Flores-González N.A., Navarro R.M., Fierro J.L.G., Campos C.H., Reyes P. Improved stability of Ni/Al<sub>2</sub>O<sub>3</sub> catalysts by effect of promoters (La<sub>2</sub>O<sub>3</sub>, CeO<sub>2</sub>) for ethanol steam-reforming reaction // *Catalysis Today*. – 2016. – V. 259. – P. 27–38.
- [179] Frusteri F., Freni S., Chiodo V., Donato S., Bonura G., Cavallaro S. Steam and auto-thermal reforming of bio-ethanol over MgO and CeO<sub>2</sub> Ni supported catalysts // *International Journal of Hydrogen Energy*. – 2006. – V. 31. – P. 2193–2199.
- [180] Zhou G., Barrio L., Agnoli S., Senanayake S.D., Evans J., Kubacka A., et al. High activity of Ce<sub>1-x</sub>Ni<sub>x</sub>O<sub>2-y</sub> for H<sub>2</sub> production through ethanol steam reforming: tuning catalytic performance through metal–oxide interactions // *Angewandte Chemie International Edition* – 2010. – V. 49. – P. 9680–9684.
- [181] Sun J., Wang Y., Li J., Xiao G., Zhang L., Li H., et al. H<sub>2</sub> production from stable ethanol steam reforming over catalyst of NiO based on flowerlike CeO<sub>2</sub> microspheres // *International Journal of Hydrogen Energy*. – 2010. – V. 35. – P. 3087–3091.
- [182] Palma V., Palo E., Castaldo F., Ciambelli P., Iaquaniello G. Catalytic activity of CeO<sub>2</sub> supported Pt–Ni and Pt–Co catalysts in the low temperature bio-ethanol steam reforming // *Chemical Engineering Transactions*. – 2011. – V. 25. – P. 947–952.
- [183] Royer S., Duprez D., Can F., Courtois X., Batiot-Dupeyrat C., Laassiri S., Alamdari H. Perovskites as Substitutes of Noble Metals for Heterogeneous Catalysis: Dream or Reality // *Chemical Reviews*. – 2014. – V. 114. – P. 10292–10368.
- [184] Nemudryi A.P. Oxygen transport in nonstoichiometric perovskites with mixed oxygen-electron conductivity based on cobaltite and strontium ferrite // Thesis for a scientific degree of Doctor of Chemical Sciences, IHTTM SB RAS, Novosibirsk, 2010.

- [185] Świerczek K., Marzec J., Pałubiak D., Zajac W., Molenda J. LFN and LSCFN perovskites — structure and transport properties // *Solid State Ionics*. – 2006. – V. 177. – P. 1811–1817.
- [186] Aleksandrov K.S., Beznosikov B.V. Perovskite-like crystals // *Novosibirsk: Nauka. Siberian Branch of RAS*. – 1997. – C. 216.
- [187] Lakshminarayanan N., Choi H., Kuhn J.N., Ozkan U.S. Effect of additional B-site transition metal doping on oxygen transport and activation characteristics in  $\text{La}_{0.6}\text{Sr}_{0.4}(\text{Co}_{0.18}\text{Fe}_{0.72}\text{X}_{0.1})\text{O}_{3-\delta}$  (where X= Zn, Ni or Cu) perovskite oxides // *Applied Catalysis B: Environmental*. – 2011. – V. 103. – P. 318–325.
- [188] Pena M.A., Fierro J.L.G. Chemical structures and performance of perovskite oxides // *Chemical Reviews*. – 2001. – V. 101. – P. 1981–2017.
- [189] Libby W.F. Promising catalyst for auto exhaust // *Science*. – 1971. – V. 171. – P. 499.
- [190] Ciambelli P., Cimino S., De Rossi S., Lisi L., Minelli G., Porta P., Russo G.  $\text{AFeO}_3$  (A=La, Nd, Sm) and  $\text{LaFe}_{1-x}\text{Mg}_x\text{O}_3$  perovskites as methane combustion and CO oxidation catalysts: structural, redox and catalytic properties // *Applied Catalysis B: Environmental*. – 2001. – V. 29. – I. 4. – P. 239-250.
- [191] Benggaard H.S., et al. Steam reforming and graphite formation on Ni catalysts // *Journal of Catalysis*. – 2002. – V. 209. – P. 365–384.
- [192] Wang Z., Wang C., Chen S., Liu Y. Co-Ni bimetal catalyst supported on perovskite-type oxide for steam reforming of ethanol to produce hydrogen // *International Journal of Hydrogen Energy*. – 2014. – V. 39. – P. 5644-5652.
- [193] de Lima S.M., da Silva A.M., da Costa L.O.O., Assaf J.M., Jacobs G., Davis B.H., Mattos L.V., Noronha F.B. Evaluation of the performance of Ni/La<sub>2</sub>O<sub>3</sub> catalyst prepared from LaNiO<sub>3</sub> perovskite-type oxides for the production of hydrogen through steam reforming and oxidative steam reforming of ethanol // *Applied Catalysis A*. – 2010. – V. 377. – P. 181–190.
- [194] Mawdsley J.R., Krause T.R. Rare earth-first-row transition metal perovskites as catalysts for the autothermal reforming of hydrocarbon fuels to generate hydrogen // *Applied Catalysis A: General*. – 2008. – V. 334. – P. 311–320.
- [195] Lin K.H., Wang C.B., Chien S.H. Catalytic performance of steam reforming of ethanol at low temperature over LaNiO<sub>3</sub> perovskite // *International Journal of Hydrogen Energy*. – 2013. – V. 38. – P. 3226-3232.
- [196] Chen H., Yu H., Peng F., Yang G., Wang H., Yang J., Tang Y. Autothermal reforming of ethanol for hydrogen production over perovskite LaNiO<sub>3</sub> // *Chemical Engineering Journal*. – 2010. – V. 160. – P. 333-339.
- [197] Marinho A.L.A., Rabelo-Neto R.C., Noronha F.B., Mattos L.V. Steam reforming of ethanol over Ni-based catalysts obtained from LaNiO<sub>3</sub> and LaNiO<sub>3</sub>/CeSiO<sub>2</sub> perovskite-type oxides for the production of hydrogen // *Applied Catalysis A: General*. – 2016. – V. 520. – P. 53–64.
- [198] De Lima S.M., Da Silva A.M., Da Costa L.O., Assaf J.M., Mattos L.V., Sarkari R., Venugopal A., Noronha F.B. Hydrogen production through oxidative steam reforming of ethanol

over Ni-based catalysts derived from  $\text{La}_{1-x}\text{Ce}_x\text{NiO}_3$  perovskite-type oxides // *Applied Catalysis B: Environ.* – 2012. – V. 1. – P. 121–122.

[199] Chen S.Q., Liu Y.  $\text{LaFe}_y\text{Ni}_{1-y}\text{O}_3$  supported nickel catalysts used for steam reforming of ethanol // *International Journal of Hydrogen Energy.* – 2009. – V. 34. – P. 4735.

[200] Chen S.Q., Wang H., Liu Y. Perovskite  $\text{La-St-Fe-O}$  ( $\text{St} = \text{Ca}, \text{Sr}$ ) supported nickel catalysts for steam reforming of ethanol: The effect of the A site substitution // *International Journal of Hydrogen Energy.* – 2009. – V. 34. – P. 7995.

[201] Zhao L., Wei Y., Huang Y., Liu Y.  $\text{La}_{1-x}\text{K}_x\text{Fe}_{0.7}\text{Ni}_{0.3}\text{O}_3$  catalyst for ethanol steam reforming — The effect of K-doping // *Catalysis Today.* – 2016. – V. 259. – P. 430–437.

[202] Natile M.M., Poletto F., Galenda A., Glisenti A., Montini T., De Rogatis L., Glisenti P.  $\text{La}_{0.6}\text{Sr}_{0.4}\text{Co}_{1-y}\text{Fe}_y\text{O}_{3-\delta}$  Perovskites: Influence of the Co/Fe Atomic Ratio on Properties and Catalytic Activity toward Alcohol Steam-Reforming // *Chemical Materials.* – 2008. – V. 20. – P. 2314.

[203] Wang Z., Wang H., Liu Y.  $\text{La}_{1-x}\text{Ca}_x\text{Fe}_{1-x}\text{Co}_x\text{O}_3$  — a stable catalyst for oxidative steam reforming of ethanol to produce hydrogen // *RSC Advances.* – 2013. – V. 3. – P. 10027-10036.

[204] Ma F., Ding Z., Chu W., Hao S., Qi T. Preparation of  $\text{LaXCoO}_3$  ( $\text{X} = \text{Mg}, \text{Ca}, \text{Sr}, \text{Ce}$ ) catalysts and their performance for steam reforming of ethanol to hydrogen // *Chinese Journal of Catalysis.* – 2014. – V. 35. – P. 1768–1778.

[205] Huang L., Zhang F., Wang N., Chen R., Hsu A.T. Nickel-based perovskite catalysts with iron-doping via self-combustion for hydrogen production in auto-thermal reforming of Ethanol // *International Journal of Hydrogen Energy.* – 2012. – V. 37. – P. 1272-1279.

[206] Pavlova S., Kapokova L., Bunina R., Alikina G., Sazonova N., Krieger T., Ishchenko A., Rogov V., Gulyaev R., Sadykov V., Mirodatos C. Syngas production by  $\text{CO}_2$  reforming of methane using  $\text{LnFeNi(Ru)O}_3$  perovskites as precursors of robust catalysts // *Catalysis Science & Technology.* – 2012. – V. 2. – P. 2099-2108.

[207] Kapokova L., Pavlova S., Bunina R., Alikina G., Krieger T., Ishchenko A., Rogov V., Sadykov V. Dry reforming of methane over  $\text{LnFe}_{0.7}\text{Ni}_{0.3}\text{O}_{3-\delta}$  perovskites: Influence of Ln nature // *Catalysis Today.* – 2011. – V. 164. – P. 227–233.

[208] Sadykov V., Mezentseva N., Alikina G., Bunina R., Pelipenko V., Lukashevich A., Vostrikov Z., Rogov V., Krieger T., Ishchenko A., Zaikovskiy V., Bobrova L., Ross J., Smorygo O., Smirnova A., Rietveld B., van Berkel F. Nanocomposite catalysts for steam reforming of methane and biofuels: Design and performance // Chapter in: B. Reddy (Eds.), *Nanocomposite Materials, Theory and Applications*, INTECH, Austria, Vienna. – 2011. – P. 909-946.

[209] Sadykov V., Bobrova L., Pavlova S., Simagina V., Makarshin L., Parmon V., Ross J.R.H., Van Veen A.C., Mirodatos C. Syngas Generation from Hydrocarbons and Oxygenates with Structured Catalysts // *Series Energy Science, Engineering and Technology*, Nova Science Publishers, Inc, New York. – 2012. – P. 140.

[210] Sadykov V., Mezentseva N., Simonov M., Smal E., Arapova M., Pavlova S., Fedorova Y., Chub O., Bobrova L., Kuzmin V., Ishchenko A., Krieger T., Roger A.C., Parkhomenko K., Mirodatos C., Smorygo O., Ross J. // *Int. J. Hydrogen Energy.* – 2015. – V. 40. – P. 7511-7522.

- [211] Sadykov V.A., Pavlova S.N., Alikina G.M., Sazonova N.N., Mezentseva N.V., Arapova M.V., Rogov V.A., Krieger T.A., Ishchenko A.V, Gulyaev R.V., Zadesenets A.V., Roger A.-C., Chan–Thaw C.E., Smorygo O.L. Perovskite-based catalysts for transformation of natural gas and oxygenates into syngas, Chapter in: J. Zhang and H. Li (Eds.), *Perovskite: Crystallography // Chemistry and Catalytic Performance*, Nova Science Publishers, Inc, New York. – 2013. – P. 1-58.
- [212] Sadykov V., Pavlova S., Zarubina V., Bobin A., Alikina G., Lukashevich A., Muzykantov V., Usoltsev V., Kharlamova T., Boronin A., Koscheev S., Krieger T., Ishchenko A., Mezentseva N., Salanov A., Smirnova A., Bobrenok O., Uvarov N. // *ECS Trans.* – 2009. – V. 25. – P. 2403.
- [213] Urasaki K., Tokunaga K., Sekine Y., Matsukata M., Kikuchi E. Production of hydrogen by steam reforming of ethanol over cobalt and nickel catalysts supported on perovskite-type oxides // *Catalysis Communications.* – 2008. – V. 9. – P. 600–604.
- [214] Jia C., Gao J., Li J., Gu F., Xu G., Zhong Z., Su F. Nickel catalysts supported on calcium titanate for enhanced CO methanation // *Catalysis Science & Technology.* – 2013. – V. 3. – P. 490.
- [215] Dacquin J.P., Cabie M., Henry C.R., Lancelot C., Dujardin C., Raouf S.R., Granger P. Structural changes of nano-Pt particles during thermal ageing: Support-induced effect and related impact on the catalytic performances // *Journal of Catalysis.* – 2010. – V. 270. – P. 299–309.
- [216] Wu G., Li S., Zhang C., Wang T., Gong J. Glycerol steam reforming over perovskite-derived nickel-based catalysts // *Applied Catalysis B: Environmental.* – 2014. – V. 144. – P. 277– 285.
- [217] Urendar M., Sagar T.V., Raveendra G., Ashwani Kumar M., Lingaiah N., Rama Rao K.S., Sai Prasad P.S. Pt doped LaCoO<sub>3</sub> perovskite: A precursor for a highly efficient catalyst for hydrogen production from glycerol // *International Journal of Hydrogen Energy.* – 2016. – V. 41. – P. 2285-2297.
- [218] Chen G., Yao J., Liu J., Yan B., Shan R. Biomass to hydrogen-rich syngas via catalytic steam reforming of bio-oil // *Renewable Energy.* – 2016. – V. 91. – P. 315–322.
- [219] Mota N., Alvarez-Galvan M.C.A., Al-Zahrani S.M., Navarro R.M., Fierro J.L.G. Diesel fuel reforming over catalysts derived from LaCo<sub>1-x</sub>Ru<sub>x</sub>O<sub>3</sub> perovskites with high Ru loading // *International Journal of Hydrogen Energy.* – 2012. – V. 37. – P. 7056-7066.
- [220] Falcon H., Baranda J., Campos-Martin J.M., Pena M.A., Fierro J.L.G. Structural features and activity for CO oxidation of LaFe<sub>x</sub>Ni<sub>1-x</sub>O<sub>3+δ</sub> catalysts // *Studies in Surface Science and Catalysis.* – 2000. – V. 130. – P. 2195–2200.
- [221] Martinelli D.M.H., Melo D.M.A., Pedrosa A.M.G., Martinelli A.E., Melo M.A.F., Batista M.K.S., Bitencourt R.C. Use of Perovskite-Type Lanthanum Nickelate Synthesized by the Polymeric Precursor Method in the Steam Reforming Reaction of Methane // *Materials Sciences and Applications.* – 2012. – V. 3. – P. 363.
- [222] Ammendola P., Cammisa E., Lisi L., Ruoppolo G. Thermochemical Stability of Alumina-Supported Rh-LaCoO<sub>3</sub> Catalysts for Tar Conversion // *Industrial and Engineering Chemistry Research* – 2012. – V. 51. – P. 7475.



- [223] Asada T., Kayama T., Kusaba H., Einaga H., Teraoka Y. Preparation of alumina-supported LaFeO<sub>3</sub> catalysts and their catalytic activity for propane combustion // *Catalysis Today*. – 2008. – V. 139. – P. 37-42.
- [224] Davshan N.A., Kustov A.L., Tkachenko O.P., Kustov L.M., Kim C.H. Oxidation of Carbon Monoxide over MLaO<sub>x</sub> Perovskites Supported on Mesoporous Zirconia // *ChemCatChem*. – 2014. – V. 6. – P. 1990.
- [225] Cimino S., Colonna S., De Rossi S., Faticanti M., Lisi L., Pettiti I., Porta P. Methane Combustion and CO Oxidation on Zirconia-Supported La, Mn Oxides and LaMnO<sub>3</sub> Perovskite // *Journal of Catalysis*. – 2002. – V. 205. – P. 309.
- [226] Zhao L., Hana T., Wang H., Zhang L., Liu Y. Ni-Co alloy catalyst from LaNi<sub>1-x</sub>Co<sub>x</sub>O<sub>3</sub> perovskite supported on zirconia for steam reforming of ethanol // *Applied Catalysis B: Environmental*. – 2016. – V. 187. – P. 19–29.
- [227] Yan X., Huang Q., Li B., Xu X, Chen Y., Zhu S., Shen S. Catalytic performance of LaCo<sub>0.5</sub>M<sub>0.5</sub>O<sub>3</sub> (M = Mn, Cr, Fe, Ni, Cu) perovskite-type oxides and LaCo<sub>0.5</sub>Mn<sub>0.5</sub>O<sub>3</sub> supported on cordierite for CO oxidation // *Journal of Industrial and Engineering Chemistry*. – 2013. – V. 19. – P. 561–565.
- [228] Zeng G.M., Shao J.J., Gu R.X., Li Y.D. Facile Fabrication of a Highly Active Shell-Core LaNi(Mg, Al)O<sub>3</sub>@Mg-Al Catalyst for Ethanol Steam Reforming // *Catalysis Today*. – 2014. – V. 233. – P. 31–37.
- [229] Voorhoeve R.J.H., Remeika J.P., Trimble L.E. Defect chemistry and catalysis in oxidation and reduction over perovskite-type oxides // *Ann. N. Y. Acad. Sci.* – 1976. – V. 272. – P. 3-21.
- [230] Taguchi H., Yamada S., Nagao M., Ichikawa Y., Tabata K. Surface characterization of LaCoO<sub>3</sub> synthesized using citric acid // *Mater Res Bull.* – 2002. – V. 37. – P. 69–76.
- [231] Molchanov V.V., Buyanov R.A. Scientific bases of application of methods of mechanochemistry for the preparation of catalysts // *Kinetics and catalysis*. – 2001. – T. 42. – C. 406-415.
- [232] Ng Lee Y., Lago R.M., Fierro J.L.G., Gonzalez. // *Applied Catalysis A: General*. – 2001. – V. 215. – P. 245-256.
- [233]. Livage J. Sol-gel synthesis of heterogeneous catalysts from aqueous solutions // *Catalysis Today*. – 1998. – V. 41. – P. 3-19.
- [234] Baythoun M.S.G., Sale F.R. Production of strontium-substituted lanthanum manganite perovskite powder by the amorphous citrate process // *Journal of Material Science*. – 1982. – V. 17. – P. 2757.
- [235] Nair M.M., Kaliaguine S., Kleitz F. Nanocast LaNiO<sub>3</sub> Perovskites as Precursors for the Preparation of Coke-Resistant Dry Reforming Catalysts // *ACS Catalysis*. – 2014. – V. 4. – P. 3837–3846.

- [236] Wang Y., Cui X., Li Y., Shu Z., Chen H., Shi J. A simple co-nanocasting method to synthesize high surface area mesoporous LaCoO<sub>3</sub> oxides for CO and NO oxidations // *Microporous and Mesoporous Materials*. – 2013. – V. 176. – P. 8–15.
- [237] Arandiyán H., Dai H., Deng J., Liu Y., Bai B., Wang Y., Li X., Xie S., Li J. Three-dimensionally ordered macroporous La<sub>0.6</sub>Sr<sub>0.4</sub>MnO<sub>3</sub> with high surface areas: Active catalysts for the combustion of methane // *Journal of Catalysis*. – 2013. – V. 307. – P. 327–339.
- [238] de Lima R.K.C., Batista M.S., Wallau M., Sanches E.A., Mascarenhas Y.P., Urquieta-Gonzalez E.A. High specific surface area LaFeCo perovskites—Synthesis by nanocasting and catalytic behavior in the reduction of NO with CO // *Applied Catalysis B: Environmental*. – 2009. – V. 90. – P. 441–450.
- [239]. Patent 3 330 697 U.S. Method of preparing lead and alkaline earth titanates and niobates and coating method using the same to form a capacitor / Pechini, M.P., – 08.1963, patented 11.07.1967.
- [240] Cimino S., Colonna S., De Rossi S., Faticanti M., Lisi L., Pettiti I., Porta P. Methane Combustion and CO Oxidation on Zirconia-Supported La, Mn Oxides and LaMnO<sub>3</sub> Perovskite // *Journal of Catalysis*. – 2002. – V. 205. – P. 309–317.
- [241] Orlik S.N., Soloviev S.A., Kapran A.Yu., Kantserova M.R., Kirienko P.I., Gubareni E.V., Structurally functional design of nanocomposite catalysts for production and ecological processes // *Chemistry, physics and surface technology*. – 2015. – T. 6. – C. 273-304.
- [242] Koo K.Y., Eom H.J., Jung U.H., Yoon W.L. Ni nanosheet-coated monolith catalyst with high performance for hydrogen production via natural gas steam reforming // *Applied Catalysis A: General*. – 2016. – V. 525. – P. 103–109.
- [243] Palma V., Martino M., Meloni E., Ricca A. Novel structured catalysts configuration for intensification of steam reforming of methane // *International Journal of Hydrogen Energy*. – 2016. – P. 1–10.
- [244] Casanovas A., de Leitenburg C., Trovarelli A., Llorca J. Catalytic monoliths for ethanol steam reforming // *Catalysis Today*. – 2008. – V. 138. – I. 3–4. – P. 187–192.
- [245] Salge J.R., Deluga G.A., Schmidt L.D. Catalytic partial oxidation of ethanol over noble metal catalysts // *Journal of Catalysis*. – 2005. – V. 235. – P. 69–78.
- [246] Lonyi F., Valyon J., Someus E., Hancsok J. Steam reforming of bio-oil from pyrolysis of MBM over particulate and monolith supported Ni/Al<sub>2</sub>O<sub>3</sub> catalysts // *Fuel*. – 2013. – V. 112. – P. 23–30.
- [247] Goyal N., Pant K.K., Gupta R., Hydrogen production by steam reforming of model bio-oil using structured Ni/Al<sub>2</sub>O<sub>3</sub> catalysts // *International Journal of Hydrogen Energy*. – 2013. – V. 38. – P. 921-933.
- [248] Laguna O.H., Domínguez M.I., Centeno M.A., Odriozola J.A. Catalysts on Metallic Surfaces: Monoliths and Microreactors // *New Materials for Catalytic Applications*, Elsevier. – 2016. – Ch. 4. – P. 81–120.

- [249] Bortolozzi J.P., Gutierrez L.B., Ulla M.A. Synthesis of Ni/Al<sub>2</sub>O<sub>3</sub> and Ni–Co/Al<sub>2</sub>O<sub>3</sub> coatings onto AISI 314 foams and their catalytic application for the oxidative dehydrogenation of ethane // *Applied Catalysis A: General*. – 2013. – V. 452. – P. 179–188.
- [250] Williams J.L. Monolith structures, materials, properties and uses // *Catalysis Today*. – 2001. – V. 69. – P. 3–9.
- [251] Smorygo O.L., Sadykov V. A., Bobrova L.N. Open Cell Foams as Substrates For Design of Structured Catalysts, Solid Oxide Fuel Cells and Supported Asymmetric Membrane // *Monograph*, Nova Science Publishers, Inc. – 2016. – P. 207.
- [252] Özkan G., Gök S., Özkan G. Active carbon-supported Ni, Ni/Cu and Ni/Cu/Pd catalysed steam reforming of ethanol for the production of hydrogen // *Chemical Engineering*. – 2011. – V. 171. – P. 1270–1275.
- [253] Soyal-Baltacıoğlu F., Erhan Aksoylu A., Önsan I. Steam reforming of ethanol over Pt–Ni Catalysts // *Catalysis Today*. – 2008. – V. 138. – P. 183–186.
- [254] Mikutski V., Smorygo O., Shchurevich D., Marukovich A., Ilyushchanka A., Gokhale A., et al. Open-cell metal–SiC composite foams made by electrolytic codeposition on polyurethane substrates. *Powder Metall Met Ceram*. – 2014. – V. 52. – P. 545–550.
- [255] Falcon H., Baranda J., Campos-Martin J.M., Pena M.A., Fierro J.L.G. Structural features and activity for CO oxidation of LaFe<sub>x</sub>Ni<sub>1-x</sub>O<sub>3+σ</sub> catalysts // *Studies in Surface Science and Catalysis*. – 2000. – V. 130. – P. 2195–2200.
- [256] Porta P., Cimino S., De Rossi S., Faticanti M., Minelli G., Pettiti I. AFeO<sub>3</sub> (A=La, Nd, Sm) and LaFe<sub>1-x</sub>Mg<sub>x</sub>O<sub>3</sub> perovskites: structural and redox properties // *Materials Chemistry and Physics*. – 2001. – V. 71. – P. 165–173.
- [257] Berenov A., Angeles E., Rossiny J., Raj E., Kilner J., Atkinson A. Structure and transport in rare-earth ferrates // *Solid State Ionics*. – 2008. – V. 179. – P. 1090–1093.
- [258] Ren Y., Küngas R., Gorte R.J., Deng C. The effect of A-site cation (Ln=La, Pr, Sm) on the crystal structure, conductivity and oxygen reduction properties of Sr-doped ferrite perovskites // *Solid State Ionics*. – 2012. – V. 212. – P. 47–54.
- [259] Singh S. J., Jayaram R. V. Oxidation of alkylaromatics to benzylic ketones using TBHP as an oxidant over LaMO<sub>3</sub> (M = Cr, Co, Fe, Mn, Ni) perovskites // *Catalysis Communications*. – 2009. – V. 10. – P. 2004–2007.
- [260] Provendier H., Petit C., Estournes C., Libsa S., Kiennemann A. Stabilisation of active nickel catalysts in partial oxidation of methane to synthesis gas by iron addition // *Applied Catalysis A: General*. – 1999. – V. 180. – P. 163–173.
- [<sup>261</sup>] G.C.de Araujo, S. M. de Lima, J. M. Assaf, M. A. Pena, J. L. G. Fierro, M. C. Rangel, Catalytic evaluation of perovskite-type oxide LaNi<sub>1-x</sub>Ru<sub>x</sub>O<sub>3</sub> in methane dry reforming // *Catalysis Today* 133–135 (2008) 129–135

- [<sup>262</sup>] M.R. Goldwasser, M.E. Rivas, E. Pietri, M.J. Perez-Zurita, M.L. Cubeiro, L. Gingembre, L. Leclercq, G. Leclercq, Perovskites as catalysts precursors: CO<sub>2</sub> reforming of CH<sub>4</sub> on Ln<sub>1-x</sub>Ca<sub>x</sub>Ru<sub>0.8</sub>Ni<sub>0.2</sub>O<sub>3</sub> (Ln = La, Sm, Nd) // *Applied Catalysis A: General* 255 (2003) 45–57
- [263] Biswas P., Kunzru D., Oxidative steam reforming of ethanol over Ni/CeO<sub>2</sub>-ZrO<sub>2</sub> catalyst // *Chemical Engineering Journal*. – 2008. – V. 136. – P. 41-49.
- [264] Batista M.S., Santos R.K.S., Assaf E.M., Assaf J.M., Ticianelli, E.A. High efficiency steam reforming of ethanol by cobalt based catalysts // *Journal of Power Sources*. – 2004. – V. 134. – P. 27-32.
- [265] Gallego G.S., Marín J.G., Batiot-Dupeyrat C., Barrault J., Mondragon F. Influence of Pr and Ce in dry methane reforming catalysts produced from La<sub>1-x</sub>A<sub>x</sub>NiO<sub>3-δ</sub> perovskites // *Applied Catalysis A: General*. – 2009. – V. 369. – P. 97–103.
- [266] Barroso M.N., Galetti A.E., Abello M.C. Ni catalysts supported over MgAl<sub>2</sub>O<sub>4</sub> modified with Pr for hydrogen production from ethanol steam reforming // *Applied Catalysis A: General*. – 2011. – V. 394. – P. 124–131.
- [267] Haryanto A., Fernando S., Murali N., Adhikari S. Current Status of Hydrogen Production Techniques by Steam Reforming of Ethanol: A Review // *Energy & Fuels*. – 2005. – V. 19. – P. 2098–2106.
- [268] Vaidya P.D., Rodrigues A.E. Insight into steam reforming of ethanol to produce hydrogen for fuel cells // *Chemical Engineering Journal*. – 2006. – V. 117. – P. 39–49.
- [269] Arapova M.V., Pavlova S.N., Rogov V.A., Krieger T.A., Ishchenko A.V., Roger A.C. Ni(Co)-Containing Catalysts Based on Perovskite-Like Ferrites for Steam Reforming of Ethanol // *Catalysis for Sustainable Energy*. – 2014. – V. 1. – P. 10–20.
- [270] Becerra M., Castro-Luna A.E., Chil J. An investigation on the presence of NiAl<sub>2</sub>O<sub>4</sub> in a stable Ni on alumina catalyst for dry reforming // *Journal of the Chilean Chemical Society*– 2005. – V. 50. – P. 465.
- [271] Lever A.B.P. *Inorganic Electronic Spectroscopy*, 2nd ed // Elsevier: Amsterdam – Oxford – New York – Tokyo. – 1987. – P. 445.
- [272] Grosvenor A.P., Biesinger M.C., Smart R.S.C., McIntyre N.S. New interpretations of XPS spectra of nickel metal and oxides // *Surface Science* – 2006. – V. 600. – P. 1771.
- [273] Sadykov V.A., Chub O., Chesalov Yu., Mezentseva N., Pavlova S.N., Arapova M.V., Rogov V.A., Simonov M.N., Roger A.C., Parkhomenko K., Van Veen A.C. Mechanism of ethanol steam reforming over Pt/(Ni+Ru)-promoted oxides by FTIRS in situ // *Topics in Catalysis*. – 2016. – V. 59. – P. 1332–1342.

## Synthèse et propriétés de catalyseurs à base de Ni pour la valorisation d'éthanol et de glycérol par vaporeformage catalytique pour la production d'hydrogène

### Résumé

Les trois familles catalytiques à base de perovskites contenant du Ni: massives  $[\text{LnFe}_{1-x-y}\text{Ni}_y\text{M}_x\text{O}_{3-\delta}]$  (Ln=La, Pr; B=Co, Mn, Ru), sur support  $[m\text{LnNi}_{0.9}\text{Ru}_{0.1}\text{O}_3/n\text{Mg-}\gamma\text{-Al}_2\text{O}_3]$  (Ln = La, Pr) et structuré  $[m\text{LaNi}_{0.9}\text{Ru}_{0.1}\text{O}_3/n\text{Mg-}\gamma\text{-Al}_2\text{O}_3/$  mousses structurées] ont été synthétisés, caractérisés et testés dans les réactions de vaporeformage de l'éthanol et de glycérol. Les effets de la composition chimique et de la méthode de synthèse sur les propriétés structurales et texturales, ainsi que sur la réductibilité des échantillons initiaux ont été évalués. L'utilisation préférentielle de Pr, Ni et Ru dans la composition de catalyseur a été démontrée pour toutes les familles. Le rôle essentiel de la modification du support  $\gamma\text{-Al}_2\text{O}_3$  avec  $\geq 10\%$  mass de Mg introduit par imprégnation humide pour le catalyseur supporté a également été prouvé. Des catalyseurs de la composition optimale fournissant une activité élevée dans le vaporeformage de l'éthanol et du glycérol à  $T = 650\text{ }^\circ\text{C}$  ont été trouvés: le meilleur catalyseur massif à base du précurseur  $\text{PrFe}_{0.6}\text{Ni}_{0.3}\text{Ru}_{0.1}\text{O}_3$  fournit une activité élevée pendant au moins 7 h, grâce à la facilité de leur réduction et les propriétés d'oxydoréduction de l'oxyde de praséodyme formé. Les catalyseurs sur support 10-20%  $\text{PrNi}_{0.9}\text{Ru}_{0.1}\text{O}_3/10\text{-}15\%\text{Mg-}\gamma\text{-Al}_2\text{O}_3$  fournissent le meilleur rendement en hydrogène ( $\sim 90\%$ ) et la stabilité pendant  $\sim 20$  heures. Le catalyseur structuré optimisé à base de la plaquette Ni-Al métallique fournit le rendement stable en hydrogène 80-87% dans l'oxy-vaporeformage d'éthanol dans les mélanges concentrés (concentration d'éthanol de 30%) dans un réacteur pilote pendant 40 heures. Les résultats obtenus rendent ces systèmes catalytiques structurés très prometteurs à utiliser dans les générateurs électrochimiques à base de piles à combustible avec l'utilisation de ressources renouvelables peu coûteuses comme bio-huile.

**Mots clés:** vaporeformage, hydrogène, bio-huiles, éthanol, glycérol, perovskites

### Résumé en Anglais

The three catalytic families based on Ni-containing perovskites: massive  $[\text{LnFe}_{1-x-y}\text{Ni}_y\text{M}_x\text{O}_{3-\delta}]$  (Ln=La, Pr; B=Co, Mn, Ru), supported  $[m\text{LnNi}_{0.9}\text{Ru}_{0.1}\text{O}_3/n\text{Mg-}\gamma\text{-Al}_2\text{O}_3]$  (Ln = La, Pr) and structured  $[m\text{LaNi}_{0.9}\text{Ru}_{0.1}\text{O}_3/n\text{Mg-}\gamma\text{-Al}_2\text{O}_3/$ structured foams] were synthesized, characterized and tested in the reactions of the ethanol and glycerol steam reforming. The effects of the chemical composition and synthesis method on the structural and textural properties, as well as on reducibility of initial samples were evaluated. The preferred use of Pr, Ni and Ru in the catalyst composition was shown for all families. The essential role of the effective  $\gamma\text{-Al}_2\text{O}_3$  support modification with the  $\geq 10\%$  wt. of Mg introduced by wetness impregnation for the supported catalyst was also proved. Catalysts of the optimal composition providing a high activity in steam reforming of both ethanol and glycerol at  $T= 650\text{ }^\circ\text{C}$  were found: the best massive catalyst based on the  $\text{PrFe}_{0.6}\text{Ni}_{0.3}\text{Ru}_{0.1}\text{O}_3$  precursor provides high activity for at least 7 hours, which is explained by the ease of their reduction and the oxidation-reduction properties of the praseodymium oxide formed. Supported 10-20%  $\text{PrNi}_{0.9}\text{Ru}_{0.1}\text{O}_3/10\text{-}15\%\text{Mg-}\gamma\text{-Al}_2\text{O}_3$  provide the greatest yield of hydrogen ( $\sim 90\%$ ) and stability for  $\sim 20$  hours. Structured catalyst based on the metal Ni-Al platelet provides the yield of hydrogen 80-87% in oxy-steam and steam reforming of ethanol in the concentrated mixtures (ethanol concentration of 30%) in a pilot reactor for 40 hours. The results obtained make these structured catalytic systems very promising to use in electrochemical generators based on fuel cells with the use of inexpensive renewable resource – bio-oil.

**Keywords:** Steam reforming, hydrogen, bio-oils, ethanol, glycerol, perovskites